A Study of Solute - Solvent Interactions in Methanol Solutions; Potential New Sustainable Technologies for Refinery Product Upgrading/Separating and Methanol Utilization

Zhaoxi Zhang

St Hugh's College

University of Oxford

A thesis submitted in partial fulfilment of

the requirements for the degree of

Doctor of Philosophy in Inorganic Chemistry

Hilary Term 2017

Abstract

The upgrading of fluid catalytic cracking (FCC) gasoline is a significant refinery process which is required to decrease FCC gasoline's alkenes and organosulfur compounds (OSCs) levels to meet stringent, regulated specifications, whilst maintaining or increasing the octane number. The separation and recovery of alkene contents in gaseous alkene and alkane mixtures produced in the refining process is presently a substantial consumer of both energy and resources. The current processes for these upgrading or separation processes rely heavily upon energy – intensive technologies which require severe conditions and complex procedures, involving the widespread use of hydrogen. In this research, I explore new routes, based on novel and innovative chemistry, to improve the considerable energy consumption and overcome the above disadvantages in current FCC gasoline upgrading and gaseous alkene and alkane separation, and to develop lower cost, less energy-intensive approaches to these significant challenges. The potentially sustainable chemical – methanol – was introduced as the key to fulfil the aim of this research.

After studying the microscopic nature of the hydrogen bond interactions between methanol and various hydrocarbons, alternative green and sustainable methanol - based "*Extractive Refining*/*Extractive Distillation*" approaches for upgrading the FCC gasoline/separating gaseous alkene and alkane has been developed to replace the conventional processes. In addition, what we define as the lower phase mixtures (LPMs) derived from the "*Extractive Refining*" processes were themselves utilised as feedstocks in a subsequent catalytic conversion process to yield high quality liquid fuel

and other products. Through these processes the LPMs is able to be efficiently converted into high added value products such as gasoline, benzene, toluene, xylenes (BTX) etc.. The feasibilities, mechanisms and advantages of these approaches and processes form the detailed investigations reported in this thesis.

At the heart of these new processes is the fundamental issue of hydrogen bond formation between the extractant solvent, methanol, and the primary constituents of FCC gasoline, that need to be extracted, namely light alkenes and organic sulphur compounds, for the latter, typically taken as thiophene in this investigation .

The work progresses from the discovery and evaluation of the applied "*Extractive Refining*/*Extractive Distillation*" process in FCC gasoline, back through to the fundamental nature, and investigation of the hydrogen bond between solute and solvent, through a variety of physicochemical techniques.

Table of Contents

Acknowledgements

I would like to express my sincere thanks and gratitude to my excellent supervisor Professor Peter P. Edwards. It has been an honour to be his D.Phil student. And I would like to offer my special thanks to Dr. Tiancun Xiao. I appreciate all their contributions of time and ideas that have made make my D.Phil experience productive and stimulating. They always stood by me and provided me with advice, guidance and support, as well as expertise in theory and methodology.

I am especially thankful to Professor Peter P. Edwards who has been a primary source of considerable inspiration and intellectual motivation through the entire process of this D.Phil dissertation from the beginning to the completion. The joy and enthusiasm he has for his research in the field fuel economy materials and new-generation catalysts was contagious and motivational for me, even during tough times in the pursuit of the D.Phil. Whenever I turned to him for help, he was always there with insight and patience.

My D.Phil program would not have been possible without the help of many people. I am thankful to Dr. Tiancun Xiao of our KOPRC group. He extended my insight into petrochemical, methanol utilization and catalyst studies and gave me plenty of inspiring and valuable advices during my D.Phil study. I am also grateful to my D.Phil transfer examiners: Professor Fraser Armstrong and Professor Kylie Vincent, for their insightful comments in my transfer examination. My special thanks go to Dr Nick Rees, who has expertise in NMR. He helped me a lot with his professional knowledge during my NMR test and analysis. I also would like to thank Dr. Vladimir Kuznetsov

of University of Oxford and Dr. Maxim L. Kuznetsov of University of Lisbon, who provided me many help and support in the aspect of computational analysis.

My study time at University of Oxford and life in Oxford were made enjoyable in large part due to the many colleagues and friends that became a part of my life. I am grateful for time spent with colleagues and many friends.

Lastly, I would like to thank my family for all their endless love and encouragement. The great love and support I received from my parents, my parents-in-law and my son have made all the hard work, late nights, and sleepless nights worth it. I am also deeply indebted to my loving, supportive, encouraging and patient wife Dr. Jing Deng. She provided her faithful support during the whole creation process of my D.Phil dissertation. Without her tolerance, motivation and support, this dissertation could not have been achieved. I enjoy so much the life we are living and studying in Oxford.

Many thanks again to all who have helped me!

–Zhaoxi Zhang

April 2017, Oxford, UK

Declaration

The work described in this thesis was performed in the Inorganic Chemistry Laboratory, University of Oxford from October 2012 until April 2017, under the complete supervision of Professor Peter P. Edwards. All the work is my own unless otherwise stated, and has not been submitted previously for any other degree at this or any other university.

Zhaoxi Zhang

April 2017

Nomenclatures and Abbreviations

Nomenclatures

pK_a logarithmic acid dissociation constant;

pK_b logarithmic base dissociation constant;

V_{IR} infrared spectrum relative shift;

ΔE the spacing of the energy levels;

h planck's constant;

ν_{NMR} frequency of *Nuclear Magnetic Resonance* (NMR);

For GC results:

Φ_i volume fraction of component ***i;***

V_i volume of component ***i;***

$\Sigma_j V_j$ the volume of all constituents of the mixture ***V;***

A_i peak area of component ***i***, the integral area of component ***i***'s peak in the *chromatogram* which is obtained from the GC analyser;

f_i relative correction factor for component ***i***, which is obtained from the component ***i***'s standard curve. The standard curve was calculated from component ***i***'s GC calibration results;

Q_i output/flow rate of component ***i;***

Φ_s volume fraction of standard component, here Nitrogen (N_2);

Q_s output/flow rate of standard component, here Nitrogen (N_2);

For GCMS results:

f_i relative correction factor for component ***i***, which is obtained from the component

i's GCMS calibration results;

A_i peak area of component ***i***, the integral area of component ***i***'s peak in the *chromatogram* which is obtained from the GCMS analyser;

A_s peak area of standard component, the integral area of standard component's peak in the *chromatogram* which is obtained from the GCMS analyser, here the standard component is dimethyl carbonate (DMC);

$W_{i\cdot GCMS}$ mass of component ***i*** in the GCMS sample;

W_s mass of standard component in the GCMS sample, here the standard component is dimethyl carbonate (DMC);

w_i mass fraction of component ***i*** in the liquid sample ***n***;

$W_{n\cdot GCMS}$ mass of liquid sample ***n*** in its GCMS sample;

$V_{n\cdot GCMS}$ certain volume of liquid sample ***n*** in its GCMS sample;

ρ_n density of liquid sample ***n***;

W_i mass of component ***i*** in the liquid sample ***n***;

W_n mass of liquid sample ***n***;

V_n volume of liquid sample ***n***;

For X-ray Diffractometer:

λ wavelength;

k wave vector;

E the energy for X-rays typically in the range of 10^2-10^5 eV;

h universal constant;

c speed of light;

2θ angle between the incident and the exit wave;

d distance between two atomic planes;

For DFT calculations:

E_{int} interaction energies (in kJ/mol) at the M06-2X/6-311+G** and CCSD(T)/6-311+G**//M06-2X/6-311+G** levels;

l(OH···π) intermolecular OH···$(C=C)_{midpoint}$ distances (in Å);

ρ electron density (in e/Å^3) at the OH···(C=C) BCP;

$\nabla^2\rho$ electron density laplacian (in e/Å^5) at the OH···(C=C) BCP;

H_b energy density at the OH···(C=C) BCP (in Hartree/Å^3);

For NMR results:

δ chemical shift;

Δδ chemical shift change;

μ permanent Dipole Moment;

For extractive refining and extractive distillation results:

Alkene(s) unsaturated hydrocarbon(s) only contain carbon-carbon double bond(s);

Gaseous alkene(s) C1-C4 unsaturated hydrocarbon(s) which in gaseous phase under room temperature and only contain carbon-carbon double bond;

Alkane(s) saturated hydrocarbon(s) i.e. n-paraffin(s), i-paraffin(s) and naphthene(s);

Gaseous alkane(s) C1-C4 saturated hydrocarbon(s) which in gaseous phase under room temperature;

S_i *(i=2,3)* the different solvent's C2 or C3 alkenes and alkanes separation performance;

$\boldsymbol{\Phi_{pi}}$ *(i=2,3)* the volume/molar fraction (mol%) of the C2 and C3 alkane;

$\boldsymbol{\Phi_{oi}}$ *(i=2,3)* the volume/molar fraction (mol%) of the C2 and C3 alkene;

$\boldsymbol{k_H}$ a temperature-dependent constant;

$\boldsymbol{p}$ the partial pressure (atm);

$\boldsymbol{c}$ the concentration of the dissolved gas in the liquid (mol/L);

$\boldsymbol{\Delta E^i}$ the induction energy, the energy required to separate the dipole (solvent) and the dielectric (solute) (J·F/m·mol);

$\boldsymbol{\epsilon}$ the dielectric constant of the dielectric medium (solute);

$\boldsymbol{\mu}$ the diploe moment of solvent (D);

$\boldsymbol{a}$ the radius of solvent molecule (nm);

For catalytic conversion results:

Gas phase product gases produced from the catalytic conversion process (e.g. H_2, C1-C4 alkene/alkane etc.);

Oil phase product two liquid phases are produced from the catalytic conversion process, the lower phase is the water phase product and the upper phase is the oil phase product;

Abbreviations

ADS adsorptive desulfurization;

BCP bond critical point;

BDS biodesulphurization;

BP boiling point;

bpd barrels per day;

BSSE basis set superposition error;

BTU British thermal units;

BTX benzene, toluene and xylenes;

CHA chabazite structure;

CFG crude FCC gasoline;

CTAB cetyl trimethyl ammonium bromide;

DFT density functional theory;

DMC dimethyl carbonate;

DME dimethyl ether;

DMSO dimethyl sulfoxide;

DOE department of energy;

ECD electron capture;

EDS extractive desulfurization;

EPA environmental protection agency;

FCC fluid catalytic cracking;

FID flame ionization;

FTIR fourier transform infrared;

GC gas chromatography;

GCMS gas chromatography mass spectrometry;

GHG green house gas;

Hβ acidic beta zeolite

HDO hydrodeoxygenation;

HDS hydrodesulphurization;

HHV higher heating value;

HMOR acidic mordenite molecular sieve

HTL hydrothermal liquefaction;

(H)ZSM-5 (acidic) zeolite socony mobil-5;

ICE internal combustion engine;

IEF-PCM integral equation-formalism polarizable continuum model;

IR infrared;

LPM lower phase mixture from "*Extractive Refining*";

MCCGM model catalytic cracking gas mixture;

ME methanol with ethylene glycol mixtures;

MFGM model FCC gasoline mixture;

M-L mesoporous zeolite L;

MOGD mobil olefins-to-gasoline and diesel;

MP2 Møller–Plesset level;

MTA methanol-to-aromatics;

MTCGM model thermal cracking gas mixture;

MTG methanol-to-gasoline;

MTH methanol-to-hydrocarbons;

MTO methanol-to-olefin;

NBO natural bond orbital;

NMR nuclear magnetic resonance;

OATS olefinic alkylation of thiophenic sulphur;

ODF organic distillate fraction;

ODS oxidative desulfurization;

OSCs organosulfur compounds;

PC propylene carbonate;

PMT photo multiplier tube;

PV pervaporation desulfurization;

SAPO-11 silicoaluminophosphate molecular sieve-11

SMD solvation model based on density;

TCD thermal conductivity;

TGA thermal gravimetric analysis;

TMS tetramethylsilane;

UCST upper critical solution temperature;

UPM upper phase mixture from "*Extractive Refining*";

UV ultraviolet;

VT variable temperature;

VTSD variable-temperature stepwise desorption;

XRD X-ray diffractometer;

^{1}H-NMR proton/protium nuclear magnetic resonance;

Chapter 1. Background

1.1 Hydrogen Bond Interactions between Methanol and Alkenes/Thiophene

The underpinning, fundamental science of the "*Extractive Refining/Distillation*" approach is outlined here. It is customary to view are two major kinds of solute – solvent interactions in solutions, one is usually seen as a "*physical interaction*" and one as a "*chemical interaction*".[1] On the physical interaction aspect, a relatively simple solution model was that proposed by Scatchard and Hildebrand for nonpolar solutions.[1-3] Then, van Arkel proposed ideas to extend the *Scatchard – Hildebrand* model to include effects due to polar – nonpolar interactions.[1] Fig. 1 shows a representation of the physical interactions in a solution containing various solute – solvent combinations.

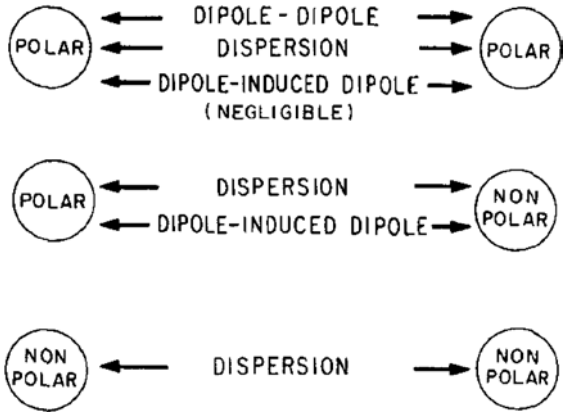

Fig. 1 Physical interactions in a solution[1]

On the other hand, the chemical interaction of species in solutions considers that effects arise because of specific association and solvation. In accordance with this concept, the species in solution are generally regarded (in the limit) as looseIy bonded aggregates consisting of two (or more) molecules of the same species (association) or of different species (the phenomenon of solvation).[1] Through, for example, hydrogen

bond interactions, these “bonded” species form complexes. A schematic diagram of one such complexes between a solute (a hydrocarbon) and solvent is given in Fig. 2.

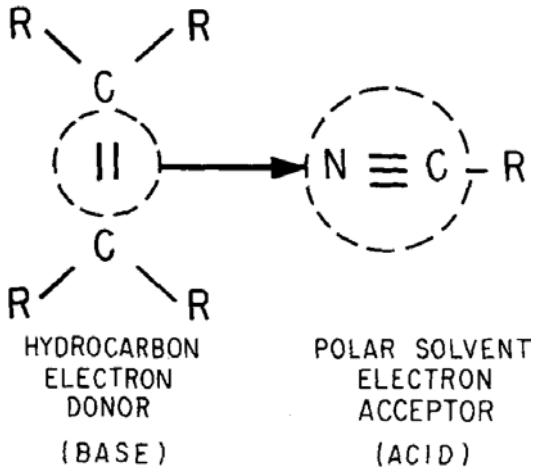

Fig. 2 Schematic diagram of a chemical interaction; arrow shows the flow comprising the flow or donation of electron density[1]

This thesis primarily focuses on the investigation and utilization of chemical interactions at the heart of a new “*Extractive Refining/Distillation*” process which centres on the nature of the hydrogen bond between methanol and light alkenes, and thiophene (thereafter as a prototypical organic sulphur compound).

1.1.1 The Hydrogen Bond

The hydrogen bond has been known since the beginning of the last century Linus Pauling introduced hydrogen bonds into the common body of knowledge in 1939, in his book, entitled *The nature of the chemical bond*.[4] Arunan et al. has recently provided a specific definition of the hydrogen bond in the paper, entitled *Definition of the hydrogen bond.*[5] Those authors define the hydrogen bond as an attractive interaction between a hydrogen atom from a molecule or a molecular fragment X–H in which X is more electronegative than H, and an atom or a group of atoms in the

same or a different molecule, in which there is specific evidence of bond formation.[5]

A typical hydrogen bond may be depicted as X–H…Y–Z, where the three dots denote the bond.[5] X–H represents the hydrogen bond donor.[5] The acceptor may be an atom or an anion Y, or a fragment or a molecule Y–Z, where Y is bonded to Z.[5] In some cases, X and Y are the same. In more specific cases, X and Y are the same and X–H and Y–H distances are the same as well leading to symmetric hydrogen bonds.[5] In any event, the acceptor is an electron rich region such as, but not limited to, a lone pair of Y or π-bonded pair of Y–Z.[5]

Arunan et al. listed some criteria useful as evidence and some typical characteristics for hydrogen bonding.[5] They are not necessarily exclusive,[5] and are listed below, respectively.

List of *criteria* for a hydrogen bond X–H…Y–Z:[5]

(1) The forces involved in the formation of a hydrogen bond include those of an electrostatic origin, those arising from charge transfer between the donor and acceptor leading to partial covalent bond formation between H and Y, and those originating from dispersion.

(2) The atoms X and H are covalently bonded to one another and the X–H bond is polarized, the H…Y bond strength increases with the increase in electronegativity of X.

(3) The X–H…Y angle is usually linear (180°) and the closer the angle is to 180°, the stronger is the hydrogen bond and the shorter is the H…Y distance.

(4) The length of the X–H bond usually increases on hydrogen bond formation

leading to a red shift in the infrared X–H stretching frequency and an increase in the infrared absorption cross-section for the X–H stretching vibration. The greater the lengthening of the X–H bond in X–H…Y, the stronger is the H…Y bond. Simultaneously, new vibrational modes associated with the formation of the H…Y bond are generated.

(5) The X–H…Y–Z hydrogen bond leads to characteristic NMR signatures that typically include pronounced proton deshielding for H in X–H, through hydrogen bond spin–spin couplings between X and Y, and nuclear Overhauser enhancements.

(6) The Gibbs energy of formation for the hydrogen bond should be greater than the thermal energy of the system for the hydrogen bond to be detected experimentally. For reference, the thermal energy at (typical) room temperature (298K) is 0.593 kcal/mol (2.481 kJ/mol).[6]

List of *characteristics* of hydrogen bonds:[5]

(1) The pK_a of X–H and pK_b of Y–Z in a given solvent correlate strongly with the energy of the hydrogen bond formed between them.

(2) Hydrogen bonds are involved in proton-transfer reactions (X–H…Y → X…H–Y) and may be considered the partially active precursors to such reactions.

(3) Networks of hydrogen bonds can show the phenomenon of co-operativity, leading to deviations from pair-wise additivity in hydrogen bond properties.

(4) Hydrogen bonds show directional preferences and influence packing modes in crystal structures.

(5) Estimates of charge transfer in hydrogen bonds show that the interaction energy correlates well with the extent of charge transfer between the donor and the acceptor.

(6) Analysis of the electron density topology of hydrogen-bonded systems usually shows a bond path connecting H and Y and a bond critical point between H and Y.

1.1.2 The Weak Hydrogen Bond

Strong and weak hydrogen bonds are discussed by Jeffrey and Saenger, in *Hydrogen Bonding in Biological Structures*.[7] They consider only those of the types F–H…F^-, O–H…O^-, and O^+–H…O, as strong hydrogen bonds which are always two-center bonds, involving short distances and strongly directional, with typical energies higher than 41 kJ mol^{-1}.[7] On the other hand, the normal or weak hydrogen bonds would be X–H…A, where the acceptor A is an electronegative atom.[7] Multicentered bonds start to appear, directionality is lost, and the bond energies drop to below 20 kJ mol^{-1}.[7] The common feature to all of these bonds is the presence of an electronegative atom A as acceptor.[7, 8]

The book by Desiraju and Steiner has indeed been motivated by the nonconventional donors and acceptors and has the title *The Weak Hydrogen Bond in Structural Chemistry and Biology*.[9, 10] In the book, Desiraju and Steiner were concerned with the weak hydrogen bond, which may be defined as an interaction X–H…A wherein a hydrogen atom forms a bond between two structural moieties X and A, of which one or even both are only of moderate to low electronegativity.[9] The

phrase '*weak hydrogen bond*' appears to be an oxymoron.[9] The text discusses C–H…O hydrogen bonds and π-acceptors in detail.[9, 10] It points out that the C–H…N hydrogen bond was discussed in 1935 by Kumler[11] and that the O–H…π interaction was discussed by Wulf et al. in 1936.[12] Rao and Jakkar published a paper in 1943 with the title "*Evidence for H bond in benzene*".[9, 10] Clearly, it has been realized that X[13] may be any element having electro negativity larger than that of H (F, N, O, C, P, S, Cl, Se, Br, and I) and Y[14] could be any of these elements and also π-electrons.[10]

Desiraju and Steiner classified hydrogen bonds as very strong, strong and weak (Table 1).[9] And they defined that, a strong hydrogen bond is one which is much stronger than a typical van der Waals interaction while a weak hydrogen bond is one which is not.[9] Table 1 lists various properties and classifications of hydrogen bonds.[9]

Table 1. Properties and classifications of hydrogen bonds[9]

Hydrogen bond	Very strong	strong	weak
Bond energy (kJ/mol)	63 to 167	17 to 63	< 17
Bond Lengths (Å)	1.2 to 1.5	1.5 to 2.2	2.0 to 3.0
θ Bond angle (X—H···A) range (°)	175 to 180	130 to 180	90 to 180
IR V_{IR} relative shift*	25%	5% to 25%	< 5%
Examples	$[F\cdots H\cdots A]^-$	O—H···O = C	C—H···O
	$[N\cdots H\cdots N]^+$	N—H···O = C	O—H···π
	P—OH···O = P	O—H···O—H	O—H···S

*define as V_{IR}= infrared spectrum relative shift.

1.1.3 The Effect of the Molecular Dipole Moment on the Hydrogen Bond

Non-uniform distributions of positive and negative electrical charges on the various atoms in the molecules lead to molecules with dipole moments.[15] The dipole moment of a molecule is an electric dipole with an inherent electric field.[15] Debye extensively studied molecular dipole moments and it calculation methods first,

therefore, the dipole moments are measured in units named *dedye* (D) in his honour.[16]

A molecular dipole moment depends on the difference in electronegativity between atoms in a molecule and the asymmetry of the molecular structure,[17] and molecules are generally classified as being non-polar if they have zero dipole moment, and polar otherwise.[18] The dipole moment (polarity) of the hydrocarbon molecule is increased by introduction of double bonds and more polar constituent groups.[19]

The hydrogen bond is described as a special case of strong dipole-dipole interaction.[20] The dipole-dipole interaction is an electrostatic interaction between permanent dipole moments in molecules.[21] Large dipole moments of both the hydrogen bond donor and acceptor give rise to a large dipole-dipole (electrostatic) interaction.[22] In the formation of the hydrogen bond due to the dipole-dipole interaction, the positive end of a molecule will attract the negative end of the other molecule and hence influence or dictate its position.[21] From this point of view, the molecular dipole moments of the hydrogen bond donor and acceptor will influence the formation (interaction) of the hydrogen bond between them, and hence the dipole moment (polarity) values will affect the strength of the hydrogen bond.[22]

1.1.4 The Hydrogen Bond between Methanol and Alkenes/Thiophene

Francis (1944) and Pavlova et al. (1975) previously reported that 1-heptene was mutually soluble in methanol above the Upper Critical Solution Temperature (UCST), of 285 K and 271.6 K, respectively.[23-25] However, these studies did not interrogate the microscopic nature of the interaction between methanol and this alkene nor indeed any other alkenes. Recently, although Heger et al. studied the hydrogen bond between

methanol and ethylene,[26] they presented a Fourier Transform Infrared (FTIR) spectroscopic study of the hydrogen-bonded methanol–ethylene complex which is the most prototypical weak intermolecular alcohol hydrogen bonding to a π cloud, O—H···π (π-type) hydrogen bond.[26, 27] Combined the FTIR study with the high-level quantum chemical calculations, Heger et al. indicated that allowing for possible anharmonic effects for this weak hydrogen bond system, a conservative estimate of 8.2±2.0 kJ mol^{-1} for the spectroscopic dissociation energy of methanol–ethylene complex appears justified.[26] However, their study did not provide any information on the interaction between methanol and other higher alkenes. Zhang et al. recently published a paper titled *Hydrogen bonds between methanol and the light liquid* alkene*s 1-pentene and 1-hexene: from application to fundamental science*.[28] In the paper, researchers investigated the dissolution of the light liquid alkenes 1-pentene and 1-hexene in methanol through computer modelling together with NMR spectroscopy, and two important hydrogen bonding modes for methanol alkene interactions – namely, O–H···π and C–H···O have been found.[28]

Nakanaga et al. studied the weakly bound clusters of aniline-ethylene, aniline-propylene and aniline-(1-butene) by infrared depletion technique and quantum chemical calculations.[29] Although it is the study of the interaction between aniline and alkenes, there are similarities to the present methanol - alkene systems. Nakanaga et al. found the N-H···π (π-type) hydrogen bond is the main interaction between the N-H bond of aniline and the double bond of the alkene for the aniline-propene and aniline-(1-butene) clusters.[29] Whilst, Nakanaga et al. also found the main interactions

in aniline-ethylene clusters are the C-H···N (σ-type) hydrogen bond between ethylene's C-H bond and the lone pair of the nitrogen atom of aniline, and the N-H···π (π-type) hydrogen bond between the N-H bond of aniline and the double bond of the alkene for aniline-ethylene clusters.[29] From this perspective, a similar hydrogen bond interaction system the weak hydrogen bond interaction could easier between alkenes and methanol molecules due mainly to the weak O—H···π (π-type) and/or C—H···O (σ-type) hydrogen bond.[27, 30]

It has been well documented that besides the rather localized electronic density (such as that found in a non-bonding "free" electron pair), delocalized electronic densities of any type may serve as proton-acceptors for this type of interactions.[31] π-electrons, such as those of aromatic rings or carbon-carbon multiple bonds, have been shown to act as weak proton acceptors in hydrogen bonding.[32, 33] This X–H···π(Y) (π-type) is weaker than the classical type,[33] probably because π bonding electrons are in general much less basic than lone pairs.[32] If the role of a proton acceptor is played by π-electronic density, the corresponding hydrogen bond is classified as a π-type hydrogen bond.[31] In this research the π-type hydrogen bond particularly means O—H···π interactions between methanol and alkenes.

The condition that allows X–H···σ(Y) (σ-type) hydrogen bonds to form strongly is that the proton acceptor,[9] YH, is an element-hydrogen bond, where the element or fragment Y is electropositive.[32] When the X–H···σ(Y) hydrogen bond forms, the σ bond electronic density from the electropositive Y atom is donated to the proton which bonded with electropositive X atom.[32, 34] As another major electrostatic

interaction between alkenes and methanol, the C—H···O (σ-type) hydrogen bond is also considered in this research. In this σ-type hydrogen bond, C–H groups acts as weak hydrogen bond donors,[35] and O atom acts as strong hydrogen acceptor.[9] The structural properties of C—H···O interactions generally parallel those of the stronger O—H···O and N—H···O hydrogen bonds.[36]

Because the O—H···π (π-type) hydrogen bond interactions between methanol and alkenes is of a strong proton donor with a weak proton acceptor,[9] the relative contribution of electrostatics should be smaller than it in the classical hydrogen bond. Thus, these interactions have been classified as week hydrogen bond interactions.[9] Nevertheless, only if the electrostatics becomes even weaker than dispersion energies of interactions,[37] the hydrogen bonds fade into the van der Waals continuum.[9]

The general belief that hydrogen bonds to oxygen are stronger obviously goes back to the observation that H bonds are dominated by electrostatic effects which are larger in O—H···O than in O—H···S systems.[38] However, the enhanced dispersion in the S-containing systems compensates the loss in the electrostatic contribution.[38] The geometry of O—H···S hydrogen bond is dominated by dipole–dipole interactions, since the van der Waals interaction is almost isotropic.[38]

Very few research appears to have covered the hydrogen bond interaction between methanol and thiophene. Wennmohs et al.[38] studied the properties of hydrogen bonds between methanol and dimethylsulfide molecules by detailed theoretical calculations. Their calculated value for the hydrogen bond energy in the dimethylsulfide-methanol complex is -5.46 kcal mol^{-1} (-22.84 kJ mol^{-1}),[38] and their natural bond orbital (NBO)

analysis identifies the dimethylsulfide's sulfur 3*p* orbital to be responsible for establishing the hydrogen bond by interacting with the methanol's H–O antibonding orbital.[38]

Huang et al. studied the structures of thiophene-hydrogen halide (HX, X=F, Cl, Br, I) complexes, these complexes were studied at the second-order Møller–Plesset (MP2) level in order to understand the hydrogen bonding between the thiophene ring and the H atom of HX, where the heteroaromatic ring of thiophene acts as a hydrogen bond acceptor.[39] In this study, a decomposition of interaction energy between the ring and HX reveals that thiophene-HX bonding is mainly through electrostatic energy contributions.[39, 40]

More recently, Singh et al. studied the thiophene's solvation in DMSO and methanol by Raman spectroscopy combined with ab initio and DFT calculations.[40] In their study, hydrogen bonded structures of thiophene with both the solvents have been optimized in gas phase and a dipole–dipole interaction energy has also been calculated using the optimized parameters.[40] Singh et al. found the optimized structure of hydrogen bonded thiophene-methanol complex is the hydrogen bond bridges methanol's OH bond to the lone pair of the sulphur atom of thiophene as O—H···S structure.[40] In their study, the dipole–dipole interaction was calculated for each hydrogen bonded complex using different levels of theory. In case of thiophene-methanol complex, the potential energy of this dipole–dipole (hydrogen bond) interaction is -1.26 kcal mol^{-1} (-5.27 kJ mol^{-1}), -0.72 kcal mol^{-1} (-3.01 kJ mol^{-1}), -1.62 kcal mol^{-1} (-6.78 kJ mol^{-1}), and the corresponding bond length is 2.799 Å, 2.669

Å, 2.983 Å, respectively.[40]

1.2 The Current Situation and Conventional Upgrading Process of Fluidized Catalytic Cracking (FCC) Gasoline

1.2.1 FCC Gasoline

Global demand for transportation fuels continues to grow (Fig. 3).

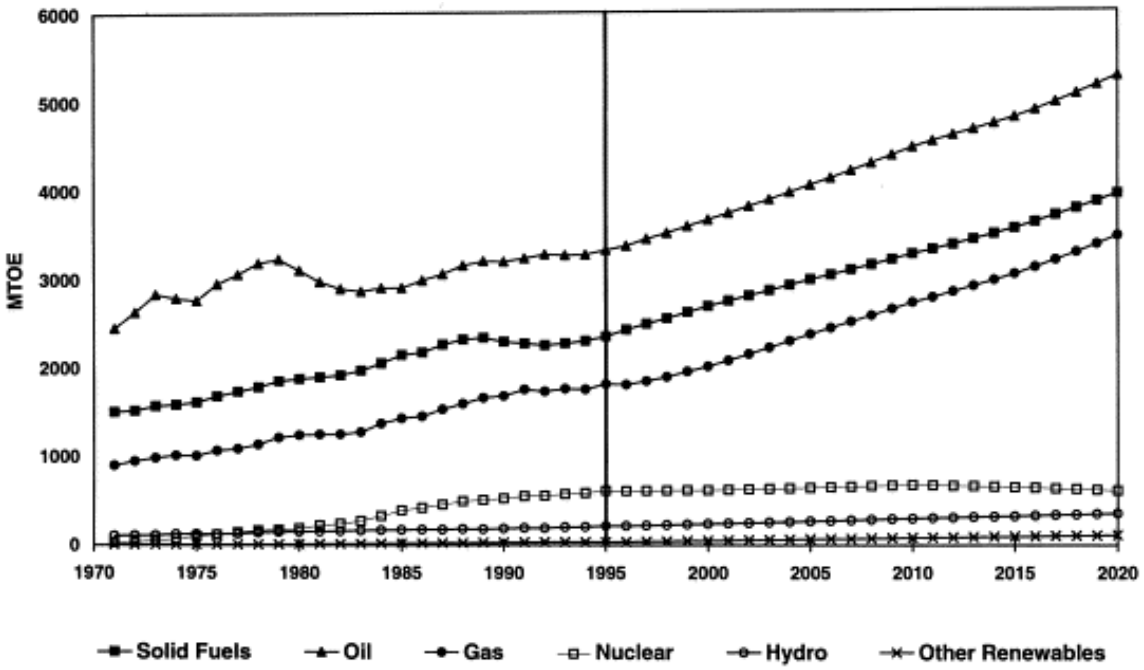

Fig. 3 Global energy demand by fuel (1971-2020)[41]

This demand will be met largely by gasoline and diesel fuels. The so-called "*Fluid Catalytic Cracking*" (FCC) process plays a key role in the modern petroleum and petrochemical integrated refinery as the primary process of crude oil conversion to lighter products (Fig. 4).[42] The principle of the FCC process showed in Fig. 5

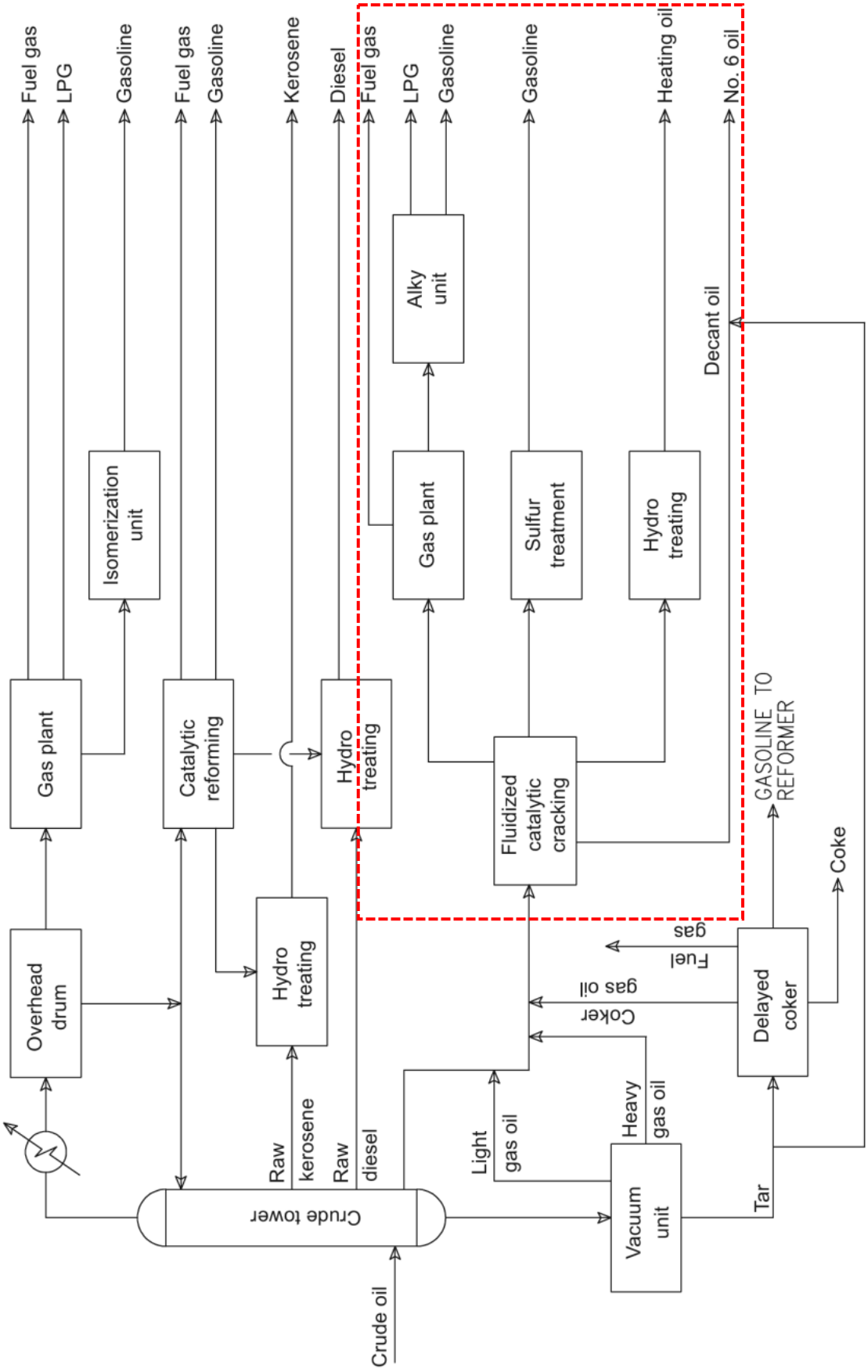

Fig. 4 The "*Fluid Catalytic Cracking*" (FCC) process in the refinery[42]

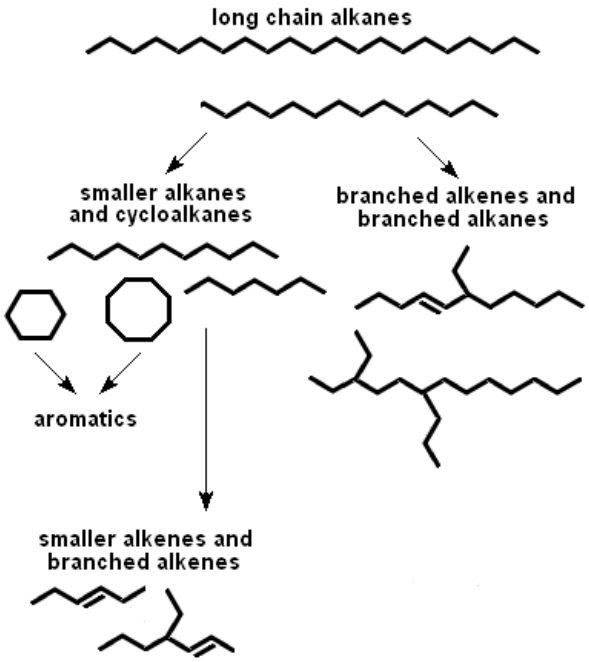

Fig. 5 Principle of the "*Fluid Catalytic Cracking*" (FCC) process[42]

As a major product of the FCC process, the resulting "*FCC gasoline*" contains large amounts of volatile, inflammable mixture composed of paraffinic, olefinic, naphthenic, and aromatic hydrocarbons (C_4- C_{12}).[43] Due to the latest environmental regulations and internal combustion engine (ICE) requirements, the contents of alkenes and organosulfur compounds (OSCs) in the FCC gasoline and other refined fuels are required to meet stringent modern product specifications. [44]

One of the primary reasons for such specifications is that, during storage, alkenes react with atmosphere oxygen and with other components. Thus, due to the ensuing polymerization reactions and formation of gums, detrimental changes in FCC gasoline's physical-chemical characteristics is promoted.[43] Because the formed materials have polymeric character, they invariably cause deposition in a vehicle's oil filters and distribution lines.[43] According to these limitations, the stability of the FCC gasoline has been defined as low.

In addition, OSCs are converted to SO_x during the engine combustion process,[45] and the exhaust gases from motor vehicles contribute to a large extent to acid rain and air pollution through their content of NO_x and SO_x.[45, 46] Moreover, OSCs may be present in varying concentrations in the refined fuels and additional contamination may take place as a consequence of transporting the refined fuel through pipelines containing sulphur contaminants. The sulphur has a particularly corrosive effect on equipment such as brass valves, gauges and in-tank fuel pump copper commutators.[47] Importantly, fuels containing impurities such as sulphur, are also slightly effective poisons for a vehicle's catalytic converters.[48-50] Therefore, OSCs is also a significant undesirable component in fuels, and this leads the governments of numerous countries to adopt new regulations which target a drastic reduction of sulphur emissions by imposing a very low concentration of this element in fuels.[51-54]

Twenty six years ago, the United States Clean Air Act Amendments of 1990 and the new regulations by the United States Environmental Protection Agency (EPA) established the need of more environmentally friendly transportation fuels with significant lower contents of sulphur (Table 2).[53, 55] In the European Union, sulphur levels in gasoline were limited to 50 ppm or less by 2005 and then below 10 ppm by 2010.[51-54, 56]

Table 2. United States EPA Tier II gasoline sulphur regulations as of 2002[55]

Category	Year				
	1988	1995	2004	2005	2006
Refinery average (ppmw)	1000 (maxium)	330	-	30	30
Coporate average (ppmw)			120	90	-
Per-gallon cap (ppmw)			300	300	80

Moreover, based on our own study, we find that commercial gasoline is made up of different fractions coming from reforming, isomerization and FCC units.[46] Those coming from the reforming and isomerization units are produced from the so-called "distillation cuts", and consequently contain little or no sulphur because the OSCs in crude petroleum have generally high boiling points [57]; and the feedstocks used in the isomerization and reforming units are generally hydrotreated to yield H_2S.[46] On the contrary, the atmospheric residues or the vacuum distillates which constitute FCC feedstocks contain significant amounts of sulphur, 0.5–1.5% in weight generally.[46] Consequently FCC gasoline, which represents 30–40% of the world's total gasoline pool, is by far the biggest sulphur contributor in gasoline, up to 85–95%.[51-54, 58] A lower sulphur content in the FCC gasoline will not only mean higher fuel quality, but also reduce the pollution from motor vehicles' exhausted gases.

For the purpose of improving the stability and quality of the FCC gasoline and reducing the pollution from motor vehicles' exhaust gases, it is critical to upgrade the gasoline which means significantly reducing the alkene and OSCs content. In the following sections we outline various current approaches to the problem.

1.2.2 Upgrading processes for FCC Gasoline

The key objects in the FCC gasoline upgrading process are (1) reducing the amount of alkene content and (2) removing the OSCs content.

Prior literature for reducing alkene content show that there are two major directions of research; *First is* to separate the alkenes through various physical approaches, s*econd*: to use specific chemical reactions to convert the alkenes into other compounds. The most typical and conventional physical separation of alkenes uses cryogenic distillation, which is both costly and energy-intensive due to the similar relative volatilities of components. In fact a large portion of the capital cost of a modern alkene plant is devoted to the large distillation columns used in the separation process.[59]

In the field of upgrading by chemical conversion, various catalysts such as SAPO-11, Hβ, HMOR, HZSM-5, HZSM-5 with Ga_2O_3, Co-Mo/Al_2O_3, Ni-Mo/Al_2O_3 and Mesoporous Zeolite L (M-L) have been introduced into the FCC process.[60-64] Through the hydroisomerization and aromatization treatments, alkenes can be selectively converted into paraffinic and aromatic hydrocarbons,[60] which are more stable and desirable. This measure reduces the alkene content in the FCC gasoline efficiently. However, this process has not only a high cost, but also requires catalysts and complex reaction conditions.

To reduce OSCs content, refiners worldwide are urgently developing technologies and strategies for economically and reliably meeting new, demanding clean fuel regulation as reviewed by Krishnaiah and Cartwright (2004).[65] As a result, technical

development for so-called "*deep desulphurization*" of FCC gasoline has attracted increasing attention.[66] In the past, various methods have been used to remove unwanted sulphur-compounds, both by chemical treatment and by hydrodesulphurization.[48]

Hydrodesulphurization (HDS) process, also known as a hydrotreating process, involves the reaction of OSCs with H_2 to yield H_2S. This is one of the most common and conventional desulfurization methods that have been used in refinery processes around world since the 1950s.[44, 48] While HDS allows the sulphur content in gasoline to be reduced to any desired level,[67] these processes require severe conditions, such as high temperatures up to 600 or 800 ℉ (316 or 427 ℃) and high-pressures which may be up to 207 bar implying that this process consumes a considerable amount of energy during operation.[48] Of course, large volumes of hydrogen are also needed for this process. Meanwhile, installing or adding the necessary hydrotreating capacity requires a substantial capital expenditure and increased operating costs. Further, alkene and cyclic alkane are susceptible to hydrogenation during hydrotreating, leading to a significant loss in octane number since alkene and cyclic alkane have higher octane numbers than paraffinic compounds.[67]

In recent decades, novel technologies with better desulfurization performance have been developed. For instance, Biodesulphurization (BDS) process based on the application of microorganisms can selectively remove sulphur atoms from OSCs[44]; Oxidative Desulfurization (ODS) process is considered as the latest unconventional desulfurization process which involves chemical oxidation of divalent organic sulphur

compounds to the corresponding hexavalent sulphur, also known as sulfone.[68-74] In Adsorptive Desulfurization (ADS) process, OSCs are absorbed into a specified solid adsorbent so as to produce zero or low-sulphur fuel [53]. Another approach is Extractive Desulfurization (EDS) process, which is based on liquid-liquid extraction using ionic liquids or acetonitrile etc. to remove sulphur-compounds, and has approximate 80% sulphur content reduction rate.[44, 48] The other sulphur reduction processes include Pervaporation Desulfurization (PV) process, which is achieved by the application of specific membrane[65-67, 75], olefinic Alkylation of Thiophenic Sulphur (OATS) desulfurization process, consisting of weighing down the sulphur compounds by catalytic alkylation with alkenes present in the feed followed by distillation,[76] and its levels of desulphurization of 99.5% with a minimal octane loss (less than two points) have been reported[49, 76], photochemical or photocatalytic desulphurization process, which can remove the sulphur compounds through photochemical reaction, and is activated by photons instead of high temperature, high pressure or other chemicals.[77] The desulphurization performance and advantages/disadvantages of these technologies are listed in Table 3. Although these novel technologies may have better desulphurization performance and energy efficiency than HDS process, they generally require severe conditions, complex procedures and specific chemicals or materials.

Table 3. Different desulfurization technologies and their advantages/disadvantages[44, 48, 49, 52, 53, 65-79]

Technology	Desulphurization performance (%)	Advantages	Disadvantages
Hydrodesulphurization (HDS)	100.0	Mature and efficient	Energy intensive, complex, need high temperature and high pressure, need numerous hydrogen supply, and leads significant loss in octane number, expensive
Biodesulphurization (BDS)	94.5	Low energy consumption	Slow, complex and requires large space
Oxidative desulphurization (ODS)	97.8	Efficient	Energy intensive, complex, need high temperature and high pressure, need oxygen or other oxidants supply, expensive
Adsorptive desulphurization (ADS)	100.0	Efficient	Complex, adsorbent need to be regenerated or replaced frequently, expensive
Extractive desulphurization (EDS)	80.0	Low energy consumption	Less efficient, extractant need to be recovered or replaced frequently
Pervaporation desulphurization (PV)	90.0	Low energy consumption	Less efficient, complex, membrane need to be replaced frequently, expensive
Olefinic alkylation desulphurization (OATS)	99.5	Efficient, low octane number loss	Energy intensive, complex, need high temperature and high pressure, need hydrogen supply, expensive
Photochemical or photocatalytic desulphurization	100.0	Low energy consumption, Efficient	Complex and expensive

1.3 The Current Situation and Conventional Separating Process of Cracking (Alkene and Alkane) Gas Mixtures

1.3.1 Cracking Gas Mixtures

Apart from liquid products from refinery industry, mixtures of light gaseous alkenes and alkanes produced in the petroleum refining process are often used as refinery fuel.[80] Since recovery of alkenes in these streams would be a substantial conservation of resources,[81] recent years there has been much interest in the recovery of light alkenes from such streams, such as the off-gas of crude oil refining and catalytic cracking process (petroleum pyrolysis gas),[80] driven largely by the escalating demand for feedstock for production of polyethylene and polypropylene.[82] Ethylene and propylene are the key building blocks for the production of a wide range of important petrochemicals, such as polyethylene, polypropylene, acrylonitrile, ethylene oxide, propylene oxide, ethylbenzene, cumene, phenol, isopropylic alcohol and many others.[83-86] Particularly for propylene, its global demand during 2006 saw a growing rate estimated at 5.5% bringing total propylene consumptions up to about 69 million metric tons.[87] And the 5-year outlook shows world propylene demand growth to average slightly less than 5% per year.[88] The production of polymers and other specialty chemicals from mono-alkenes such as ethylene and propylene requires the alkenes to be of extremely high purity (>99.9%), and since light alkenes are commonly produced together with alkane hydrocarbons (e.g., ethane and propane), the techniques for separating the both hydrocarbons are of primary importance in the petrochemical industry.[89]

On other aspects, environmental regulations such as the Clean Air Act will require reduction of hydrocarbon emissions from chemical processing facilities to low levels.[81] Waste hydrocarbon streams from polyolefin processes and polymer storage facilities, which are typically flared, must be dealt with in an environmentally acceptable manner.[81] These regulation requirements also drive the industries and research institutions to develop more efficient and sustainable methods to treat the emissions, then, recover and utilize the light alkenes/alkanes from these streams.

1.3.2 Separating Process for Gaseous Alkene and Alkane Mixtures

As a major and conventional mixture gas separation process, industrial alkenes/alkanes separations heavily rely upon energy intensive technologies, which represent a class of the most important and also most costly separations in the chemical and petrochemical industry.[90, 91] It is also extremely challenging due to the physicochemical similarities between those two types of molecules.[81, 88, 92, 93]

The most traditional separation process, cryogenic distillation has been used for over 60 years for these separations.[94] Ethane/ethylene and propane/propylene separations are being performed by such highly energy-intensive distillations.[87, 90] Ethane/ethylene separation is carried out at about 248K and 23bar in a column containing over 100 trays, and propane/propylene separation is process with 150–200 trays at cryogenic temperatures between 233 and 183K and pressures ranging from 16 to 20bar.[87, 90, 94] The reason for the extreme conditions used in such distillations is the relatively similar volatilities and boiling points of these alkenes and alkanes.[87, 90, 92]

A 1991 DOE study estimated that 122BTU of energy was used yearly for

alkene/alkane distillation.[80] Even at that time, the capital cost for a world-class ethylene unit had already exceeded 500 million U.S. dollars.[80] The alkene/alkane separations train contributed a major part of this cost.[80] This large energy and capital investment requirement provides the incentive for ongoing alkene/alkane separation technology research.

Alkene/alkane separations performed by molecular sieves have been investigated by numerous researchers. Studies with various molecular sieves such as 13X, 5A and ion-exchanged molecular sieves indicated that alkenes and alkanes can be separated using an equilibrium adsorption step followed by a stepwise thermal regeneration so-called variable-temperature stepwise desorption (VTSD).[80, 95-97] Based on this technology a commercial process for alkene/alkane separation is licensed by UOP Inc.[80, 98] The pilot plant results indicate that high recoveries (99.7 wt %) and purities (99.6 wt % on a desorbent-free basis) can be obtained.[80, 98] However, an economic comparison indicated that the VTSD energy costs were lower, but capital costs were higher than a comparable distillation process.[80, 99]

Besides the physical absorption methods, the chemical absorption technologies have also been investigated. π-complexation absorption is a well known technique. The basis of this chemisorption is the alkene π bonds interacting with the σ and π bonds of a metal.[80] Copper and silver ions are commonly used as complexing metals.[80] The separation factors of π-complexation absorption can achieve 17/1 for ethylene/ethane and 10/1 for propylene/propane using cuprous diketonate in an α-methylstyrene solvent.[100] The agent is also capable of separating branched and

unbranched alkenes based on steric effects.[80, 100] One shortcoming is that this process requires significant feed pre-treatment to remove feed contaminants, such as H_2S and CO_2, which will interfere with the complex formation and/or destroy the complexing agent.[80]

On the other hand, the metal-based facilitated transport membranes have been introduced into alkene/alkane separation process. The alkene forms a reversible complex with the metal carrier.[80] The complex migrates across the swollen membrane film releasing the alkene on the opposite side of the membrane.[80] A 60-day continuous test of silver-impregnated commercial hollow fibre membrane indicated that the permeation rate decreased by a factor of 5 during the test, with a steady decrease the first 15 days of the test.[101] The alkene selectivity remained above 92% for the entire test.[101] The loss in performance was attributed to the loss of water and Ag^+ from the membrane film.[80, 101] As the π-complexation absorption technology, facilitated transport membranes also have similar contamination problems, along with the need for water content control.[80] The addition of water into the separating device's feed stream can also cause problems in downstream processes.[80] And water must be removed from the alkene stream prior to introduction into the polymerization reactor when the process applied in the polyolefin plant.[80] Hence, the cost of the separation system is raised by this dehydration step.

To sum up, alkene loadings by physical adsorption are low, and the process and regeneration cycles are complicated.[80] On the other hand, chemical adsorption systems suffer from low alkene loadings (<5 wt %) and contamination problems.[80]

With all these complications and problems, development of sustainable and economically viable alkene/alkane separation processes is becoming increasingly important.

1.4 The Importance of Methanol

1.4.1 Methanol Production

Methanol, which is prepared from fossil-fuel-based syn-gas and bio-mass, can also be prepared by direct oxidative conversion of natural gas (methane) or reductive conversion of atmospheric carbon dioxide with hydrogen.[102] In this way, hydrogen can be stored by converting it into methanol—a convenient liquid fuel and raw material for synthetic hydrocarbons and their products—with carbon dioxide from industrial effluents or the atmosphere.[102] This opens up the possibility of an alternative energy source to diminishing oil and gas resources and would lead to a feasible “methanol economy”.[102]

Although methanol is becoming a commodity chemical and can be produced from various resources, it presents excellent utilizability. However, the excess in methanol production capability cannot be ignored.[103] As the largest methanol consumer and producer in the world, accounting for >20% of global methanol output (Fig. 6), China could play a leading role in a transition to the “methanol economy”.[103] Also due to the increasingly available feed stock from shale gas,[104] the United States is experiencing the fastest expansion of methanol production in recent years of any country. Thus, the methanol industry development status in these two countries will surely reflect the tendency of a global methanol industry.

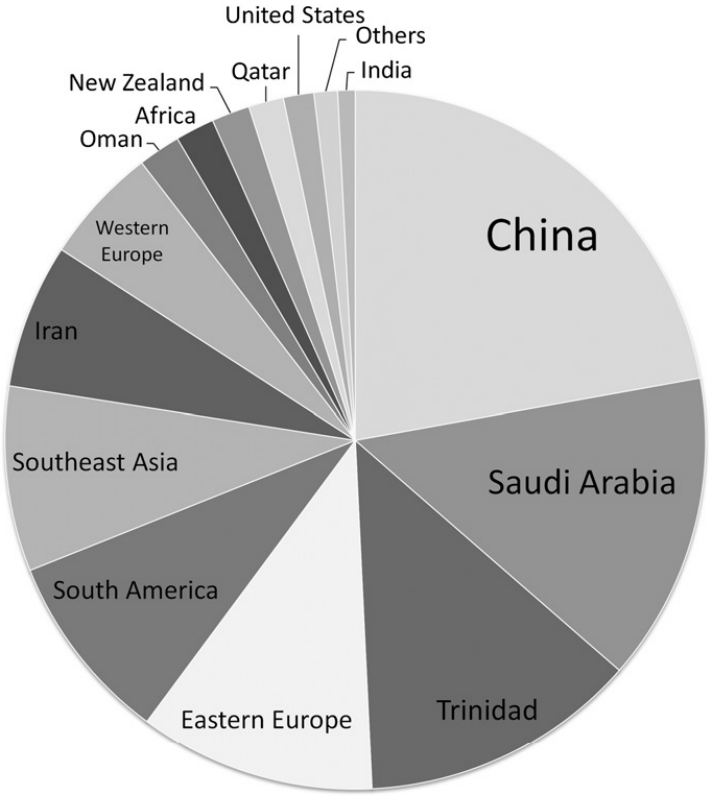

Fig. 6 Global methanol production in 2009[103]

In the United States, the methanol production capacity is expected to increase from 1.6 million metric tons in 2013 to over 12 million metric tons per year by 2018, and nearly 30 million metric tons per year by the early 2020s.[104] This is driven by readily available shale-derived feedstock.[102] This is likely to have serious impact on global trade and shipping, because the United States domestic consumption of methanol has remained relatively stable at about 6 million metric tons per year, the expansion will transform the United States from a net importer to a major exporter of methanol in the very near future.[104]

On the other hand, China is the world's largest methanol consumer and the major destination for United States methanol export.[104] In 2014, China consumed about 41 million metric tons of methanol, which account for 55% of global demand.[104] To meet the huge market demand of methanol, China has been building a unique

coal-to-methanol industry.[105] Many coal-producing regions have encouraged investments in coal conversion to boost demand for coal. However, coal-to-methanol is carbon intensive. Making a metric ton of methanol from coal emits roughly 5.3 ton of carbon dioxide, while making the same amount from natural/shale gas emits only 1.7 tons. Moreover, the capital investment for a coal-to-methanol plant is roughly twice as much as a methane-to-methanol plant of comparable capacity, while the feedstock costs are comparable (Fig. 7).[106] Even these could not stop the methanol industry expansion in China, which already has had more than enough methanol production capacities to meet its demand, yet it continues to build more production facilities.[104]

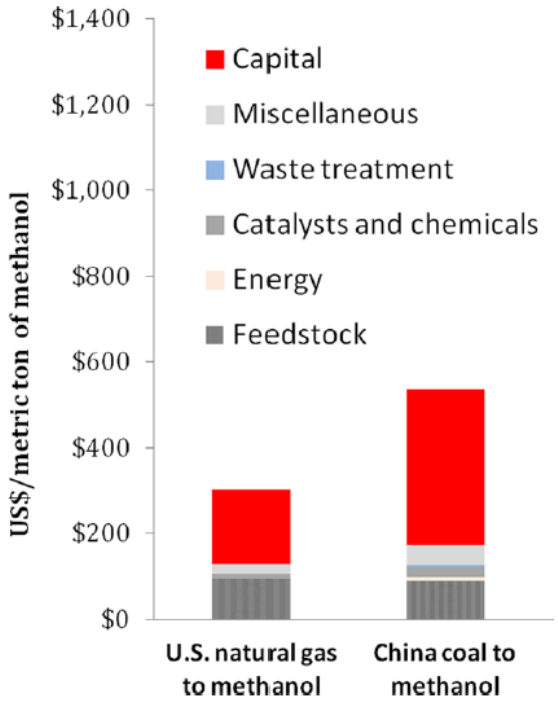

Fig. 7 Costs of the natural/shale gas and coal- derived methanol[106]

Conclusively, shale/coal-derived methanol production is becoming or will undoubtedly soon become a serious excess capacity.[107] To relieve this the methanol-to-hydrocarbons (MTH) reaction is considered as an alternative way of the

large scale utilization of methanol.

1.4.2 Methanol Utilization

Although methanol itself is a potential motor fuel that also can be blended with gasoline, it would require large investments to overcome the technical problems connected with the direct use of methanol as a motor fuel.[108] In addition, there are lingering concerns as to the toxicity of methanol. Therefore, various methanol-to-hydrocarbons technologies are being developed, and this conversion becomes one of the most studied reactions in the field of industrial chemistry since its discovery in 1977.[109, 110]

In the methanol-to-hydrocarbons process methanol is converted to an equilibrium mixture of methanol, dimethyl ether and water, which can be processed catalytically to alkenes (methanol-to-olefin, MTO), aromatics (methanol-to-aromatics, MTA), or gasoline (methanol-to-gasoline, MTG), depending on the catalyst and/or the process operation conditions.[108]

It is found that methanol can be conveniently converted into ethylene or propylene in the MTO process (Fig. 8).[102] These methanol-based alkenes can be an alternative way to produce hydrocarbon fuels and their products,[111] which are presently obtained from oil and gas.[102]

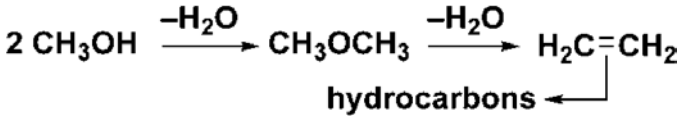

Fig. 8 Conversion of methanol into ethylene (or propylene) on the way to hydrocarbons and their products[102]

The selectivity towards light alkenes was significantly improved by the discovery

of H-SAPO-34 by researchers at Union Carbide (now UOP).[112, 113] Through its chabazite (CHA) structure of large cavities connected by 8-rings, selectivity to light alkenes (ethene/propene) may exceed 80% and conditions may be tuned to make propene the favorable product.[112] Unfortunately as opposed to H-ZSM-5, coking of H-SAPO-34 is rapid, hence during the MTO process catalyst requires frequent regeneration.[112] In 2009 a semi-commercial demonstration unit in Feluy, Belgium, processing up to 10 t per day of methanol feed was brought on-stream, and in 2011 the construction of a 295 kt per year plant in Nanjing, China was announced.[112]

Moreover, aromatics especially benzene, toluene, and xylenes (BTX) are important raw chemical materials conventionally produced from feedstock of crude oil.[107] Controversy exists regarding the shortage of crude oil supply in the future,[114] and the gradual depletion of oil reserves has resulted in a tight supply and high cost of aromatics.[115] In the past two decades, the route of converting methanol into aromatics (MTA) has received extensive attention, since methanol was readily available from wide resources such as coal, natural gas, shale gas and biomasses.[115-117] Typically, the single pass conversion of methanol, over ZSM-5 catalyst at 470–500℃, gave the aromatics yield of 50–70% (carbon base), the yield (25–40%) of gaseous hydrocarbon (C1–C5) and 3–4% yield for coke.[112, 115-121]

The product evolution route of MTA is different from that of MTO.[122-125] The MTA process mainly followed a consecutive reaction route from methanol to dimethyl ether (DME), C1–C5 hydrocarbons and finally to aromatics. Moreover, para-xylene was confirmed as the primary product of aromatics, while other isomers of xylene

were produced by the isomerization of para-xylene subsequently, and benzene, toluene and trimethylbenzene was produced by the de-alkylation and alkylation of X finally.[115]

Furthermore, it is generally recognised that methanol-to-gasoline process (MTG) should be the first commercialized process among these three methanol conversion processes. In 1985, the MTG process was commercialized in New Zealand, where Mobil, in a partnership with the New Zealand government, built a 14500 bpd plant based on natural gas, converted through synthesis gas into methanol and other organics.[112, 126, 127]

In the MTG process crude methanol is dehydrated over a slightly acidic catalyst (typically alumina-based, such as H-ZSM-5) into an equilibrium mixture of methanol, dimethyl ether, and water before entering the gasoline synthesis loop (Fig. 9).[112] In the gasoline reactor, the feed mixture is converted into C1–C11 hydrocarbons with C5+ (benzene fraction) selectivity of about 80%.[112] As the final product the gasoline from the MTG process consists of (predominantly iso-) paraffins, aromatics (predominantly methyl substituted), naphthenes, and alkenes.[112]

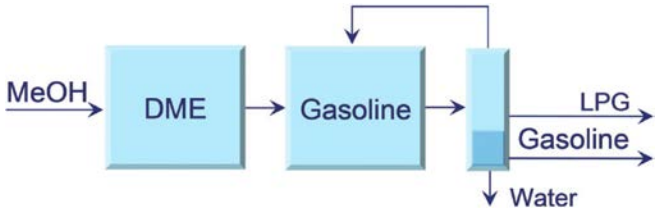

Fig. 9 Methanol-to-gasoline (MTG) process: adiabatic dehydration reactor for DME synthesis and parallel adiabatic gasoline reactors[112]

The reaction is strongly exothermic and to control the temperature in the adiabatic reactor light hydrocarbons, hydrogen, and carbon oxides (formed in small

amounts by cracking reactions) are recycled to dilute the feed.[112] Typical inlet and exit temperatures are 350 and 410℃ and the pressure is around 20 bar.[112] Despite the unique properties of H-ZSM-5, inevitable slow coke formation does take place and any catalyst must be regenerated by controlled coke burn-off.[112] Therefore, the MTG section consists of parallel reactors allowing for intermittent regeneration (Fig. 9).[112]

1.4.3 The Co-feeding Catalytic Conversion

Compared with pure methanol methanol-to-hydrocarbons (MTH) conversion process, the co-feeding MTH conversion has many advantages, such as (1) thermoneutral and low energy consumption, (2) the improvement of hydrocarbons cracking, (3) the reduction of coke disposition, (4) the high yield and selectivity, and (5) the simplification of reactor design.[128-132]

The Alkene Co-feeding Effect on Methanol-to-Hydrocarbon (MTH) Conversion

Ronning et al. reported the results of co-feeding propylene with methanol on ZSM-5 with isotopic labeling.[133] They concluded that propylene is reactive in the methanol-to-hydrocarbons conversion process, and propene methylation is a non-negligible part of the reaction network.[133] Möller et al., confirmed that co-feeding methanol and ethylene or propylene in the MTO process over HZSM-5 strongly increase the yield of propylene and butenes, respectively.[134]

On the other hand, Wu and Anthony observed that, over SAPO-34 during the conversion of methanol, the presence of propene in the feed increases the selectivities to ethene and butenes, which may be due to the competition for stronger acidic sites

for the reactions of ethene with methanol and of propene with methanol. The presence of ethene in the feed increases the selectivities to propene and butenes.[133]

The Effect of Alkane Co-feeding on the MTH Conversion

Roohollai et al., observed that propylene yield would be enhanced when i-butane fed to the reactor along with methanol.[135] The rising growth of the propylene yield continued to peak on till the balance in thermal condition established.[135] Since methanol transformation was an exothermic reaction, co-feeding of isobutane with methanol might have compensated for the acid strengths and reduced temperature associated with the endothermic individual isobutane cracking reaction. Furthermore, when different methanol to isobutane ratio fed with water in equal mass methanol to water ratio, a considerable propylene enhancement was obtained.[135]

The Effect of Aromatics Co-feeding on the MTH Conversion

Mole et al. observed that, the rate of conversion of methanol to hydrocarbons over HZSM-5 zeolite is enhanced by the addition of aromatic hydrocarbons to the feed.[136] They concluded that toluene promotes the catalytic activity of the catalyst for conversion of methanol to hydrocarbons.[136] Various other aromatic hydrocarbons likewise increase the activity: namely benzene, ethylbenzene, and p-xylene. All these are readily sorbed into the channels of HZSM-5 zeolite.[136]

The Effect of Water Co-feeding on the MTH Conversion

The effect of co-feeding water on the MTH reaction has been studied for decades.[134, 137-142] Through these studies co-feeding water have been found to improve the alkene selectivity.[134] Qi et al. observed that during the MTH conversion the coke

formation on the catalyst can be attenuated by the presence of water, but the effect of water weakens gradually with the progress of the reaction.[143]

It has also been reported that the yield of lower alkenes from MTO conversion increases when the methanol feed is diluted with water.[134, 141, 142] This was ascribed to reduced methanol partial pressure,[141] to the preferential adsorption of water on acid sites, thus facilitating the desorption of the lower alkenes and inhibiting further chain growth,[137, 138] or to reduced contact time and the corresponding decrease in methanol conversion.[134, 142]

The latter research indicates that water can moderate the formation of bulky hydrocarbon pool species that cannot diffuse through the small-pore material.[144] The occupation of the acid sites by water ultimately leads to reduced pore blocking, enhancing the diffusion of methanol and small alkenes deeper into the crystals to undergo reactive events.[144]

The Effect of Co-extractant Ethylene Glycol Co-feeding on the MTH Conversion

Ethylene glycol is one of the co-extractants in the "*Extractive Refining*" process. As an important content in the lower phase post extraction process, ethylene glycol will also enter the reactor as a co-feed. There is no any research mentioned the co-feeding effect of the ethylene glycol in the methanol-to-hydrocarbons conversion process.

Other alcohols e.g. ethanol's performance in their conversion to hydrocarbons over HZSM-5 was studied by Derouane et al.[124] Compared with methanol conversion over HZSM-5, ethanol produces more C3 and C4 aliphatics when the conversion

temperature is above 300 ℃, and it has higher conversion rate than methanol.[124] From this point of view, it has been predicted the conversion rate and yield of the co-feeding of methanol with ethylene glycol is higher than the pure methanol feeding.

The Effect of Organosulfur compounds (OSCs) on the MTH Conversion

Small impurities of sulfur compounds such as mercaptans, thiophenes, etc., present in the feed stream may deactivate the catalyst,[145] because, zeolite catalyst acidity is affected by the chemisorption of basic compounds containing nitrogen, as well as compounds containing oxygen or sulfur.[145]

Metal-ZSM-5 like Pt-HZSM-5, Ni-HZSM-5 and Pt-NiHZSM-5 are reported to be used for catalytic transformation of C8 aromatics.[146] In xylene isomerization over Ni-HZSM-5, the presence of 2 ppm thiophene in the feed resulted in the loss of xylenes.**[146]** Thiophene is converted into H_2S which then reacts with zeolite surface, generating stronger acidic sites and, thus, enhancing the disproportionation reaction.[145]

The resistance to sulfur poisoning is suggested to come from the small bonding energy of electronegative atoms with electron-deficient metal clusters.[145] Hence, the higher is the electron deficiency, the better will be the sulfur resistance.[145] Beside electron deficiency of metal aggregates, the other effect which could account for the sulfur resistance of encaged metal are the differential accessibility of the aggregate surface between hydrogen and poison, and thus maintaining the hydrogenation function and helping the removal of poison.[145]

1.5 Zeolite Socony Mobil-5 (ZSM-5) Catalyst

The synthesis of Zeolite Socony Mobil-5 (so-called ZSM-5) in the early 1970s along with the discovery of its unique catalytic properties by researchers at Mobil triggered an immense interest in industry and academia.[112, 147]

ZSM-5 is a member of shape-selective zeolite catalysts with unique channel structures which are distinctly different from and intermediate in pore dimension to the familiar large-pore faujasites and the very narrow-pore zeolites such as Zeolite A and eriomite.[148-150] ZSM-5 also possesses unusual catalytic properties and has high thermal stability.[150]

The framework of ZSM-5 contains a novel configuration of linked tetrahedra and consisting of eight five-membered rings.[150] ZSM-5 is the first zeolite reported with the characteristic structure of ideal 4_1m2 (D_{2d}) symmetry.[150] These ZSM-5 units join through edges to form chains, and these chains can be connected to form sheets and the linking of the sheets lead to a three dimensional framework structure which the chains extend along the z-axis.[150] ZSM-5 crystallises in the idealised orthorhombic system,[150] the unit cell contents of its Na form are $Na_nAl_nSi_{96-n}O_{192}\cdot \sim 16H_2O$, where $n < 27$ and typically about 3.[148] The ZSM-5 framework contains two intersecting channel systems, one sinusoidal running parallel to [001] and the other straight and parallel to [010].[150] The elliptical 10-membered ring openings controlling the channels have an effective diameter between those of zeolite Linde type A and faujasite.[150] The general structure of ZSM-5's monocrystal and its pore structure are indicated in Fig. 10.

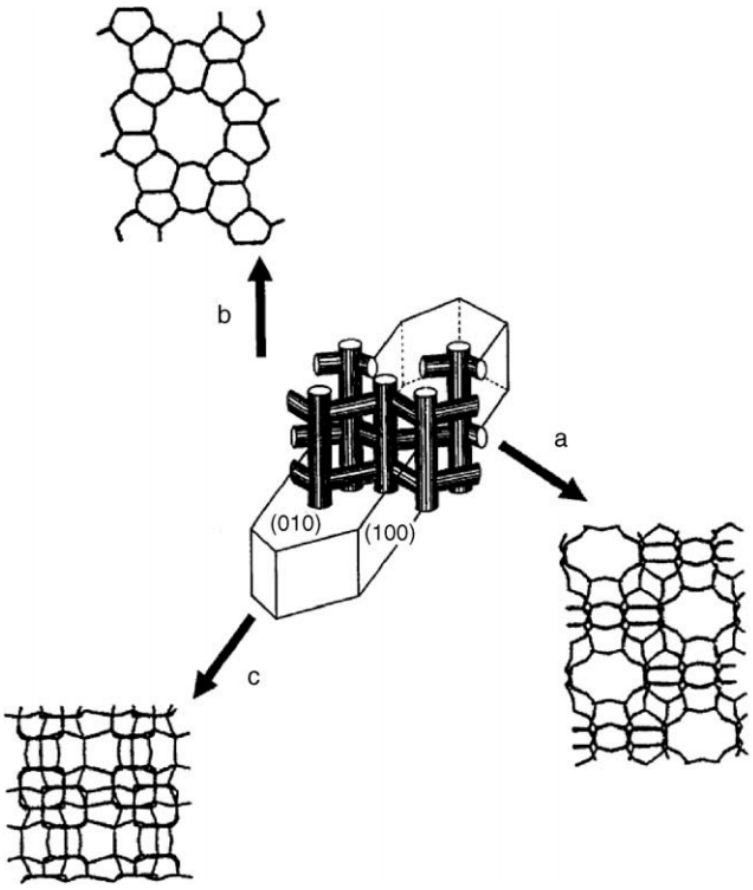

Fig. 10 General sketch of monocrystal and pore structure of ZSM-5[151]

1.5.1 The Application of HZSM-5 in Methanol-to-Hydrocarbon (MTH) Conversion

The zeolite-catalyzed conversion of methanol to hydrocarbons is commonly referred to as the methanol-to-hydrocarbon (MTH) reaction, but because process conditions and catalyst choice alter product selectivity, the abbreviations methanol-to-olefins (alkenes) (MTO), methanol-to-aromatics (MTA) and methanol-to-gasoline (MTG) are frequently used depending on the desired products.[125]

The original interest of the conversion of methanol to hydrocarbons was focused on obtaining automotive fuels by the MTG and MOGD (Mobil olefins-to-gasoline

and diesel) processes on HZSM-5 zeolite catalysts, which is the the acidic form of the ZSM-5 catalyst.[149, 152, 153] At the same time, due to the growing demand for alkenes and aromatics, the MTO and MTA processes have become as important as the other methanol conversion processes, which have also been originally proposed on a HZSM-5 zeolite,[142] and MTO process currently contributes to 10% of the world alkene production.[153]

On the other hand, the conversion of methanol to hydrocarbons over acidic zeolites has been studied for decades.[107, 154-158] In recent years, the conversion of methanol-to-hydrocarbons over HZSM-5 is attracting increasing attention. The concept of the methanol-to-hydrocarbons conversion process over HZSM-5 is presented in Fig. 11.[112, 125, 159, 160] Svelle et al. and Bjørgen et al. suggested that two mechanistic cycles run simultaneously during the MTH reaction over HZSM-5: ethene (and propene)[156] formation from the lower methylbenzenes followed by re-methylation, and methylation/cracking involving only the C3+ alkenes (not ethene).[112, 125, 159, 160] The idea is referred to as the dual-cycle concept and is summarized in Fig. 11.[112, 125, 159, 160] Cycle I on the right is the aromatics/ethene (with aromatics formally represented by toluene and trimethylbenzene) cycle, whereas cycle II on the left is the alkene-based cycle.[125] According to a study by Bjørgen et al.,[125] there is a continuous production of aromatics during the reaction; hence there must be a corresponding aromatization of higher alkenes formed in cycle II. This implies that cycle I cannot run without cycle II over H-ZSM-5.[125] This dual-cycle concept constitutes a refinement of the hydrocarbon-pool mechanism as proposed by Dahl and

Kolboe.[112, 161-163]

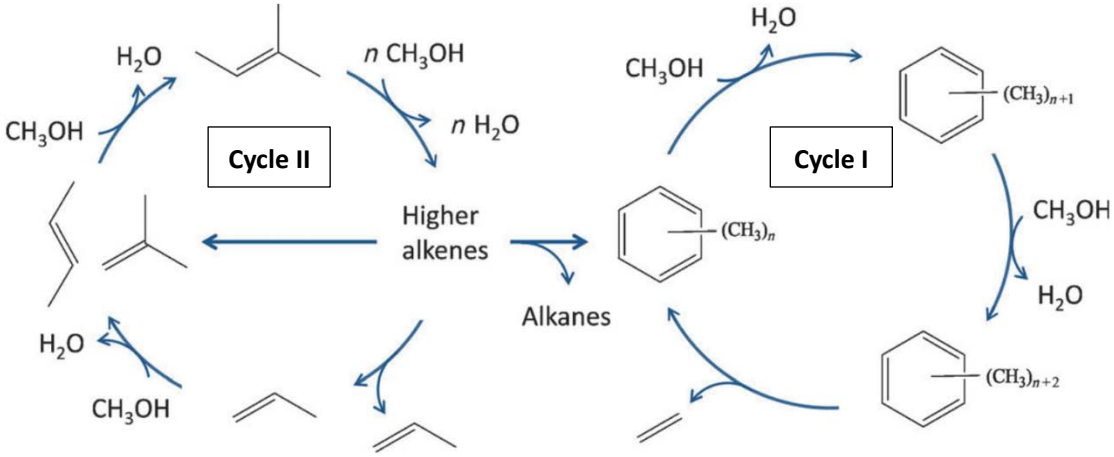

Fig. 11 Dual-cycle concept for the conversion of methanol over HZSM-5[112, 125, 159, 160]

1.5.2 The Development of Mesoporous HZSM-5

HZSM-5 is a highly porous catalytic material.[150, 164] These micro-pores of the catalyst give rise to its shape selective catalytic characteristics.[164] However, the beneficial properties of the small definite pore openings cause diffusion limitations of larger reacting molecules, leading to restrictions in the catalyst activity and lifetime during the conversion process.[164, 165] Hence, improvements and modification of the diffusion properties might lead to improved catalyst performance.[164] To overcome this problem a lot of research has been done to shorten the diffusion length in zeolites, one of the most popular research directions is by introducing an additional mesoporous transport network to the zeolite catalysts.[165-169] The property differences and advantages obtained from published studies when comparing conventional (microporous) and mesoporous HZSM-5 are listed in Table 4. Also, as outlined by Hartman[170] and Gorden et al.[171], different studies have been performed to meet this purpose which may be categorized as post-synthetic correlated to direct zeolite synthesis.[164]

Table 4. Property differences and advantages of mesoporous HZSM-5 compare to microporous HZSM-5

Property differences of mesoporous HZSM-5	Advantages of mesoporous HZSM-5
Microporous HZSM-5 (pore diameter < 2 nm) and mesoporous HZSM-5 (pore diameter 2–50 nm)[172]	Significantly improved diffusional properties[172]
Increase in catalyst porosity[165]	Improvement of overall conversion and activity[173]
High increase in external surface area and broad pore size distribution[165]	Lower coke formation and more ability to convert methanol[174, 175]
Increase in both acidity and Bronsted acid sites[176, 177]	Longer catalyst lifetime and higher gasoline product selectivity in MTG conversion[164, 175, 177-179]

Removal of Si in the framework of HZSM-5 by desilication has been confirmed as a result of the formation of the mesopore structure in HZSM-5 zeolites.[180-185] Desilication of HZSM-5 using alkali treatment had been studied by Mochizukiet al..[186] They treated HZSM-5 with different concentrations of NaOH solution, and they examined different crystallite size, external surface area and deactivation of the catalysts and claimed that Lewis acid sites may be generated by treating with high concentrations of NaOH.[186] Ni et al.[157] found that mesopores in zeolites was formed by alkali treatment. In their study, they modified the hierarchical mesoporous ZSM-5 zeolite catalyst with NaOH treatment and Zn impregnation.[157] In the other studies, Groen et al.[180-185] did a series of researches on the formation of mesopores in HZSM-5 by desilication with NaOH, which effectively created two hierarchical pore systems. Also, improvement of the catalytic performance by NaOH treatment in the MTG process has been reported by Bjøgen et al.[175]. From a study by Fathi et al.[164], it has been shown that mild alkaline solutions like 0.1 M Na_2CO_3 solutions result in HZSM-5 catalysts with enhanced yield characteristics with respect to the gasoline

range of products. Although treatment with 0.1 M NaOH solutions results in a slightly higher desilication, the final catalyst is more prone to deactivation compared with Na_2CO_3 treated HZSM-5 catalysts.[164]

Another approach generating mesoporosity by dissolution involves the simultaneous re-assembly of amorphous silica directed by surfactant molecules.[165] Ying and García-Martínez adapted the concept of pseudomorphic transformation for zeolitic systems.[187] Slightly alkaline and hydrothermal reaction conditions enabled the introduction of mesoporosity in zeolite FAU, MOR and MFI.[187] Ying and García-Martínez also proposed a surfactant-assisted crystal rearrangement mechanism.[188, 189] Yoo et al. published a dissolution re-assembly process under different synthesis conditions close to the conditions described for pure desilication procedures.[190] In their procedures, dissolved fragments of ZSM-5 were reassembled around Cetyl Trimethyl Ammonium Bromide (CTAB) molecules and re-deposited on the zeolite surface.[190] Recently, alkaline desilication of ZSM-5 with a surfactant was studied by Schmidt et al..[165] They showed that a high increase in external surface area, a decreased Bronsted acidity and a narrow pore size distribution could be achieved by the use of a surfactant CTAB throughout the alkaline treatment.[165] As the result of applying a co-surfactant during the alkaline treatment, both HZSM-5 activity and lifetime can be improved. The catalytic conversion of methanol to hydrocarbons confirmed the beneficial properties received by the physiochemical characterization.[165] A further improvement in catalyst lifetime was achieved by introducing more surfactant molecules, leading to an increased catalyst porosity.[165]

1.6 Towards the Refinery of the Future

The modern petroleum refining industry comprises many integrated processes and operations that are used in refining crude petroleum into a myriad of petroleum products, liquid fuels – notably gasoline and diesel in particular.[191] It also provides raw materials for the petrochemical industry

Petroleum refining in this century will continue to be shaped by many factors, but environmental and energy/CO2 emission challenges will necessitate changes in refinery technology. In parallel, increasingly stringent anti – pollution regulations are forcing greater restrictions on fuel specifications. So also, one expects that "conventional" oil production will decline and production of oil from residua, heavy oils etc. will become increasingly important.

It is quite clear also that over the coming decades, refineries will have to adapt to receiving such heavy oils as swell as a range of bio – based feedstocks.

As such feedstocks change, there must be an accompanying change in refinery technology.

One overriding issue – with whatever changes will be forthcoming- is that refineries use huge amounts of thermal energy to process crude oil.[192] Purifying, separating and extracting processes without using fossil – fuel – generated heat would reap global benefits in lower energy use, emissions and pollution. In parallel such advances would open up new routes to resources.

It is clear, therefore, that petroleum refining technology must become more innovative, driven not only by the increasing supply of lower – quality heavy oils but

also by the demand for energy-conscious processes to clean and ultra – clean vehicle fuels and petrochemical raw materials.

Thus, as skillfully highlighted by Speight the *refinery of the future* will be a *clean refinery* built around high – value,[191] energy – efficient processes to make it both environmentally benign *and* with a negligible footprint. It will also be a *smart refinery*, accepting a wide variety of feedstocks, including biomass. All these developments will stem from innovations derived from, and managed by, sound chemical principles and chemical reaction concepts. We hope that this critical transition will derive from evolutionary changes from my fundamental studies reported here of new extractive and (catalytic) processing.

For example, it has been realised that the current processes for FCC gasoline upgrading or hydrocarbon mixtures separation processes rely heavily upon energy – intensive technologies, involving the widespread use of hydrogen. In this work, I would like to explore new routes, based on novel, innovative chemistry, to overcome the considerable energy consumption and environmental disadvantages in current FCC gasoline upgrading, cracking gas separating and methanol utilization processes, and to develop a lower cost, less energy – intensive approach to the problem. These approaches are the new methanol based "*Extractive Refining*", "*Extractive Distillation*" and post extraction, developing catalytic conversion processes for the extracted phase. The potentially sustainable chemical – methanol – was introduced as the key to fulfil the aim of this research. At the heart of these new approaches is the fundamental issue

of hydrogen bond formation between the extractant solvent methanol and the extract light alkenes and organic sulphur compounds.

References

1 J. Prausnitz, R. Anderson, *AIChE Journal* 1961, *7*, 96-101.

2 J. H. Hildebrand, *Journal of the American Chemical Society* 1929, *51*, 66-80.

3 G. Scatchard, *Chemical Reviews* 1931, *8*, 321-333.

4 L. Pauling, in *The nature of the chemical bond*, 1st ed., Irnoil University Press, New York, 1939, Chap. 12.

5 E. Arunan, G. R. Desiraju, R. A. Klein, J. Sadlej, S. Scheiner, I. Alkorta, D. C. Clary, R. H. Crabtree, J. J. Dannenberg, P. Hobza, *Pure and Applied Chemistry* 2011, *83*, 1637-1641.

6 C. Zhang, C. Lu, Q. Wang, J. W. Ponder, P. Ren, *Journal of Chemical Theory and Computation* 2015, *11*, 5326-5339.

7 W. Saenger, G. Jeffrey, *Hydrogen bonding in biological structures*. Springer-Verlag, Berlin, 1991.

8 M. J. Calhorda, *Chemical Communications* 2000, 801-809.

9 G. R. Desiraju, T. Steiner, *The weak hydrogen bond: in structural chemistry and biology*. Oxford University Press, New York, 2001.

10 E. Arunan, R. Desiraju Gautam, A. Klein Roger, J. Sadlej, S. Scheiner, I. Alkorta, C. Clary David, H. Crabtree Robert, J. Dannenberg Joseph, P. Hobza, G. Kjaergaard Henrik, C. Legon Anthony, B. Mennucci, J. Nesbitt David, *Pure and Applied Chemistry* 2011, *83*, 1619 10.1351/PAC-REP-10-01-01.

11 W. Kumler, *Journal of the American Chemical Society* 1935, *57*, 600-605.

12 O. R. Wulf, U. Liddel, S. B. Hendricks, *Journal of the American Chemical Society* 1936, *58*, 2287-2293.

13 L. Allen, P. Kollman, *Chemical Reviews* 1972, *72*, 283.

14 E. Kryachko, A. Karpfen, F. Remacle, *The Journal of Physical Chemistry A* 2005, *109*, 7309-7318.

15 W. M. Haynes, in *CRC handbook of chemistry and physics*. CRC press, Boca Raton, 2014, Sec. 9.

16 P. Debye, *The dipole moment and chemical structure*. Blackie and Son, London, 1931.

17 H. Pritchard, H. Skinner, *Chemical Reviews* 1955, *55*, 745-786.

18 T. Brinck, J. S. Murray, P. Politzer, *Molecular Physics* 1992, *76*, 609-617.

19 W. N. Maclay, *Journal of Colloid Science* 1956, *11*, 272-285.

20 K. W. Whitten, R. E. Davis, M. L. Peck, G. G. Stanley, *Chemistry,* 10th ed., Brooks Cole, Belmont, 2014, Chap. 7.

21 R. John, *Solid State Physics*. McGraw Hill Education, New Dehil, 2014.

22 K. Morokuma, *Accounts of Chemical Research* 1977, *10*, 294-300.

23 A. W. Francis, *Industrial & Engineering Chemistry* 1944, *36*, 764-771.

24 O. P. Pavlova, A. A. Gaile, K. A. Proskuryokov, I. F. Li, *Zh. Fiz. Khim.* 1975, *49*, 2874.

25 J. W. Lorimer, F. W. Getzen, C. L. Young, P. D. Gujral, *IUPAC, Solubility Data Series Volume 56 Alcohols With Hydrocarbons*. Oxford University Press, Oxford, 1994.

26 M. Heger, R. A. Mata, M. A. Suhm, *Chemical Science* 2015, *6*, 3738-3745.
27 K. Oku, H. Watanabe, M. Kubota, S. Fukuda, M. Kurimoto, Y. Tsujisaka, M. Komori, Y. Inoue, M. Sakurai, *Journal of the American Chemical Society* 2003, *125*, 12739-12748.
28 Z. Zhang, T. Xiao, H. Al-Megren, S. A. Aldrees, M. Al-Kinany, V. L. Kuznetsov, M. L. Kuznetsov, P. P. Edwards, *Chemical Communications* 2017, *53*, 4026-4029.
29 T. Nakanaga, K. Buchhold, F. Ito, *Chemical Physics* 2002, *277*, 171-178.
30 D. J. SUTOR, *Nature* 1962, *195*, 68-69.
31 L. Pejov, M. Solimannejad, V. Stefov, *Chemical Physics* 2006, *323*, 259-270.
32 R. H. Crabtree, O. Eisenstein, G. Sini, E. Peris, *Journal of Organometallic Chemistry* 1998, *567*, 7-11.
33 J. L. Atwood, F. Hamada, K. D. Robinson, G. W. Orr, R. L. Vincent, *Nature* 1991, *349*, 683-684.
34 B. M. Kariuki, K. D. Harris, D. Philp, J. M. Robinson, *Journal of the American Chemical Society* 1997, *119*, 12679-12680.
35 G. Desiraju, *Chemical Communications* 1998, 891-892.
36 T. Steiner, *Journal of the Chemical Society, Perkin Transactions 2* 1995, 1315-1319.
37 T. van Mourik, F. B. van Duijneveldt, *Journal of Molecular Structure: THEOCHEM* 1995, *341*, 63-73.
38 F. Wennmohs, V. Staemmler, M. Schindler, *The Journal of Chemical Physics* 2003, *119*, 3208.
39 D.-M. Huang, Y.-B. Wang, L. M. Visco, F.-M. Tao, *Chemical Physics Letters* 2005, *407*, 222-226.
40 D. K. Singh, S. K. Srivastava, A. K. Ojha, B. P. Asthana, *Journal of Molecular Structure* 2008, *892*, 384-391.
41 F. Birol, M. Argiri, *Energy* 1999, *24*, 905-918.
42 R. Sadeghbeigi, *Fluid catalytic cracking handbook: An expert guide to the practical operation, design, and optimization of FCC units*. Elsevier, Oxford, 2012.
43 R. C. Pereira, V. Pasa, *Fuel* 2006, *85*, 1860-1865.
44 E. Kowsari, in *Ionic Liquids - New Aspects for the Future*. InTech, Rijeka, 2013, Chap. 11.
45 T. Hirai, Y. Shiraishi, K. Ogawa, I. Komasawa, *Industrial & Engineering Chemistry Research* 1997, *36*, 530-533.
46 S. Brunet, D. Mey, G. Pérot, C. Bouchy, F. Diehl, *Applied Catalysis A: General* 2005, *278*, 143-172.
47 M.-A. Poirier, J. B. Gilbert, US 5199978 A, 1993.
48 A. Ibrahim, S. B. Xian, Z. Wei, *Petroleum Science and Technology* 2003, *21*, 1555-1573.
49 M. Arias, D. Laurenti, C. Geantet, M. Vrinat, I. Hideyuki, Y. Yoshimura, *Catalysis Today* 2008, *130*, 190-194.
50 R. R. Gatte, R. Harding, T. Albro, D. Chin, R. Wormsbecher, *ACS Preprints* 1992, *137*, 33-40.
51 T. Kaufmann, A. Kaldor, G. Stuntz, M. Kerby, L. Ansell, *Catalysis Today* 2000,

62, 77-90.
52 C. Marcilly, *Studies in Surface Science and Catalysis* 2001, *135*, 37-60.
53 C. Song, X. Ma, *Applied Catalysis B: Environmental* 2003, *41*, 207-238.
54 I. Babich, J. Moulijn, *Fuel* 2003, *82*, 607-631.
55 C. Song, *Catalysis Today* 2003, *86*, 211-263.
56 M. F. Ali, A. Al-Malki, B. El-Ali, G. Martinie, M. N. Siddiqui, *Fuel* 2006, *85*, 1354-1363.
57 R. L. Martin, J. A. Grant, *Analytical Chemistry* 1965, *37*, 644-649.
58 J. Miller, W. Reagan, J. Kaduk, C. Marshall, A. Kropf, *Journal of Catalysis* 2000, *193*, 123-131.
59 F. Song, Y. Yu, J. Chen, *Tsinghua Science & Technology* 2008, *13*, 730-735.
60 Y. Fan, X. Bao, D. Lei, G. Shi, W. Wei, J. Xu, *Fuel* 2005, *84*, 435-442.
61 Y. Fan, X. Lin, G. Shi, H. Liu, X. Bao, *Microporous and Mesoporous Materials* 2007, *98*, 174-181.
62 N. Viswanadham, B. Negi, M. Garg, M. Sundaram, B. Sairam, A. Agarwal, *Fuel* 2007, *86*, 1290-1297.
63 P. Zhang, X. Guo, H. Guo, X. Wang, *Journal of Molecular Catalysis A: Chemical* 2007, *261*, 139-146.
64 Q. Huo, T. Dou, Z. Zhao, H. Pan, *Applied Catalysis A: General* 2010, *381*, 101-108.
65 G. Krishnaiah, T. Cartwright, *S-brane technology brings flexibility to refiners' clean fuel solutions*, in: Proceedings of the 2004 NPRA Annual Meeting, San Antonio, TX, 2004.
66 L. Lin, Y. Kong, G. Wang, H. Qu, J. Yang, D. Shi, *Journal of Membrane Science* 2006, *285*, 144-151.
67 L. Lin, G. Wang, H. Qu, J. Yang, Y. Wang, D. Shi, Y. Kong, *Journal of Membrane Science* 2006, *280*, 651-658.
68 M. Te, C. Fairbridge, Z. Ring, *Applied Catalysis A: General* 2001, *219*, 267-280.
69 S. Mondal, Y. Hangun-Balkir, L. Alexandrova, D. Link, B. Howard, P. Zandhuis, A. Cugini, C. P. Horwitz, T. J. Collins, *Catalysis Today* 2006, *116*, 554-561.
70 J. L. García-Gutiérrez, G. A. Fuentes, M. E. Hernández-Terán, F. Murrieta, J. Navarrete, F. Jiménez-Cruz, *Applied Catalysis A: General* 2006, *305*, 15-20.
71 V. Hulea, F. Fajula, J. Bousquet, *Journal of Catalysis* 2001, *198*, 179-186.
72 A. V. Anisimov, E. V. Fedorova, A. Z. Lesnugin, V. M. Senyavin, L. A. Aslanov, V. B. Rybakov, A. V. Tarakanova, *Catalysis Today* 2003, *78*, 319-325.
73 J. Palomeque, J.-M. Clacens, F. Figueras, *Journal of Catalysis* 2002, *211*, 103-108.
74 Y. Shiraishi, T. Naito, T. Hirai, *Industrial & Engineering Chemistry Research* 2003, *42*, 6034-6039.
75 L. S. White, R. F. Wormsbecher, M. Lesemann, US 7018527 B2, 2006.
76 G. A. Huff Jr, O. S. Owen, B. D. Alexander, D. N. Rundell, W. J. Reagan, J. S. Yoo, US 5863419 A, 1999.
77 A. Samokhvalov, *Catalysis Reviews* 2012, *54*, 281-343.
78 P. Xu, J. Feng, B. Yu, F. Li, C. Ma, in *Biotechnology in China I*, ed. by J.-J.

Zhong, F.-W. Bai, W. Zhang, Springer, Berlin, 2009, Vol. 113, Chap. 16.
79 L. Lin, Y. Zhang, Y. Kong, *Fuel* 2009, *88*, 1799-1809.
80 R. B. Eldridge, *Industrial & Engineering Chemistry Research* 1993, *32*, 2208-2212.
81 D. J. Safarik, R. B. Eldridge, *Industrial & Engineering Chemistry Research* 1998, *37*, 2571-2581.
82 D. M. Ruthven, S. C. Reyes, *Microporous and Mesoporous Materials* 2007, *104*, 59-66.
83 A. Corma, F. Melo, L. Sauvanaud, F. Ortega, *Catalysis Today* 2005, *107*, 699-706.
84 L. M. Baker, W. L. Carrick, *The Journal of Organic Chemistry* 1970, *35*, 774-776.
85 P. Kilty, W. Sachtler, *Catalysis Reviews Science and Engineering* 1974, *10*, 1-16.
86 Y. Du, H. Wang, S. Chen, *Journal of Molecular Catalysis A: Chemical* 2002, *179*, 253-261.
87 A. Ortiz, A. Ruiz, D. Gorri, I. Ortiz, *Separation and Purification Technology* 2008, *63*, 311-318.
88 I. C. Chemical Market Associates, *World Light Olefins Analysis*, 2006.
89 T. A. Reine, R. B. Eldridge, *Industrial & engineering chemistry research* 2005, *44*, 7505-7510.
90 R. Yang, E. Kikkinides, *AIChE Journal* 1995, *41*, 509-517.
91 A. Ortiz, L. María Galán, D. Gorri, A. B. de Haan, I. Ortiz, *Industrial & Engineering Chemistry Research* 2010, *49*, 7227-7233.
92 F. Krull, M. Medved, T. Melin, *Chemical Engineering Science* 2007, *62*, 5579-5585.
93 R. Bryan, *Separation and Purification Reviews* 2004, *33*, 157-182.
94 G. E. Keller, A. E. Marcinkowsky, S. K. Verma, K. D. Williamson, *Olefin recovery and purification via silver complexation*. Marcel Dekker, New York, 1992.
95 C. Shu, S. Kulvaranon, M. Findley, A. Liapis, *Separations Technology* 1990, *1*, 18-28.
96 S. Kulvaranon, M. E. Findley, A. I. Liapis, *Industrial & Engineering Chemistry Research* 1990, *29*, 106-115.
97 R. Schoellner, U. Mueller, *Adsorption Science & Technology* 1986, *3*, 167-171.
98 D. Tajbl, J. Kanofsky, J. Braband, *Energy Process./Can. 1980, 72 (5), 61* 1987, *63*.
99 R. Faiz, K. Li, *Desalination* 2012, *287*, 82-97.
100 W. W. Ho, G. Doyle, D. W. Savage, R. L. Pruett, *Industrial & Engineering Chemistry Research* 1988, *27*, 334-337.
101 R. Hughes, J. Mahoney, E. Steigelmann, *Recent Developments in Separation Science* 1986, *9*, 173-195.
102 G. A. Olah, *Angewandte Chemie International Edition* 2005, *44*, 2636-2639.
103 C.-J. Yang, R. B. Jackson, *Energy Policy* 2012, *41*, 878-884.
104 C.-J. Yang, *Environmental Science & Technology* 2015, *49*, 9501-9502.
105 D. Xiang, Y. Qian, Y. Man, S. Yang, *Applied Energy* 2014, *113*, 639-647.

106 J. Goellner, N. Kuehn, V. Shah, C. White III, M. Woods, *Baseline Analysis of Crude Methanol Production from Coal and Natural Gas*, National Energy Technology Laboratory, 2014.
107 Y. Xin, P. Qi, X. Duan, H. Lin, Y. Yuan, *Catalysis Letters* 2013, *143*, 798-806.
108 M. Stöcker, *Microporous and Mesoporous Materials* 1999, *29*, 3-48.
109 M. Conte, J. A. Lopez-Sanchez, Q. He, D. J. Morgan, Y. Ryabenkova, J. K. Bartley, A. F. Carley, S. H. Taylor, C. J. Kiely, K. Khalid, *Catalysis Science & Technology* 2012, *2*, 105-112.
110 A. Corma, *Chemical Reviews* 1997, *97*, 2373-2420.
111 G. A. Olah, H. Doggweiler, J. D. Felberg, S. Frohlich, M. J. Grdina, R. Karpeles, T. Keumi, S.-i. Inaba, W. M. Ip, K. Lammertsma, *Journal of the American Chemical Society* 1984, *106*, 2143-2149.
112 U. Olsbye, S. Svelle, M. Bjørgen, P. Beato, T. V. Janssens, F. Joensen, S. Bordiga, K. P. Lillerud, *Angewandte Chemie International Edition* 2012, *51*, 5810-5831.
113 J. Q. Chen, A. Bozzano, B. Glover, T. Fuglerud, S. Kvisle, *Catalysis Today* 2005, *106*, 103-107.
114 R. A. Kerr, *Science* 2005, *309*, 101-101.
115 T. Wang, X. Tang, X. Huang, W. Qian, Y. Cui, X. Hui, W. Yang, F. Wei, *Catalysis Today* 2014, *233*, 8-13.
116J.-G. ZHANG, W.-Z. QIAN, X.-P. TANG, K. SHEN, T. WANG, X.-F. HUANG, F. WEI, *Acta Physico-Chimica Sinica* 2013, *29*, 1281-1288.
117 Y. Inoue, K. Nakashiro, Y. Ono, *Microporous Materials* 1995, *4*, 379-383.
118 J. A. Lopez-Sanchez, M. Conte, P. Landon, W. Zhou, J. K. Bartley, S. H. Taylor, A. F. Carley, C. J. Kiely, K. Khalid, G. J. Hutchings, *Catalysis Letters* 2012, *142*, 1049-1056.
119 T. TIAN, W.-Z. QIAN, X.-P. TANG, S. YUN, F. WEI, *Acta Phys Chim Sin* 2010, *26*, 3305-3309.
120 D. Freeman, R. P. Wells, G. J. Hutchings, *Chemical Communications* 2001, 1754-1755.
121 H. Zaidi, K. Pant, *Catalysis Today* 2004, *96*, 155-160.
122D. M. McCann, D. Lesthaeghe, P. W. Kletnieks, D. R. Guenther, M. J. Hayman, V. Van Speybroeck, M. Waroquier, J. F. Haw, *Angewandte Chemie* 2008, *120*, 5257-5260.
123 S. Ilias, R. Khare, A. Malek, A. Bhan, *Journal of Catalysis* 2013, *303*, 135-140.
124 E. G. Derouane, J. B. Nagy, P. Dejaifve, J. H. van Hooff, B. P. Spekman, J. C. Védrine, C. Naccache, *Journal of Catalysis* 1978, *53*, 40-55.
125 M. Bjørgen, S. Svelle, F. Joensen, J. Nerlov, S. Kolboe, F. Bonino, L. Palumbo, S. Bordiga, U. Olsbye, *Journal of Catalysis* 2007, *249*, 195-207.
126 S. Yurchak, *Studies in Surface Science and Catalysis* 1988, *36*, 251-272.
127 C. D. Chang, *Catalysis Today* 1992, *13*, 103-111.
128 T. Gong, X. Zhang, T. Bai, Q. Zhang, L. Tao, M. Qi, C. Duan, L. Zhang, *Industrial & Engineering Chemistry Research* 2012, *51*, 13589-13598.
129 B. Lücke, A. Martin, H. Günschel, S. Nowak, *Microporous and Mesoporous Materials* 1999, *29*, 145-157.

130 D. Mier, A. T. Aguayo, A. G. Gayubo, M. Olazar, J. Bilbao, *Applied Catalysis A: General* 2010, *383*, 202-210.
131 D. Mier, A. T. Aguayo, A. G. Gayubo, M. Olazar, J. Bilbao, *Chemical Engineering Journal* 2010, *160*, 760-769.
132 Z. Wang, G. Jiang, Z. Zhao, X. Feng, A. Duan, J. Liu, C. Xu, J. Gao, *Energy & Fuels* 2009, *24*, 758-763.
133 X. Wu, R. Anthony, *Applied Catalysis A: General* 2001, *218*, 241-250.
134 K. Möller, W. Böhringer, A. Schnitzler, E. Van Steen, C. O'Connor, *Microporous and Mesoporous Materials* 1999, *29*, 127-144.
135 G. Roohollahi, M. Kazemeini, A. Mohammadrezaee, R. Golhosseini, *Journal of Industrial and Engineering Chemistry* 2013, *19*, 915-919.
136 T. Mole, J. A. Whiteside, D. Seddon, *Journal of Catalysis* 1983, *82*, 261-266.
137 A. J. Marchi, G. F. Froment, *Applied Catalysis* 1991, *71*, 139-152.
138 W. Dehertog, G. Froment, *Applied catalysis* 1991, *71*, 153-165.
139 A. A. Cichowlas, P. Wierzchowski, L. Zatorski, *Reaction Kinetics and Catalysis Letters* 1986, *32*, 341-346.
140 D. Prinz, L. Riekert, *Applied catalysis* 1988, *37*, 139-154.
141 S. Tabak, S. Yurchak, *Catalysis Today* 1990, *6*, 307-327.
142 C. D. Chang, *Catalysis Reviews Science and Engineering* 1984, *26*, 323-345.
143 G. Qi, Z. Xie, W. Yang, S. Zhong, H. Liu, C. Zhang, Q. Chen, *Fuel Processing Technology* 2007, *88*, 437-441.
144 K. De Wispelaere, C. S. Wondergem, B. Ensing, K. Hemelsoet, E. J. Meijer, B. M. Weckhuysen, V. Van Speybroeck, J. Ruiz-Martínez, *ACS Catalysis* 2016, 1991-2002 10.1021/acscatal.5b02139.
145 S. Bhatia, J. Beltramini, D. Do, *Catalysis Reviews—Science and Engineering* 1989, *31*, 431-480.
146 G. Babu, M. Santra, V. Shiralkar, P. Ratnasamy, *Journal of Catalysis* 1986, *100*, 458-465.
147 H. Johan, H. L. Gunnar, N. Vegard, S. Sigbjorn, US 3702866 A, 1972.
148 S. Meisel, J. McCullough, C. Lechthaller, P. Weisz, *Chem-Tech*, 1976, *6*, 86-89.
149 C. D. Chang, A. J. Silvestri, *Journal of Catalysis* 1977, *47*, 249-259.
150 G. Kokotailo, S. Lawton, D. Olson, *Nature* 1978, *272*, 437-438.
151 Y. Fan, D. Lei, G. Shi, X. Bao, *Catalysis Today* 2006, *114*, 388-396.
152 R. J. Quann, L. A. Green, S. A. Tabak, F. J. Krambeck, *Industrial & Engineering Chemistry Research* 1988, *27*, 565-570.
153 A. T. Aguayo, D. Mier, A. G. Gayubo, M. Gamero, J. Bilbao, *Industrial & Engineering Chemistry Research* 2010, *49*, 12371-12378.
154 J. Li, Y. Wei, J. Chen, P. Tian, X. Su, S. Xu, Y. Qi, Q. Wang, Y. Zhou, Y. He, *Journal of the American Chemical Society* 2011, *134*, 836-839.
155 N. Tajima, T. Tsuneda, F. Toyama, K. Hirao, *Journal of the American Chemical Society* 1998, *120*, 8222-8229.
156 M. Bjørgen, F. Joensen, K.-P. Lillerud, U. Olsbye, S. Svelle, *Catalysis Today* 2009, *142*, 90-97.
157 Y. Ni, A. Sun, X. Wu, G. Hai, J. Hu, T. Li, G. Li, *Journal of Natural Gas*

Chemistry 2011, *20*, 237-242.
158 Y. Ono, H. Adachi, Y. Senoda, *Journal of the Chemical Society, Faraday Transactions 1: Physical Chemistry in Condensed Phases* 1988, *84*, 1091-1099.
159 S. Svelle, F. Joensen, J. Nerlov, U. Olsbye, K.-P. Lillerud, S. Kolboe, M. Bjørgen, *Journal of the American Chemical Society* 2006, *128*, 14770-14771.
160 M. Bjørgen, K.-P. Lillerud, U. Olsbye, S. Svelle, *Studies in Surface Science and Catalysis* 2007, *167*, 463-468.
161 I. M. Dahl, S. Kolboe, *Catalysis Letters* 1993, *20*, 329-336.
162 I. M. Dahl, S. Kolboe, *Journal of Catalysis* 1994, *149*, 458-464.
163 I. M. Dahl, S. Kolboe, *Journal of Catalysis* 1996, *161*, 304-309.
164 S. Fathi, M. Sohrabi, C. Falamaki, *Fuel* 2014, *116*, 529-537.
165 F. Schmidt, M. R. Lohe, B. Büchner, F. Giordanino, F. Bonino, S. Kaskel, *Microporous and Mesoporous Materials* 2013, *165*, 148-157.
166 C. J. Jacobsen, C. Madsen, J. Houzvicka, I. Schmidt, A. Carlsson, *Journal of the American Chemical Society* 2000, *122*, 7116-7117.
167 K. Egeblad, C. H. Christensen, M. Kustova, C. H. Christensen, *Chemistry of Materials* 2007, *20*, 946-960.
168 J. Pérez-Ramírez, C. H. Christensen, K. Egeblad, C. H. Christensen, J. C. Groen, *Chemical Society Reviews* 2008, *37*, 2530-2542.
169 M. Choi, K. Na, J. Kim, Y. Sakamoto, O. Terasaki, R. Ryoo, *Nature* 2009, *461*, 246-249.
170 M. Hartmann, *Angewandte Chemie International Edition* 2004, *43*, 5880-5882.
171 J. C. Groen, J. A. Moulijn, J. Pérez-Ramírez, *Journal of Materials Chemistry* 2006, *16*, 2121-2131.
172 J. C. Groen, L. A. Peffer, J. Pérez-Ramírez, *Microporous and Mesoporous Materials* 2003, *60*, 1-17.
173 M. Ogura, S.-y. Shinomiya, J. Tateno, Y. Nara, M. Nomura, E. Kikuchi, M. Matsukata, *Applied Catalysis A: General* 2001, *219*, 33-43.
174 U. V. Mentzel, K. T. Højholt, M. S. Holm, R. Fehrmann, P. Beato, *Applied Catalysis A: General* 2012, *417*, 290-297.
175 M. Bjørgen, F. Joensen, M. S. Holm, U. Olsbye, K.-P. Lillerud, S. Svelle, *Applied Catalysis A: General* 2008, *345*, 43-50.
176 R. Wei, C. Li, C. Yang, H. Shan, *Journal of Natural Gas Chemistry* 2011, *20*, 261-265.
177 P. L. Benito, A. G. Gayubo, A. T. Aguayo, M. Olazar, J. Bilbao, *Journal of Chemical Technology and Biotechnology* 1996, *66*, 183-191.
178 A. A. Rownaghi, F. Rezaei, J. Hedlund, *Catalysis Communications* 2011, *14*, 37-41.
179 A. A. Rownaghi, J. Hedlund, *Industrial & Engineering Chemistry Research* 2011, *50*, 11872-11878.
180 J. Groen, L. Peffer, J. Moulijn, J. Pérez-Ramırez, *Colloids and Surfaces A: Physicochemical and Engineering Aspects* 2004, *241*, 53-58.
181 J. C. Groen, J. C. Jansen, J. A. Moulijn, J. Pérez-Ramírez, *The Journal of Physical Chemistry B* 2004, *108*, 13062-13065.

182 J. C. Groen, T. Bach, U. Ziese, A. M. Paulaime-van Donk, K. P. de Jong, J. A. Moulijn, J. Pérez-Ramírez, *Journal of the American Chemical Society* 2005, *127*, 10792-10793.
183 J. C. Groen, J. A. Moulijn, J. Pérez-Ramírez, *Microporous and Mesoporous Materials* 2005, *87*, 153-161.
184 J. C. Groen, W. Zhu, S. Brouwer, S. J. Huynink, F. Kapteijn, J. A. Moulijn, J. Pérez-Ramírez, *Journal of the American Chemical Society* 2007, *129*, 355-360.
185 J. C. Groen, J. A. Moulijn, J. Pérez-Ramírez, *Industrial & Engineering Chemistry Research* 2007, *46*, 4193-4201.
186 H. Mochizuki, T. Yokoi, H. Imai, S. Namba, J. N. Kondo, T. Tatsumi, *Applied Catalysis A: General* 2012, *449*, 188-197.
187 J. Ying, J. Martinez, CA 2565435 A1, 2005.
188 J. Garcia-Martinez, US 7976696 2011.
189 J. García-Martínez, M. Johnson, J. Valla, K. Li, J. Y. Ying, *Catalysis Science & Technology* 2012, *2*, 987-994.
190 W. C. Yoo, X. Zhang, M. Tsapatsis, A. Stein, *Microporous and Mesoporous Materials* 2012, *149*, 147-157.
191 J. G. Speight, in *The Refinery of the Future*, William Andrew Publishing, Boston, 2011.
192 D. S. Sholl, R. P. Lively, *Nature* 2016, *532*, 435-438.

Chapter 2. Aims of the Thesis

2.1 Nature of the *"Extractive Refining and Distillation"* Process

There are many critical reasons why methanol should be central and utilized in the processes. With its advantages of low cost, extensive supplies and a solvent easily produced from a wide variety of raw materials, such as natural gas, coal, biomass and even carbon dioxide,[1] methanol is an ideal choice.[2,1] Moreover, the rapid expansion of the methanol production industry in many countries such as China, USA, appears to strengthen Nobel Laureate George Olah's vision of "*The Methanol Economy*".[3, 4] Indeed, there current exists an excess capacity of methanol.[5, 6]

In order to understand the underlying solvent (methanol) extraction or solubilisation processes, one needs to consider the universally - classified nine types of solution.[7] This study concerns with two types of that nine, the "*Gas in liquid*" and "*Liquid in liquid*" dissolution processes. In order to study the nature of the hydrogen bond between methanol and alkenes/thiophene – as it turns out the key interaction in these processes –, we have investigated the dissolution of the gaseous alkenes, various liquid alkenes and thiophene in methanol through a combination of visual observation and NMR spectroscopy, together with a computer modelling study.

Contributing factors such as the magnitude of the Upper Critical Solution Temperature (UCST), as well as molecular dipole moment of both solutes' and solvents' molecules are taken into account in this research.

Therefore, one aim of this research is to explore the fundamental science and the application of methanol as a solvent/co-solvent for specifically removing/separating

alkenes or organic sulphur contents (OSCs) from liquid/gaseous mixtures. The mechanisms and processes for these solvent extraction and solubilization are investigated in detail in Chapter 4.

2.2 A New Process for FCC gasoline Upgrading

In order to overcome the disadvantages apparent in both the current alkene and sulphur reduction processes, and achieve high alkene and sulphur removal efficiency, a novel and sustainable FCC gasoline upgrading process with catalyst will be developed in this study. Fig. 12 shows a schematic representation of the new processes for FCC gasoline upgrading.

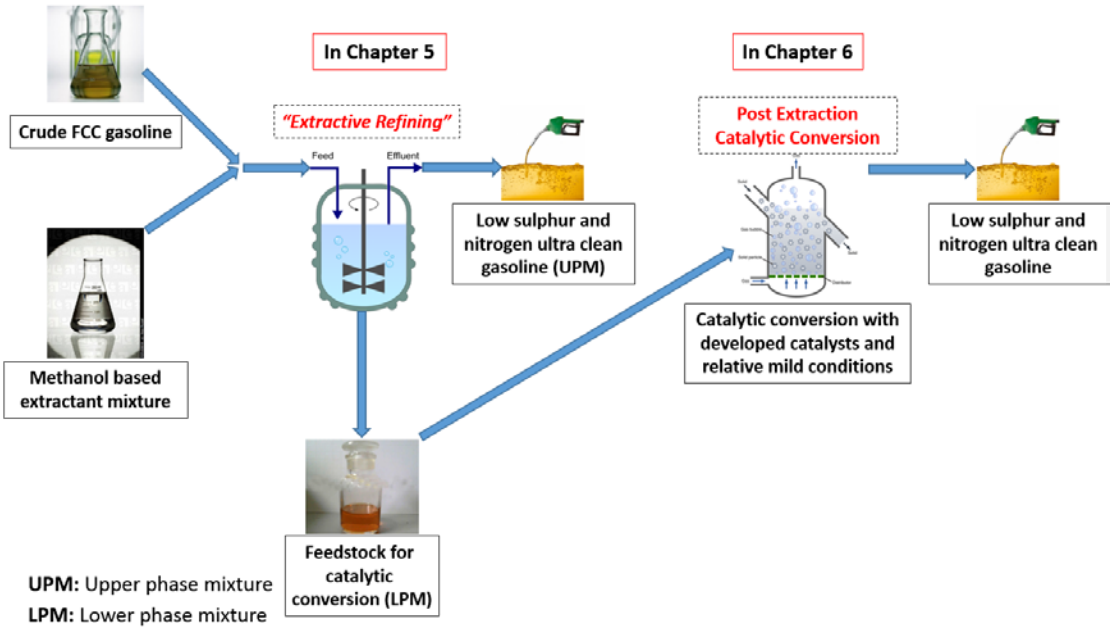

Fig. 12 The new process for FCC gasoline upgrading

The detailed studies of the "*Extractive Refining*" and post extraction catalytic conversion for the new FCC gasoline upgrading process are presented in the following Chapter 5 and Chapter 6 respectively.

2.3 A New Process for Cracking Gas Separating

Compared to those highly energy-intensive distillations and physical/chemical adsorption technologies, the relatively low energy consuming of our developed "*Extractive Distillation*" has become our process principle. Based on this principle a new process for cracking gas separating would be developed. The detailed studies are presented in Chapter 5. Fig. 13 shows this new process for cracking gas separating.

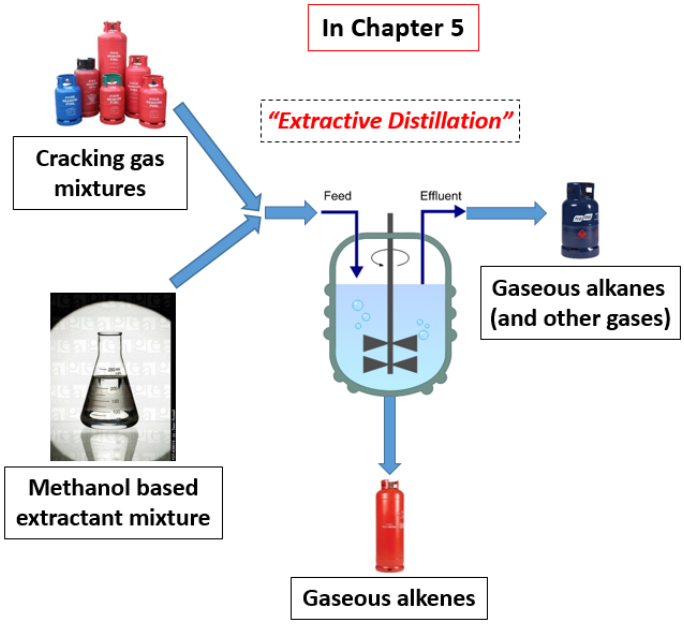

Fig. 13 The new process for cracking gas separating

References

1 S. Ilias, A. Bhan, *Journal of Catalysis* 2012, *290*, 186-192.
2 A. W. Francis, *Journal of Chemical Engineering Data* 1966, *11*, 96-101.
3 G. A. Olah, A. Goeppert, G. K. S. Prakash, *The Journal of Organic Chemistry* 2008, *74*, 487-498.
4 G. A. Olah, *Angewandte Chemie International Edition* 2005, *44*, 2636-2639.
5 C.-J. Yang, R. B. Jackson, *Energy Policy* 2012, *41*, 878-884.
6 C.-J. Yang, *Environmental Science & Technology* 2015, *49*, 9501-9502.
7 A. G. Sharpe, *Education in Chemistry* 1964, *1*, 75.

Chapter 3. Experimental Methods, Materials Preparation and Products Analysis

3.1 Mechanism Study of the Extraction Process

For the purpose of examining and verifying the feasibility of the extraction process, and to enhance the efficiency of the process and with that the maximization of the environmental gain, it is necessary to have a fundamental understanding of the interaction, for example, between the extracting solvent, methanol and the constituent solutes alkenes and thiophene. Therefore, this research starts with the solubilisation analysis of the solvent and solutes then the computational quantum chemical calculations of the interactions between the solvent and solutes and nuclear magnetic resonance analysis of "model" solvent and solutes mixtures. The preparation and the source of the raw materials used in this mechanism study are stated in the following part and Appendix 1.

3.1.1 Preparation of Raw Materials

1-pentene, 1-hexene, thiophene, methanol and tetramethylsilane (TMS) with analytical standard purity, methanol-d_4 with purity of 99.8% and cyclohexane-d_{12} with purity of 99.6% were purchased from Sigma Aldrich Company. Gas cylinders of pure grade ethylene, propylene, 1-butene, isobutylene, cis-2-butene and trans-2-butene were purchased from the BOC Group plc. These agents were used without further purification.

3.1.2 Solubilisation Analysis

First, to examine and verify the feasibility of the extraction process, the

dissolving capability of liquid solutes in the solvent methanol and the absorption capability of gases in absorber (solvent) need to be analysed.

In order to investigate the dissolving capacity of our selected prototypical liquid solutes 1-pentene, 1-hexene and thiophene in the solvent methanol under room temperature and atmosphere pressure, their solubilities in methanol have been measured shake-flask method. According to this method the liquid solute is added in surplus to a certain amount of methanol and shaken at a predetermined time at room temperature. The saturation is confirmed by observation of the presence of phase separation.

For the gaseous alkenes, how much of each gaseous alkene in volume (ml) can be adsorbed by a unit of liquid methanol (100 ml) in 30 minutes time has been measured. During the experiment, each gaseous alkene was diverted into the methanol container, and left in contact for 30 minutes under 20℃/293.15 K and 1.8 bar pressure by pumping the gaseous alkenes into a pressure vessel which contains a certain amount of methanol. The methanol adsorbed alkene's weight can be obtained by measuring the mass difference of the pressure vessel before and after 30 minutes contact. Then the adsorbed volume of each gaseous alkene by the solvent methanol can be calculated from the mass difference of the vessel before and after the absorption process divided by the alkene's density.

3.1.3 Computational Quantum Chemical Calculations

As a recently developed technology, computational methods can be used to study domains of the potential energy surface which are far from the equilibrium structure.[1,

[2] To establish the possible origins of the interaction between solute alkene and solvent methanol, 1-hexene with methanol was chosen as prototypical example for the computational quantum chemical calculations. The use of ab initio and DFT (Density Functional Theory[3]) calculations seems to be the most appropriate approach to calculate hydrogen bond interaction energy as the difference between the energy of dimer and the energies of corresponding monomers.[4, 5] During the calculations, the full geometry optimization at the DFT level of 1-hexene with methanol has been carried out by Dr. Maxim L. Kuznetsov at Centro de Química Estrutural, Instituto Superior Técnico, University of Lisbon. These calculations are carried out in both gas phase and solution (SMD model,[6] 1-hexene or methanol as solvent) using the M06-2X functional[7] and the 6-311+G** basis set with the help of the Gaussian-09[8] program package.

The continuum solvation model based on the quantum mechanical charge density of a solute molecule interacting with a continuum description of the solvent,[6] called SMD was applied in the calculations, where the “D” stands for “density” to denote that the full solute electron density is used without defining partial atomic charges.[6] “Continuum” denotes that the solvent is not represented explicitly but rather as a dielectric medium with surface tension at the solute-solvent boundary.[6]

SMD is a universal solvation model, where “universal” denotes its applicability to any charged or uncharged solute in any solvent or liquid medium for which a few key descriptors are known (in particular, dielectric constant, refractive index, bulk surface tension, and acidity and basicity parameters).[6] The model separates the

observable solvation free energy into two main components.[6]

The first component is the bulk electrostatic contribution arising from a self-consistent reaction field treatment that involves the solution of the nonhomogeneous Poisson equation for electrostatics in terms of the integral equation-formalism polarizable continuum model (IEF-PCM).[6] The cavities for the bulk electrostatic calculation are defined by super positions of nuclear-centered spheres.[6]

The second component is called the cavity-dispersion-solvent-structure term and is the contribution arising from short-range interactions between the solute and solvent molecules in the first solvation shell.[6] This contribution is a sum of terms that are proportional (with geometry-dependent proportionality constants called atomic surface tensions) to the solvent-accessible surface areas of the individual atoms of the solute.[6]

In my research, the full geometry optimization of 1-hexene, methanol and their clusters has been carried out at the DFT level of theory in both gas phase and solution (SMD model,[6] 1-hexene or methanol as solvent) using the M06-2X functional[7] and the 6-311+G** basis set with the help of the Gaussian-09[8] program package. It was shown that the M06-2X functional describes reasonably the weak dispersion forces.[9, 10] No symmetry operations have been applied. The Hessian matrix was calculated analytically in order to prove the location of correct minima (no imaginary frequencies). The topological analysis of the electron density distribution with the help of the AIM method of Bader[11] was performed using the program AIMAll. The

atomic charges and bond orbital nature were analyzed by using the natural bond orbital (NBO) partitioning scheme.[12]

For the clusters 1-hexene···methanol, several initial geometries with various mutual positions of the hexene and methanol molecules were used. The 1-hexene···methanol interaction energies were calculated at both M06-2X/6-311+G** and CCSD(T)/6-311+G**//M06-2X/6-311+G** levels as the difference between the enthalpy at 0 K of the cluster 1-hexene···methanol and the sum of enthalpies of isolated 1-hexene and methanol. Counterpoise estimates of the basis set superposition error (BSSE)[13, 14] were made using the Counterpoise keyword in Gaussian 09.

3.1.4 Nuclear Magnetic Resonance (NMR)

Of the important spectroscopic aids that at the disposal of the chemist for use in elucidating molecular structures, molecular motions, interactions and reactions, *Nuclear Magnetic Resonance* (NMR) spectroscopy is one of the major tools.[15, 16] In the mid of 1940s, Purcell, Torrey, and Pound at Harvard University and Bloch, Hansen, and Packard at Stanford University first succeeded in observing the phenomenon of NMR in solid and liquids and these pioneers set the starting point for the quite remarkable development of a new branch of science,[15] used in every chemistry departments across the world.

The physical foundation of NMR spectroscopy lies in the magnetic properties of atomic nuclei.[15] Nuclear magnetic moments are exquisitely sensitive to their surroundings such as an external magnetic field.[15, 16] A magnetic nucleus placed in a magnetic field has a small number of quantized energy levels. The energy levels differ

in the orientation of the nuclear magnetic moment which can point in the same direction as the magnetic field or in the opposite direction. The spacing of the energy levels, ΔE, depends on the size of the nuclear magnetic moment and the strength of the magnetic field. ΔE may be measured by using electromagnetic radiation to induce transitions between the energy levels. This can occur when the frequency, ν_{NMR}, of the applied radiation satisfies the resonance condition $\Delta E = h\nu_{NMR}$, where h is Planck's constant. This is *Nuclear Magnetic Resonance* (NMR) spectroscopy.

The radiation required to induce NMR transitions is consequently referred to as the *radiofrequency field*.[16] Magnetic fields in the range 2.35-23.5 T are commonly used, giving ^{1}H (proton/protium) resonance frequencies of 100-1000 MHz. Since ^{1}H is by far the most popular NMR nucleus, NMR spectrometers are usually classified by their ^{1}H frequencies, rather than the strengths of their magnetic fields. Of all the nuclei (^{1}H, ^{2}H, ^{13}C, ^{14}N, ^{15}N, etc.), ^{1}H has the largest magnetogyric ratio and magnetic moment.[16] Only the magnetogyric ratio of the radioactive isotope tritium, ^{3}H which has very low natural abundance, exceeds that of ^{1}H.[16] Therefore, with high resolution and high sensitive, *Proton/Protium Nuclear Magnetic Resonance* (^{1}H-NMR) spectroscopy was applied in this research.

Considering the application of NMR in the study of hydrogen bond interactions, Arunan et al. indicated that NMR spectroscopy offers the next best evidence for hydrogen bonding after IR spectroscopy.[17] The partial covalent nature of the hydrogen bond has been experimentally verified during the last decade by NMR spin–spin coupling and Compton scattering measurements.[17-19] In general, the proton magnetic

resonance of X—H moves toward lower field compared to non-hydrogen-bonded X—H.[17] This is the result of strong deshielding of the protons, which is a direct consequence of electron redistribution around the H atom following the H bond formation.[17] NMR spectroscopy has provided direct evidence for through-bond coupling between X and Y in a X—H…Y hydrogen-bonded system,[18, 20] here, Y could be any element having electronegativity larger than that of H and also π-electrons.[21]

To probe further the nature of the interaction of hydrogen bonds between various alkenes or thiophene and methanol, in this research ^{1}H-NMR spectra analysis was therefore carried out.

For studying the liquid - liquid mixtures i.e. 1-pentene in methanol, 1-hexene in methanol and thiophene in methanol, 5 mm (7 inches, 300 MHz) NMR tubes were used as the sample holder. The mixtures were studied at 293.1 K and under atmospheric pressure (101 kPa) by ^{1}H-NMR spectroscopy using a Bruker Advance III HD Nanobay 400MHz NMR spectrometer (repeated for 10 times). Deuterated methanol-d_4 and cyclohexane-d_{12} were utilised in the tests to render these solvents "invisible" in the ^{1}H spectra. Here, the non-polar solvent cyclohexane-d_{12} (0.000 D) was chosen as the reference solvent and lock in this series of tests.[22] It is because, as a solvent, cyclohexane-d_{12} will not affect the chemical shift or give any proton signal when obtaining the ^{1}H-NMR spectrum, and it is also mutually soluble with the liquid solutes (alkenes and thiophene). Tetramethylsilane (TMS) was added into each sample as the internal standard, which is assigned the chemical shift zero (0 ppm). The

mixing ratio of the solute (alkenes/thiophene) and solvent (methanol-d_4/cyclohexane-d_{12}) in each samples were 1:10 molar ratio, and six samples were prepared for acquiring the ^{1}H-NMR spectra, they are:

(1) 1-pentene with methanol-d_4;

(2) 1-pentene with cyclohexane-d_{12};

(3) 1-hexene with methanol-d_4;

(4) 1-hexene with cyclohexane-d_{12};

(5) Thiophene with methanol-d_4;

(6) Thiophene with cyclohexane-d_{12};

To investigate the gas - liquid mixtures i.e. ethylene in methanol, propylene in methanol, 1-butene in methanol, isobutene in methanol, cis-2-butene in methanol and trans-2-butene in methanol, the ^{1}H-NMR spectrums were recorded at 293.1 K with Bruker Advance III 500 MHz NMR spectrometer using a 5mm thick wall high pressure NMR tube (repeated 10 times). Various gaseous alkenes were pumped into the NMR tube with 1.8 bar pressure to ensure in each sample there is sufficient gaseous alkene dissolved in the solvent phase for acquiring the ^{1}H-NMR spectrum.

The non-polar (0.000 D) solvent cyclohexane-d_{12} was introduced into this ^{1}H-NMR spectrum measuring process as a reference solvent and a lock,[22] and tetramethylsilane (TMS) was also added into each sample as the internal standard. Twelve mixed samples were prepared for acquiring the ^{1}H-NMR spectra, they are:

(7) Ethylene with methanol-d_4;

(8) Ethylene with cyclohexane-d_{12};

(9) Propylene with methanol-d_4;

(10) Propylene with cyclohexane-d_{12};

(11) 1-butene with methanol-d_4;

(12) 1-butene with cyclohexane-d_{12};

(13) Isobutene with methanol-d_4;

(14) Isobutene with cyclohexane-d_{12};

(15) Cis-2-butene with methanol-d_4;

(16) Cis-2-butene with cyclohexane-d_{12};

(17) Trans-2-butene with methanol-d_4;

(18) Trans-2-butene with cyclohexane-d_{12};

Moreover, previous studies indicate that, the hydrogen bonding complex eventually phase separates (or precipitates) with decreasing temperature.[23-26] Therefore, in order to study the temperature influence on the hydrogen bond interactions between alkenes or thiophene and methanol, Variable Temperature (VT) ^{1}H-NMR spectroscopy analysis was introduced into this research. The VT ^{1}H-NMR spectra were recorded at 183.1 K, 193.1 K, 243.1 K, 253.1 K, 273.1 K and 293.1K under atmospheric pressure using an Agilent Mercury 300 MHz spectrometer (repeated 10 times). The 5 mm (7 inches, 300 MHz) NMR tubes were used as the sample holder. Six samples were prepared for acquiring the ^{1}H-NMR spectra, and the composition and VT ^{1}H-NMR test temperature of these samples are listed in Table 5 In the VT ^{1}H-NMR tests the residual solvents (methanol-d_4) peaks were used as the internal standard for referencing chemical shift in the spectra.

Table 5. The composition and test temperature of VT ^{1}H-NMR samples

Samples composition (1:10 in molar)	VT ^{1}H-NMR test temperature					
	183.1 K	193.1 K	243.1 K	253.1 K	273.1 K	293.1 K
1-pentene with methanol-d_4	√	√	√	√	√	√
1-hexene with methanol-d_4		√	√	√	√	√
Thiophene with methanol-d_4				√	√	√

3.2 FCC Gasoline "*Extractive Refining*" Performance Test

The feasibility and effectiveness of the "*Extractive Refining*" was examined and verified through series of experiments. Whilst, in order to obtain the best extraction performance, the optimized conditions for the laboratory scale "*Extractive Refining*" process have been studied in this research. The preparation and the source of the raw materials used in this study are stated in the following part and Appendix 1 and 2.

3.2.1 Preparation of Raw Materials

1-pentene, 1-hexene and thiophene with analytical standard purity, n-octane with purity of 99.0%, ethylbenzene with purity of 99.9%, methanol with purity of 99.9%, ethylene glycol with purity of 99.0% and dimethyl carbonate (DMC) with purity of 99.0% were purchased from Sigma Aldrich Company. Two batches of raw and crude FCC gasoline (unpurified) were purchased from SINOPEC Company, China and Petroineos Manufacturing Scotland LTD, UK. These agents were used without further purification. Distilled water was prepared in our laboratory. Because 1-pentene is a volatile substance with a low boiling point of 303 K,[27] the liquid components of solutions were measured by weight rather than volume. All the experiments were carried out at room temperature 298 K and under atmosphere pressure 101 kPa.

Model FCC Gasoline Mixture (MFGM)

To study the alkene and OSCs reduction effectiveness of the process, firstly, the "*Extraction Refining*" process was applied to deal with a so-called Model FCC Gasoline Mixture (MFGM).

Preparation of the MFGM was referred to the existing literature, which illustrated the required composition of FCC gasoline. In the FCC gasoline, the major part of the alkene content is consists of C5 to C8 alkenes, [28, 29] while C5, C6 alkenes contribute more to the alkene content.[30] Therefore, C5 alkene 1-pentene and C6 alkene 1-hexene were chosen as the model, target alkenes used in this work. Moreover, due to the fact that C8 aromatics contributed as the largest portion among all the aromatics in the FCC gasoline,[29] ethylbenzene was chosen as the model aromatic. The abundance of each compound in the MFGM was based on a crude FCC gasoline, Daqing FCC gasoline.[29] The group composition listed in the Table 6.[29] From the table, the mass fraction of C5, C6 alkenes and C8 Aromatics contents in Daqing FCC gasoline are 5.65%, 11.83% and 7.51%, respectively. Here the mass fraction is the percentage ratio of the weight of one substance to the weight of the total mixture.

Table 6. Group composition of Daqing fluid catalytic cracking (FCC) gasoline [29]

Carbon Number	Composition (Wt), %				
	n-Paraffins	i-Paraffins	Alkenes	Naphthene	Aromatics
3	0.11	0.00	0.10	0.00	0.00
4	0.21	0.00	1.09	0.00	0.00
5	0.46	2.68	5.65	0.53	0.00
6	0.98	0.80	11.83	1.33	0.60
7	1.16	5.26	9.40	2.27	0.29
8	1.27	6.08	9.71	1.35	7.51
9	0.57	3.92	3.54	1.25	7.01
10	0.42	1.49	1.71	0.00	1.31
11	0.00	4.36	2.20	0.00	0.23
12	0.00	1.30	0.00	0.00	0.00
Total	5.18	25.89	45.23	6.73	16.95

Based on the literature survey, the most important class of sulfur compounds presenting in FCC gasoline is thiophene and its light alkyl derivatives in addition to benzothiophene.[31-33] Thus, thiophene was chosen as the target sulfur-compound of this study, which makes the largest contribution to FCC gasoline's sulfur-content. The general concentration of OSCs in FCC gasoline is approximately 1000 ppm (0.1% by weight).[34-36] Thus, to replace all the other OSCs in FCC gasoline, the mass fraction of thiophene in the MFGM was set at 0.1%.

For the purpose of optimizing the experimental procedure, in the MFGM I for the "*Extractive Refining*" performance test, the mass fraction of 1-pentene, 1-hexene, ethylbenzene and thioiphene have been set as 6.0%, 12.0%, 8.0% and 0.1%, respectively. And all the other components have been balanced with n-octane, whose mass fraction is 73.9%.

Crude FCC Gasoline (CFG)

Two batches of crude FCC gasoline (CFG) applied in different parts of this

research were purchased from Sinopec Company, China and Petroineos Manufacturing Scotland LTD, UK, and their group compositions are listed in the Table 7. These composition analysis results of the CFG samples were analysed by a professional petroleum research institution of PetroChina Company in Beijing, China.

Table 7. Group composition of CFG I from Sinopec Company, China and CFG II from Petroineos Manufacturing Scotland LTD, UK

FCC Gasoline	CFG I	CFG II
n-Paraffins (Wt%)	7.25	4.23
i-Paraffins (Wt%)	18.12	20.31
Naphthenes (Wt%)	20.31	13.27
Total Alkane (Wt%)	45.68	37.81
Alkene (Wt%)	49.27	30.39
Aromatics (Wt%)	5.05	31.80
OSCs (ppm)	750	960

Extractant Mixtures

With regard to another important part in the extraction process, various extractant/ extractant mixtures were tested in this research. Pure methanol was used as the extractant to deal with the MFGM I. Methanol with ethylene glycol mixtures (ME) under different mixing ratios was used as the extractant or extractant mixtures in the CFG I "*Extractive Refining*" tests, respectively. In order to test the more economical and sustainable crude methanol (containing water) extractive purification performance,[37, 38] a methanol with distilled water mixture under a certain mixing ratio was used as the extractant mixture in the "*Extractive Refining*" test of CFG II.

3.2.2 *"Extractive Refining"* Test

These series of extraction experiments adopted careful mixing and separating methods, and the general process picture of all the "*Extractive Refining*" tests is presented in Fig. 14.

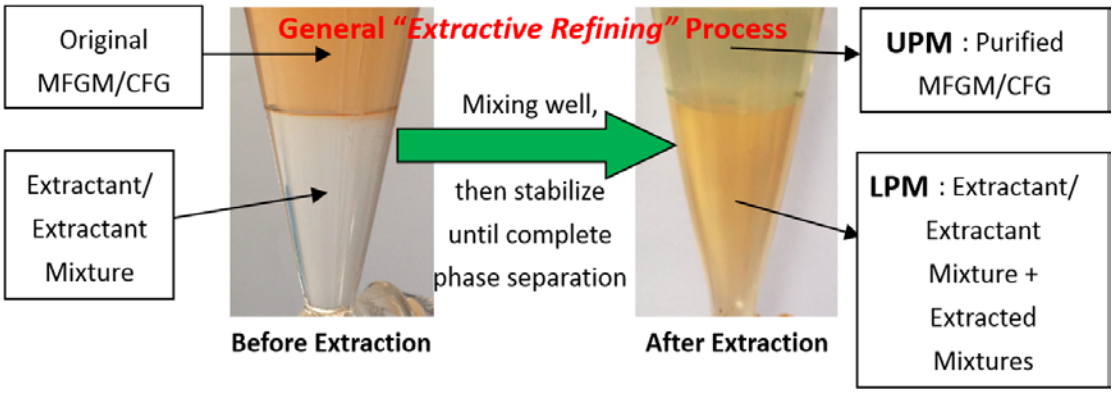

Fig. 14 General process picture of the "*Extractive Refining*" test

For the primary MFGM test, a specific quantity of MFGM I and methanol were premixed in the separating funnel to produce different extracted ratio solutions. Five 10 g MFGM I samples were prepared, and different quantities of methanol were added into these samples. Because the liquid-liquid phase separation was not observed in a 4:1 ratio mixture (under 101kPa, 298 K), in this study, the maximum extractant to gasoline mixing ratio was chosen as 3:1. The weight ratios of extractant methanol to MFGM I in each sample are (i) 3:1, (ii) 2:1, (iii) 1:1, (iv) 1:2 and (v) 1:3.

The mixture was mixed thoroughly by shaking the funnel approx. 200 times. After complete phase separation (two liquid phases) was observed in the mixture, the mixture was stabilized for 5 minutes, and these resulting mixtures were separated and analysed. Then, two liquid phases titled "Upper Phase Mixture" (UPM) and "Lower Phase Mixture" (LPM) based on their vertical order were weighed and recorded.

Table 8 suggests the extractant methanol and extracted compounds are located in the lower phase of the samples, because methanol has the higher density.[39]

Table 8. The density of each component [27, 39]

	n-octane	**1-pentene**	**1-hexene**	**thiophene**	**ethylbenzene**	**methanol**
Density (g/cm^3)	0.703	0.640	0.673	1.051	0.867	0.792

To deal with CFG I, five 10 g CFG I samples (vi) – (x) were premixed with ME mixture under different mixing ratios. The weight ratios of extractant ME mixture to FCC gasoline in each sample are all equal to 1:1. Similar to the MFGM I tests, these resulting mixtures were separated and analysed after mixing and complete phase separation was observed. Then, the UPM and LPM were separated and analysed, respectively.

In the "*Extractive Refining*" tests of CFG II, methanol and distilled water with 9:1 mixing ratio in weight was used as the extractant mixture. During the tests, CFG II and this extractant mixtures were fed into the separating funnel under 5:1 CFG to extractant (mass) ratio, respectively. Then the mixtures were mixed well by shaking the funnel 200 times. After complete phase separation (two liquid phases) was observed in the mixture, the mixture was stabilized for 5 minutes. Then, the UPM and LPM were separated, and fresh extractant was added into the UPM with 5:1 UPM to extractant ratio. This extractive purification process was repeated five times. Finally, the UPM and LPM resultant mixtures were separated and analysed. Here, LPM is the total mixture of all the LPM from five time extractions.

3.3 Cracking Gas "*Extractive Distillation*" Performance Test

In the tests of the "*Extractive Distillation*" process for separating the cracking gas,

the various solvents, methanol and n-hexane with stated purity of 97.0%, propylene carbonate (PC) with purity of 99.7%, and dimethyl carbonate (DMC) with purity of 99% were all purchased from Sigma Aldrich Company. The model cracking gas mixture cylinders were prepared and purchased from CK Special Gases Ltd, UK. These agents were used without further purification. The preparation and the source of the raw materials used in this study are stated in the following part and Appendix 1 and 2.

3.3.1 Preparation of Raw Materials

Two major types of petroleum pyrolysis/cracking gas were mostly mentioned in the literature, they are the catalytic cracking gas and thermal cracking gas.[40, 41] These cracking gas mixtures are produced from refineries' catalytic cracking process and thermal cracking process, respectively.[40]

Model Catalytic Cracking Gas Mixtures (MCCGM)

In this research, model catalytic cracking gas mixture (MCCGM) is composed of 14.97% ethylene, 24.97% ethane, 19.87% propylene and 40.19% propane in mol%. The components of the MCCGM are obtained from the Gas Market Research Report of China (2011).[40]

Model Thermal Cracking Gas Mixtures (MTCGM)

According to Safarik and Eldridge research,[41] the components of our model thermal cracking gas mixture (MTCGM) are of 15.00% hydrogen, 4.01% carbon monoxide, 24.76% methane, 45.21% ethylene, 4.99% ethane, 5.02% propylene and 1.01% propane in mol%.

Extractant Mixtures

Several organic solvents were also introduced into the "*Extractive Distillation*" process for preparing different extractant/solvent mixtures. Because almost all the organic solvents are miscible with DMC, DMC has used as a basic solvent. Two groups of four extractant mixture samples were prepared, the components in each sample are (i) 140ml n-hexane with 140 ml DMC; (ii) 280ml pure DMC; (iii) 140 ml methanol with 140 ml DMC and (iv) 140 ml PC with 140 ml DMC. Each group of these extractant mixture samples have been applied in the "*Extractive Distillation*" process to separate different gaseous contents in MCCGM and MTCGM. Moreover, these solvent mixtures are homogeneous under the experiment conditions.

3.3.2 "*Extractive Distillation*" Test System

The "*Extractive Distillation*" process was processing by the Parr 4560 Mini Bench Top Reactor. The picture of the process equipment's detail structure is displayed in Fig. 15. Each extractant mixture was transferred into the reactor column as prepared. Then the reactor column was installed and the air tightness had been checked. Two major steps were carefully processed in the experiment, the adsorption process and the desorption process.

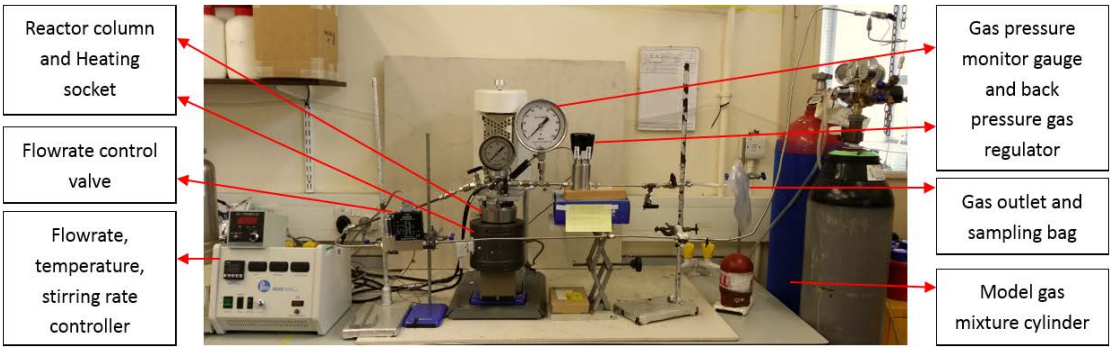

Fig. 15 Picture and the detail structure of the separation equipment

During the adsorption process constant input gas flow (10ml/min) was maintained for 3 hours. The stirrer was kept rotating to ensure the model gas mixture can be maximally adsorbed. Samples were collected from the gas outlet of the reactor. In the desorption step, the gas inlet was switched off. Then, the reactor was heated periodically until the temperature in the reactor reached the lower boiling point of the solvent in the mixture. The stirrer kept running for 30 minutes under a stable temperature to ensure the gas desorption. The released gas from desorption step was also collected and stored with the gas sampling bags.

Lewis and Whitman (1924) indicated that changes in temperature affect several factors, and it is necessary to distinguish clearly between the effect of temperature on the equilibrium and its effect on the coefficients of diffusion.[42] Increase in temperature makes the gas less soluble, thus tending to lower the rate of absorption.[42] The diffusion coefficients themselves may, however, be either raised or lowered by temperature, depending upon changes in film thickness and in specific diffusivity.[42] Therefore, in this research the same process (except the heat process) was repeated to test the pure methanol's gas separation performance under various temperatures (-18 ℃, room temperature/25 ℃ and 40 ℃).

3.4 Catalytic Conversion Tests in Micro-Reactor

In this series of tests, the co-feeding effect of several organic chemicals during methanol-to-gasoline (MTG) catalytic conversion were studied. In the following step of the "*Extractive Refining*" process, as a feedstock, lower phase mixtures (LPM) were fed into the reactor and converted into more valuable gasoline range products

through the catalytic conversion process. The effectiveness of these conversions and the performance of different catalysts used in these conversion process were also carefully examined. The preparation and the source of the raw materials used in this study are stated in the following part and Appendix 1 and 2.

3.4.1 Preparation of Feedstocks and Catalysts

1-hexene and thiophene with analytical standard purity, n-octane with purity of 99.0%, p-xylene with purity of 99.0%, methanol with purity of 99.9% and ethylene glycol with purity of 99.0% were purchased from Sigma Aldrich Company. Sodium carbonate (Na_2CO_3) with purity of 99.95%, CTAB with purity of 99.0%, and Ammonium nitrate (NH_4NO_3) with purity of 99.5% was purchased from Sigma Aldrich Company. HZSM-5 with the Si/Al ratio of 60 had been chosen as the directly used catalyst/basic catalyst for modification in the post extraction conversion process, and this catalyst was purchased from ZEOLYST international Company, USA. These agents were used without further purification. Distilled water was prepared in our laboratory.

Preparation of Co-feeding Catalytic Conversion Feedstocks

In order to study the co-feeding effect in the MTG process, methanol was mixed with various organic chemicals under different mass fractions. All these samples are list in Table 9. Here, the maximum dissolvable mass fraction of n-octane in methanol is 15%; hence 15% in wt. was chosen as the highest n-octane concentration when preparing co-feeding feedstock mixture of n-octane with methanol.

Table 9. Detail composition of each co-feeding test sample

Group	Contents	Mass Fraction (wt)
methanol with alkene mixtures	methanol+1-hexene	95.0%+5.0%
	methanol+1-hexene	90.0%+10.0%
	methanol+1-hexene	80.0%+20.0%
methanol with alkane mixtures	methanol+n-octane	95.0%+5.0%
	methanol+n-octane	90.0%+10.0%
	methanol+n-octane	85.0%+15.0%
methanol with aromatics mixtures	methanol+p-xylene	95.0%+5.0%
	methanol+p-xylene	90.0%+10.0%
	methanol+p-xylene	80.0%+20.0%
methanol with co-extractant mixtures	methanol+ ethylene glycol	95.0%+5.0%
	methanol+ ethylene glycol	90.0%+10.0%
	methanol+ ethylene glycol	80.0%+20.0%
methanol with OSCs mixtures	methanol+thiophene	99.9%+1000 ppm (0.1%)
	methanol+thiophene	99.8%+2000 ppm (0.2%)
	methanol+thiophene	99.6%+4000 ppm (0.4%)

Preparation of after "*Extractive Refining*" Catalytic Conversion Feedstocks

The LPM from the MFGM's "*Extractive Refining*" process was applied as the first feedstock in the after "*Extractive Refining*" catalytic conversion test. In order to obtain the LPM with more simple and accurate constituents, MFGM II was used instead of MFGM I during "*Extractive Refining*" process.

Preparation of the MFGM II was also referred to the existing literature.[28, 29] C6 alkene 1-hexene were chosen as the model, target alkenes used in MFGM II, while C6 alkenes contribute more to the alkene fraction than C5.[30] Its fraction in the MFGM II was equal to the total fraction of C5 and C6 alkenes in MFGM I. Moreover, due to the fact that C8 aromatics is the prevailing mass fraction among all the aromatics in FCC gasoline,[29] p-xylene was chosen as the model aromatic rather than ethylbenzene. The concentrations of constituents in the MFGM II were based on the Daqing FCC gasoline.[29]

In the MFGM II, the mass fraction of 1-hexene, p-xylene, thiophene and n-octane (for balancing) were equal to 18.0%, 8.0%, 0.1% (1000 ppm) and 73.9%, respectively. Methanol (75%, in wt.) with ethylene glycol (25%, in wt.) was used as the extractant mixture to obtain LPM from MFGM II. The extraction process is same as MFGM I's "*Extractive Refining*" process, and the extraction ratio of MFGM II to extractant mixture is 1:1.

For a more practical performance test, lower phase mixtures (LPM) from previous "*Extractive Refining*" process of CFG II was also used as the feedstock of the post extraction catalytic conversion process.

Preparation of Modified 0.10C60 Catalysts

The HZSM-5 sample was treated twice with 0.1 M of Na_2CO_3 (about 15mL/g of zeolite) and CTAB (0.1g CTAB/g of zeolite) solution for 3 hours at 75℃ followed by washing with de-ionized (distilled) water until the pH of the washing water was neutral. Experimental runs to find out the optimum concentration of the solutions were applied at 0.05, 0.1 and 0.2 M of Na_2CO_3 solutions, and at 0.1g, 0.2g, 0.3g and 0.4g of CTAB per one gram of zeolite which 0.1 M of Na_2CO_3 solution and 0.1g CTAB/g of zeolite exhibited the best performance.

After the first 3 hours of treatment, the sample was filtered and will washed with de-ionized (distilled) water and then exposed to another 3 hours of treatment with a fresh solution of the same primary concentration. After drying overnight at 80℃, the sample was ion exchanged twice with a 1.0 M solution of ammonium nitrate NH_4NO_3 (about 15 mL/g of zeolite) for 3 hours at 75℃.After the first 3 hours of treatment, the

sample was filtered and will washed with de-ionized (distilled) water until the pH of washing water was neutral and then exposed to another 3 hours of treatment with a fresh solution of the same primary concentration. After drying overnight at 80℃, the sample was calcined at 500℃ for 6 hours to obtain the protonated sample. The latter was labelled as 0.10C60, which represents the HZSM-5 with a Si/Al ratio of 60 sample treated with 0.1 M solution of Na_2CO_3 and 0.1g CTAB/g of zeolite.

3.4.2 Catalytic Conversion System

A fixed bed microreactor system was applied following the extraction catalytic conversion process, and the schematic structure of the whole process including the analysis equipment (GC and GCMS) is displayed in Fig. 16. The microreactor applied in this research is a MicroReactor 10A system designed and constructed by KLYT Catalysis Science & Technology CO., LTD, and the detailed structure of the microreactor system is indicated in Fig. 17.

In this process, as the raw material, methanol with other organic chemical mixtures or the LPMs of the after "*Extractive Refining*" test (extraction) mixtures were fed into the microreactor by a HPLC pump. The pumping flow rate of these mixtures into the reactor was 2g/hour or 4g/hour. The carrier gas of the conversion process was nitrogen and its flow rate had been set to 20ml/min. During the reaction preparation of each test, 1 or 2 gram of unmodified HZSM-5 (HZSM-5) or modified HZSM-5 (0.10C60) catalyst was added into the reactor tube with the carborundum sand and quartz wool which can prevent the catalyst from blowing away from the reactor tube by the carrier gas. Based on the parameters of the conversion process

above, we calculate the weight hour space velocity (WHSV) of the system is equal to 2 $hour^{-1}$, and this WHSV rate was kept constant through all the catalytic conversion tests. The temperature of the reaction system was from 300℃ to 400℃, and the pressure was from atmosphere pressure (1atm) to 1atm+2bar. The detailed operation conditions such as reaction temperature and pressure settings for different catalytic conversion tests are described in the results and discussion chapters.

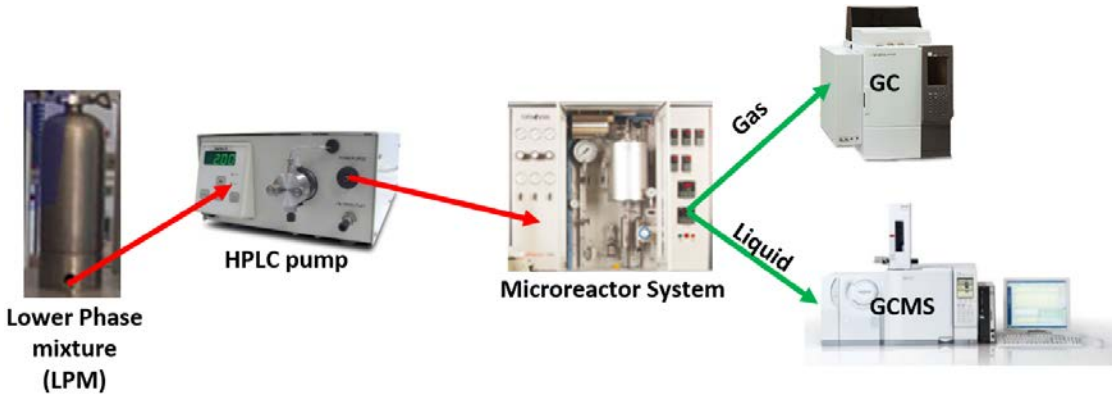

Fig. 16 Schematic setup of the post extraction conversion system and analysis equipment

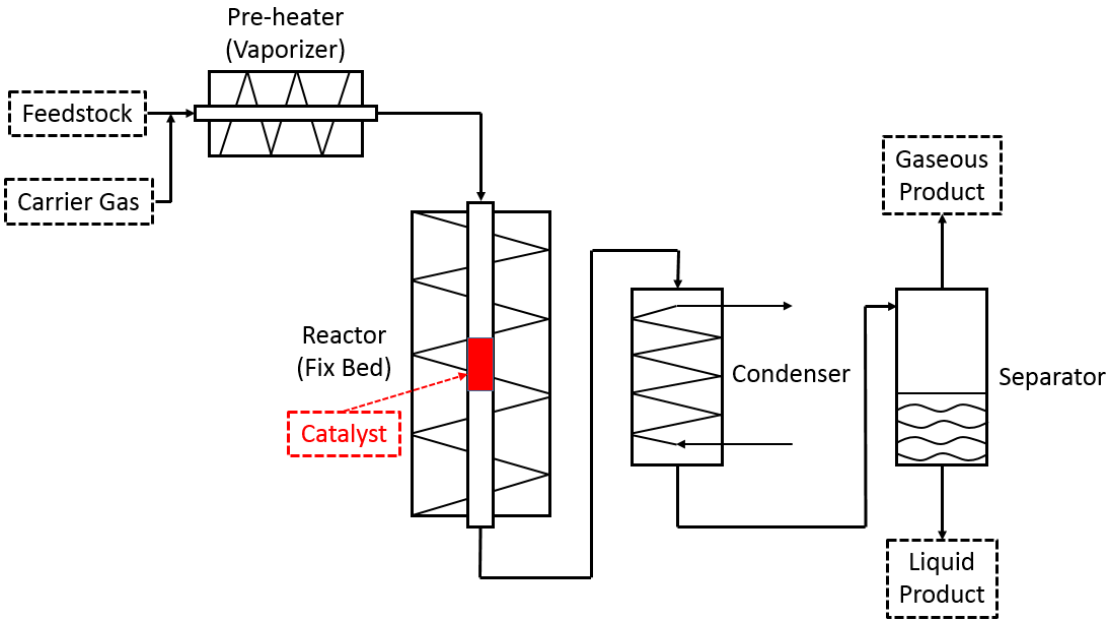

Fig. 17 Schematic setup of the micro-reactor system

The gas chromatography (GC) spectrometer was linked with the gas outlet of the microreactor to analyse online the gaseous product from the conversion process. The

gaseous product was injected into the GC analyser once an hour during the conversion process.

After each completion of the reactor test, the liquid product was collected from the liquid outlet of the microreactor. Two phases were observed in the liquid product, the Oil Phase at the top and Water Phase at the bottom. We separated these two phases and measured the volume and weight of the Oil Phase. Then, the Oil Phase was sent to the chromatography mass (GCMS) spectrometer to quantify the target organic chemicals in it.

3.5 Feedstocks, Products Analysis

In this research, various properties of the feedstocks and products from different "*Extractive Refining*" or "*Extractive Distillation*" processes were analysed by eye and by weight measurement, Gas Chromatography (GC), Gas Chromatography Mass Spectrometry (GCMS) and Thermal Gravimetric Analysis (TGA).

3.5.1 Colour Change and Mass Balance Analysis

The colour change was monitored during the "*Extractive Refining*" processes by eye. Because the organic chemicals contained in the MFGMs and the extractant/extractant mixtures are all colourless, no colour change should be observed in both feedstock and product before and after the MFGMs' "*Extractive Refining*". Compared to the colourless MFGMs, CFGs are coloured due to the OSCs and other chemicals in it. Therefore, the colour changes for the CFGs are much easier to monitor during the "*Extractive Refining*" processes.

Mass balance measurement is another primary analysis for the feedstocks and

products from the "*Extractive Refining*" processes. Unlike the colour change monitoring, this measurement was applied in all the extraction tests. During the "*Extractive Refining*" processes, after complete phase separation was observed in the mixture, the mixture was stabilized for 5 minutes, and then the two liquid phase mixtures UPM and LPM were separated based on their vertical order and transferred into separate containers (weighed when they are empty) and sealed in order to avoid volatilization. These mixtures were weighed by a high accuracy electronic scale and recorded. For the CFG II tests, the "*Extractive Refining*" process was repeated five time and therefore differs from the other tests in that the final LPM is the total mixture of all the LPM from five time extractions.

3.5.2 Gas Absorption Volume Analysis

As described in the previous "*Extractive Distillation*" tests, in the desorption step of the process, the released gas was collected and stored with a gas sampling bag. Because all the gases desorbed from the extractant/extractant mixtures are insoluble in the water, the volume of the desorbed gas was carefully determined by the water gas displacement. In other words, the volume of the gas absorbed by/dissolved in the extractant/extractant mixture was obtained.

3.5.3 Gaseous Product Analysis

Gas Chromatography (GC) technology was employed to quantify the different contents in the gaseous products from different "*Extractive Distillation*" tests and catalytic conversion tests in this research.

Many publications have discussed or detailed the history and development of

chromatography.[43-46] Among all the chromatography technologies gas chromatography (GC), probably has been the most widely investigated since the early 1970s.[46] GC is a unique and versatile technique. In its initial stage of development it was applied to the analysis of gases and vapours from very volatile components.[46] The work of Martin and Synge[47] and James and Martin[48] in gas-liquid chromatography (GLC) or simply gas chromatography (GC) opened the door for an analytical technique that has revolutionized chemical separations and analyses.[46, 49] As an analytical tool, GC can be used for the direct separation and analysis of gaseous samples, liquid solutions, and volatile solids.[46] Both organic and inorganic materials can be analysed, and molecular weight can range from 2 to over 1000 Daltons.[50] GC technology has many advantages such as fast analysis, efficiency, high resolution, sensitivity, highly accurate quantitative analysis, requires small samples, reliable and relatively simple, and is also non-destructive and inexpensive.[50]

In GC a carrier gas is the moving phase, usually an inert gas such as helium, argon or an unreactive gas such as nitrogen.[50] The use of a gas for the mobile phase requires that the system be contained and leak-free, and this is accomplished with a glass or metal tube referred to as the column.[50] Since the column contains the stationary phase which is a microscopic layer of liquid or polymer on an inert solid support, it is common to name the column by specifying the stationary phase.[50]

The gaseous compounds being analysed interact with the walls of the column, which is coated with a stationary phase.[49] This causes each compound to elute at a different time, known as the *retention time* of the compound.[49] The comparison of

retention times is what gives GC its analytical usefulness.[49] Fig. 18 is a schematic representation of the chromatographic process.[50, 51] The horizontal lines represent the column; each line is like a snapshot of the process at a different time (increasing in time from top to bottom).[50] In the first snapshot, the sample, composed components A and B, is introduced onto the column in a narrow zone.[50] It is then carries through the column (from left to right) by the moving phase.[50]

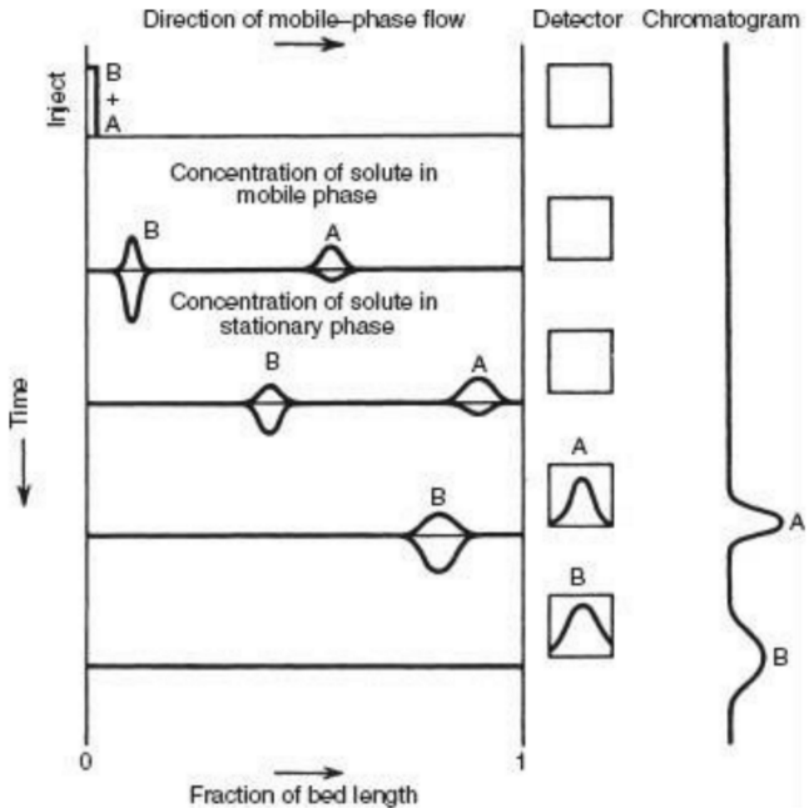

Fig. 18 Schematic representation of the chromatographic process[50, 51]

Each component partitions between the two phases, as shown by the distributions or peaks above and below the line.[50] Peaks above the line represent the amount of a particular component in the moving phase, and peaks below the line represent the amount in the stationary phase.[50] Component A has a greater distribution in the mobile phase and as a consequence it is carried down the column faster than component B,

which spends more of its time in the stationary phase.[50] Thus, separation of A from B occurs as they pass through the column.[50] Eventually the components leave the column and pass through the detector (Fig. 18). Then, the output signal obtained from the detector gives rise a *chromatogram* shown at the right side of Fig. 18.[50, 51] Several kinds of detectors and carrier gases have been applied in the existing GC analyser system, and they are listed in Table 10.

Table 10. Detectors and carrier gases applied in the GC analyser[50]

Detector	Carrier Gas
Thermal Conductivity (TCD)	Helium or argon
Flame Ionization (FID)	Helium, argon or nitrogen
Electron Capture (ECD)	Very dry nitrogen

The GC analyser used in this research was a SHIMADZU GC2014 gas chromatography spectrometer with TCD and FID detector. The main operating parameters of the GC meter were: Column Oven Temperature 45 ℃; Injection Temperature 300 ℃; At 45 ℃ system held 4 minutes, then temperature rising rate from 45 to 200 ℃ was 50 ℃/min, and after 200 ℃ system held for another 7.8 minutes, the temperature rising rate was changed to 10 ℃/min, until it reached 300 ℃. Collected gaseous samples from the "*Extractive Distillation*" tests were manually injected into the analyser through a 20 ml syringe. The on-line gaseous products from the catalytic conversion tests were automatically injected into the GC analyser through the GC's auto sampler per hour during the conversion process.

The volume fraction for all the contents in the different gaseous products analysed by the GC analyser were calculated according to the following expressions [52]:

$$\Phi_i = \frac{V_i}{\Sigma_j V_j} = \frac{A_i}{f_i} \qquad (1)$$

$\boldsymbol{\Phi_i}$ volume fraction of component ***i***;

$\boldsymbol{V_i}$ volume of component ***i***;

$\boldsymbol{\Sigma_j V_j}$ the volume of all constituents of the mixture ***V***;

$\boldsymbol{A_i}$ peak area of component ***i***, the integral area of component ***i***'s peak in the *chromatogram* which is obtained from the GC analyser;

$\boldsymbol{f_i}$ relative correction factor for component ***i***, which is obtained from the component ***i***'s standard curve. The standard curve was calculated from component ***i***'s GC calibration results.

For the catalytic conversion tests, the on-line period output rate of different gaseous product during each tests were calculated according to:

$$Q_i = (\frac{\Phi_i}{\Phi_s}) \cdot Q_s \qquad (2)$$

$\boldsymbol{Q_i}$ output/flow rate of component ***i***;

$\boldsymbol{\Phi_i}$ volume fraction of component ***i***;

$\boldsymbol{\Phi_s}$ volume fraction of standard component, here Nitrogen (N_2);

$\boldsymbol{Q_s}$ output/flow rate of standard component, here Nitrogen (N_2).

3.5.4 Liquid Raw Materials and Products Analysis

In this research, the different contents in the raw materials (CFGs) and products from different "*Extractive Refining*" tests and catalytic conversion tests were quantifying by the Gas Chromatography Mass Spectrometry (GCMS) analyser.

Unlike the Gas Chromatography (GC), which has already been introduced in

previous part, the commercial mass spectrometer/mass spectrometry (MS) analyser was used almost entirely for quantitative analysis of volatile hydrocarbons for the first decade after its introduction in 1942.[53-56] Reports of the mass spectrometry of other compound types were appearing in the early 1950s when the Gohlke and MaLafferty joined the Spectroscopy Laboratory at the Dow Chemical Company.[56-59]

A MS analyser is an analytical instrument that produces a beam of gas phase ions from samples (*analytes*), sorts the resulting mixture of ions according to their *mass-to-charge* (*m/z*) ratios using electrical or magnetic fields (or combinations), and provides analog or digital output signals (*peaks*) from which the mass-to-charge ratio and the *intensity* (abundance) of each detected ionic species may be determined.[60] The basic sequence of events in all MS analyser are presented in Fig. 19, firstly introducing the sample, then operate on the premise that the samples is ionized, and the resulting ions are separated according to a parameter related to their mass-to-charge ratio and finally detected.[60]

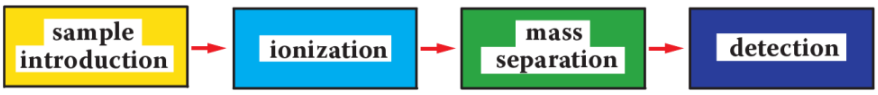

Fig. 19 The basic sequence of events in a mass spectrometers (MS)[60]

For a typical MS analyser, there are six major components: (1) sample introduction system, (2) ion source where the analytes are vaporized and ions are produced, (3) mass analyser where the ions are separated according to their *m/z* ratios, (4) ion detector where the signal intensities of each separated *m/z* value are determined, (5) vacuum system, needed to prevent the loss of ions through collisions with neutral gas molecules as well as with the walls of the mass analyser, the detector,

and sometimes the ion source, and (6) computers, to control the operation of the instrument, record, and process the data generated.[60] These major components of a MS analyser are shown in Fig. 20.

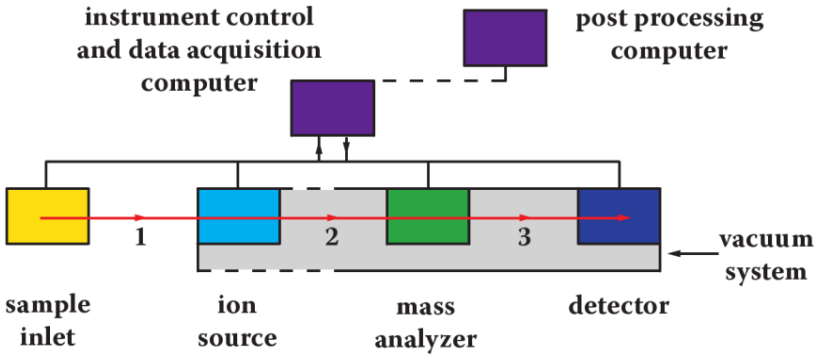

Fig. 20 The major components of a typical mass spectrometer[60]

MS can provide detailed structural information on most compounds such that they can be exactly identified, but it cannot readily separate them.[61] GC can separate volatile and semivolatile compounds with great resolution, but it cannot identify them.[61] Therefore, it was not surprising that the combination of the two techniques was suggested shortly after the development of GC in the mid-1950s.[61] Gas chromatography and mass spectrometry are highly compatible techniques.[61] In both techniques, the sample is in the vapor phase, and both techniques deal with about the same amount of sample (typically less than 1 ng).[61] Gas chromatographic mass spectrometry (GCMS) is the single most important tool for the identification and quantitation of volatile and semi volatile organic compounds in complex mixtures.[61] As such, it is very useful for the determination of molecular weights and the elemental compositions of unknown organic compounds in complex mixtures.[61]

The GCMS is composed of two major building blocks: the gas chromatograph and the mass spectrometer.[62] The gas chromatograph utilizes a

capillary column which depends on the column's dimensions (length, diameter, film thickness) as well as the phase properties.[62] The difference in the chemical properties between different molecules in a mixture and their relative affinity for the stationary phase of the column will promote separation of the molecules as the sample travels the length of the column.[49-51, 62] The molecules are retained by the column and then elute from the column at different times (i.e. *retention time*), and this allows the mass spectrometer downstream to capture, ionize, accelerate, deflect, and detect the ionized molecules separately.[49-51, 61, 62] The mass spectrometer does this by breaking each molecule into ionized fragments and detecting these fragments using their mass-to-charge ratio.[60, 62] The typical schematic of a GCMS analyser is shown in Fig. 21.

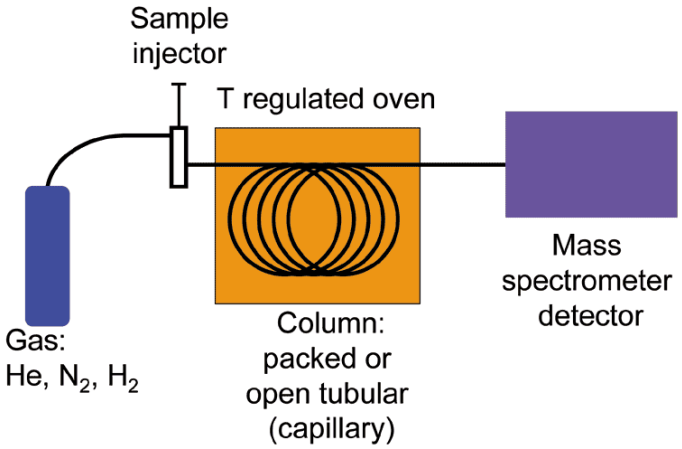

Fig. 21 The typical schematic of a GCMS analyser[62]

To use a GCMS analyser, the organic compounds must be in solution for injection into the gas chromatograph.[61] The solvent must be volatile and organic (for example, hexane or dichloromethane).[61] Depending on the ionization method, analytical sensitivities of 1 to 100 pg per component are routine.[61] GCMS is used both

for the qualitative identification and for the quantitative measurement of individual components in complex mixtures.[61] There are three ways of examining GCMS data. First, the analyst can go through the gas chromatogram (as reproduced by the mass spectrometer) and look at the mass spectra scanned at each GC peak maximum.[61] The second approach is to look at each mass spectrum in turn, in essence stacking up the mass spectra one behind the other and examining them individually.[61] The third approach is to look at the intensity of one particular mass as a function of time.[61] Quantitation can be based on peak areas from mass chromatograms or from selected ion monitoring.[61]

The GCMS analyser used in this research was a SHIMADZU GCMS-QP2010 SE gas chromatography mass spectrometer. The main operating parameters of the GCMS were: Column Oven Temperature 30 ℃/303K; Injection Temperature 200 ℃/473 K; Injection Mode Split; Temperature rising rate from 30 to 35 ℃ was 1 ℃/min, and after 35 ℃ the rate was changed to 10 ℃/min, until it reached 200 ℃. During the preparation of the GCMS samples, 1.0 ml of acetone, 0.2 ml of standard compound dimethyl carbonate (DMC) and 0.5 ml of liquid sample were added in to a 2ml glass GCMS sample tube and mixing well. Then, the sample tube was put in the rack of the GCMS auto sampler. After completion of the GCMS program, the sample was automatically injected into the GCMS analyser by the auto sampler.

In order to quantify specific components in the liquid raw material or products through the GCMC analyser, the component correction factors need to be determined first. The correction factors for all the components analysed by the GCMS were

calculated according to[61, 63]:

$$f_i = \frac{W_{i\cdot GCMS}}{A_i} \Big/ \frac{W_s}{A_s} \quad (3)$$

$\boldsymbol{f_i}$ relative correction factor for component ***i***, which is obtained from the component ***i***'s GCMS calibration results;

$\boldsymbol{A_i}$ peak area of component ***i***, the integral area of component ***i***'s peak in the *chromatogram* which is obtained from the GCMS analyser;

$\boldsymbol{A_s}$ peak area of standard component, the integral area of standard component's peak in the *chromatogram* which is obtained from the GCMS analyser, here the standard component is dimethyl carbonate (DMC);

$\boldsymbol{W_{i\cdot GCMS}}$ mass of component ***i*** in the GCMS sample;

$\boldsymbol{W_s}$ mass of standard component in the GCMS sample, here the standard component is dimethyl carbonate (DMC).

In the GCMS quantification process, the densities of all the liquid raw materials and products were measured before the GCMS analysis, and during the analysis a certain volume of each liquid sample (raw materials or products) *n* was used for preparing its GCMS sample. Therefore, the mass fraction of component *i* in the liquid sample *n* was calculated according to:

$$w_i = \frac{W_{i\cdot GCMS}}{W_{n\cdot GCMS}} \quad (4)$$

$$W_{i\cdot GCMS} = \frac{W_s}{A_s} \cdot f_i \cdot A_i \quad (5)$$

$$W_{n\cdot GCMS} = V_{n\cdot GCMS} \cdot \rho_n \quad (6)$$

$\boldsymbol{w_i}$ mass fraction of component ***i*** in the liquid sample ***n***;

$\boldsymbol{W_{n\cdot GCMS}}$ mass of liquid sample ***n*** in its GCMS sample;

$V_{n\cdot GCMS}$ certain volume of liquid sample ***n*** in its GCMS sample;

ρ_n density of liquid sample ***n***.

The total mass of component *i* in the liquid sample *n* was calculated according to:

$$W_i = w_i \cdot W_n \quad (7)$$

$$W_n = V_n \cdot \rho_n \quad (8)$$

W_i mass of component ***i*** in the liquid sample ***n***;

W_n mass of liquid sample ***n***;

V_n volume of liquid sample ***n***.

3.5.5 Organic Sulphur Contents (OSCs) Analysis

For analysing the total organic sulphur contents (OSCs) in the liquid feedstocks and products, the ultraviolet (UV) fluorescent sulphur detector was used. The structure of an UV fluorescent sulphur detector is illustrated in Fig. 22. The UV fluorescent sulphur detector is based on classical fluorescence spectroscopy principles. The measurement principle relies on the excitation of SO_2 which occurs in the presence of a specific wavelength (220 nanometers) of UV light and subsequent relaxation which produces a photon of light.[64] A photo multiplier tube (PMT) allows the light emissions to be measured as the SO_2 molecule returns to a ground state.[64]

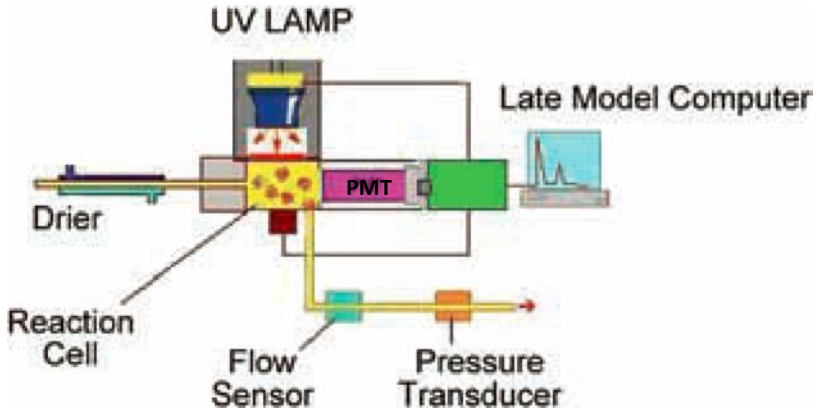

Fig. 22 The structure of the UV fluorescent sulphur detector[64]

During the analysis process, sulphur-containing molecules in the sample stream are oxidised to SO_2 by oxygen.[64] The water formed in this process is removed by the drier.[64] The SO_2 formed, as it enters the reaction cell, is excited with a specific wavelength of UV light.[64] Excited SO_2 decays, emitting a second, specific wavelength of light.[64] This light is detected by a photomultiplier tube, amplified and the software converts it to a peak that can be measured.[64]

These OSCs analysis results of the liquid feedstock and product samples were analysed by the UV fluorescent sulphur detector at a professional petroleum research institution of PetroChina Company in Beijing, China. The model of the UV fluorescent sulphur detector is ZDS-2000. Argon, high-purity grade was used as carrier gas at a flow rate of 100 ml/min. There, the sample was subjected to pyrolysis in the stream of argon. Oxygen, high-purity grade was used for oxi-combustion and ozone generation. The gases from the pyrolysis were completely oxidised in the stream of oxygen (300 ml/min). The furnace oxidative temperature was kept at 1050℃. The gas to be analysed was dried and then passes to the reaction cell of the UV fluorescence detector. The wavelength with is used to excite the SO_2 molecules with the UV fluorescence detector is 220 nm.[65]

3.5.6 Boiling Point (BP) Analysis of Liquid Products

Thermal methods of investigation, generally referred to as thermo- or thermal analysis or thermo-analytical techniques, have found wide application in recent years.[66] These may be defined as experimental methods for characterising a system

(element, compound or mixture) by measuring changes in physical-chemical properties at elevated temperatures as a function of increasing temperature.[66, 67] The two chief methods are *(a)* differential thermal analysis,[66, 68] in which changes in "heat content" are measured as a function of increasing temperature and *(b)* thermogravimetric analysis, in which changes in weight are measured as a function of increasing temperature.[66] Table 11 presents the information that can be provided by methods *(a)* and *(b)*.[66] These information are relating to certain physical and chemical phenomena.

Table 11. Information provided by differential thermal analysis and thermogravimetric analysis[66]

Physical Phenomena	Chemical Phenomena
Crystalline transition	Chemisorption
Second-order transition	Desolvation (especially dehydration)
Fusion	Decomposition
Vaporisation	Oxidative degradation
Sublimation	Solid-state reactions
Absorption	Solid-gas reactions (e.g., oxidation or reduction
Adsorption	
Desorption	

Thermogravimetric analysis (TGA) has come into wide use in the 1950s for rapidly assessing the thermal stability of various substances.[69] A number of workers have demonstrated its usefulness.[69-72] The basic instrumental requirements for thermogravimetric analysis are a precision balance and a furnace that is programmed for a linear rise of temperature with time.[66] Thermogravimetric analysis can provide information on all the phenomena listed above, except crystalline transitions, fusions and those solid-state reactions that occur without change in weight.[66] The results from a thermogravimetric analysis may be presented by-[66]

(i) Weight**,** versus temperature (or time) curve, referred to as the thermogravimetric curve;

(ii) Rate of loss of weight versus temperature curve, referred to as the differential thermogravimetric curve.

In a thermogravimetric curve, the weight axis may be scaled in one of several ways, *e.g.*, (*a*) as a true weight scale, (*b*) as a percentage of the total weight, (*c*) as a percentage of the total weight loss or as a fraction of the total weight lost, (*d*) in terms of molecular-weight units, or (*e*) expressed in terms of fraction decomposed.[66]

As a powerful thermal analysis method, TGA has also been utilized in the distillation study of fuel products for investigating their distillation properties such as a fuel's boiling point or boiling range.[73]

In this research, during the boiling point analysis of the liquid product which are the UPMs from CFG II's "*Extractive Refining*" tests and the CFG II's post extraction LPMs catalytic conversion final products (oil phase products), Thermogravimetric Analysis (TGA) was applied. These UPMs and oil phase products after each process were collected and analysed by the TGA analyser, respectively. The weight versus temperature curve (thermogravimetric curve) of each liquid product was obtained as the result from the TGA analyser, and the weight axis is scaled as a percentage of the total weight. The analyser is a TA Instruments SDT Analyzer Model Q600. The analysis program was: 100ml/min carrier gas flow rate (N_2), 5℃/min heating rate, final temperature is 600℃.

3.6 Catalyst Characterization

In order to investigate the catalysts' characterization and performance during the more practical CFG II after "*Extractive Refining*" catalytic conversion processes, the catalysts were analysed by X-ray diffractometer (XRD), Laser Raman Spectrometer and TGA analyser to investigate their crystallinity, coke deposition and lifetime/catalytic performance, respectively.

3.6.1 Solid Analysis by X-ray Diffraction

X-ray diffraction is a very important technique for qualitative and quantitative analyses.[74] It has been used for many years to study the structural properties and fundamental of crystalline and amorphous materials on an atomic scale.[75] One of the basic advantages is that in many cases X-rays only interact weakly with matter and a single scattering (kinematical) approach is sufficient to analyze the experimental data.[75-77] Moreover, the nondestructive nature of the technique makes it particularly valuable because one frequently needs to obtain a large amount of information about a relatively small sample of material.[74]

The basic concept behind X-ray diffraction is the elastic scattering of an electromagnetic wave by the electrons present in the sample.[78] An X-ray wave is scattered elastically if the scattering process does not cause a change of wavelength, but only of its direction.[78] The elastic scattering is a conserving process, it does not involve any energy loss, neither by transfer of energy to the electrons, nor by generation of electronic or phonon excitation of the sample.[78]

X-rays, as electromagnetic waves, are described by a wave vector *k*, related to the

wavelength λ by the following equation[78]:

$$k = \frac{2\pi}{\lambda} \qquad (9)$$

where λ depends on the energy E (for X-rays typically in the range of 10^2-10^5 eV) in the following relation[78]:

$$\lambda = \frac{hc}{E} \qquad (10)$$

where h is the universal constant and c is the speed of light.[78]

The phenomenon of diffraction consists of the interference of waves elastically scattered by all the electrons present in the material illuminated by the radiation.[78] This interference produces an angular distribution of intensity of radiation that holds information about density and distribution of electrons inside the specimen.[78] The scattering process can be described as follows: electromagnetic waves with wave vector k_i impinge on a specimen along the direction k_i and are scattered in all directions in space; only the waves exiting in a specific direction k_f can have the same phase and can interfere constructively.[78] These waves add up in a coherent way and produce a measurable intensity only along the directions for which the path difference between the waves scattered by different atoms is equal to an integer number of the wavelength λ.[78] This leads to the formulation of Bragg's law[78, 79]:

$$2d\sin\theta = \mathrm{n}\lambda \qquad (11)$$

where 2θ is the angle between the incident and the exit wave and d is the distance between two atomic planes.[78, 79] In an analogous description of the scattering process, the electrons invested by the electromagnetic wave start to oscillate with the same frequency.[78] Each oscillating atom produces a spherical wave of the same frequency

of the original one.[78] Only specific directions will produce constructive interference which will depend on the distance between atoms inside the specimen and the radiation wavelength.[78] For specimens where atomic positions follow a very ordered path, the diffraction process yields more specific features.[78]

X-ray diffraction is widely used to determine the degree of the so-called "X-ray crystallinity" of zeolites and zeolite-like materials.[80] The intensities of one or more arbitrarily selected X-ray reflections of the studied zeolite are simply related to those of the respective peaks in the XRD pattern of a standard material containing the zeolite in a known or presumed amount, and this intensity ratio is generally believed to reflect the crystallinity, i.e., the amount of the crystalline zeolitic phase in the studied material.[80]

In this research, X-ray Diffraction (XRD) patterns were used to identify the phase and assess the crystallinity of the catalysts powder samples. XRD patterns were recorded using a PANalytical (X'Pert PRO model) diffractometer with Cu K_∞ radiation in the 2θ range of 2-60°. The acquisition time was 55mins and increment was 0.0084°. Modified and unmodified HZSM-5 catalysts were tested to study their crystallinity change before and after the modification.

3.6.2 Analysis by Laser Raman Spectrometer

The Raman effect, discovered in 1928 and seemingly of enormous potential, has been widely applied.[81] Raman spectroscopy is a light-scattering process which may be *illustrated* as follows.[82] If a medium, whose molecular energy is divided between molecules in the ground state (E_0) and in an excited state (E_1), is illuminated with

monochromatic radiation of frequency ν_0 when $\nu_0 > [(E_1 - E_0)/h]$, then examination of the scattered radiation will show that it contains radiation of that frequency (Raleigh scattering), plus other of frequencies $\nu_0 \pm [(E_1 - E_0)/h]$ (Raman scattering).[82] Typically, the intensity of this latter effect is $\sim 10^{-5}$ of the former which is in turn of the intensity of the source.[82] The intensity of the scattered radiation is dependent upon the sense of polarization of the incident beam and the direction of view.[82]

Raman spectroscopy/scattering can result from rotational, vibrational or even electronic transitions.[81] As it is a light-scattering process (the exciting radiation is normally in the visible region), standard spectrographic *(i.e.,* photographic) methods can be used.[81] The Raman effect is weak (about 10^{-3} $Intensity_{Rayleigh}$, which is in turn about 10^{-3} $Intensity_{Source}$) and this leads to several experimental difficulties.[81] To solve this problem, in the early 1960's, the laser was applied as a source and it rapidly became clear that a renaissance was possible because of an increase in versatility and the removal of most of the experimental limitations of the technique.[81] The first Raman laser, realized in 1962, used nitrobenzene as the gain medium, which was intra-cavity-pumped inside a Q-switching ruby laser.[83, 84]

Raman spectra arise because the polarisability of a bond is sensitive to its orientation (for rotations), length (vibrations) or nature (electronic transitions).[81] The vibrational spectrum of a compound can be an excellent guide to its structure and general chemical composition.[81] Thus the intensity of a vibrational Raman line is related to the rate of change of polarizability *(a)* as a function of change in bond length (Υ), *i e* , $(da/d\Upsilon)$.[81] The shape of the polarizability against bond length curve

for a symmetrical vibration is such that as *a* increases so too will the slope, and similarly the slope reduces with *a*.[82] The relationship between intensity and bond order can thus crudely be explained, because *a* is directly related to the bond strength and hence the bond order.[82]

There are four major components contained in a Laser Raman spectrometer. The first one is the laser source, for most purposes, the helium-neon and argon ion lasers are accepted as being most satisfactory for Raman spectroscopy.[82] As the Raman effect yields, in essence, a weak set of emissions surrounding an intense monochromatic line, the monochromator in a Raman spectrometer must possess a high discrimination.[82] The sampling system is the third major component in a Laser Raman spectrometer, and the classic method of illuminating a Raman sample is to irradiate it at a right angle to the direction of view.[82] The last but most important component is the detector. Basically, the Vast majority of Raman spectrometers which incorporate photoelectric detection systems consist of a photomultiplier-amplifier-recorder chain.[82]

Raman spectroscopy is a widely used technique for studying carbons and coke samples. One of the first attempts to explain the Raman spectra of graphite-like materials was published in 1970 by Tuinstra and Koenig.[85, 86] In the research aspect of coke deposition on the catalyst, Espinat et al., indicated that, Laser Raman spectroscopy can provide very useful information on the coke deposits on the catalysts, over a large range of carbon contents, and especially in the initial stages of coking.[87]

During the post reaction analysis of catalysts in this research, Laser Raman Spectroscopy was used to analyse the coke deposited on the catalysts by subtracting the fluorescence caused by coke. The measurements were done on 3 – 5 mg of post reaction (spent) catalyst. Laser Raman spectra were obtained from a Perkin Elmer Raman Station 400F spectrometer. The spectra obtained conditions were -49℃, exposure time 5 seconds, scanned 4 times and minimizing exposure to air to avoid coke oxidation. The Laser Raman spectra were obtained over 1000-2000 cm^{-1} wavenumber.

3.6.3 Analysis by TGA Analyser

Thermogravimetric Analysis (TGA) techniques have been particularly useful for relating coking to specific reaction conditions and for developing a more comprehensive understanding of the process under observation.[88, 89] In the catalyst study, TGA has been used as a tool to characterise the activity, regenerability and deactivation behaviour of spent catalyst.[90] Analysis of the TGA results allowed a relationship between catalyst activity and coke content to be derived.[90] During the analysis process, TGA was always used to analyse weight loss during heat treatment and to estimate the amount of coke deposited on the catalyst surface after reaction.[91]

In this research, TGA were applied to analysis the carbon deposition of the post reaction catalysts. In order to compare the catalysts anti-coke (lifetime) performance between unmodified and modified catalysts during the CFG II after "*Extractive Refining*" catalytic conversion process, TGA analysis was used to analyse the post reaction samples of both kinds of catalysts.

The catalyst after each reaction test were collected and a 30-50mg catalyst sample was analysed by the TGA/DSC analyser. The analyser is a TA Instruments SDT Analyzer Model Q600. The analysis program was: 100ml/min carrier gas flow rate (Air), 10℃/min heating rate, final temperature is 1000℃.

References

1 A. C. Scheiner, J. Baker, J. W. Andzelm, *Journal of Computational Chemistry* 1997, *18*, 775-795.
2 G. R. Desiraju, T. Steiner, *The weak hydrogen bond: in structural chemistry and biology*. Oxford University Press, New York, 2001.
3 R. G. Parr, in *Horizons of Quantum Chemistry edited by* K. Fukui, B. Pullman. Springer, Dordrecht, 1980, Chap. 1.
4 S. J. Grabowski, *Chemical Physics Letters* 2001, *338*, 361-366.
5 M. S. Gordon, J. H. Jensen, *Accounts of Chemical Research* 1996, *29*, 536-543.
6 A. V. Marenich, C. J. Cramer, D. G. Truhlar, *The Journal of Physical Chemistry B* 2009, *113*, 6378-6396.
7 Y. Zhao, D. G. Truhlar, *Theoretical Chemistry Accounts* 2008, *120*, 215-241.
8 R. A. Gaussian09, *Inc., Wallingford CT* 2009.
9 L. A. Burns, Á. Vázquez-Mayagoitia, B. G. Sumpter, C. D. Sherrill, *The Journal of Chemical Physics* 2011, *134*, 084107.
10 M. Sumimoto, Y. Kawashima, D. Yokogawa, K. Hori, H. Fujimoto, *International Journal of Quantum Chemistry* 2013, *113*, 272-276.
11 R. F. Bader, *Atoms in Molecules: A Quantum Theory*. Oxford University Press, Oxford, 1990.
12 A. E. Reed, L. A. Curtiss, F. Weinhold, *Chemical Reviews* 1988, *88*, 899-926.
13 S. F. Boys, F. d. Bernardi, *Molecular Physics* 1970, *19*, 553-566.
14 S. Simon, M. Duran, J. Dannenberg, *The Journal of Chemical Physics* 1996, *105*, 11024-11031.
15 H. Günther, *NMR spectroscopy: basic principles, concepts and applications in chemistry*. John Wiley & Sons, Weinheim, 2013.
16 P. Hore, *Nuclear magnetic resonance*, Oxford University Press, New York, 2015.
17 E. Arunan, R. Desiraju Gautam, A. Klein Roger, J. Sadlej, S. Scheiner, I. Alkorta, C. Clary David, H. Crabtree Robert, J. Dannenberg Joseph, P. Hobza, G. Kjaergaard Henrik, C. Legon Anthony, B. Mennucci, J. Nesbitt David, *Pure and Applied Chemistry* 2011, *83*, 1619-1636.
18 A. J. Dingley, S. Grzesiek, *Journal of the American Chemical Society* 1998, *120*, 8293-8297.
19 E. Isaacs, A. Shukla, P. Platzman, D. Hamann, B. Barbiellini, C. Tulk, *Physical Review Letters* 1999, *82*, 600.
20 M. Pecul, J. Leszczynski, J. Sadlej, *Journal of Chemical Physics* 2000, *112*, 7930-7938.
21 E. Kryachko, A. Karpfen, F. Remacle, *The Journal of Physical Chemistry A* 2005, *109*, 7309-7318.
22 W. M. Haynes, in *CRC handbook of chemistry and physics*. CRC press, Boca Raton, 2014, Sec. 9.
23 E. Tsuchida, K. Abe, *Advances in Polymer Science* 1982, *45*, 1-119.
24 H. Katono, A. Maruyama, K. Sanui, N. Ogata, T. Okano, Y. Sakurai, *Journal of Controlled Release* 1991, *16*, 215-227.

25 D. Eustace, D. Siano, E. Drake, *Journal of Applied Polymer Science* 1988, *35*, 707-716.
26 L. Deng, C. Wang, Z.-C. Li, D. Liang, *Macromolecules* 2010, *43*, 3004-3010.
27 IFA., in *Book GESTIS Substance Database 2012*, 2012.
28 W. Kiatkittipong, S. Wongsakulphasatch, N. Tintan, N. Laosiripojana, P. Praserthdam, S. Assabumrungrat, *Fuel Processing Technology* 2011, *92*, 1999-2004.
29 Z. Rusong, G. Junbin, Z. Juanjuan, *Petrochemical Technology* 2009, *3*, 009.
30 N. Viswanadham, B. Negi, M. Garg, M. Sundaram, B. Sairam, A. Agarwal, *Fuel* 2007, *86*, 1290-1297.
31 T. G. Albro, P. A. Dreifuss, R. F. Wormsbecher, *Journal of High Resolution Chromatography* 1993, *16*, 13-17.
32 W.-C. Cheng, G. Kim, A. Peters, X. Zhao, K. Rajagopalan, M. Ziebarth, C. Pereira, *Catalysis Reviews* 1998, *40*, 39-79.
33 M. Absi-Halabi, J. Beshara, H. Qabazard, A. Stanislaus, in *Catalysts in Petroleum Refining and Petrochemical Industries 1995*. Elsevier, Amsterdam, 1996, Chap. 3.
34 L. Lin, G. Wang, H. Qu, J. Yang, Y. Wang, D. Shi, Y. Kong, *Journal of Membrane Science* 2006, *280*, 651-658.
35 L. Lin, Y. Kong, G. Wang, H. Qu, J. Yang, D. Shi, *Journal of Membrane Science* 2006, *285*, 144-151.
36 H.-m. QU, Y. KONG, *Acta Petrolei Sinica (Petroleum Processing Section)* 2008, *2*, 232-236.
37 V. Vishwanathan, K.-W. Jun, J.-W. Kim, H.-S. Roh, *Applied Catalysis A: General* 2004, *276*, 251-255.
38 F. J. Keil, *Microporous and Mesoporous Materials* 1999, *29*, 49-66.
39 R. H. Perry, D. W. Green, J. O. Maloney, *Perry's chemical engineers' handbook*. McGraw-Hill, New York, 2008, Vol. 7.
40 CNCIC, *Gas Market Research Report of China*. China National Chemical Information Center, 2012.
41 D. J. Safarik, R. B. Eldridge, *Industrial & Engineering Chemistry Research* 1998, *37*, 2571-2581.
42 W. Lewis, W. Whitman, *Industrial & Engineering Chemistry* 1924, *16*, 1215-1220.
43 V. Heines, *Chemical Technology* 1971, 280-288.
44 L. S. Ettre, *Analytical Chemistry* 1971, *43*, 20-31.
45 G. Zweig, J. Sherma, *Journal of Chromatographic Science* 1973, *11*, 279-283.
46 R. L. Grob, E. F. Barry, *Modern practice of gas chromatography*. John Wiley & Sons, Hoboken, 2004.
47 A. Martin, R. M. Synge, *Biochemical Journal* 1941, *35*, 1358.
48 A. James, A. Martin, *Biochemical Journal* 1952, *50*, 679.
49 S. Ghoshal, *Fundamentals of bioanalytical techniques and instrumentation*. PHI Learning Pvt. Ltd., New Delhi, 2009.
50 H. M. McNair, J. M. Miller, *Basic gas chromatography*. John Wiley & Sons, Hobken, 2011.
51 J. M. Miller, *Chromatography: concepts and contrasts*. John Wiley & Sons,

Hobken, 2005.
52 V. Gold, K. Loening, A. McNaught, P. Shemi, *Iupac compendium of chemical terminology*. Blackwell Science, Oxford, 1997.
53 M. O'Neal Jr, T. Wier Jr, *Analytical Chemistry* 1951, *23*, 830-843.
54 A. Quayle, *Organic Mass Spectrometry* 1987, *22*, 569-585.
55 V. Dibeler, *Analytical Chemistry* 1954, *26*, 58-65.
56 R. S. Gohlke, F. W. McLafferty, *Journal of the American Society for Mass Spectrometry* 1993, *4*, 367-371.
57 S. Rock, *Analytical Chemistry* 1951, *23*, 261-268.
58 J. Momigny, *Bulletin de la Société Royale des Sciences de Liège* 1953, *22*, 541-560.
59 J. Beynon, *Naure* 1954, 174, 735-737.
60 J. Greaves, J. Roboz, *Mass spectrometry for the novice*. CRC Press, Boca Raton, 2013.
61 R. A. Hites, in *Handbook of instrumental techniques for analytical chemistry*. Prentice Hall PTR, Upper Saddle River, 1997, Chap. 3.
62 Y. G. Li, D. Lu, C. Wong, *Electrical conductive adhesives with nanotechnologies*. Springer Science & Business Media, New York, 2009.
63 F. Song, Y. Yu, J. Chen, *Tsinghua Science & Technology* 2008, *13*, 730-735.
64 A. International, *ASTM D 5453-09*, ASTM International, 2009.
65 A. Pavlova, P. Ivanova, T. Dimova, *Petroleum & Coal* 2012, *54*, 9-13.
66 A. Coats, J. Redfern, *Analyst* 1963, *88*, 906-924.
67 S. Gordon, *Encyclopedia of Science and Technology*. McGraw-Hill, New York, 1960.
68 R. Mackenzie, B. Mitchell, *Analyst* 1962, *87*, 420-434.
69 H. H. Horowitz, G. Metzger, *Analytical Chemistry* 1963, *35*, 1464-1468.
70 D. A. Anderson, E. S. Freeman, *Journal of Polymer Science* 1961, *54*, 253-260.
71 H. C. Anderson, *Polymer* 1961, 2, 451-453.
72 C. Doyle, *Analytical Chemistry* 1961, *33*, 77-79.
73 H. E. Schwartz, R. G. Brownlee, M. M. Boduszynski, F. Su, *Analytical Chemistry* 1987, *59*, 1393-1401.
74 A. L. Ryland, *Journal of Chemical Education* 1958, *35*, 80.
75 R. Feidenhans, *Surface Science Reports* 1989, *10*, 105-188.
76 R. James, *Chap* 1954, *2*, 54.
77 B. E. Warren, *X-ray Diffraction*. Courier Corporation, 1969.
78 J. Stangl, C. Mocuta, V. Chamard, D. Carbone, *Nanobeam X-ray Scattering: Probing matter at the nanoscale*. John Wiley & Sons, Weinheim, 2013.
79 W. H. Bragg, W. L. Bragg, *Proceedings of the Royal Society of London. Series A, Containing Papers of a Mathematical and Physical Character* 1913, *88*, 428-438.
80 J. Weitkamp, L. Puppe, *Catalysis and zeolites: fundamentals and applications*. Springer Science & Business Media, Berlin, 2013.
81 P. Hendra, C. Vear, *Analyst* 1970, *95*, 321-342.
82 P. J. Hendra, P. Stratton, *Chemical Reviews* 1969, *69*, 325-344.
83 E. Woodbury, W. Ng, *Proceedings of the Institute of Radio Engineerings* 1962, 50,

2367.
84 G. Eckhardt, R. Hellwarth, F. McClung, S. Schwarz, D. Weiner, E. Woodbury, *Physical Review Letters* 1962, *9*, 455.
85 B. M. Vogelaar, A. D. van Langeveld, S. Eijsbouts, J. A. Moulijn, *Fuel* 2007, *86*, 1122-1129.
86 F. Tuinstra, J. L. Koenig, *The Journal of Chemical Physics* 1970, *53*, 1126-1130.
87 D. Espinat, H. Dexpert, E. Freund, G. Martino, M. Couzi, P. Lespade, F. Cruege, *Applied catalysis* 1985, *16*, 343-354.
88 J. W. Dean, D. B. Dadyburjor, *Industrial & Engineering Chemistry Research* 1988, *27*, 1754-1759.
89 F. Massoth, *Chemical Technology* 1972, 285.
90 Y.-H. Lin, M.-H. Yang, *Thermochimica Acta* 2008, *470*, 52-59.
91 H. Zaidi, K. Pant, *Industrial & Engineering Chemistry Research* 2008, *47*, 2970-2975.

Chapter 4. A Study of the Extractive Process and the Solvent – Solutes Interactions

This research is to understand, identity and quantify the nature of the hydrogen bond between methanol and alkenes. Such an investigation will help to overcome the considerable energy and environmental disadvantages in current alkene or organic sulphur contents (OSCs) reduction/separation processes, and to develop lower cost, less energy-intensive approaches to the clean fuel industry. The approaches are new methanol - based "*Extractive Refining*" and "*Extractive Distillation*" techniques; the underpinning, fundamental science is outlined here.

To understand the underlying solvent (methanol) extraction or solubilisation processes, one needs to consider the universally - classified nine types of solvation and solubility (From A G Sharpe, "Solubility Explained ", Education in Chemistry, 1, 75 (1964))[1]; these are listed in Table 12. This mechanism study is concerned about the "*Gas in liquid*" and "*Liquid in liquid*" solution processes. Ethanol in water is perhaps the most typical of such known solutions. Solubility arises as a result of the particular intermolecular interactions between the ethanol and water molecules above,[2] therefore, ethanol is completely miscible with water.

Table 12. The nine types of solutions[1]

Solution	Gas in gas	Liquid in gas	Solid in gas	Gas in liquid	Liquid in liquid	Solid in liquid	Gas in Liquid	Liquid in solid	Solid in solid
Example	Air	H_2O (vapour) in N_2	I_2 (vapour) in N_2	CO_2 in H_2O	Ethanol in H_2O	NaCl in H_2O	H_2 in Palladium	Mercury in Silver	Copper in nickel

This intermolecular interaction, *"the hydrogen bond"*, is a critically important attractive interaction between polar molecules in which hydrogen is bonded to a

highly electronegative atom.[3] The bond energy range of a hydrogen bond is typically between 2 kJ/mol. to 167 kJ/mol.[3] Fig. 23 indicates the hydrogen bond strength (in so-called Associating Fluids) is intermediate between that of a strong chemical bond and the weak van der Waals interactions.[4] The chemical bond typically ranges from 63 kJ/mol to 1050 kJ/mol.[5] On the other hand, van der Waals interactions, originating from the instantaneous attractive or dispersion forces between molecular entities, have characteristic energies normally less than 42 kJ/mol.[5] The hydrogen bond structure between ethanol and water is presented in Fig. 24.[6]

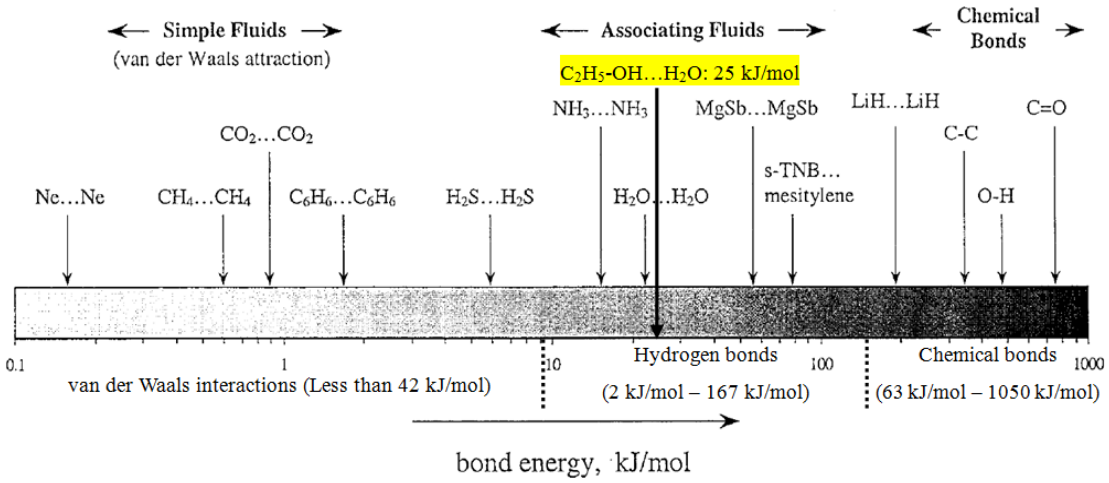

Fig. 23 The continuous distribution of bond strengths, showing the span from-Simple Fluids, through Associating Fluids to the formation of Chemical Bonds[3-5, 7] *The continuous evolution of characteristic bond energies takes one from ca 0.1 through to > 1000 kJ mol^{-1}

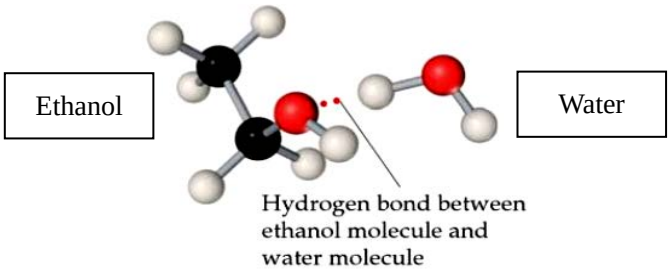

Fig. 24 Hydrogen-bonding interactions between ethanol and water[6]

Other contributing factors such as the magnitude of the Upper Critical Solution Temperature (UCST) as well as so-called molecular dipole moment of both solute and solvent molecules are taken into account in this study.

4.1 Is the Extraction Process Feasible - and what are the Nature of the Interactions between the Solvent and Solutes?

First, in order to verify the feasibility of the methanol - based "*Extractive Refining*" and "*Extractive Distillation*" approaches, the solubility of various liquid solutes (alkenes/thiophene) and gaseous solutes (alkenes) in solvent methanol was examined. Then this study investigates the dissolution of the alkenes and thiophene in methanol through a combination of observations together with a computer modelling study.

4.1.1 On the Nature and Importance of the Upper Critical Solution Temperature

The Upper Critical Solution Temperature (UCST), T_{uc} (or *Upper Consolute Temperature*), is the highest temperature at which phase separation occurs. Above the upper critical temperature the two components are fully miscible.[8] In molecular terms, this temperature exists because the greater thermal motion overcomes any potential energy advantage in molecules of one type being close together. The thermodynamic interpretation of the UCST focuses on the Gibbs energy of mixing and its variation with temperature.[8]

The UCST phenomena are commonly found in mixtures of hydrocarbon and polar liquids.[9] At lower temperatures the energy of interaction of the dipoles in the pure polar liquid is strong enough to dominate the free energy expression, i.e., the

enthalpy change of mixing nonpolar molecules into a fluid held together by strong dipole-dipole interactions is large and positive. As the temperature is raised, the entropy term becomes more important; thus, miscibility increases with temperature.[9] The Gibbs energy of mixing becomes negative above a certain temperature (UCST), regardless of the composition.[8] The balance of the kinetic energy by the energy of dipolar attraction of the pure component molecules leads to the UCST.[9]

One example is the methanol/cyclohexane and several isomers of hexane systems shown in Fig. 25. Trejo et al. reported the liquid-liquid miscibility temperatures as a function of mole fraction for binary systems formed by methanol with cyclohexane and several isomers of hexane at 0.1 MPa.[10] All the studied coexistence curves present an UCST from 293.02 K to 321.62 K, and they reported the UCST of n-hexane with methanol is 313.42 K (Fig. 25).[10]

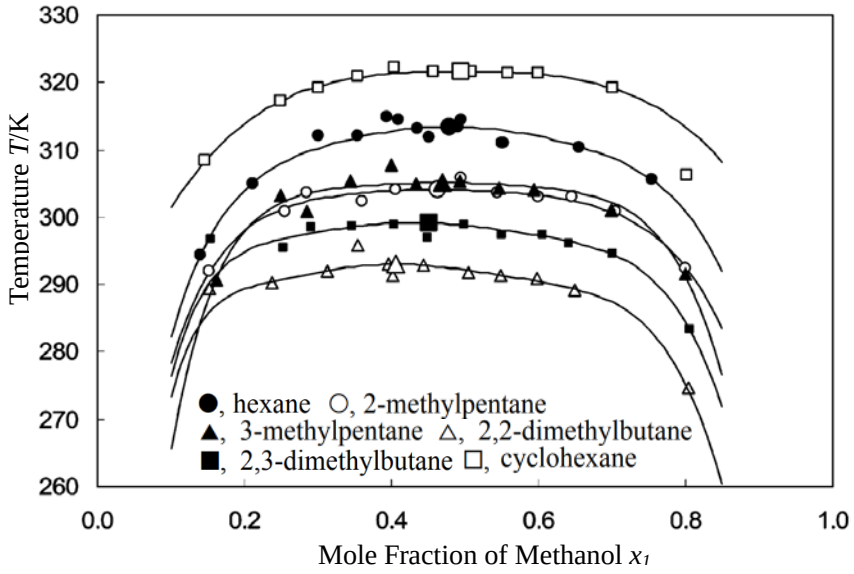

Fig. 25 Liquid-liquid miscibility behaviour for six x_1 methanol + (1- x_1) hydrocarbon systems, the UCST of each system is indicated with a larger symbol[10]

In this study, the unsaturated 1-hexene has the same carbon number as n-hexane,

but 1-hexene's UCST with methanol is much lower than n-hexane, which has been observed below room temperature (298K). A potential explanation for this result is that the hydrogen bond interaction between the solvent methanol and the solute 1-hexene reduces the UCST.

The two main factors generating a UCST are the contribution of the entropy of mixing *S*. Since this is positive and the Gibbs free energy $G = H - ST$, the entropy always causes mixing on raising the temperature *T*. In alkane methanol mixtures this is opposed by the enthalpy of mixing *H* which is positive for the alkane methanol mixtures. For the alkene – methanol system the hydrogen bonding makes the enthalpy of mixing less positive and the UCST is lowered to below room temperature.

4.1.2 Solubilisation Measurements

With regards to the alkenes' solubility, very few reports have been published on the UCST or solubility of alkenes in methanol. The only data were reported previously by Francis (1944) and Pavlova et al. (1975) that 1-heptene is mutually soluble in methanol above the UCST, of 285 K and 271.6 K, respectively.[11-13]

From the observation results of the solubilisation experiments, the solubility of 1-pentene and 1-hexene in methanol was investigated. The solubility of alkenes in methanol is defined as being that no phase separation is observed in the solution after each alkene mixed with solvent methanol, a i.e. homogeneous solution in taken to demonstrate that the alkenes are soluble in methanol at 298 K (Fig. 26b). Further experimental results indicated that the solubility of 1-pentene and 1-hexene in the methanol solvent are mutually soluble almost any ratio, which means 1-pentene and

1-hexene are miscible with methanol in all proportions at room temperature. Table 13 shows the reference data and the results from the tests.

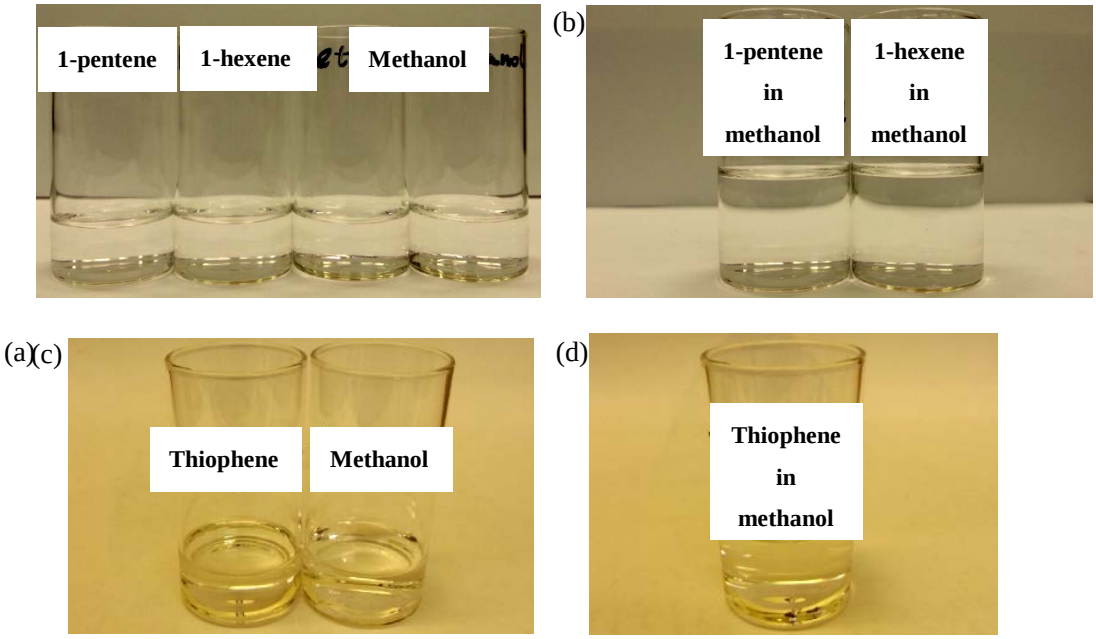

Fig. 26 Photos of the solutions to illustrate the solubility of the alkenes and thiophene in methanol: (a) Pure alkenes and methanol before mixing; (b) Alkenes and methanol solutions after mixing; (c) Pure thiophene and methanol before mixing; (d) Thiophene and methanol solution after mixing

Table 13. Solubility of various solutes in methanol at room temperature

Solvent \ Solute	1-heptene[11-13]	1-pentene	1-hexene	thiophene
methanol	Miscible	Miscible	Miscible	Miscible

From the thiophene with methanol solubilisation experiment, the result also showed no phase separation in the solutions after the thiophene mixed with methanol (Fig. 26d). Similarly, further experiments indicated that, thiophene is complete miscible in methanol at room temperature (Table 13).

The solubility of the various *gaseous* alkenes in methanol obtained from the alkenes solubility tests are listed in Table 14. The error estimate analysis is outlined in

detail in Appendix 3.1. Among all the gaseous alkenes, ethylene shows the lowest solubility in methanol at 20℃/293.15 K and 1.8 bar pressure (Table 14). In contrast, isobutene presents the best solubility among all the gaseous alkenes in methanol under the same conditions (Table 14).

Table 14. Solubility of specified gaseous alkenes in methanol under 20 ℃/293.15 K and 1.8 bar

Compounds	Solubility (ml) per 100 ml methanol (±2 ml)
Ethylene	60
Propylene	513
1-butene	556
Isobutene	1067
Cis-2-butene	302
Trans-2-butene	68

In general, these solubilisation results of alkenes/thiophene in methanol basically support and confirm the feasibility of the "*Extractive Refining*" and "*Extractive Distillation*" processes. The following part of this study focuses on the investigation of the mechanism of these solubilisation phenomena and the interaction between various solutes and solvent methanol.

4.1.3 Computational Quantum Chemical Calculations

In order to investigate the possible origins of the interaction between solute alkenes and solvent methanol, 1-hexene with methanol was chosen as prototypical example for the computational quantum chemical calculations which were processed and obtained with the help of our colleague Dr. Maxim L. Kuznetsov at Centro de Química Estrutural, Instituto Superior Técnico, University of Lisbon.

The full geometry optimization at the DFT level of 1-hexene with a single methanol molecule was carried out first and the results indicated the stable structure

of 1-hexene surrounded by 8 methanol molecules. In the most stable equilibrium structure of the 1-hexene···methanol complex, the hydrogen atom of methanol interacts with the π (C=C double) bond of the alkene with the OH···$(C=C)_{midpoint}$ distances of 2.36–2.41 Å (Table 15, Fig. 27).

Table 15. The calculated parameters of the 1-hexene···methanol and 1-hexene···8 methanol complexes[14]

	1-hexene···methanol			1-hexene···8 methanol[a,c]
	Gas phase[a]	in 1-hexene solution[b]	in methanol solution[b]	
E_{int}[d]	–19.6 (–17.2)[e]	–19.8	–13.6	
E_{int}[f]	–15.8	–14.8	–11.3	
l(OH···π)[g]	2.409	2.376	2.360	2.361
ρ[h]	0.082	0.090	0.088	0.096
$\nabla^2\rho$[i]	0.859	0.912	0.919	1.012
H_b[j]	0.010	0.011	0.012	0.010

[a] Isolated molecular complex without bulky solvent effects. [b] SMD model. [c] Molecular complex with a 1-hexene molecule surrounded by 8 methanol molecules. [d] Binding energies (in kJ/mol) at the M06-2X/6-311+G** level. [e] BSSE corrected value. [f] Binding energies (in kJ/mol) at the CCSD(T)/6-311+G**//M06-2X/6-311+G** level. [g] Intermolecular OH···$(C=C)_{midpoint}$ distances (in Å). [h] Electron density (in e/Å^3) at the OH···(C=C) BCP. [i] Laplacian (in e/Å^5) at the OH···(C=C) BCP. [j] Energy density at the OH···(C=C) BCP (in Hartree/Å^3).

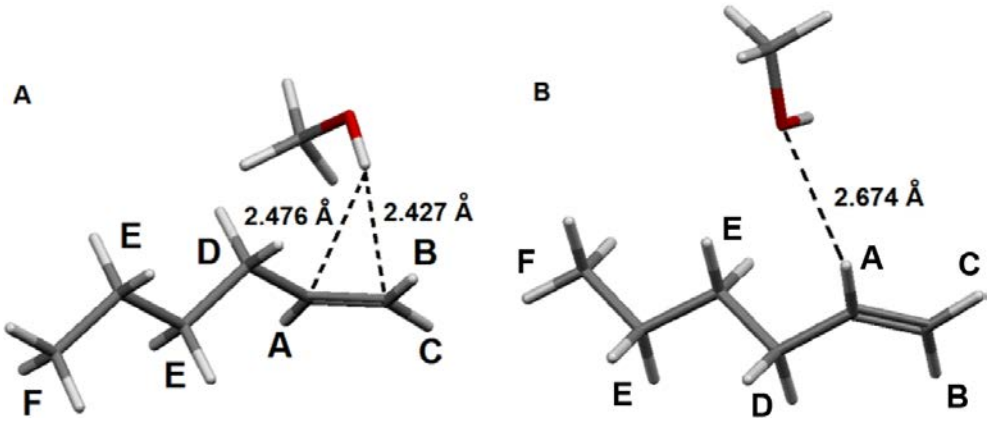

Fig. 27 Equilibrium structures of the 1-hexene···methanol associates exhibiting the O–H···(C=C) (**A**), the most stable structure) and C–H···O (**B**) interactions[14]

The methanol···1-hexene (O—H···π) interaction energies computed at the M06-2X and CCSD(T) levels, both with and without basis set superposition error (BSSE) correction, are given in Table 16. Their values [–11.3 to –19.6 kJ/mol] are comparable at both levels, and the BSSE correction is rather insignificant (–17.2 kJ/mol).

The topological analysis of the electron density distribution (the AIM method) revealed the existence of a bond critical point (BCP) corresponding to the interaction between the methanol hydroxyl hydrogen atom and the π bond in the 1-hexene···methanol complex. The electron density values (ρ) at this BCP do not exceed 0.10 e/Å^3 (Table 15), the electron density Laplacian ($\nabla^2\rho$) is positive and the energy density values (H_b) are slightly positive. All these values are typical for the weak hydrogen bonding which is predominantly electrostatic in nature.[15]

The natural bond orbital analysis demonstrates very small charge transfer (0.003 e) from 1-hexene to the methanol molecule in the complex 1-hexene···methanol which is associated with the π (C=C)→ σ*(OH) transition with the E(2) energy of 10.5 kJ/mol**.** Both models, *i.e.* 1-hexene···methanol cluster with bulky solvent effects and 1-hexene···8 methanol cluster with explicit first solvation shell around alkene molecule, demonstrate very similar bonding features. According to the classifications for the bond energy of various hydrogen bonds (Table 1),[3] combined with these computational quantum chemical calculations, the hydrogen bond interactions between 1-hexene and methanol molecules are shown to be weak hydrogen bonds.

These calculations indicate that the dissolution process can involve weak

hydrogen bonds formed between the alkenes and methanol, via O—H···π and C—H···O interactions and these will be illustrated in the following parts experimentally.[14, 16, 17]

4.2 Hydrogen Bond Interactions between Solvent – Solutes

As in previous descriptions, *"the hydrogen bond"* is a critically important attractive interaction between polar molecules in which hydrogen is bonded to a highly electronegative atom.[3] In this study, the *"polar molecules"* refer to solvent and solute molecules.

Arunan et al. indicated that NMR spectroscopy offers excellent evidence for hydrogen bonding.[18] Therefore, to probe further the nature of the hydrogen bond interactions between various solutes (gaseous and liquid alkenes/thiophene) and hydroxyl group in solvent methanol, the various mixture samples were studied by Proton Nuclear Magnetic Resonance (^{1}H-NMR) spectroscopy.

4.2.1 NMR Analysis of Methanol with Various Gaseous Alkene Mixtures

In this research, methanol with gaseous alkene mixtures were analysed using ^{1}H-NMR spectroscopy. It should be noted that the chemical shifts observed from the spectra are outside of the experimental error estimates (+/- 0.004ppm) in carefully measured chemical shifts of multiple calibration samples. The error estimates analysis of the ^{1}H-NMR spectrum test is described in Appendix 3.2.

Ethylene···methanol H-bond interaction

The numerical chemical shift of the ethylene protons from its ^{1}H-NMR spectrum has been indicated, and the location (A) of these protons in corresponding to their

geometric positions is given in Fig. 28. It can be seen from these ^{1}H-NMR spectra, when ethylene is dissolved in reference solvent cyclohexane d12, the chemical shift of ethylene's protons are located at 5.31 ppm (Fig. 28), and for the ethylene in methanol d4 sample the chemical shift of ethylene's protons appear at 5.38 ppm (Fig. 28). There has a positive chemical shift change $\Delta\delta$ of 0.07 ppm for the ethylene's protons when the solvent has been changed from cyclohexane d12 to methanol d4 (Table 16).

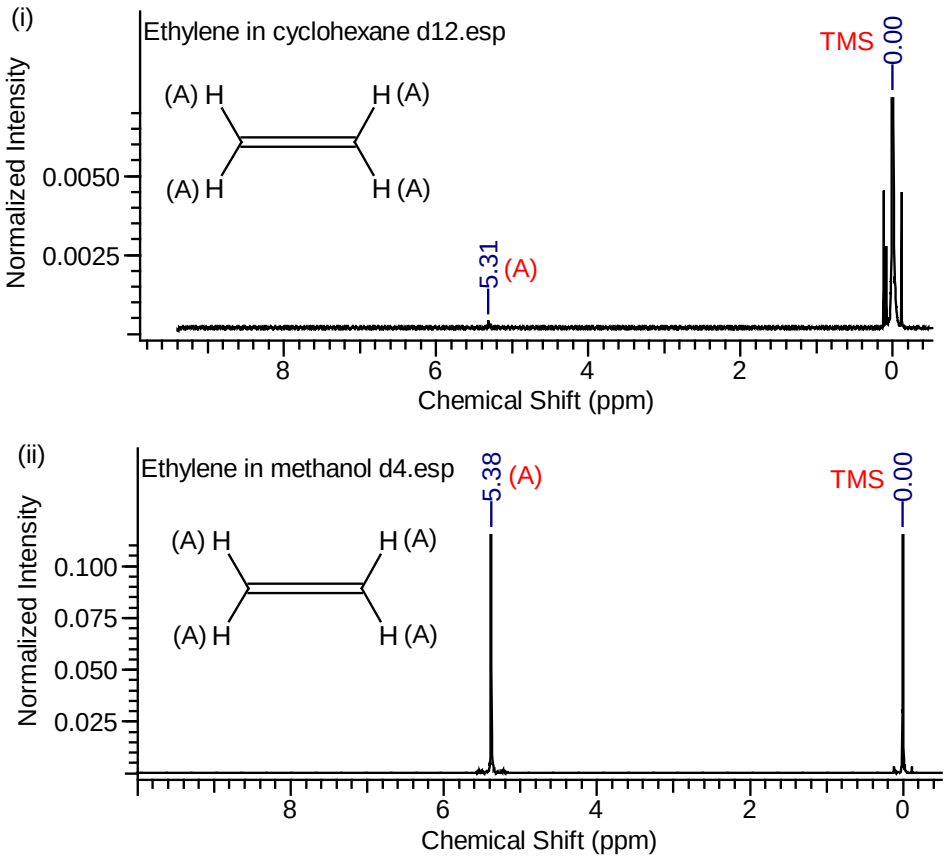

Fig. 28 ^{1}H-NMR spectra of ethylene in cyclohexane-d_{12} (i) and in methanol-d_4 (ii)

Table 16. ^{1}H-NMR results for the ethylene in methanol-d_4 or cyclohexane-d_{12}

Alkene / Proton	Ethylene in cyclohexane-d_{12} δ^a	Ethylene in methanol-d_4 δ^a ($\Delta\delta^b$)
A	5.31	5.38 (0.07)

^{a} Chemical shift (in ppm). ^{b} Corresponding chemical shift change (in ppm).

Matthias et al. studied of the weak hydrogen bond interactions in the methanol-ethylene clusters, they concluded the main interaction in methanol-ethylene was the O—H···π (π-type) hydrogen bond interaction.[19] This hydrogen bond interaction forms between ethylene's π-electron system and hydrogen atom of methanol's hydroxyl group.[16, 17] Due to the electrostatic interaction the electron density from the alkene's π-electron system is donated to the acidic proton (σ* orbital) of the methanol's hydroxyl, and this reduces the electron density of the protons (A) and enhance the deshielding effect on these protons.[3, 20]

Propylene···methanol H-bond interaction

The ^{1}H-NMR spectra of solutions of propylene in both of these solvents are shown in Fig. 29. The numerical chemical shift of the various protons has also been indicated, and the location (A-D) of the propylene's protons in corresponding to their geometric positions are also labelled in Fig. 29.

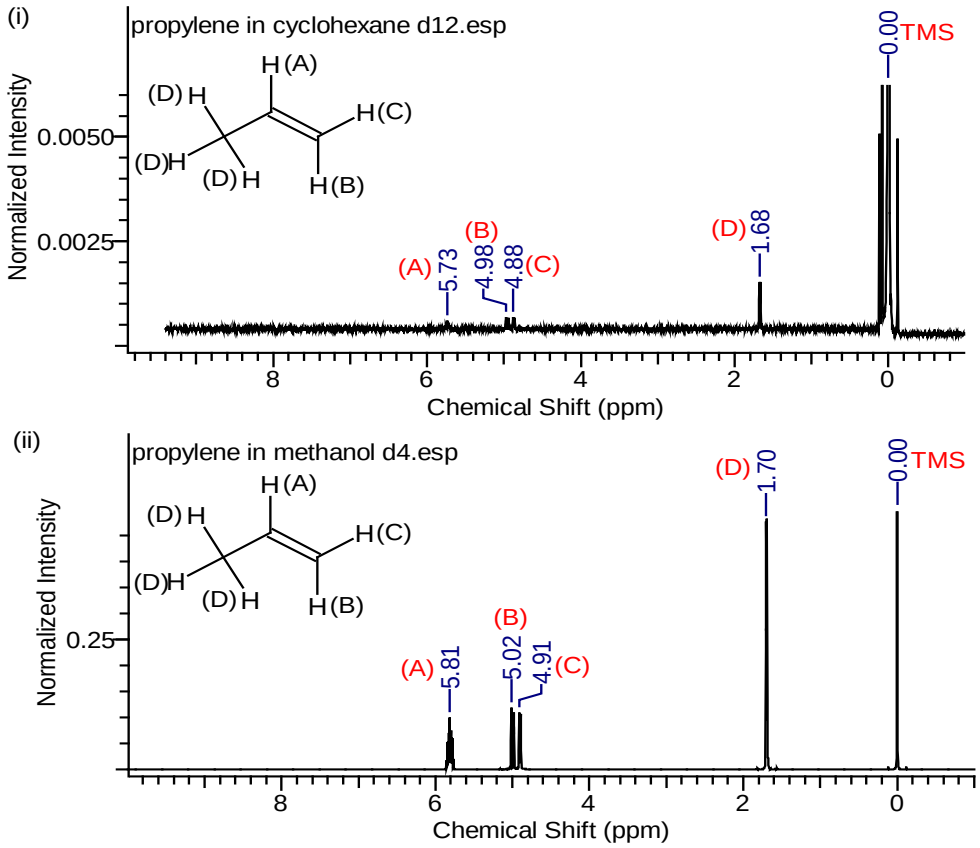

Fig. 29 ^{1}H-NMR spectra of propylene in cyclohexane-d_{12} and in methanol-d_4

Table 17. ^{1}H-NMR results for the propylene in methanol-d_4 or cyclohexane-d_{12}

Alkene / Proton	Propylene in cyclohexane-d_{12} δ^a	Propylene in methanol-d_4 δ^a ($\Delta\delta^b$)
A	5.73	5.81 (0.08)
B	4.98	5.02 (0.04)
C	4.88	4.91 (0.03)
D	1.68	1.70 (0.02)

^{a} Chemical shift (in ppm). ^{b} Corresponding chemical shift change (in ppm).

The NMR data reveal that when propylene is dissolved in methanol, all the protons are deshielded relative to those in cyclohexane solutions with chemical shifts moving downfield. The chemical shift change of the protons located at D (Fig. 29) is due to methanol's solvent effect.[21, 22] Bulk magnetic susceptibility differences between cyclohexane and methanol will make contributions to the magnetic shielding of all

alkene's constituent protons but these would be identical and independent of their position along the hydrocarbon chain. The fact that the observed chemical shifts are different in magnitude for all constituent carbon atoms points to site-specific interactions contributions to the magnetic shielding (Table 17). The protons located at B and C now become more deshielded as compared to the corresponding values in cyclohexane. These chemical shift changes (Δδ in Table 17) for the proton located at (A), (B) and (C) were 0.08 ppm, 0.04 ppm and 0.03 ppm (Table 17). These shifts are outside of the error estimates (+/- 0.004ppm) in carefully measured chemical shifts of multiple samples.

It also has been noted that these (A), (B) and (C) protons are located on the unsaturated carbon atom. These shifts are proposed originate from the weak O—H···π (π-type) and C—H···O (σ-type) hydrogen bond.[16, 17]

When the π-type weak hydrogen bond is formed, propylene therefore acts as a base and due to the electrostatic interaction, the electron density from the propylene's π-electron system is donated to acidic proton (σ* orbital) of the methanol's hydroxyl.[20]

For the σ-type hydrogen bond interaction, where the oxygen atom on methanol acts as an hydrogen bond acceptor and due to an electrostatic interaction;[3] the electron density from the methanol's oxygen atom is donated to protons (B) and (C) of propylene.[23]

Because of the formation of these weak hydrogen bonds the electron density of the protons linked to the alpha carbon atom is thereby decreased. This leads to the

enhancement of the deshielding effect on these protons. As a result, the chemical shift of these protons moved to downfield (the chemical shift became bigger). It is particularly noteworthy, that the chemical shift change of the protons (A), (B) and (C) is larger than that of the remaining protons (D).

Compared with the energy of O—H···π interaction, the C—H···O interaction between propylene and the methanol molecule is weaker.[16] This can be observed from the shielding effect of these hydrogen bond interactions which reflected by the ^{1}H-NMR spectra (Fig. 29). The (D) proton's Δδ towards downfield is smaller than (B) and (C) protons' (Table 17).

1-butene···methanol H-bond interaction

It can be observed from the^{1}H-NMR spectra (Fig. 30) that all the protons are deshielded relative to those in cyclohexane solutions with chemical shifts moving downfield (Table 18),[39, 41] when 1-butene is dissolved in methanol.

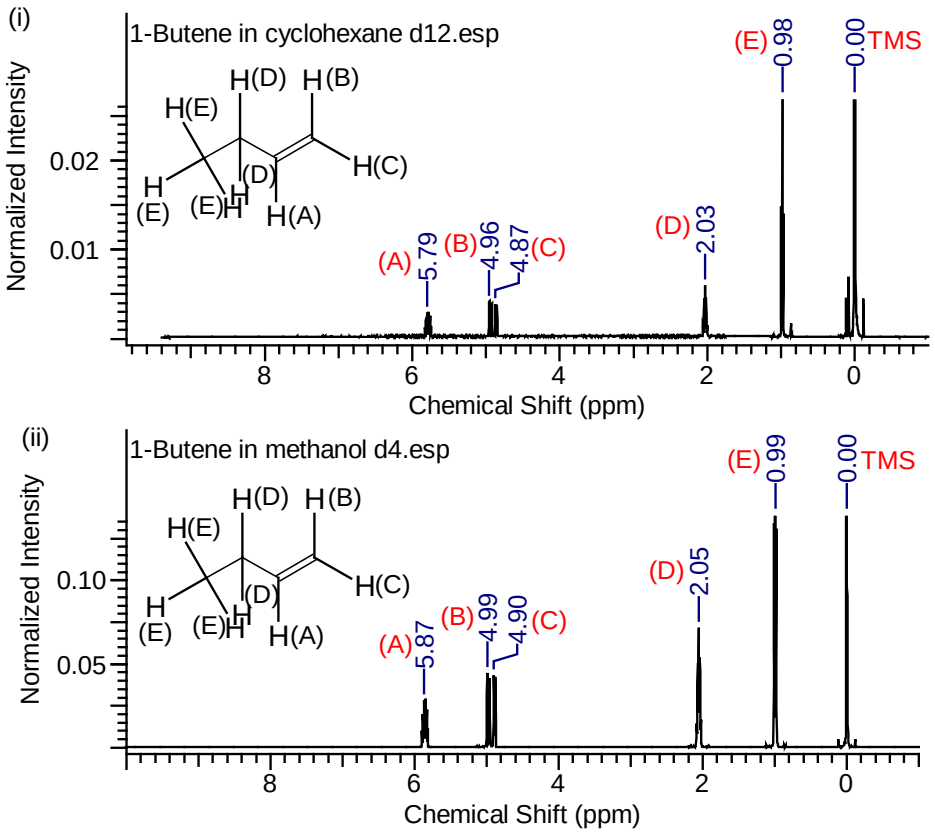

Fig. 30 ^{1}H-NMR spectra of 1-butene in cyclohexane-d_{12} (i) and in methanol-d_4 (ii)

Table 18. ^{1}H-NMR results for the 1-butene in methanol-d_4 or cyclohexane-d_{12}

Alkene / Proton	1-butene in cyclohexane-d_{12} δ^a	1-butene in methanol-d_4 δ^a ($\Delta\delta^b$)
A	5.79	5.87 (0.08)
B	4.96	4.99 (0.03)
C	4.87	4.90 (0.03)
D	2.03	2.05 (0.02)
E	0.98	0.99 (0.01)

[a] Chemical shift (in ppm). [b] Corresponding chemical shift change (in ppm).

Protons (A), (B) and (C)'s chemical shift changes (Δδ in Table 18) were 0.08 ppm, 0.03 ppm and 0.03 ppm (Table 18), and as compared to the corresponding values in cyclohexane they become deshielded. These shifts are also believed to originate from the weak O—H···π (π-type) and C—H···O (σ-type) hydrogen bond.[16, 17] As for

propylene in methanol, when the π-type or σ-type weak hydrogen bond are formed between 1-butene and methanol, due to the electrostatic interaction,[3] the electron density from the alkene's π-electron system or from methanol's oxygen atom are donated to acidic proton (σ* orbital) of the methanol's hydroxyl or protons (B) and (C),[20, 23] respectively.

Compared with the energy of π-type interaction, the σ-type interaction between 1-butene and the methanol molecule is much weaker.[16] Thus, the formation of these weak hydrogen bonds leads to the reduction of the electron density of these protons (A), (B) and (C), it enhances the deshielding effect on these protons as consequence. Therefore, the chemical shift of these protons all moved to downfield. This also can be observed from the deshielding effect of these hydrogen bond interactions which are reflected by the ^{1}H-NMR spectra (Fig. 30), the (D) and (E) protons' chemical shift change towards downfield is smaller than (B) and (C) protons' Δδ (Table 18).

Isobutene···methanol H-bond interaction

The ^{1}H-NMR spectrum of the isobutene in cyclohexane and methanol are presented in Fig. 31, the alkene protons' chemical shift and chemical shift change of these protons relative to those in cyclohexane solutions are shown in Table 19.

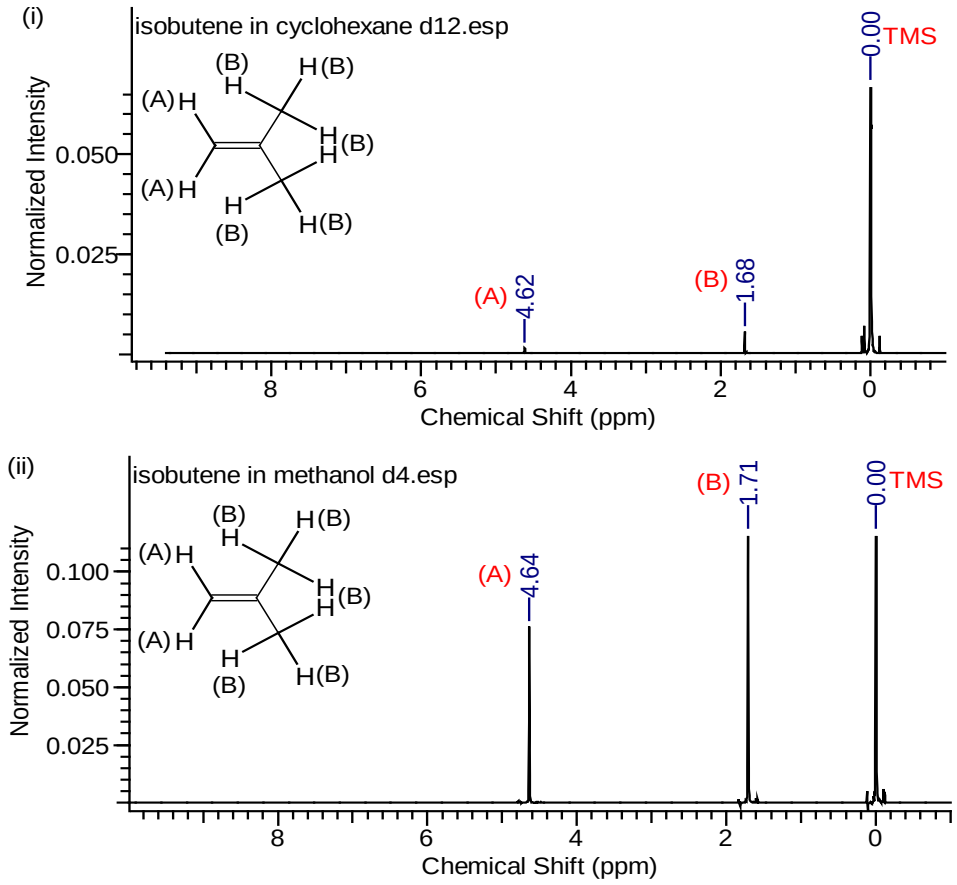

Fig. 31 ^{1}H-NMR spectra of isobutene in cyclohexane-d_{12} and in methanol-d_4

Table 19. ^{1}H-NMR results for the isobutene in methanol-d_4 or cyclohexane-d_{12}

Alkene / Proton	Isobutene in cyclohexane-d_{12} δ^a	Isobutene in methanol-d_4 δ^a ($\Delta\delta^b$)
A	4.62	4.64 (0.02)
B	1.68	1.71 (0.03)

[a] Chemical shift (in ppm). [b] Corresponding chemical shift change (in ppm).

When 1-butene is dissolved in methanol, protons (A)'s chemical shift changes ($\Delta\delta$ in Table 19) were 0.02 ppm (Table 19), and as compared to the corresponding values in cyclohexane they become deshielded. It has been supposed that the protons (A)'s positive $\Delta\delta$ is because of the weak O—H···π and weaker C—H···O interaction, which formed between isobutene's π cloud and proton of methanol's hydroxyl group

or between isobutene's protons (A) and oxygen atom of methanol's hydroxyl group.[16, 17] When these hydrogen bonds are formed, due to the electrostatic interaction,[3] the electron density from the isobutene's π-electron system or from methanol's oxygen atom are donated to the acidic proton (σ* orbital) of the methanol's hydroxyl or to protons (A), respectively.[20, 23] Since the σ-type C—H···O interaction is weaker than the π-type O—H···π interaction,[16] as a consequence, the electron density of protons (A) decreased, this enhances the deshielding effect on these protons and leads their chemical shift move to downfield (Fig. 31).

Cis-2-butene···methanol H-bond interaction

It can be observed from the cis-2-butene in methanol ^{1}H-NMR spectra (Fig. 32), compared to the corresponding chemical shift value of the this alkene's protons in cyclohexane, protons (A)'s chemical shift changes (Δδ in Table 20) were 0.04 ppm (Table 20), that means when cis-2-butene dissolved in methanol protons (A) are become deshielded.

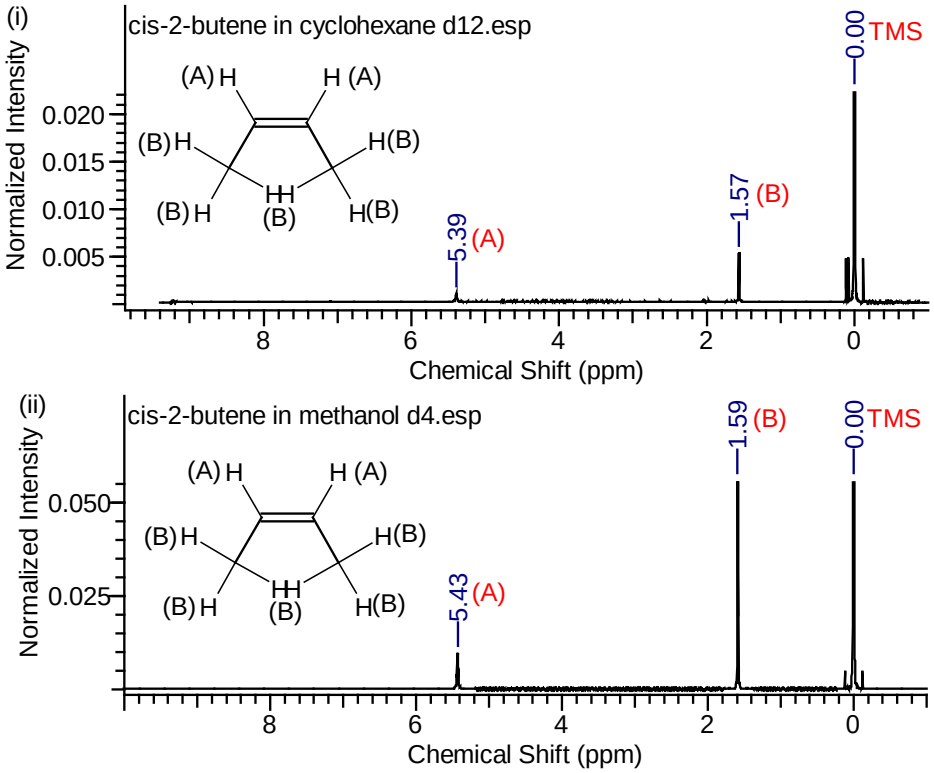

Fig. 32 ^{1}H-NMR spectra of cis-2-butene in cyclohexane-d_{12} (i) and in methanol-d_4 (ii)

Table 20. ^{1}H-NMR results for the cis-2-butene in methanol-d_4 or cyclohexane-d_{12}

Alkene / Proton	Cis-2-butene in cyclohexane-d_{12} δ^a	Cis-2-butene in methanol-d_4 δ^a ($\Delta\delta^b$)
A	5.39	5.43 (0.04)
B	1.57	1.59 (0.02)

[a] Chemical shift (in ppm). [b] Corresponding chemical shift change (in ppm).

The shielding effect leads the protons (A)'s chemical shift move to downfield. This deshielding effect is supposed to be influenced by the combination of the weak O—H···π interaction formed between cis-2--butene's π cloud and proton of methanol's hydroxyl group, and C—H···O interaction between cis-2-butene's protons and oxygen atom of methanol's hydroxyl group.[16, 17] When the O—H···π hydrogen bonds and C—H···O hydrogen bonds are formed, the electron density from the

alkene's π-electron system or from methanol's oxygen atom are donated to the acidic proton (σ* orbital) of the methanol's hydroxyl or to cis-2-butene's protons (A) due to the electrostatic interaction, respectively.[3, 20, 23] Since the σ-type C—H···O interaction is weaker than the π-type O—H···π interaction,[16] the overall consequence is that this leads these protons' chemical shift move to downfield (Fig. 32).

Trans-2-butene···methanol H-bond interaction

Fig. 33 shows the ^{1}H-NMR spectrum of the trans-2-butene in cyclohexane d12 and methanol d4, and the numerical data of the alkene protons' chemical shift and their chemical shift changes observed from the spectrum is presented in Table 21.

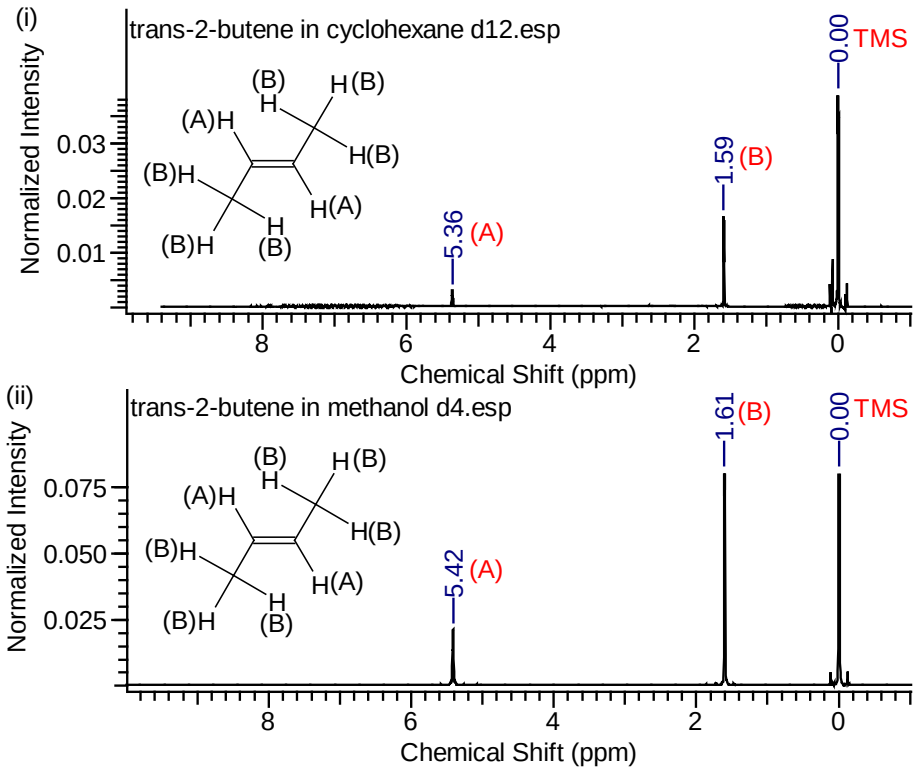

Fig. 33 ^{1}H-NMR spectra of trans-2-butene in cyclohexane-d_{12} (i) and in methanol-d_4 (ii)

Table 21. ^{1}H-NMR results for the trans-2-butene in methanol-d_4 or cyclohexane-d_{12}

Alkene / Proton	Trans-2-butene in cyclohexane-d_{12} δ^a	Trans-2-butene in methanol-d_4 δ^a ($\Delta\delta^b$)
A	5.36	5.42 (0.06)
B	1.59	1.61 (0.02)

^{a} Chemical shift (in ppm). ^{b} Corresponding chemical shift change (in ppm).

As a very similar case, Lester et al. 1982 indicated that, in the FTIR matrix spectra when trans-2-butene mix with hydrogen fluoride, a weak 996 cm^{-1} band was observed above the 977 cm^{-1} C—H wagging mode of the base (trans-2-butene) in argon.[24] This 19 cm^{-1} blue shift is assigned to the C—H···F (σ-type) hydrogen bond interaction (complex) between trans-2-butene and hydrogen fluoride molecules, which always lead the blue shift to the C—H's rocking absorption in the FTIR spectra.[24, 25]

Based on Matthias et al., Lester et al. and Taisuke et al.'s previous studies and according to the very similar symmetric molecular structure of trans-2-butene and ethylene,[24, 26] it is believed that interactions between trans-2-butene and methanol molecules is the π-type and σ-type hydrogen bond interaction.[16, 17] The π-type hydrogen bond is formed between trans-2--butene's π cloud and proton of methanol's hydroxyl group, the σ-type hydrogen bond is formed between trans-2-butene's (A) protons and oxygen atom of methanol's hydroxyl group.[16, 17] When the O—H···π hydrogen bonds and C—H···O hydrogen bonds are formed, the electron density from the trans-2--butene's π-electron system or from methanol's oxygen atom are donated to the proton (σ* orbital) of the methanol's hydroxyl or to trans-2-butene's protons (A)

due to the electrostatic interaction, respectively.[3, 17, 20] The shielding effect caused by the σ-type hydrogen bond interaction between trans-2-butene and methanol is weaker than the π-type interaction.[16] Therefore, when trans-2-butene dissolved into methanol instead of cyclohexane, downfield direction chemical shift change (positive Δδ) 0.06 ppm of protons (A) can be observed (Table 21).

4.2.2 NMR Analysis on Methanol with Various Liquid Alkene Mixtures

For the methanol with liquid alkenes mixtures, 1-pentene and 1-hexene are considered as the solutes and methanol as the host solvent. The numerical NMR chemical shifts of the various protons are indicated in Figs. 32 and 33 and the location (A-F) of the 1-pentene and 1-hexene's protons are also labelled. These chemical shifts observed from the spectra are outside of the experimental error estimates (+/- 0.004ppm). The error estimates analysis of the ^{1}H-NMR spectrum test is described in Appendix 3.2.

The NMR data reveal that when 1-pentene and 1-hexene are dissolved in methanol, all the protons are de-shielded relative to those in cyclohexane solutions with chemical shifts moving downfield. The chemical shift change of the protons located at D, E and F (Fig. 34 and 33) is due to methanol's solvent effect.[21, 22] The protons located at A, B and C become more de-shielded as compared to the other protons located at D, E and F (Fig. 34 and 33). The chemical shift changes (denoted as Δδ in Table 22) for the 1-pentene's proton located at (A), (B) and (C) were 0.06 ppm, 0.04 ppm and 0.03 ppm, for the 1-hexene's proton located at (A), (B) and (C) were 0.06 ppm, 0.03 ppm and 0.03 ppm (Table 22).

These (B) and (C) protons are located on the outermost alpha, unsaturated carbon atom (Fig. 34 and 33).

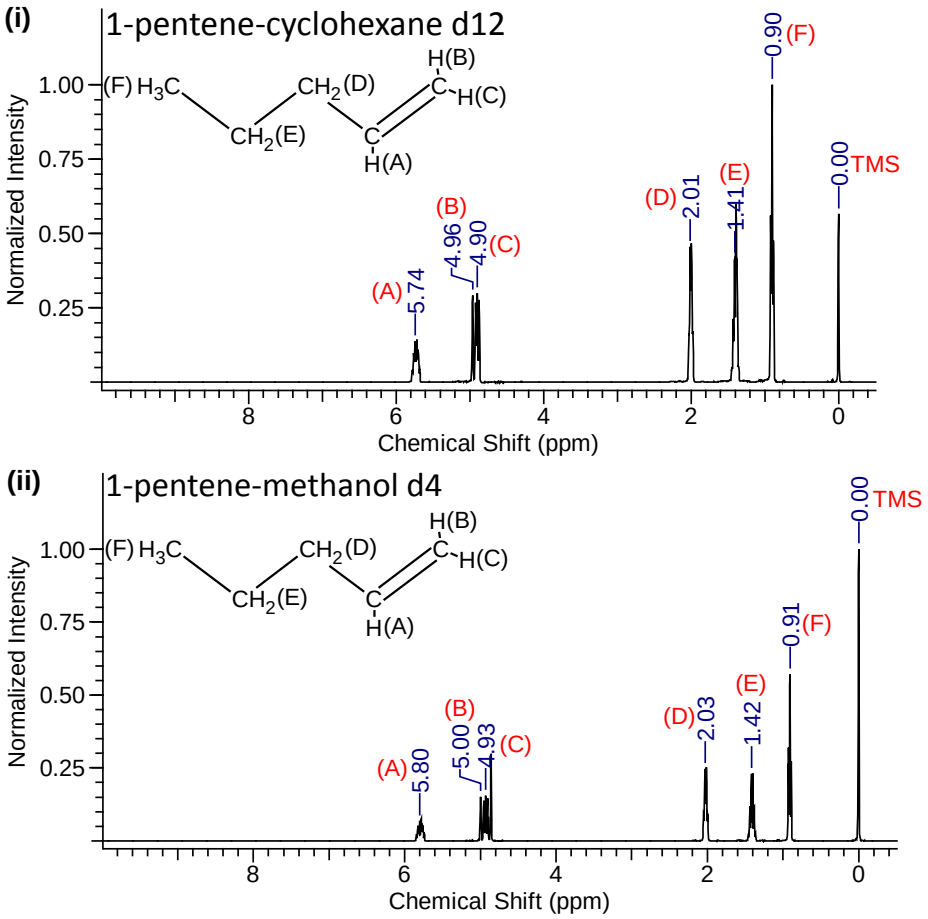

Fig. 34 ^{1}H-NMR spectra of 1-pentene in cyclohexane-d_{12} (i) and in methanol-d_4 (ii)[14]

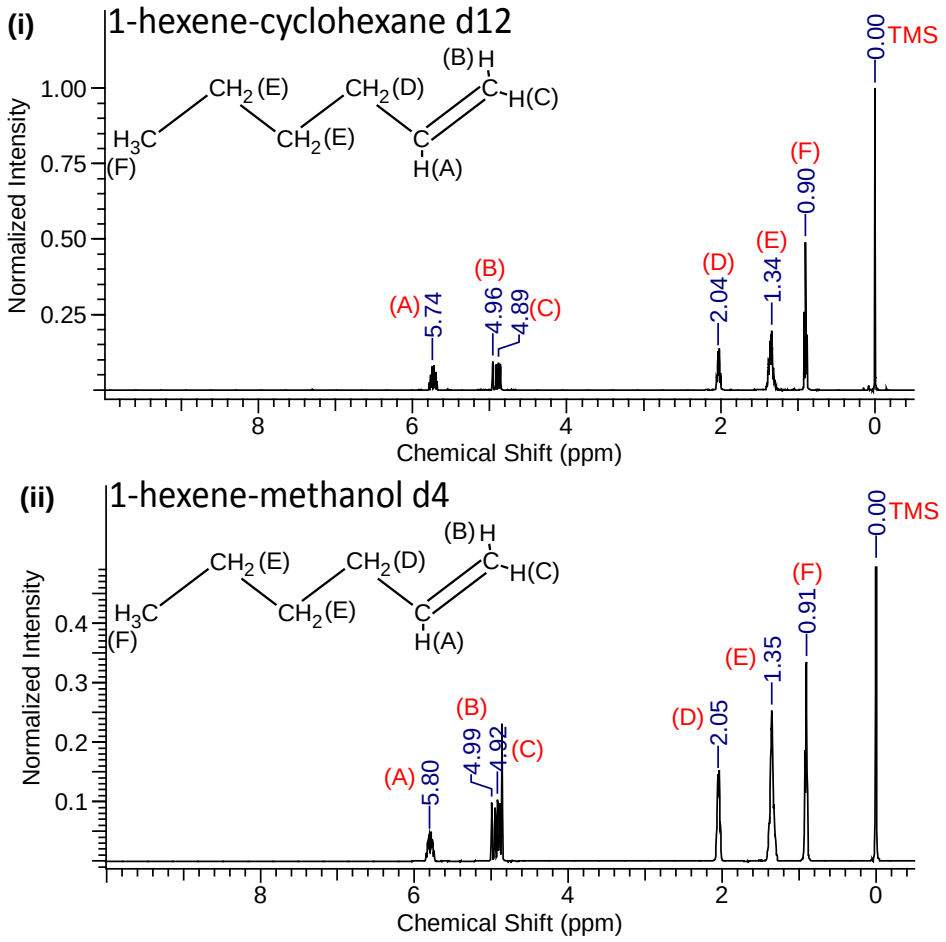

Fig. 35 ^{1}H-NMR spectra of 1-hexene in cyclohexane-d_{12} (i) and in methanol-d_4 (ii)[14]

The complete ^{1}H-NMR results for the mixture of 1-pentene and 1-hexene in cyclohexane-d_{12} or methanol-d_4 are listed in Table 24, respectively.

Table 22. ^{1}H-NMR results for the mixtures of 1-pentene and 1-hexene in methanol-d_4 or cyclohexane-d_{12}

Alkene / Proton	1-pentene in cyclohexane-d_{12} δ^a	1-pentene in methanol-d_4 δ^a ($\Delta\delta^b$)	1-hexene in cyclohexane-d_{12} δ^a	1-hexene in methanol-d_4 δ^a ($\Delta\delta^b$)
A	5.74	5.80 (0.06)	5.74	5.80 (0.06)
B	4.96	5.00 (0.04)	4.96	4.99 (0.03)
C	4.90	4.93 (0.03)	4.89	4.92 (0.03)
D	2.01	2.03 (0.02)	2.04	2.05 (0.01)
E	1.41	1.42 (0.01)	1.34	1.35 (0.01)
F	0.90	0.91 (0.01)	0.90	0.91 (0.01)

[a] Chemical shift (in ppm). [b] Corresponding chemical shift *change* (in ppm).

Bulk magnetic susceptibility differences between cyclohexane and methanol will make contributions to the magnetic shielding of all constituent protons; and these should be identical and independent of their position along the hydrocarbon chain. The fact that the observed chemical shifts for the H associated with all constituent carbon atoms are different – importantly in magnitude (Table 22) – reflect site-specific interactions which contribute to the magnetic shielding of individual protons.

The combination of the spectroscopic data enable us to propose that these NMR chemical shifts originate from the two types of alkene-methanol interactions highlighted in our computational studies (Fig. 27)

The first is the O—H···π interaction.[16, 19] When the O—H···π weak hydrogen bond is formed, the 1-pentene or 1-hexene acts as a π base (hydrogen bond acceptor) where the electron density from the alkene's π-electron system is donated to the acidic proton (σ* orbital) of the methanol's hydroxyl, and this reduces the electron density of the protons (A), (B) and (C) which are linked with the unsaturated carbon atom in the alkenes.[14, 18, 20, 27]

The second type is the C—H···O interaction,[17] where the oxygen atom on methanol acts as an hydrogen bond acceptor,[18, 27] and due to an electrostatic interaction the electron density from the methanol's oxygen atom is donated to the protons located at (B) and (C) of 1-pentene or 1-hexene.[3, 14, 23, 28] However, compared with the energy of O—H···π interaction, the C—H···O interaction between these alkenes and methanol molecule is weaker.[16]

Because of the formation of these hydrogen bonds, the electron density of the protons linked to the unsaturated carbon atom is thereby decreased. This leads to the reduction of the shielding effect on these protons. It is particularly noteworthy that the chemical shift changes of the protons (A) to (C) increases more than the remaining protons (D) to (F) (Table 22).

Hence, through the analysis of these ^{1}H-NMR results, it has been found that weak hydrogen bonds are formed between methanol and alkenes through the interaction of the π-electron cloud of alkenes and the hydrogen atom of methanol's hydroxyl group,[16, 29] together with the interaction of a proton of these alkenes and the oxygen atom of the hydroxyl group in methanol.[14, 23]

4.2.3 NMR Analysis on Methanol with Thiophene Mixture

Regarding another liquid mixture system, the methanol with thiophene mixture, the O—H···S interaction is the accepted hydrogen bond which is formed between thiophene and methanol molecules.[30] The sulphur atom in the thiophene molecule acts as the electron donor in the hydrogen bond,[31] and the proton donor (electron acceptor) O—H is the hydroxyl group in methanol.[3, 32] Accordingly, it is proposed that during the solubilisation process, a hydrogen bond is formed between the thiophene and methanol molecule as the O—H···S structure. The ^{1}H-NMR spectra of thiophene with methanol d_4 and cyclohexane d_{12} are shown in Fig. 36, and the chemical shift of each proton has been marked in this figure with their locations. The chemical shifts are also outside of the experimental error estimates (+/- 0.004ppm). The error estimates analysis of the ^{1}H-NMR spectrum test is described in Appendix 3.2.

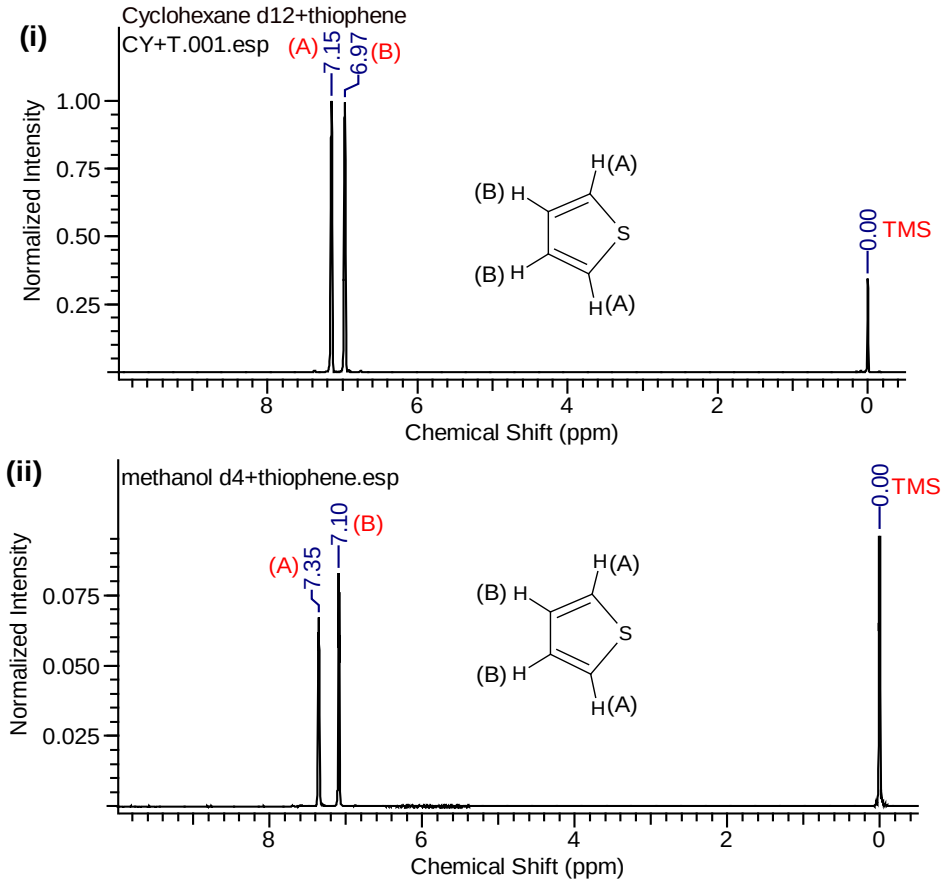

Fig. 36 ^{1}H-NMR spectra of thiophene in cyclohexane-d_{12} (i) and in methanol-d_4 (ii)

Table 23. ^{1}H-NMR results for the thiophene in methanol-d_4 or cyclohexane-d_{12}

Thiophene / Proton	Thiophene in cyclohexane-d_{12} δ^a	Thiophene in methanol-d_4 δ^a ($\Delta\delta^b$)
A	7.15	7.35 (0.20)
B	6.97	7.10 (0.13)

[a] Chemical shift (in ppm). [b] Corresponding chemical shift change (in ppm).

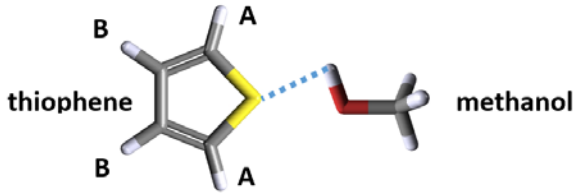

Fig. 37 Proposed structures of hydrogen bond (dashed line) between the molecule of thiophene and methanol

^{1}H-NMR results indicates that there is a downfield chemical shift change (deshielded) for every thiophene proton in methanol as compared to the NMR of thiophene in a reference non-polar solvent, here cyclohexane. This difference in chemical shifts is defined as Δδ. The chemical shift change of the thiophene's protons (A) (Δδ=0.20 ppm) is 0.07 ppm larger than that of protons (B) (Δδ=0.13 ppm) (Table 23). Protons (A) in the thiophene are linked to the carbon atoms which directly links with the sulphur atom.

The hydrogen bonds between methanol and thiophene molecules are thought to link the proton in the methanol's hydroxyl group with the thiophene's sulphur atom through the O—H···S hydrogen bond. Here, the sulphur atom in thiophene acts as electron donor with its electron density donated to the methanol's hydroxyl-moiety. Thus, the sulphur atom's electron density decreased. Thereafter, the electron density of the protons linked to the carbon atoms attached to the sulphur atom (protons A) and linked to other carbon atoms (protons B) is also decreased because of the electrostatic interaction. This leads to the reduction of the shielding effect on these protons (A) and (B), and hence downfield chemical shift of these protons. Moreover, since protons (B) not linked to the carbon atom which attached to the sulphur atom directly, these protons lose less electron density than protons (A). Thus, protons (B)'s shielding effect is stronger than protons (A). As consequence, when thiophene dissolved in methanol, thiophene's protons (B) indicate smaller chemical shift change than protons (A) (Table 23).

Therefore, these ^{1}H-NMR results suggest that the hydrogen bond formed between

the thiophene and methanol is bridged by the sulphur atom's electron cloud of the thiophene and the proton of methanol's hydroxyl group (Fig. 37).[30]

4.2.4 The Effect of Molecular Dipole Moment

From the results of the previous solubility tests, without considering the miscible liquid alkenes, the gaseous alkenes solubility in methanol indicate an obvious positive correlation with the dipole moment of these alkenes (Fig. 38). Among all the gaseous alkenes, ethylene has no dipole moment (Table 24), and it also has the lowest solubility in methanol at 20℃/293.15 K and with 1.8 bar pressure (Fig. 38).[33-35] In contrast, isobutene with the largest dipole moment (0.500 D) presents the best solubility in methanol under the same conditions (Fig. 38).[33-35]According to these results, it can be tentatively concluded that there should have some connections between the dipole moments of the various alkenes and their solubility in the solvent methanol at the microscopic hydrogen bond interaction aspect.

Table 24. Gaseous alkenes' dipole moments[33-35]

Compounds	Permanent Dipole Moment μ (D)
Ethylene	0.000
Propylene	0.350
1-butene	0.380
Isobutene	0.500
Cis-2-butene	0.257
Trans-2-butene	0.001
1-pentene	0.483
1-hexene	0.490

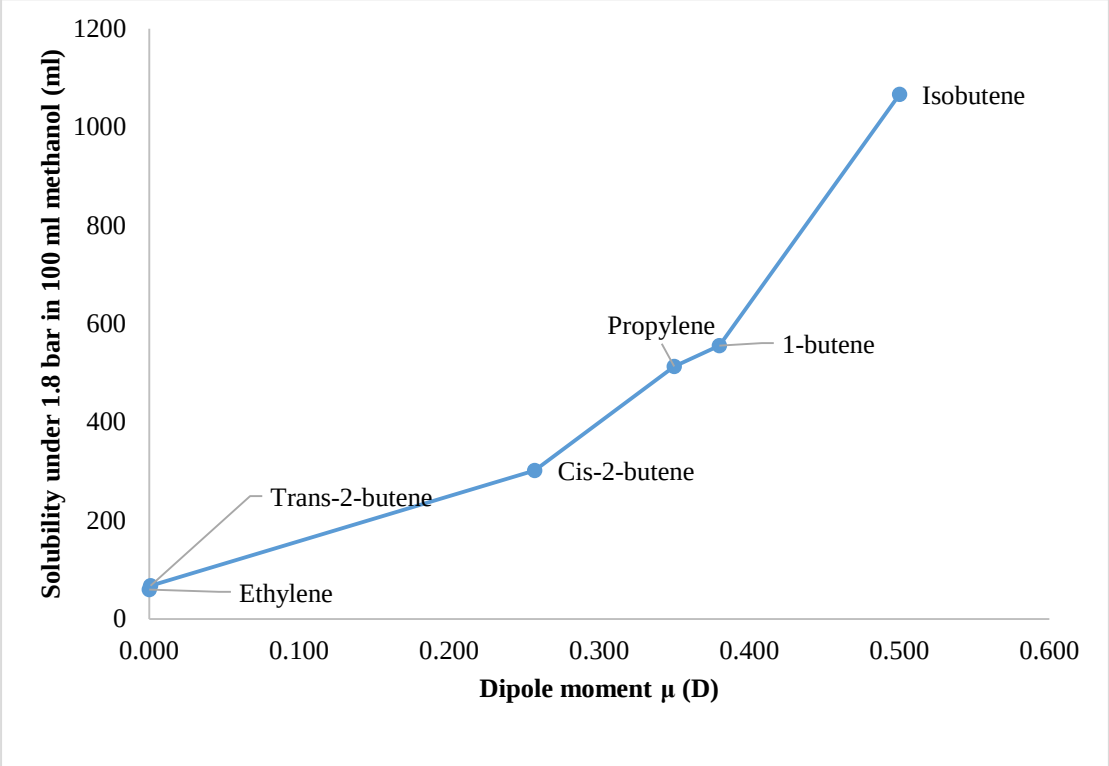

Fig. 38 Solubility of each gaseous alkenes in methanol under 20 ℃/293.15 K and 1.8 bar

From the ^{1}H-NMR spectrum of various alkenes with solvent methanol, it has been found when smaller dipole moment alkenes dissolved in methanol, the former protons' chemical shift change Δδ becomes more positive relative to it dissolved in cyclohexane (Fig. 39).

This study focuses on the olefinic protons. Due to the molecular steric shielding effects during the formation of hydrogen bond between alkenes and methanol, these olefinic protons require the electron density the most.[36] These target protons are controlling where and from what direction a intermolecular interaction like hydrogen bond can take place.[37]

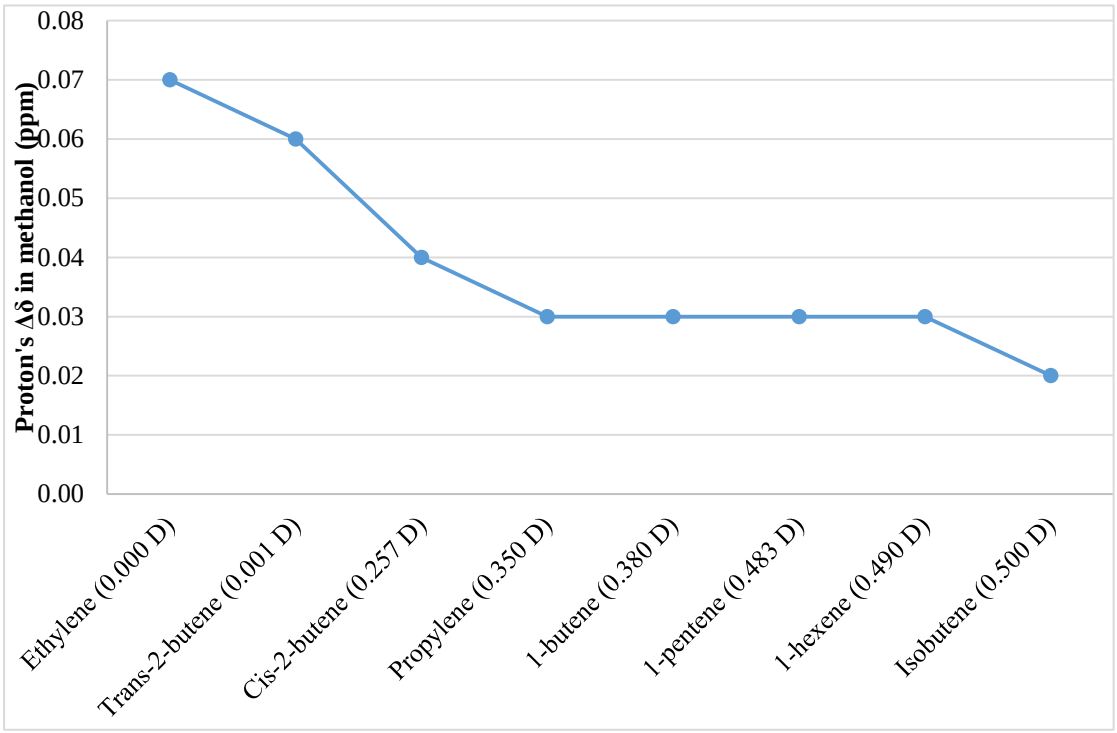

Fig. 39 Chemical shift change Δδ of the target protons for the alkenes in methanol-d_4 when compared with corresponding solutions in cyclohexane-d_{12}

In the ^{1}H-NMR spectra, a more positive chemical shift change, Δδ, means the protons are influenced by stronger deshielding effect, and this deshielding effect is negatively correlated to the electron density of these protons.[3, 23] Whilst the electron density change of the target proton indicates the strength of the electrostatic (π-type and σ-type hydrogen bond) interaction between the various alkenes and methanol molecules, and they present negative correlation with each other since the stronger π-type hydrogen bond withdraw the electron density from the target proton and the weaker σ-type hydrogen bond donate the electron density to the target proton.[3, 16, 17, 20, 23] Thus, the strength of the hydrogen bond formed between alkenes and methanol is reflected by the constituent proton's chemical shift change Δδ in the ^{1}H-NMR spectrum; namely the stronger hydrogen bond is, the less positive Δδ will be.

We note that ethylene, having no dipole moment generates the weakest hydrogen bond interaction with methanol,[33] and isobutene with the largest dipole moment (0.500 D) among all the light alkenes forms the strongest hydrogen bond with methanol (Fig. 39). In general, the hydrogen bond strength between alkene and methanol molecules therefore presents an important positive correlation with the alkene's dipole moment, and also the solubility, as shown in Fig. 38.

From a molecular aspect, many factors affect the various alkenes' dipole moment, and these obviously influence the hydrogen bond interaction between an alkene and methanol. The molecular dipole moment depends on the difference in electronegativity between atoms in a molecule and the asymmetry of the molecular structure.[38]

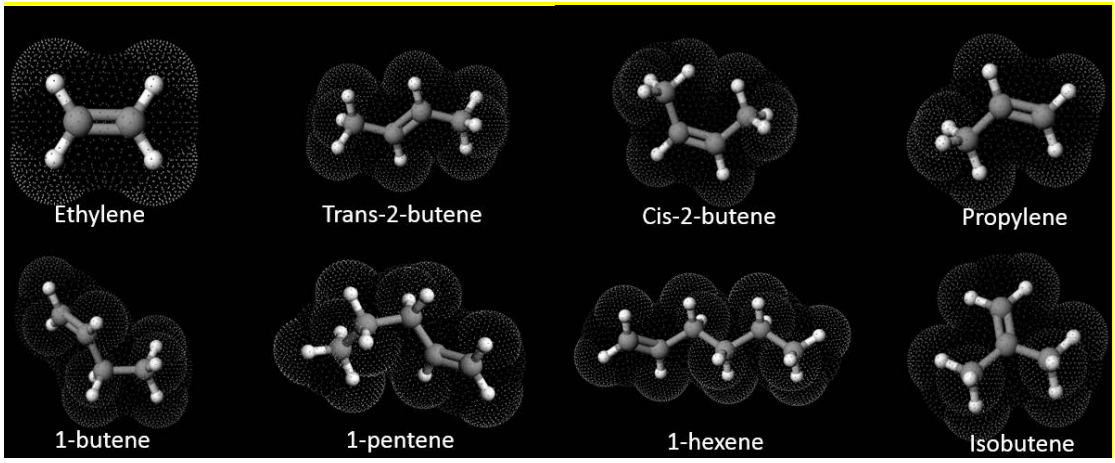

Fig. 40 Structure of alkene molecules[39]

Ethylene is the most symmetric structure molecule among all the other alkenes (Fig. 40), leading ethylene to have zero dipole moment,[33] and the solvent methanol's dipole moment is 1.69 D. Meanwhile, as the dipole moments of both the hydrogen bond donor and acceptor indicates positive correlation to the dipole-dipole (electrostatic) interaction,[40] that means large dipole moment of both hydrogen bond donor and

acceptor give rise to a large dipole-dipole (hydrogen bond) interaction.[40-42] The symmetric structure also brings much lower proton affinities (680 kJ/mol) to ethylene than other alkenes, such as propylene (751 kJ/mol),[43] it is clear that the former is a much reduced proton acceptor (hydrogen bond).[26] In general, ethylene's zero dipole moment induces a very weak hydrogen bond interaction between methanol and this hydrogen bond interaction is even weaker than the solvent effect of methanol.[39, 41] Hence, as observed from the ^{1}H-NMR spectrum, the protons (A) present the largest positive chemical shift change (0.08 ppm) when ethylene dissolved in methanol than cyclohexane (Fig. 28).

The dipole moment of the alkene molecule is increased by the introduction of more polar constituent groups,[44] such as alkene's alkyl chain, which brings small and limited dipole moment to the alkenes.[45] Trans-2-butene also has very symmetric molecular structure which is very similar to the ethylene's. However, it has two polar constituent methyl groups (Fig. 40). This brings a very small dipole moment (0.001 D) to trans-2-butene than the completely symmetric ethylene.[33-35] Hence, trans-2-butene's hydrogen bond strength with methanol is stronger than that with ethylene. This is reflected by the reduced (positive) chemical shift change $\Delta\delta$ (0.07 ppm) of trans-2-butene in methanol than ethylene in methanol (Fig. 39).

Compared with trans-2-butene, cis-2-butene molecule has an even more asymmetric structure (Fig. 40). Thus, cis-2-butene gets relative larger dipole moment (0.257 D).[33-35] When dissolved in methanol, cis-2-butene target protons' $\Delta\delta$ is 0.04 ppm (Fig. 39), that means a stronger hydrogen bond has been formed between

methanol and cis-2-butene than trans-2-butene.

With a more asymmetric structure than ethylene and trans/cis-2-butene (Fig. 40), propylene present a larger dipole moment 0.350 D than those three alkenes.[34] Therefore, one sees a less positive Δδ (0.03 ppm) of the propylene's target protons as shown in Fig. 39. These indicate a stronger hydrogen bond formed between methanol and propylene than ethylene, trans-2-butene or cis-2-butene.

The dipole moment of the constituent alkene is also related to the length of the alkene's alkyl chain.[46] Because of the ethyl group constituent (Fig. 40), 1-butene shows a slightly larger dipole moment (0.380 D) than propylene.[34] Thus, when 1-butene dissolves in methanol, the slightly stronger hydrogen bond interaction between the solute - solvent and generates similar chemical shift change Δδ (0.03 ppm) of the 1-butene's target proton in ^{1}H-NMR spectra as propylene in methanol (Fig. 39).

With a longer alkyl chain (Fig. 40), 1-pentene exhibits a larger dipole moment (0.483 D) than 1-butene.[33, 46] 1-pentene can form stronger hydrogen bond interaction with methanol when it dissolves in methanol as liquid mixture. The stronger hydrogen bond interaction between them leads to more negative chemical shift change Δδ (0.03 ppm) of the 1-pentene's target proton in ^{1}H-NMR spectra than ethylene, trans-2-butene or cis-2-butene in methanol (Fig. 39).

Moreover, 1-hexene has an even longer alkyl chain than 1-pentene (Fig. 40), and this makes 1-hexene have slightly larger dipole moment (0.490 D) than 1-pentene.[33, 46] Thus, the hydrogen bond interaction formed between 1-hexene and methanol molecules are slightly stronger than it formed between 1-pentene and methanol.[46] This

can be observed from the similar chemical shift change Δδ (0.03 ppm) of the 1-hexene's target proton in ^{1}H-NMR spectra (Fig. 39).

Two methyl groups present higher electron donating/ lower withdrawing ability for donating electron density to the nearby electron withdrawing group (π cloud in alkenes) than the ethyl group.[47, 48] According to this, isobutene's dipole moment (0.500 D) is larger than 1-hexene's (0.490 D),[33, 44, 46] and it is the largest among all the gaseous alkenes/alkenes studied in this research. Compared to the hydrogen bond formed between other alkenes and methanol, the hydrogen bond interaction between isobutene and methanol is the strongest. This can be observed through the least positive chemical shift change Δδ (0.02 ppm) of the isobutene's target protons in Fig. 39.

Combining the results of previous solubility analysis with the ^{1}H-NMR analysis, it can be concluded that, the larger the dipole moment of the alkene leads to a stronger hydrogen bond interaction between the alkene and methanol molecules. Therefore, the stronger the hydrogen bond the more this contributes to the enhanced solubility of the gaseous alkene in methanol. [49, 50]

4.2.5 The Effect of Temperature

Based on literature with in the research field of behaviour with upper critical solution temperature (UCST) that, the hydrogen bonding complex eventually phase separates (or precipitates) with decreasing temperature.[51-54] Therefore, Variable Temperature (VT) ^{1}H-NMR analysis was employed in this research to further explore the existence and investigate the other characteristics of the hydrogen bonds between

1-pentene/1-hexene/thiophene and methanol. The results obtained from the VT-^{1}H-NMR experiment are presented in Table 25.

Interestingly, for the hydrogen bond between 1-pentene/1-hexene and methanol, the results of the VT-^{1}H-NMR experiment show that, except for the proton located at (B) and (C) position of these alkenes, other protons' chemical shifts are not affected by temperature changes. As indicated in Table 25, with decreasing temperature (from 293.1 K to 183.1 K), the chemical shift of (B) and (C) position protons chemical shifts moved downfield. According to the literature, this phenomenon can be explained by the decreasing temperature causing the hydrogen bond between the alkene and methanol molecules to become strengthened and eventually phase separation.[51-54] Thus, due to the electrostatic interaction, more electron density was donated to the hydroxyl of methanol from the alkene's π-electron system with lower temperature. As a result, electron density of protons at position (B) and (C) is declining. It gives rise to the deshielding effect of these protons, which contributes to protons' chemical shift and leads it moving to downfield.[22]

The VT-^{1}H-NMR results of thiophene in methanol-d_4 displayed in Table 25 indicate the chemical shift of the thiophene protons at position (A) increases from 7.19 ppm to 7.20 ppm when the temperature dropped from 293.1±0.05 K to 253.1±0.05 K. Similarly, because the lower temperature makes the hydrogen bond between the thiophene and methanol molecules strengthen,[51-54] the electron density of the thiophene's sulfur atom gets smaller. Thus, due to the electrostatic interaction, the electron density of the thiophene's protons at position (A) gets smaller as well. This

result gives rise to the enhanced deshielding effect of these protons, which contributes to the proton's chemical shift and leads it moving to downfield.[22] It is important to note that, in the VT-^{1}H-NMR analysis the chemical shifts observed from the spectra are outside of the experimental error estimates (+/- 0.004 ppm). The error estimates analysis of the ^{1}H-NMR spectrum test is described in Appendix 3.2.

Through the VT-^{1}H-NMR analysis, not only the effect of various temperatures on the hydrogen bond between 1-pentene/1-hexene/thiophene and methanol has been investigated, but also the existences of these hydrogen bonds have been further confirmed. It is believed that the so called UCST phenomena might be the results of the hydrogen bond formation between the solvent and solutes.

Table 25. Chemical shift (δ) of 1-pentene, 1-hexene and thiophene in methanol-d_4 under variable temperature from the VT-^{1}H-NMR results

Temperature	Proton position of alkene	1-pentene in methanol-d_4 δ (ppm)	1-hexene in methanol-d_4 δ (ppm)	Proton position of thiophene	thiophene in methanol-d_4 δ (ppm)
293.1 K	**B**	4.94	4.93	**A**	7.19
	C	4.9	4.91		
273.1 K	**B**	4.94	4.94	**A**	7.20
	C	4.91	4.93		
253.1 K	**B**	4.95	4.95	**A**	7.20
	C	4.91	4.93		
243.1 K	**B**	N/A	4.95	**A**	N/A
	C	N/A	4.94		
193.1 K	**B**	4.96	4.97	**A**	N/A
	C	4.93	4.95		
183.1 K	**B**	4.96	N/A	**A**	N/A
	C	4.93	N/A		

4.3 Conclusions

In this work, the underlying science of the "*Extractive Refining*" and "*Extractive Distillation*" processes was first studied from the view of the solubility analysis of various liquid/gaseous solutes in solvent methanol. Then the computational quantum chemical calculations modelled the possible origins of the interaction between solute alkenes and solvent methanol, which is the hydrogen bond formation.

The weak hydrogen bonds are confirmed to be present between methanol and alkenes through the interaction of the π-electron cloud of alkenes and methanol's hydroxyl group (O—H···π),[16, 29] together with the interaction of a proton of these alkenes and the oxygen atom of methanol's hydroxyl group (C—H···O),[23] through the analysis of the ^{1}H-NMR results. The ^{1}H-NMR results also suggest that the hydrogen bond formed between the thiophene and methanol is bridged by the thiophene's sulphur atom and methanol's hydroxyl group (O—H···S).[30] Further investigation into the nature of the hydrogen bond between alkenes and methanol, and the various alkene dipole moments gives a positive correlation with the strength of these hydrogen bond, and this also affect the solubility of gaseous alkenes in methanol.

Furthermore, the VT-^{1}H-NMR analyses for various liquid mixture samples indicate that the hydrogen bond between different liquid solutes and solvent methanol becomes strengthened when a lower temperature than room temperature (20 ℃/293.1 K) is reached.

References

1 A. G. Sharpe, *Education in Chemistry* 1964, *1*, 75.

2 F. t. Franks, D. Ives, *Quarterly Reviews, Chemical Society* 1966, *20*, 1-44.

3 G. R. Desiraju, T. Steiner, *The weak hydrogen bond: in structural chemistry and biology*. Oxford University Press, New York, 2001.

4 E. A. Müller, K. E. Gubbins, *Industrial & Engineering Chemistry Research* 2001, *40*, 2193-2211.

5 L.-H. Lee, in *Fundamentals of adhesion*. Springer, New York, 1991, Chap. 1.

6 T. L. Brown, *Chemistry: the central science*. Pearson Education, Upper Saddle River, 2009.

7 C.-J. Yang, R. B. Jackson, *Energy Policy* 2012, *41*, 878-884.

8 P. Atkins, P. W. Atkins, J. de Paula, in *Atkins' Physical Chemistry*, 10th ed., Oxford University Press, Oxford, **2014**, Chap. 5, pp. 208-215.

9 F. Leder, C. A. Irani, *Journal of Chemical & Engineering Data* 1975, *20*, 323-327.

10 A. Trejo, P. Yañez, R. Eustaquio-Rincón, *Journal of Chemical & Engineering Data* 2006, *51*, 1070-1075.

11 A. W. Francis, *Industrial & Engineering Chemistry* 1944, *36*, 764-771.

12 O. P. Pavlova, A. A. Gaile, K. A. Proskuryokov, I. F. Li, *Zh. Fiz. Khim.* 1975, *49*, 2874.

13 J. W. Lorimer, F. W. Getzen, C. L. Young, P. D. Gujral, *IUPAC, Solubility Data Series Volume 56 Alcohols With Hydrocarbons*. Oxford University Press, Oxford, 1994.

14 Z. Zhang, T. Xiao, H. Al-Megren, S. A. Aldrees, M. Al-Kinany, V. L. Kuznetsov, M. L. Kuznetsov, P. P. Edwards, *Chemical Communications* 2017, *53*, 4026-4029.

15 I. Rozas, I. Alkorta, J. Elguero, *Journal of the American Chemical Society* 2000, *122*, 11154-11161.

16 K. Oku, H. Watanabe, M. Kubota, S. Fukuda, M. Kurimoto, Y. Tsujisaka, M. Komori, Y. Inoue, M. Sakurai, *Journal of the American Chemical Society* 2003, *125*, 12739-12748.

17 D. J. SUTOR, *Nature* 1962, *195*, 68-69.

18 E. Arunan, R. Desiraju Gautam, A. Klein Roger, J. Sadlej, S. Scheiner, I. Alkorta, C. Clary David, H. Crabtree Robert, J. Dannenberg Joseph, P. Hobza, G. Kjaergaard Henrik, C. Legon Anthony, B. Mennucci, J. Nesbitt David, *Pure and Applied Chemistry* 2011, *83*, 1619-1636.

19 M. Heger, R. A. Mata, M. A. Suhm, *Chemical Science* 2015, *6*, 3738-3745.

20 D. E. Rosenfeld, Z. Gengeliczki, M. Fayer, *The journal of physical chemistry. B* 2009, *113*, 13300.

21 R. J. Abraham, J. J. Byrne, L. Griffiths, M. Perez, *Magnetic Resonance in Chemistry* 2006, *44*, 491-509.

22 A. A. Bothner-By, *J. Mol. Spectrosc* 1960, *5*, 52-61.

23 B. M. Kariuki, K. D. Harris, D. Philp, J. M. Robinson, *Journal of the American Chemical Society* 1997, *119*, 12679-12680.

24 L. Andrews, G. L. Johnson, B. J. Kelsall, *Journal of the American Chemical Society* 1982, *104*, 6180-6186.
25 J. Joseph, E. D. Jemmis, *Journal of the American Chemical Society* 2007, *129*, 4620-4632 10.1021/ja067545z.
26 T. Nakanaga, K. Buchhold, F. Ito, *Chemical Physics* 2002, *277*, 171-178.
27 E. Arunan, G. R. Desiraju, R. A. Klein, J. Sadlej, S. Scheiner, I. Alkorta, D. C. Clary, R. H. Crabtree, J. J. Dannenberg, P. Hobza, *Pure and Applied Chemistry* 2011, *83*, 1637-1641.
28 G. R. Desiraju, *Chemical Communications* 2005, 2995-3001.
29 K. Kowski, W. Lüttke, P. Rademacher, *Journal of Molecular Structure* 2001, *567–568*, 231-240.
30 D. K. Singh, S. K. Srivastava, A. K. Ojha, B. P. Asthana, *Journal of Molecular Structure* 2008, *892*, 384-391.
31 S. A. Cooke, G. K. Corlett, A. Legon, *Journal of the Chemical Society, Faraday Transactions* 1998, *94*, 1565-1570.
32 Q. Li, G. Wu, Z. Yu, *Journal of the American Chemical Society* 2006, *128*, 1438-1439.
33 W. M. Haynes, in *CRC handbook of chemistry and physics*. CRC press, Boca Raton, 2014, Sec. 9.
34 C. Bowman, D. Gordon, *The Journal of Chemical Physics* 1967, *46*, 1878-1883.
35 W. J. Hehre, J. A. Pople, *Journal of the American Chemical Society* 1975, *97*, 6941-6955.
36 S. Liu, *The Journal of Chemical Physics* 2007, *126*, 244103.
37 B. Ośmiałowski, E. Kolehmainen, M. Kowalska, *The Journal of Organic Chemistry* 2012, *77*, 1653-1662.
38 H. Pritchard, H. Skinner, *Chemical Reviews* 1955, *55*, 745-786.
39 W. G. M. P.J. Linstrom, *NIST Chemistry WebBook*. National Institute of Standards and Technology, 2015.
40 K. Morokuma, *Accounts of Chemical Research* 1977, *10*, 294-300.
41 K. W. Whitten, R. E. Davis, M. L. Peck, G. G. Stanley, *Chemistry,* 10th ed., Brooks Cole, Belmont, 2014, Chap. 7.
42 R. John, *Solid State Physics*. McGraw Hill Education, New Dehil, 2014.
43 S. G. Lias, J. F. Liebman, R. D. Levin, *Journal of Physical and Chemical Reference Data* 1984, *13*, 695-808.
44 W. N. Maclay, *Journal of Colloid Science* 1956, *11*, 272-285.
45 S. Ahuja, *Chromatography and Separation Science*. Academic Press, San Diego, 2003.
46 L. Xu, H.-Y. Wang, Q. Su, *Computers & Chemistry* 1992, *16*, 187-194.
47 S. Prasad, R. Vetrivel, *The Journal of Physical Chemistry* 1992, *96*, 3092-3096.
48 A. A. Bothner-By, C. Naar-Colin, *Journal of the American Chemical Society* 1961, *83*, 231-236.
49 A. F. M. Barton, *Chemical Reviews* 1975, *75*, 731-753.
50 A. F. Barton, *CRC handbook of solubility parameters and other cohesion parameters*. CRC press, Boca Raton, 1991.

51 E. Tsuchida, K. Abe, *Advances in Polymer Science* 1982, *45*, 1-119.
52 H. Katono, A. Maruyama, K. Sanui, N. Ogata, T. Okano, Y. Sakurai, *Journal of Controlled Release* 1991, *16*, 215-227.
53 D. Eustace, D. Siano, E. Drake, *Journal of Applied Polymer Science* 1988, *35*, 707-716.
54 L. Deng, C. Wang, Z.-C. Li, D. Liang, *Macromolecules* 2010, *43*, 3004-3010.

Chapter 5. Performance Study of the Extractive Refining and Distillation Process

In the previous chapters it has been demonstrated that, with the help of the hydrogen bond interactions between various target solutes and solvent methanol, the "*Extractive Refining*" process is able to remove the undesired alkenes and OSCs from crude FCC gasoline. Furthermore the "*Extractive Distillation*" process can successfully separate the gaseous alkenes and alkanes from the hydrocarbon mixtures. In this study both processes are applied with real crude raw or the modelled materials and their performances were analysed, respectively.

Error estimates analyses for the experimental data are described in Appendix.

Those for:

1) The analysis of these mass loss results in Appendix 3.3;
2) The analysis of the liquid contents' composition in Appendix 3.4;
3) The analysis of the OSCs fraction in Appendix 3.5;
4) The analysis of the sample's boiling point in Appendix 3.6;
5) The analysis of the total adsorbed gas volume in Appendix 3.7;
6) The analysis of the gaseous contents' composition in Appendix 3.8.

5.1 Extractive Refining

As described previously, the motivation for developing the "*Extractive Refining*" process is to overcome the inherent disadvantages in both the current alkene and sulphur reduction processes, and achieves high alkene and sulphur removal efficiency. And the "*Extractive Refining*" process is particular for dealing with the raw materials

in the liquid phase. Thus, a novel and sustainable lower-energy methanol based "*Extractive Refining*" process was developed in this study.

5.1.1 Model FCC Gasoline Mixtures (MFGMs)

In order to verify the feasibility of the "*Extractive Refining*" approach in the practical process, and analyse its performance, Model FCC Gasoline Mixture I (MFGM I) was introduced into the "*Extractive Refining*" process as the raw material at the first place. The abundance of each compound in the MFGM I was based on a crude FCC gasoline, Daqing FCC gasoline,[1] and having the mass fraction of 1-pentene, 1-hexene, ethylbenzene and thioiphene have been set as 6.0%, 12.0%, 8.0% and 0.1%, respectively. During the experiment, various conditions (e.g. MFGM I to extractant ratio) were tested for obtaining the best alkene reduction and desulphurization performance.

To verify the practical feasibility and examine the performance of the "*Extractive Refining*", the mass loss taking place during application was first analysed. Here, the mass (weight) loss represents the reduced weight when comparing the original weight of the added gasoline as a feed to the weight of the after "*Extractive Refining*" process upper phase mixture (UPM) as a product. The mass (weight) loss is quite important and vital to be considered in the practical application.[2] The results of mass loss analysis experiments are listed in Table 26, and these results are outside of the experimental error estimates (± 0.05 g). After the extraction, sample (i) to (iv)'s product (UPM) was 8.15 g, 7.04 g, 3.61 g, 1.64 g and 0.67 g less than the original weight of the added gasoline, respectively. It means that, in the (i) to (v) samples, part

of the solutes either moved from MFGM I to solvent methanol or were extracted by methanol from the MFGM I. With different ratios of extractant methanol to MFGM I, the LPM weight gain was determined. This weight gain exhibited a positive correlation with the methanol to MFGM I ratio. According to the results shown in Fig. 41, which are based on the mass loss analysis results, the practical feasibility of the extraction process could be established through the mass loss of MFGM I phase.

Table 26. The mass of two phase mixture for samples (i) to (v) before and after extraction

Sample number and methanol to MFGM I ratio	MFGM I weight before extraction (g)	UPM weight after extraction(g)	Methanol weight before extraction (g)	LPM weight after extraction(g)
i, 3 to 1	10.00	1.85	30.00	38.15
ii, 2 to 1	10.00	2.96	20.00	27.04
iii, 1 to 1	10.00	6.39	10.00	13.61
iv, 1 to 2	10.00	8.36	5.00	6.64
v, 1 to 3	10.00	9.33	3.33	4.00

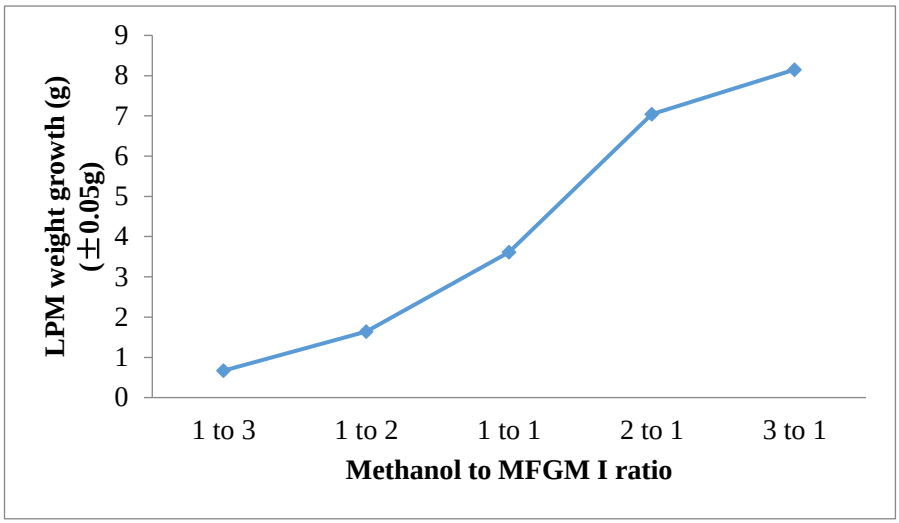

Fig. 41 The Methanol phase weight gain versus the extractant for MFGM I ratio

Secondly, GCMS was employed to identify the various alkenes and thiophene, and to analyze the efficiency of this "*Extractive Refining*" approach for the MFGM I. The GCMS results of the sample's LPM indicated that, in the chromatogram the peaks

appearing at retention times of 2.3 min, 3.1 min and 4.6 min were identified as 1-pentene, 1-hexene and thiophene by the system, respectively. These peaks were present in all the five samples LPM in the GC-MS profiles. Hence, alkenes and thiophene were confirmed to exist in the lower phase of the mixture following the extraction process. Consequently, the feasibility of the extraction process was confirmed by these GCMS results in the aliquot which demonstrated the existence of 1-pentene, 1-hexene and thiophene.

To determine the performance/effectiveness of this "*Extractive Refining*" process, the UPM of each sample was measured using GCMS. Through the chromatograms from GCMS analysis results of sample (i) to (v) UPMs, one can determine the content of the UPM. After the quantitative analysis of these GCMS results, the mass fractions of 1-pentene, 1-hexene, thiophene, n-octane and ethylbenzene in the UPM were derived. Comparing each compound's mass fraction after the extraction with its original mass fraction in the MFGM I, the effectiveness of the extraction, with different extractant methanol to simulated gasoline MFGM I proportion was obtained. These results are presented in Table 27 and Fig. 42.

Table 27. UPM composition of each sample after the extraction

Fraction % (±0.005%) Sample / Compound	**MFGM**	**i (3:1)**	**ii (2:1)**	**iii (1:1)**	**iv (1:2)**	**v (1:3)**
1-pentene	6.00	0.87	1.06	1.05	1.50	4.16
1-hexene	12.00	3.96	4.92	5.10	5.98	9.29
Thiophene	0.10	0.00	0.00	0.00	0.01	0.02
n-octane	73.90	90.49	88.76	86.66	83.68	78.25
Ethylbenzene	8.00	4.60	5.22	7.13	8.71	8.29

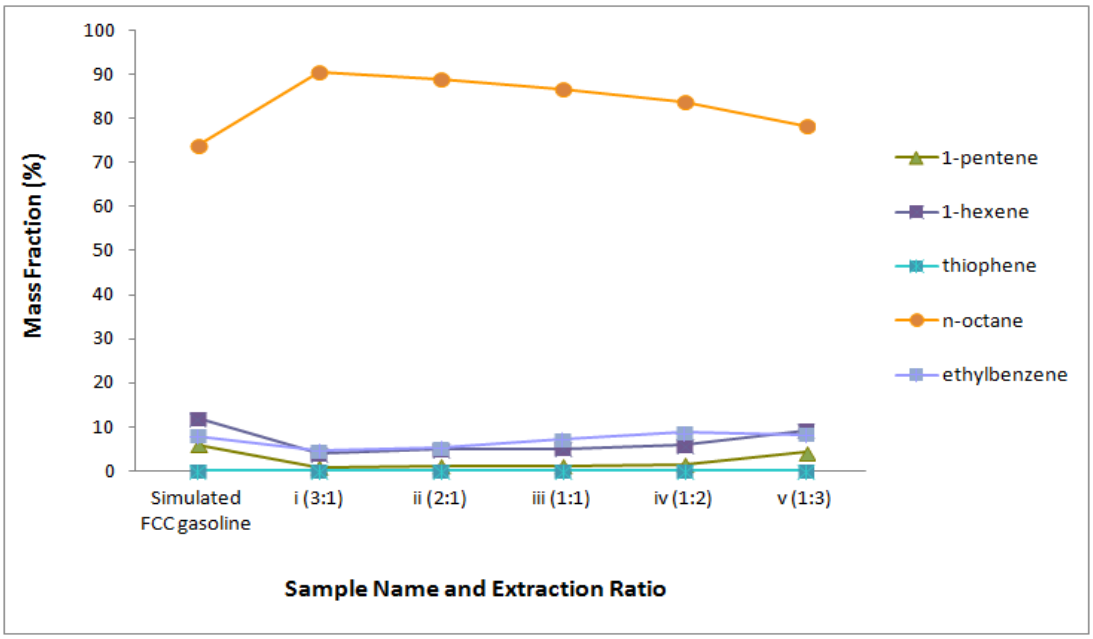

Fig. 42 UPM composition of each sample after the extraction compare with the original mass fraction

As mentioned previously, in the experiment on the 4:1 ratio mixture, liquid-liquid phase separation was not observed (under ambient conditions, 298 K). That demonstrates that the MFGM I underwent complete dissolution in the methanol phase. Hence, except for the 4:1 sample, the maximum extraction rate occurred at sample (i), in which the extractant to gasoline ratio was 3:1 before the extraction. The reduced mass fraction of 1-pentene, 1-hexene and thiophene was from 6.00% to 0.87%, 12.00% to 3.96% and 0.10% to 0.00%, respectively. Whilst, the n-octane's mass fraction was increased from 73.90% to 90.49%, the aromatic ethylbenzene was reduced from 8.00% to 4.60%.

From the composition results after extraction, the minimum methanol to MFGM I ratio for effective extraction is clearly demonstrated to be 1:3. With 1:3 extracted ratio, the 1-pentene fraction was reduced to 4.16%, 1-hexene fraction was reduced to 9.29%,

and the thiophene fraction was reduced to 0.02%. However, the n-octane and ethylbenzene mass fractions were raised 4.35% and 0.29% compared with the original MFGM I, respectively. Then, considering the 1-pentene, 1-hexene and thiophene mass fraction in the original MFGM I, the gasoline phase alkene and thiophene (OSCs) reduction rate of sample (i) to (v) is shown in Table 28. Table 29 and 30 show the different technologies with various catalysts/processes and their alkene reduction or desulfurization rate after refining, respectively.

Table 28. Sample (i) to (v) alkene and thiophene (OSCs) reduction rate

Sample / Fraction	i (3:1)	ii (2:1)	iii (1:1)	iv (1:2)	v (1:3)
Alkene reduction rate % (±0.005%)	73.20	66.80	65.80	58.50	25.30
Thiophene (OSCs) reduction rate % (±0.005%)	100.00	100.00	100.00	94.70	83.30

Table 29. Hydroisomerization and aromatization methods with various catalysts and their alkene reduction rate[3-7]

Catalyst	Original Alkene content (%)	Alkene content after refining process (%)	Alkene reduction rate (%)
Co-Mo/Al_2O_3 and Ni-Mo/Al_2O_3	30.30	14.00	53.80
HZSM-5	39.80	18.30	54.02
nanoscale HZSM-5 (20-50 nm) with Ga_2O_3	49.60	15.10	69.56
SAPO-11 with HZSM-5	41.70	11.10	73.38
HMOR with HZSM-5	41.70	9.80	76.50
Hβ with HZSM-5	41.70	8.70	79.14
SAPO-11, Hβ, HMOR with HZSM-5	41.70	6.50	84.41
SAPO-11, HMOR with HZSM-5	41.70	7.30	82.49
Mesoporous Zeolite L (M-L)	33.90	5.15	84.81
SAPO-11, Hβ with HZSM-5	41.700	6.300	84.892

Table 30. Different technologies with various processes and their OSCs reduction rate[8-17]

Technology and process	OSCs reduction rate (%)
Hydrodesulfurization (HDS)	100.00
Biodesulfurization (BDS)	94.50
Oxidative desulfurization (ODS)	97.80
Adsorptive desulfurization (ADS)	100.00
Extractive desulfurization (EDS)	80.00
Pervaporation desulfurization (PV)	90.00
Olefinic alkylation desulfurization (OATS)	99.50
Photochemical or photocatalytic desulfurization	100.00

Compared with other catalysts in Table 29, the alkene reduction rate obtained the

highest rate 84.89% by applying SAPO-11, Hβ with HZSM-5 mixture catalyst (Table 29). Nevertheless, this refining process based on the use of heterogeneous catalysts not only consumes considerable energy, but also requires severe conditions, such as high temperature, high pressure and a hydrogen reactor. By contrast, with relatively higher alkene reduction rate (73.20%) and more easily accessible conditions than the other methods in the table (room temperature and atmospheric pressure), the advantages of the methanol based "*Extractive Refining*" approach become obvious.

Considering the desulfurization aspect, obviously, the "*Extractive Refining*" process by methanol extraction in this study is able to provide higher OSCs reduction rate than extractive desulfurization (EDS), prevaporation desulfurization (PV), biodesulfurization (BDS), oxidative desulfurization (ODS) and olefinic alkylation desulfurization (OATS) process (Table 30 and Table 3).

Moreover, due to the simplest treatment process, this novel "*Extractive Refining*" process is expected to consume much less energy and upon industrial application have a lower capital or operational cost than hydrodesulfurization (HDS), adsorptive desulfurization (ADS) and photochemical or photocatalytic desulfurization process during the practical industry application (Table 30 and Table 3). Thus, it is believed and expected that this liquid extraction method could be a most efficient novel desulfurization process.

5.1.2 Crude FCC Gasoline (CFG)

The feasibility of the "*Extractive Refining*" process during the practical application were preliminarily confirmed through the above modelled FCC gasoline

tests. From the results of the mass loss and GCMS analysis, the "*Extractive Refining*" presented very good alkene reduction and desulphurization performance when dealing with MFGM I. However, it was found the phase separation could not be observed when only methanol was used as the extractant to deal with one of the crude FCC gasoline (CFG II). That means it is not desirable to utilise only methanol as the extractant during "*Extractive Refining*" process to remove the alkene and sulphur content in all kinds of CFG from a refinery.

Therefore, in the following study, in order to optimize the performance of any "*Extractive Refining*" process and introduce the approach into the CFG upgrading process, it is necessary to modify the constituents of the extractant and investigate the most suitable ratio between gasoline and extractant during the "*Extractive Refining*" process.

The "*Extractive Refining*" approach was applied to deal with the CFG I and II. In this series of tests, co-solvents (co-extractants) ethylene glycol or water was added into the extractant methanol, and different gasoline and extractant ratios were applied to achieve the most efficient performance during the "*Extractive Refining*" process.

"*Extractive Refining*" approach for CFG I

Ethylene glycol was introduced into the "*Extractive Refining*" process as the first kind of co-extractant with methanol. In this study, the extraction effectiveness of a methanol-ethylene glycol mixture (ME) with CFG I has been analysed. CFG I is the crude FCC gasoline from SINOPEC, China, its detail composition is listed in Appendix 2.1.

Observation of the mixture solution during the extraction by eye, it was found that the dark content in the upper phase moved to the lower phase after the extraction process. This dark content always consisted of OSCs. This means that the extractant ME mixture can extract the OSCs content from CFG I. This phenomenon can be observed from Fig. 43 as an example.

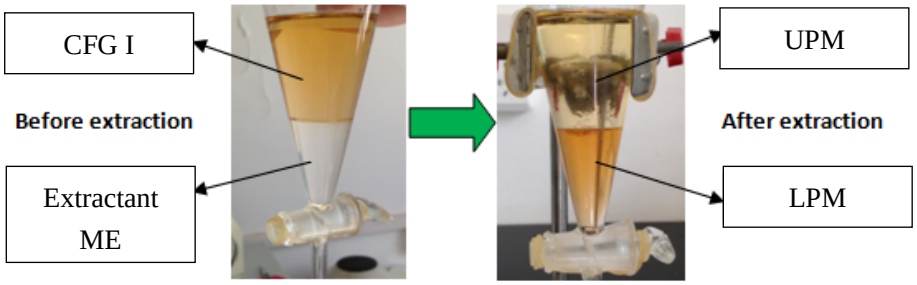

Fig. 43 Mixture solution before and after the "*Extractive Refining*" test for CFG I which utilises methanol-ethylene glycol mixture (ME) as the extractant

The results of mass loss analysis are listed in Table 31. These results are outside the experimental error estimates (± 0.05 g). The results listed in the Table 31 indicate that, unlike the results of pure methanol with MFGM I, after the extraction with ME a positive change of UPMs was observed in these tests. The mass loss became obvious when ethylene glycol was applied together with methanol as the co-extractant. Based on the mass loss analysis results in the Table 33, the weight gain of the LPM after extraction exhibited a positive correlation with methanol's mass fraction in the extractant ME (Fig. 44). Through these results, the feasibility of the "*Extractive Refining*" process for the crude feedstock is able to be preliminarily confirmed.

Table 31. The weight of two phase mixture for (vi) to (x) samples before and after "*Extractive Refining*" processes utilise different ethylene glycol to methanol mixing ratio methanol-ethylene glycol mixtures (ME) as the extractant

Sample number and ethylene glycol to methanol ratio	CFG I weight before extraction (g)	UPM weight after extraction(g)	ME mixture weight before extraction (g)	LPM weight after extraction(g)
vi, 80% to 20%	10.00	10.36	10.00	9.64
vii, 60% to 40%	10.00	10.04	10.00	9.96
viii, 40% to 60%	10.00	9.44	10.00	10.56
ix, 20% to 80%	10.00	7.88	10.00	12.12
x, 10% to 90%	10.00	3.24	10.00	16.76

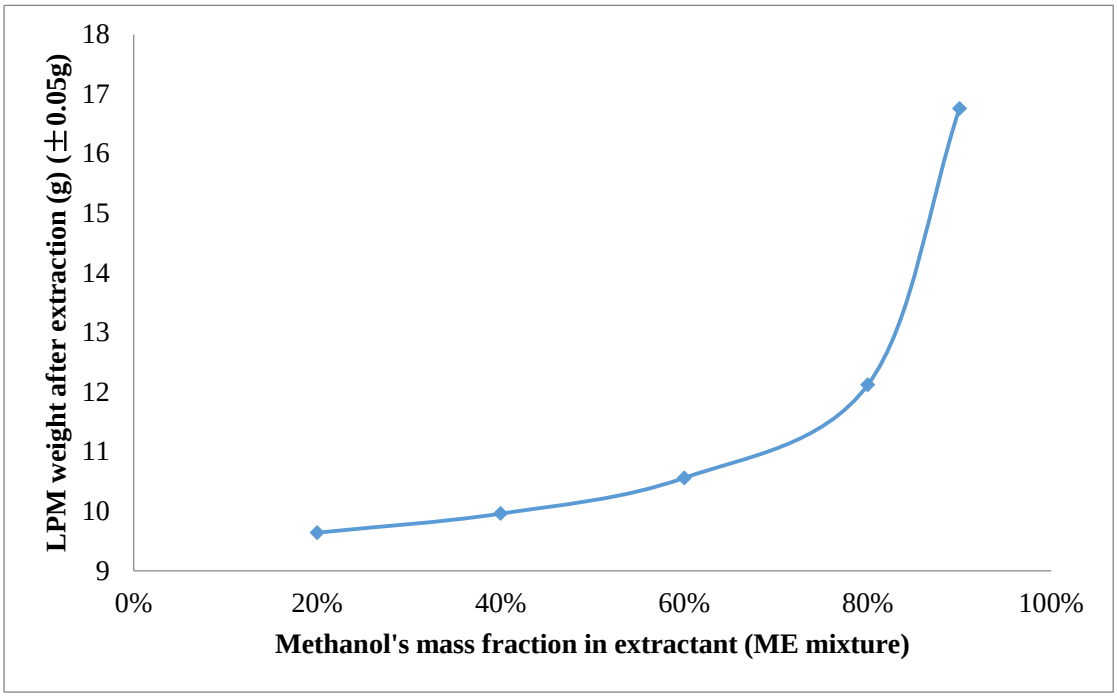

Fig. 44 LPM weight after the "*Extractive Refining*" processes utilise different ethylene glycol to methanol mixing ratio methanol-ethylene glycol mixtures (ME) as the extractant

After the quantitative analysis of the GCMS results, the mass fractions of each group composition in the upper phase were derived (Fig. 45). Comparing each group composition's mass fraction after the "*Extractive Refining*" process with its original mass fraction in the FCC gasoline phase, the performance of the process, with

different methanol to ethylene glycol proportion was obtained.

The results of applying ME as the extractant are presented with the data in Fig. 45. The mixing ratio between ME and FCC gasoline is fixed, and it is equal to 1:1.

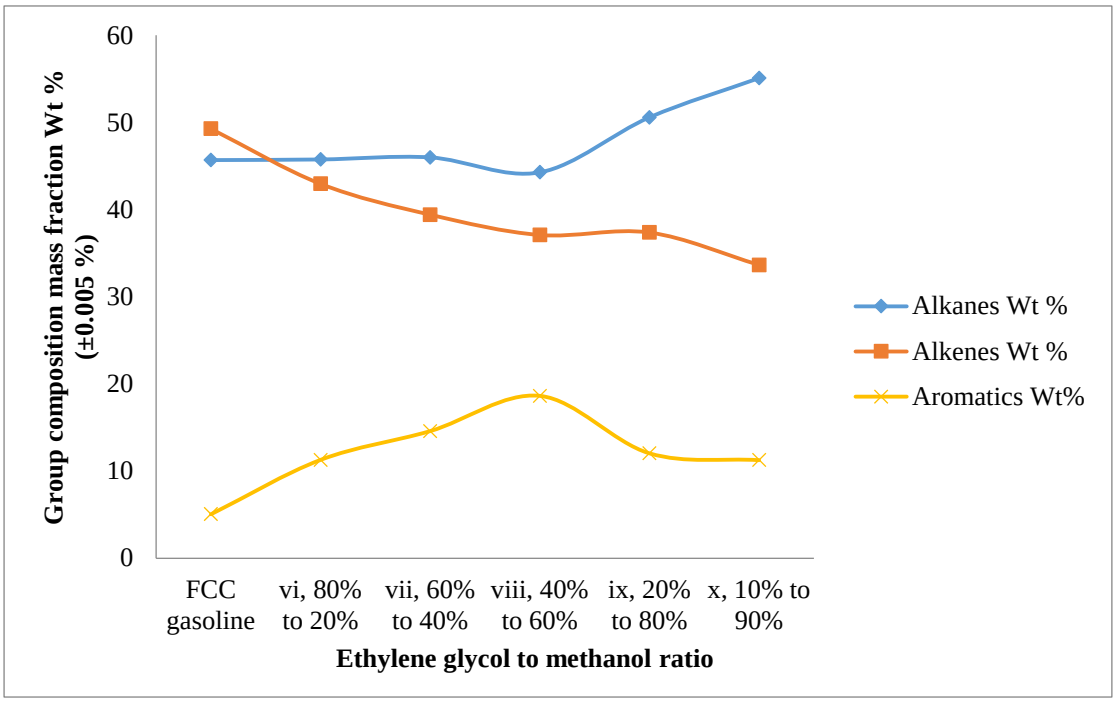

Fig. 45 UPM composition of each sample after the "*Extractive Refining*" processes utilising different ethylene glycol to methanol mixing ratio methanol-ethylene glycol mixtures (ME) as the extractant

Given these GCMS results, combined with the previous mass loss analysis results, with a larger proportion of methanol in the extractant ME, the extraction process gives a higher alkene reduction rate. However, the weight of the CFG phase is reducing with the increasing methanol proportion in the ME, and this will lead low gasoline productivity during practical industrial production.

After analysis of the OSCs content concentration of each sample, a positive correlation between the methanol fraction in the ME mixture and the desulphurization performance of the "*Extractive Refining*" process can be obtained (Fig. 46). Although

extractant x (90% methanol and 10% ethylene glycol in wt.) showed the highest mass loss among all the ME, it presented the best OSCs reduction performance.

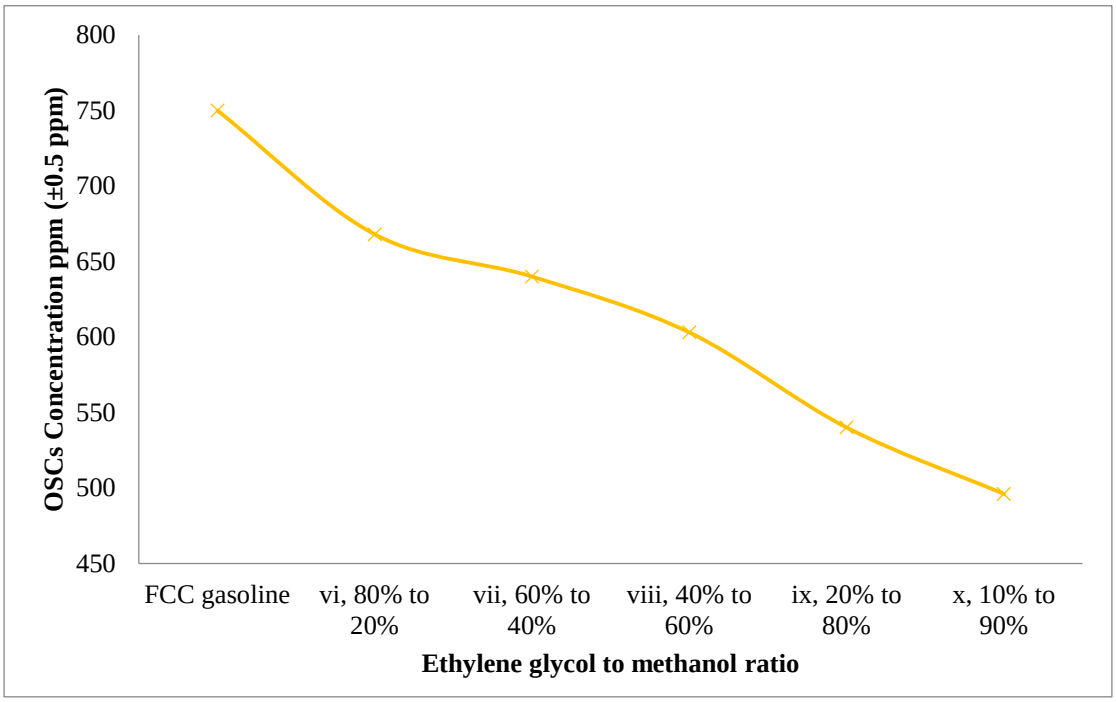

Fig. 46 UPM OSCs concentration of each sample after the "*Extractive Refining*" processes utilise different ethylene glycol to methanol mixing ratio methanol-ethylene glycol mixtures (ME) as the extractant

In addition, because aromatics have higher octane number than alkane and alkene [18], not only a lower alkene and OSCs content means better gasoline, but a larger fraction of aromatics in the gasoline represents higher quality of the gasoline as well. Based on this point of view, the ME with 60% methanol and 40% ethylene glycol presented the highest aromatics content (18.63%) after the "*Extractive Refining*" process. At the same time, applying the ME under this methanol to ethylene glycol ratio also can lead to a relatively better desulphurization and alkene reduction performance and gasoline productivity than the ME with other proportions.

In combining these results, it can be concluded that, the best performance of

"*Extractive Refining*" under 1:1 extractant mixture to CFG I ratio is achieved by applying the ME with 60% methanol and 40% ethylene glycol.

"*Extractive Refining*" approach for CFG II

On the other hand, compared to the low cost and high production capacity of methanol,[19] ethylene glycol is much more expensive and with lower production capacity in global industries. Also because one aim of this "*Extractive Refining*" approach is to reduce the cost of the upgrading process, considering the usage amount of the raw material and in order to develop a more sustainable and efficient "*Extractive Refining*" process, it is necessary to replace ethylene glycol with another more suitable co-extractant.

Surprisingly, from the literature it has been found that, the crude methanol consists of around 20% mol (12% in wt.) of water.[20] More importantly, it already exists at a considerable level (around 12% in wt.) in the crude methanol, which means except methanol no extra cost for the extractant's raw material is needed. Hence, in the following study water was introduced into the "*Extractive Refining*" process as the co-extractant of methanol to dealing with CFG II. CFG II is the crude FCC gasoline from Petroineos, Scotland. Its detailed composition is listed in Appendix 2.2.

As described in the previous experimental part, methanol and distilled water with 9:1 mixing ratio in weight was used as the extractant mixture that means in this study the extractant mixture for the CFG II contains 10% of water (in wt.).

The colour change of the mixture solution during the extraction is shown in Fig. 47. From the figure it is clear that the dark content which always consisted of OSCs in

the upper phase moved to the lower phase after the "*Extractive Refining*" process. This also means the extractant mixture consist of 90% methanol and 10% water (in wt.) can extract the OSCs content from CFG II.

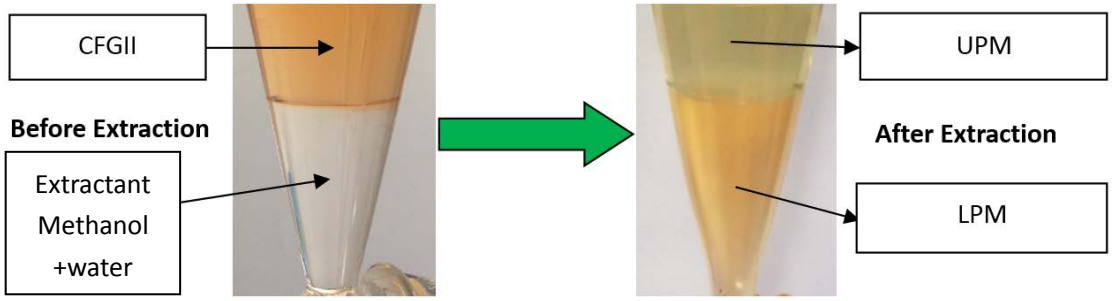

Fig. 47 Mixture solution before and after the "*Extractive Refining*" test for CFG II which utilises 9:1 methanol-water mixture as the extractant

Meanwhile, from the mass loss analysis result of applying this 9:1 methanol-water mixture as the extractant in the "*Extractive Refining*" process to refine CFG II, a relatively low total mass loss 10.73% (in wt.) was observed after five time extractions (Fig. 48). That means the "*Extractive Refining*" approach is able to upgrade CFG more efficiently when utilising the more economical methanol-water mixture instead of ME as the extractant, and five time extraction process was applied instead of single extraction. Fig. 48 shows the mass loss after each extraction during the CFG II "*Extractive Refining*" test when applying 90% methanol and 10% water (in wt.) mixture as the extractant. Therefore, the feasibility of applying this extractant in the "*Extractive Refining*" process of CFG II is able to be preliminarily confirmed.

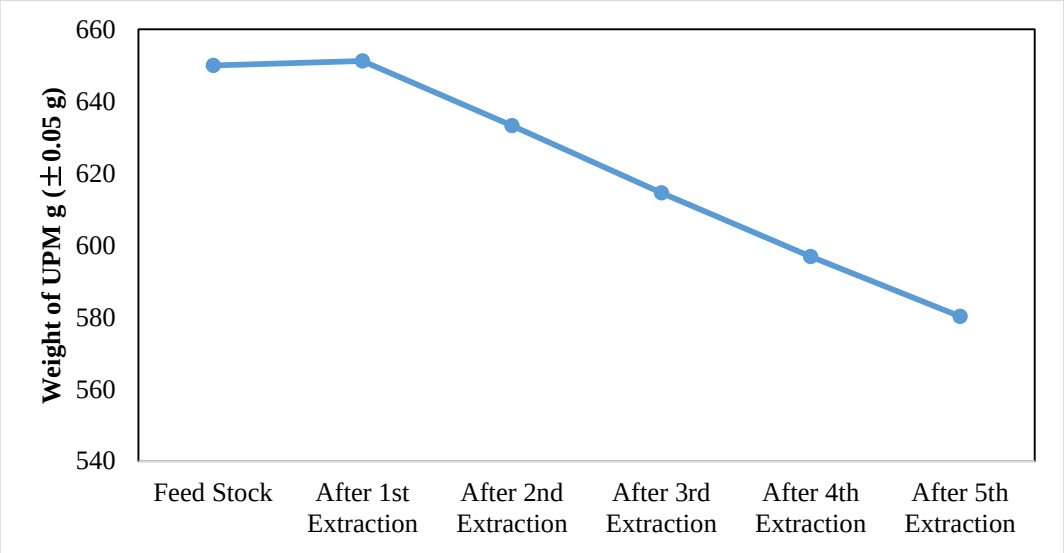

Fig. 48 UPM mass loss after each extraction in the "*Extractive Refining*" process utilises 9:1 methanol-water mixture as the extractant

Gasoline consists a complex mixture of n-paraffins, i-paraffins, alkenes, naphthenics, aromatics and other compounds, with chains containing 4 to 12 atoms of carbon, with a range of ebullition from 30 to 225℃.[21] In order to define the products from the "*Extractive Refining*" process when applying 90% methanol and 10% water (in wt.) mixture as the extractant can be treated as the gasoline range product, the "*Extractive Refining*" process final product UPM's boiling point under atmosphere was analysed.

TGA analysis was carried out on the UPM and it confirmed all the contents in the UPM evaporated before the temperature of the furnace reached 146℃ (Fig. 49). The results are outside the experimental error estimates (± 0.005% wt and ± 0.5℃). Meanwhile, this UPM consists of two parts of mixtures with different ebullition temperature. Before 78℃ the first and major part (73.57% wt) of UPM was evaporated, and from 78 to 146℃ the rest (second part) of UPM was evaporated (Fig.

49). Therefore, through the boiling point analysis of these products, it was confirmed that the liquid product from this "*Extractive Refining*" process is in the gasoline range.

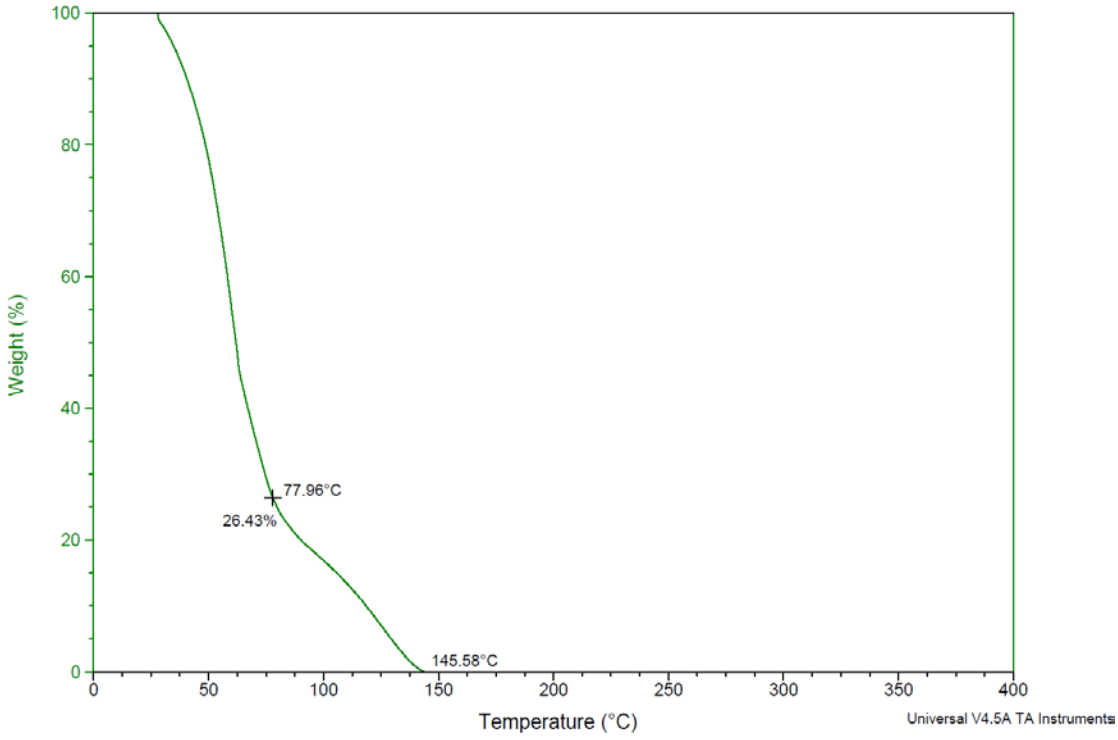

Fig. 49 Boiling point (TGA) analysis result of UPM from the "*Extractive Refining*" process utilises 9:1 methanol-water mixture as the extractant

Similarly, GCMS was applied for the content quantification analysis of CFG II, and CFG II after "*Extractive Refining*" process of the UPM. The GCMS analysis results indicates that after the "*Extractive Refining*" process when applying 90% methanol and 10% water (in wt.) mixture as the extractant, the alkene content in the UPM was reduced from 30.39% (in CFG II in wt.) to 25.37% (in UPM in wt.), the total alkane content was increased from 37.81% (in CFG II in wt.) to 43.89% (in UPM in wt.), and the aromatics content was slightly reduced from 31.80% (in CFG II in wt.) to 30.74% (in UPM in wt.). Thus, the process is effective for reducing the alkene content in the CFG II, and it can maintain the valuable aromatics content at

maximum level.

With regard to the OSCs content change before and after the "*Extractive Refining*" process, a drop from 960 ppm (in CFG II) to 778 ppm (in UPM) was obtained from the GCMS analysis results. Therefore, the effective desulphurization performance was confirmed when applying 90% methanol and 10% water (in wt.) mixture as the extractant during the "*Extractive Refining*" process.

Considering the above colour change, mass loss and GCMS analysis results, it can be concluded that the economical mixture of 90% methanol and 10% water (in wt.%) extractant presented highly efficient alkene reduction and desulphurization performance when applied in the "*Extractive Refining*" process. Compared with the ME mixture, this extractant's desulphurization performance results is not at those levels, but this relative efficient extractant is clearly the most economical one. Moreover, through the boiling point analysis of the purified CFG II (post extraction UPM), the final product from the "*Extractive Refining*" process was further confirmed eligible to be directly used as the transport fuel in the gasoline vehicles.

5.2 Extractive Distillation

As described in the earlier, a major aim of this research is to develop a lower cost, less energy-intensive process to separate the alkene/alkane in gaseous hydrocarbon mixtures such as cracking gases, and in order to overcome the disadvantages in current separation processes, a new "*Extractive Distillation*" process was also developed in this study.

Our earlier study of the extractive process and solvent-solute interactions, the

molecular dipole moment of a target solute shows a positive correlation to the strength of the hydrogen bond interaction between solvent (extractant) and solutes (extracts). Since hydrogen bond interactions between extractant and extracts are critical to the performance of the extraction, it was supposed that extractant with different molecular dipole moments will also present different extraction performance during the corresponding "*Extractive Distillation*" process.

5.2.1 Experimental Method

In this study, in order to examine the performances of extractant/extractant mixtures having different constituent molecular dipole moments during the "*Extractive Distillation*" process, dimethyl carbonate (DMC) was used as the base extractant which shows excellent miscibility with other organic solvents. Various organic solvents with different molecular dipole moments were then added into the DMC to form the co-extractant mixture, then these extractant/extractant mixtures showed in Table 32 were applied in the "*Extractive Distillation*" process to separate different gaseous contents in model catalytic cracking gas mixture (MCCGM) and model thermal cracking gas mixture (MTCGM).

Table 32. Contents in extractant sample (i) to (iv), dipole moment of the added co-extractant and lower boiling point of the solvent in the extractant mixture[22-25]

Extractant Sample No.	Extractant/Extractant Mixture (1:1 in volume)	Dipole Moment of Added Co-extractant μ (D)	Lower Boiling Point of the Extractant ℃
i	DMC+**n-hexane**	0.08	68.00
ii	pure **DMC**	0.90	90.00
iii	DMC+**methanol**	1.70	64.70
iv	DMC+**Propylene Carbonate**	5.00	68.00

A new formalism for evaluating the alkene selectively and alkene and alkane separation performance, by applying various extractants during the "*Extractive Distillation*" process was set up in this study.

$$S_i = \frac{\Phi_{pi}}{\Phi_{oi}} \qquad (12)$$

$\boldsymbol{S_i}$ *(i=2,3)* the different solvent's C2 or C3 alkenes and alkanes separation performance;

$\boldsymbol{\Phi_{pi}}$ *(i=2,3)* the volume/molar fraction (mol%) of the C2 and C3 alkane;

$\boldsymbol{\Phi_{oi}}$ *(i=2,3)* the volume/molar fraction (mol%) of the C2 and C3 alkene.

Based on the molar fraction of different contents in the MCCGM/MTCGM, two individual evaluation systems were constructed, respectively.

1) For the MCCGM:

The ethane/ethylene molar ratio in the original MCCGM is 1.67.

The propane/propylene molar ratio in the original MCCGM is 2.02.

If the value of C2 alkene selectively S_2 is higer than 1.67 at adsorption stage and lower than 1.67 at desorption (lower boiling point of the solvent in the extractant mixtures) stage of the "*Extractive Distillation*" process, it indicates through the novel process the light alkenes have been concentrated. This means the extractant can successfully separate the C2 alkene and alkane contents in the MCCGM. Otherwise, the extractant is defined as noneffective.

It is similar in the C3 alkene selectivity calculation. If S_3 is higher than 2.02 at adsorption stage and lower than 2.02 at desorption stage, it means extractant can successfully separate the C3 alkene and alkane contents in the MCCGM.

2) For the MTCGM:

The ethane/ethylene molar ratio in the original MTCGM is 0.11.

The propane/propylene molar ratio in the original MTCGM is 0.20.

Except the different reference value of C2 and C3 alkene selectively, all the evaluation processes are identical to the processes of the MCCGM separation.

5.2.2 Model Catalytic Cracking Gas Mixtures (MCCGM)

As one of the major type of petroleum pyrolysis/cracking gases, the "*Extractive Distillation*" approach was first applied in the separation process for the catalytic cracking gas mixtures. [26] In our study a model catalytic cracking gas mixture (MCCGM) was prepared by a special gas product company base on the components listed in the Gas Market Research Report of China (2011).[26]

Firstly, in order to study the feasibility of the "*Extractive Distillation*" approach, the adsorption capacity of each extractant sample was examined. The total volume of MCCGM adsorbed by various extractant/extractant mixtures is listed in Table 33.

Table 33. Sample (i) to (iv) total adsorbed gas volume with MCCGM[22-25]

Extractant Sample No.	Extractant/Extractant Mixture (1:1 in volume)	Dipole Moment of Added Co-extractant μ (D)	Total Adsorbed Gas Volume ml (±5 ml)
i	DMC+**n-hexane**	0.08	2540
ii	pure **DMC**	0.90	1915
iii	DMC+**methanol**	1.70	1655
iv	DMC+**Propylene Carbonate**	5.00	910

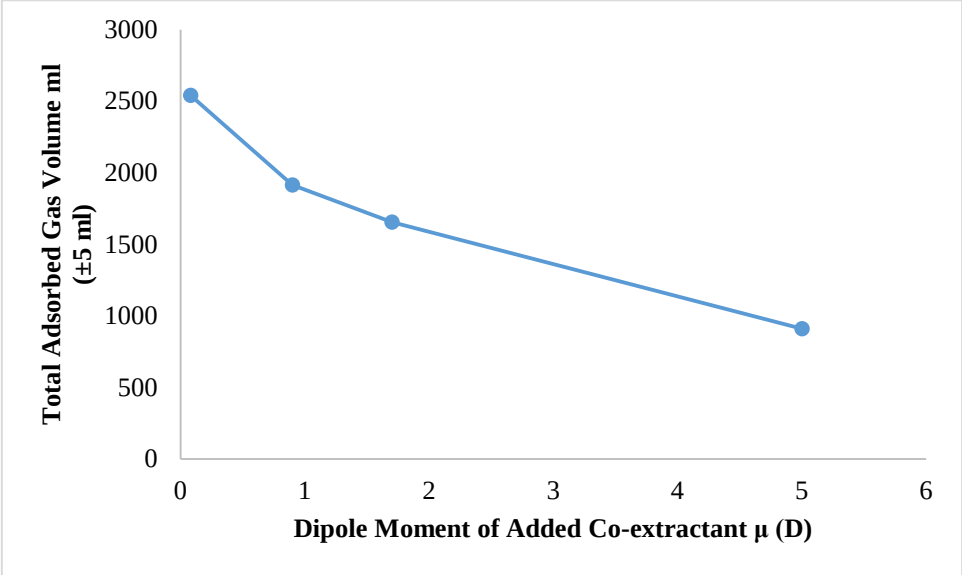

Fig. 50 Total adsorbed gas volume vs. dipole moment of added co-extractant μ (D) (MCCGM)

In these results, the total adsorbed gas volume exhibits a reduction when considered with the increasing dipole moment of added co-extractant (Fig. 50). Considering the reason of this phenomenon, it has been described previously that molecules are generally classified as being non-polar if they have zero dipole moment, and polar otherwise,[27] and according to the "*like-dissolves-like*" theory,[28] which indicates solutes will dissolve most effectively in solvents with similar polarity/dipole moment to themselves. Due to the gaseous contents in the MCCGM all have very small or zero dipole moment. Therefore, during the adsorption stage of the "*Extractive Distillation*" process for the MCCGM the extractant mixture consisted of n-hexane which has the smallest dipole moment and DMC presented the largest adsorption capacity.

Through the adsorption capacity analysis, two points were confirmed. The feasibility of the "*Extractive Distillation*" approach was proved by the adsorption capacity of the process with various extractants. The second point is the

extractant/extractant mixture with the smallest dipole moment can absorb the largest volume of the low dipole moment hydrocarbon mixture during the adsorption stage of the MCCGM's "*Extractive Distillation*" process.

To further investigate the effectiveness and performance of the "*Extractive Distillation*" process, gas chromatography (GC) was used analyse the gaseous contents in the output gas mixtures during adsorption and desorption stage of the "*Extractive Distillation*" process.

Extractant samples with number (i) to (iv) were applied in the "*Extractive Distillation*" process to examine their effectiveness for separating the alkene and alkane content in the MCCGM. Their separation performance S_i results were indicated in Table 34.

Table 34. Sample (i) to (iv) separation performance with MCCGM[22-25]

Extractant Sample No.	Extractant/Extractant Mixture (1:1 in volume)	Dipole Moment of Added Co-extractant μ (D)	S_i Alkane/Alkene ratio (adsorption)	S_i Alkane/Alkene ratio (desorption)
		C2 Content		
MCCGM			**1.67**	**1.67**
i	DMC+**n-hexane**	0.08	1.47	2.12
ii	pure **DMC**	0.90	2.11	1.52
iii	DMC+**methanol**	1.70	2.25	1.52
iv	DMC+**Propylene Carbonate**	5.00	2.33	1.41
		C3 Content		
MCCGM			**2.02**	**2.02**
i	DMC+**n-hexane**	0.08	2.42	2.02
ii	pure **DMC**	0.90	3.65	1.99
iii	DMC+**methanol**	1.70	4.13	1.90
iv	DMC+**Propylene Carbonate**	5.00	5.60	1.78

In order to examine the extractant molecular dipole moment effect on the

separation performance, various co-extractant with different molecular dipole moment were added in to the DMC with 1:1 volume ratio in all samples. The dipole moments of these added organic co-extractants are also displayed in Table 34. Obviously, compared with the pure DMC as the separation solvent in sample (ii), the differences of the added solvents' polarity in other samples lead to some changes which are reflected in their separation performance. These changes have similar trends. Based on the results in Table 34, Fig. 51 and 52 have been drawn for easier understanding the extractant dipole moment effect and the influence's trends.

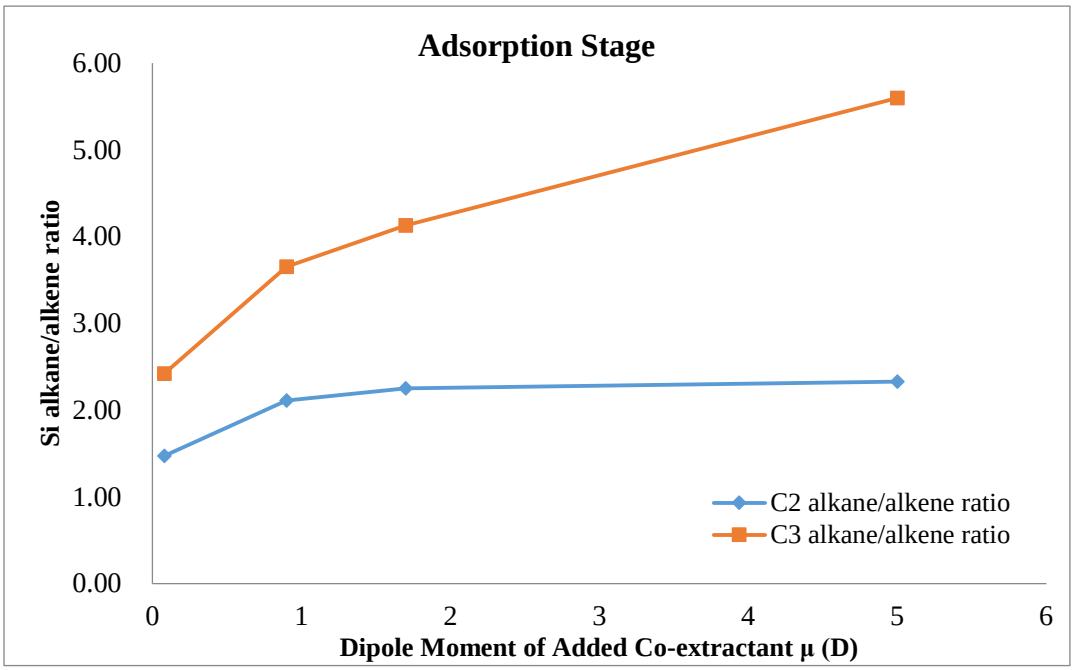

Fig. 51 Relation between the co-extractant's dipole moment and the separation performance in the "*Extractive Distillation*" process's adsorption stage with MCCGM

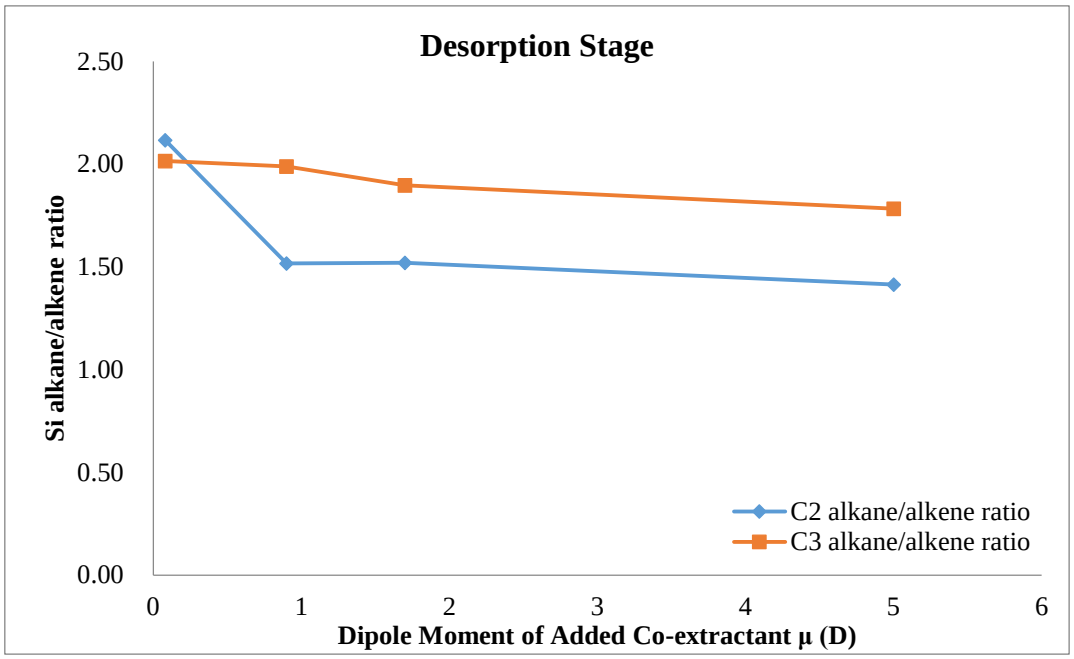

Fig. 52 Relation between the co-extractant's dipole moment and the separation performance in the "*Extractive Distillation*" process's desorption stage with MCCGM

Fig.51 indicates that in the adsorption stage of the "*Extractive Distillation*" process, both the C2 and C3 alkane/alkene ratio in the gas outlet stream are increasing with the rising value of the added co-extractant dipole moment. That means the alkene are adsorbed more than the alkane into the extractant with larger extractant dipole moment.

Combined with the previous mechanism study, it is believed that these results can be explained by the hydrogen bond interaction between solutes/the extractant alkenes and the solvents/extractants molecular structure. Compared to the zero dipole moment alkane contents in the MCCGM, alkenes such as propylene have higher dipole moments. This is clearly critical for the formation of hydrogen bond between them and the extractant solvent molecules, because the larger dipole moment results in stronger hydrogen bond interactions between solute and solvent, and stronger

hydrogen bond formed between two compounds clearly enhances the solubility of one in the other.[29, 30] Moreover, compared with the alkanes in MCCGM, the alkenes are more prone to form hydrogen bond through O—H···π and/or C—H···O structure.[31-33]

The recognised Prausnitz and Anderson theory also can be used to explain that the extractant dipole moment can influence the separation performance.[34] The theory proposes that the hydrocarbon separation selectivity depends on the extractant molecular polarity/ dipole moment and molar volume.[34, 35] With larger polarity/dipole moment the extractant will have higher light alkene selectivity.[34, 35] Therefore, as obtained from the GC analysis results, the alkenes are adsorbed more than the alkanes during the adsorption stage of the "*Extractive Distillation*" process.

On the other hand, except sample (i) the n-hexane and DMC mixture, which has the smallest dipole moment among (i) to (iv) samples, all the other samples achieve higher alkane/alkene ratio than the original alkane/alkene ratio in the MCCGM. Therefore, it has been confirmed that in the adsorption stage extractant sample (ii) to (iv) can achieve effective alkane and alkene separation.

From the desorption results displayed in Fig.52, it is found that the C2 and C3 alkane/alkene ratio in the gas outlet stream present a negative correlation with the value of the added co-extractant dipole moment. It indicates that, because of the larger dipole moment of the co-extractant, more alkene contents adsorbed in the adsorption stage. Thus, during desorption extractants/extractant mixtures with larger dipole moment discharges more alkene to the gas outlet stream. Based on the previous evaluation method, extractants (ii) to (iv) are confirmed to have the feasibility for

separating the light alkene and alkane mixtures through the "*Extractive Distillation*" process.

Furthermore, with regard to the best co-extractant, propylene carbonate showed the highest light alkene selectivity among all the other extractant/co-extractant. However, it presented the lowest hydrocarbon gas mixture adsorption capability. On the contrary, although n-hexane presented the highest adsorption capability, it exhibits the lowest light alkene selectivity during the "*Extractive Distillation*"process. Combining the results of various extractant/extractant mixture's adsorption capacity and alkenes/alkanes separation performance (light alkene selectivity) during the "*Extractive Distillation*" process, the co-extractant methanol with relative high adsorption capacity and high light alkene selectivity presents the most equilibrium performance. Therefore, methanol is proposed as the best co-extractant in the "*Extractive Distillation*" process of the MCCGM.

5.2.3 Temperature Effect

The temperature effect on the "*Extractive Distillation*" approach was also investigated in this study. Since methanol presented the most equilibrium performance during the "*Extractive Distillation*" process, it was used as the extractant during the temperature effect test.

Table 35. Pure methanol separation performance at different temperature with MCCGM

Temperature (℃)	S_i Alkane/Alkene ratio (adsorption)	S_i Alkane/Alkene ratio (desorption)
	C2 Content	
-18	2.06	1.60
25	1.87	1.67
40	1.75	1.70
	C3 Content	
-18	3.10	1.78
25	3.04	1.85
40	3.00	1.88

Table 35 presents the pure methanol separation performance at different temperatures and constant pressures. The results clearly indicate that, the increasing temperature causes the C2 and C3 contents' S_i value to drop during the adsorption stage. The reason is that the increase of temperature makes the gas less soluble, thus tending to lower the rate of absorption.[36] Also because in the MCCGM, both the C2 and C3 alkane have higher concentration than the alkene contents, the partial pressures of the alkanes are higher than the alkenes'.[36, 37] Based on Henry's law, compared with the low temperature situation, methanol absorbs more alkanes at high temperature than alkenes.[36, 37]

Therefore, during the desorption stage, the higher the operation temperature is, the bigger the alkane/alkene ratio is observed from the gas outlet stream. From this point of view, it can be confirmed that the "*Extractive Distillation*" approach's separation performance has a clear negative correlation with the operation temperature. That means a lower operation temperature during the "*Extractive Distillation*" process gives rise to a better alkene and alkane separation performance, as might be anticipated.

5.2.4 Model Thermal Cracking Gas Mixtures (MTCGM)

Thermal cracking gas is another major type of the petroleum pyrolysis/cracking gases,[26] similar to the catalytic cracking gas. The conventional separation technologies (such as cryogenic distillation) for separating the alkene and alkane contents in the thermal cracking gas are always energy-intensive and have high capital costs.[38] In order to reduce the cost and the energy consumption of this separation process, the "*Extractive Distillation*" approach was also applied in the separation process for the thermal cracking gas.

In this study, model thermal cracking gas mixtures (MTCGM) was used as gaseous feedstock in the "*Extractive Distillation*" process. The contents in the MTCGM was referred to the Safarik and Eldridge research,[39] which consisted of 15.00% hydrogen, 4.01% carbon monoxide, 24.76% methane, 45.21% ethylene, 4.99% ethane, 5.02% propylene and 1.01% propane in mol%.

The total volume of MTCGM adsorbed by the various extractant/extractant mixture was first examined in this study. As listed in Table 36 and shown in Fig 53, the total adsorbed gas volume presents a positive correlation with an increase of the value of the co-extractant molecular dipole moment. This result is different from the negative trend between the co-extractant molecular dipole moment and extractant's adsorption capacity, which was obtained from the "*Extractive Distillation*" process of the MTCGM.

Table 36. Sample (i) to (iv) total adsorbed gas volume with MTCGM[22-25]

Extractant Sample No.	Extractant/Extractant Mixture (1:1 in volume)	Dipole Moment of Added Co-extractant μ (D)	Total Adsorbed Gas Volume ml (±5 ml)
i	DMC+**n-hexane**	0.08	345
ii	pure **DMC**	0.90	405
iii	DMC+**methanol**	1.70	415
iv	DMC+**Propylene Carbonate**	5.00	430

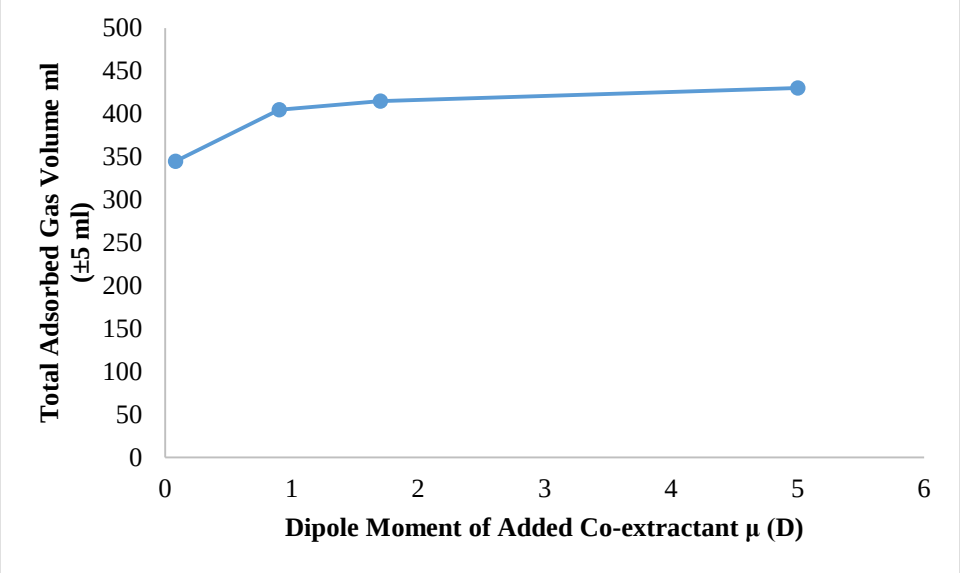

Fig. 53 Total adsorbed gas volume vs. dipole moment of added co-extractant μ (D) (MTCGM)

It has also been found from these results, unlike the "*Extractive Distillation*" process for the MCCGM, that the various extractant/extractant mixture showed similar gas adsorption capacity during the process, but the gas adsorption capacity of various extractants in the "*Extractive Distillation*" process for the MTCGM were much smaller than the MCCGM process. From the gas adsorption capability aspect of the process, it is assumed that the "*Extractive Distillation*" approach may be more suitable for the catalytic cracking gas treatment.

The reason for the different results obtained from MCCGM and MTCGM

"*Extractive Distillation*" process has also been studied. These results were due to the different concentration of the various contents in the MCCGM and MTCGM. In MCCGM the gaseous contents are all C2-C3 hydrocarbons (mainly alkanes), however the MTCGM are consisted of hydrogen, carbon monoxide and C1-C3 hydrocarbons (mainly alkenes). Henry's law,[36, 37] which can be described as the equation below has been introduced to help to explain the above results:

$$p = k_{\mathrm{H}} c \qquad (13)$$

$\boldsymbol{k_{\mathrm{H}}}$ a temperature-dependent constant;

$\boldsymbol{p}$ the partial pressure (atm);

$\boldsymbol{c}$ the concentration of the dissolved gas in the liquid (mol/L).

The temperature in the reactor was kept constant at room temperature 25 ℃ during adsorption step of the "*Extractive Distillation*" process. And in the MTCGM, the alkene contents have higher concentration than the alkane contents. Thus, with higher concentration in the gaseous mixtures the alkenes partial pressure is bigger than the alkanes,[36, 37] and according to Henry's law, more alkene contents should dissolve into the extractant phase during the adsorption step of the "*Extractive Distillation*" process.[36, 37]

On the other hand, considering the hydrogen bonds formed between various solutes and solvents/extractants, as discussed in the mechanism study of the extraction process of this research, hydrogen bonds are stronger and easier to form between alkenes and extractant which has higher molecular dipole moment. Hence, extractant with higher molecular dipole moment can adsorb more alkene contents during the

"*Extractive Distillation*" process. Combined with the above discussion based on Henry's law, it can be proposed that extractant with higher molecular dipole moment will present larger gas adsorption capacity during the "*Extractive Distillation*" process for the MTCGM.

As obtained from the MCCGM's "*Extractive Distillation*" tests, the small/zero dipole moment gaseous contents in MTCGM also are supposed to dissolve more in the extractant mixture of small dipole moment n-hexane and DMC than other extractants based on the "*like-dissolves-like*" theory at beginning.[28] However, due to the much higher concentration of alkene contents in the MTCGM than in the MCCGM, and according to Henry's law and the hydrogen bond interaction between alkene contents and extractant, it was observed during the MTCGM's "*Extractive Distillation*" tests that the co-extractant with higher dipole moment presented larger gas adsorption capacity (Fig. 53).

The separation performance of extractant sample (i) to (iv) were also tested when applied to the "*Extractive Distillation*" process for MTCGM. Their separation results which obtained from the gas chromatography (GC) spectrometer were analysed and listed in Table 37. According to the results data presented in Table 37, Fig. 54 and 55 have been constructed.

Table 37. Sample (i) to (iv) separation performance with MTCGM[22-25]

Extractant Sample No.	Extractant/Extractant Mixture (1:1 in volume)	Dipole Moment of Added Co-extractant μ (D)	S_i Alkane/Alkene ratio (adsorption)	S_i Alkane/Alkene ratio (desorption)
		C2 Content		
MCCGM			**0.11**	**0.11**
i	DMC+**n-hexane**	0.08	0.25	0.12
ii	pure **DMC**	0.90	0.12	0.09
iii	DMC+**methanol**	1.70	0.14	0.09
iv	DMC+**Propylene Carbonate**	5.00	0.16	0.08
		C3 Content		
MCCGM			**0.20**	**0.20**
i	DMC+**n-hexane**	0.08	1.92	0.82
ii	pure **DMC**	0.90	0.47	0.26
iii	DMC+**methanol**	1.70	0.49	0.18
iv	DMC+**Propylene Carbonate**	5.00	0.56	0.17

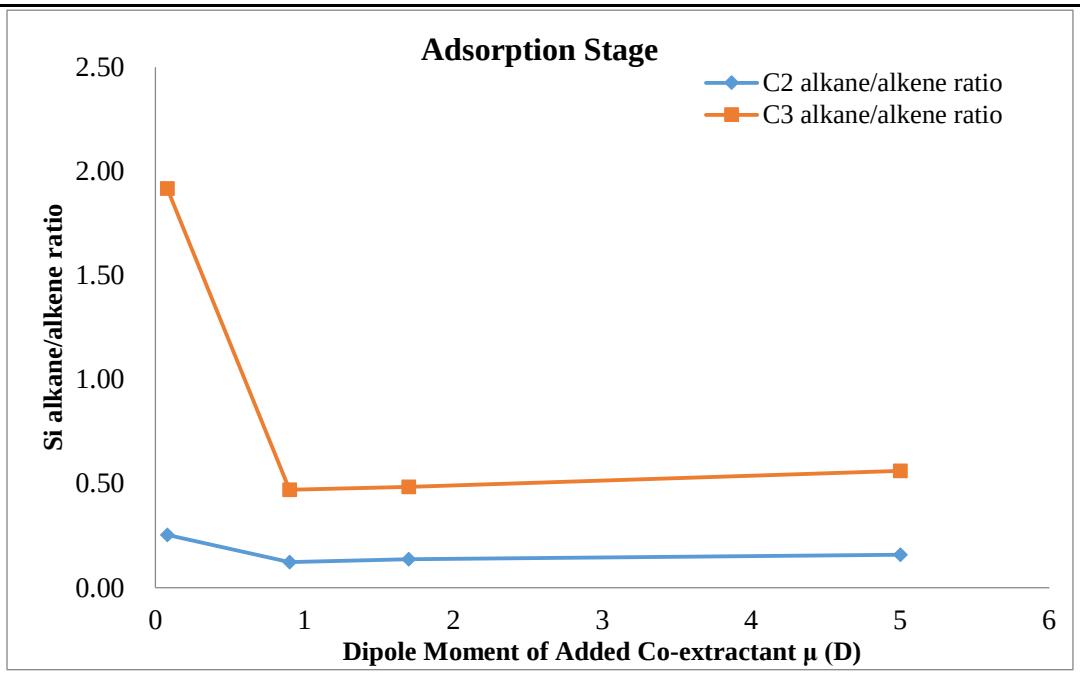

Fig. 54 Relation between the co-extractant's dipole moment and the separation performance in the "*Extractive Distillation*" process's adsorption stage with MTCGM

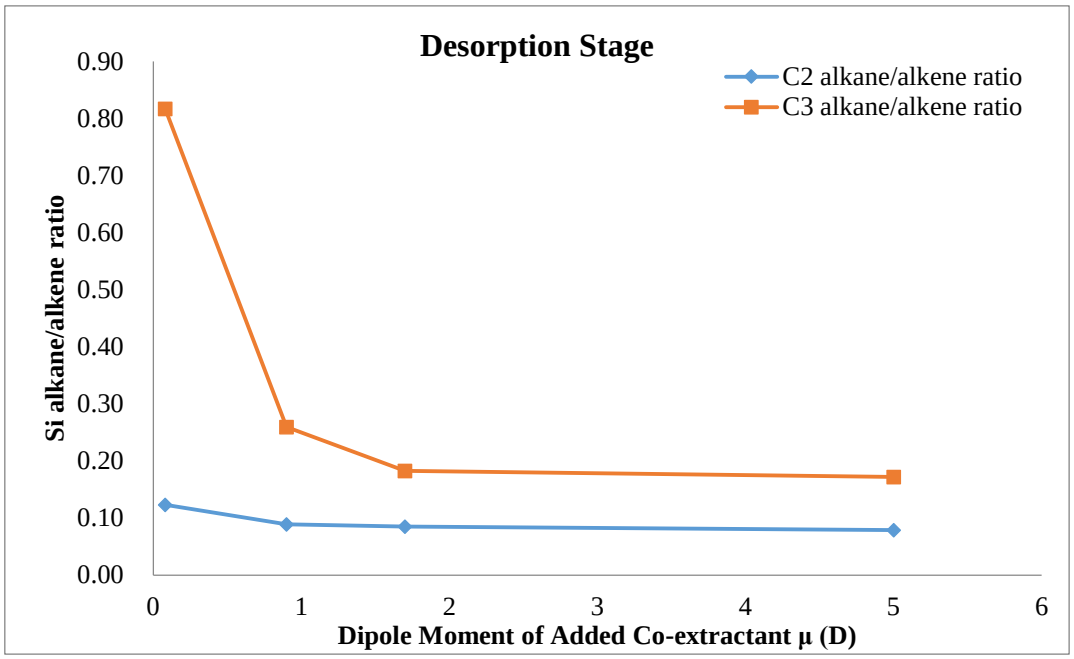

Fig. 55 Relation between the co-extractant's dipole moment and the separation performance in the "*Extractive Distillation*" process's desorption stage with MTCGM

As can be observed from Fig.54, extractant sample (i)'s C2 and C3 contents S_i values during the adsorption stage are relatively higher than the other samples. This is because compared with other extractants, the molecular dipole moment of co-extractant n-hexane (0.08 D) and gaseous hydrocarbon contents are closer,[22-25] and the partial pressure of alkenes in MTCGM is much higher than the alkanes. Therefore, due to "*like-dissolves-like*" theory and Henry's law,[28, 36, 37] more gaseous alkenes were adsorbed by extractant sample (i) than the other samples in the adsorption stage of the "*Extractive Distillation*" process.

Considering the other samples, it indicates that in the adsorption stage of the "*Extractive Distillation*" process, both the C2 and C3 alkane/alkene ratio in the gas outlet stream are increasing with the rising value of the added co-extractant molecular dipole moment (Fig. 54). This trend is the same as in the MCCGM test, which means

the absorbance of gaseous alkenes has a positive correlation with the extractant dipole moment. Moreover, during the tests, higher a alkane/alkene ratio in the outlet stream than the original alkane/alkene ratio in the MTCGM was observed. Thus, it can be confirmed that alkenes can be successfully adsorbed by extractants (i) to (iv) in the adsorption stage of the "*Extractive Distillation*" process.

The desorption results shown in Fig.55 indicates that the C2 and C3 alkane/alkene ratio in the gas outlet stream present a negative correlation with co-extractant molecular dipole moment. Through these results, sample (ii) to (iv) are confirmed to have the feasibility for separating the C2 alkene and alkane content; sample (iii) and (iv) are confirmed to have the feasibility for separating the C3 alkene and alkane content as the reason of their alkane/alkene ratio S_i are lower than 0.11 and 0.20, respectively.

The origin of these differences in the separation performance caused by the extractant molecular dipole moment has been explained in details in the previous part of the MCCGM's "*Extractive Distillation*" process.

Except C2/C3 contents there are three kinds of other gases existing in the MTCGM, which are hydrogen, carbon monoxide and methane. Therefore, in order to further confirm the feasibility of the "*Extractive Distillation*" process applied in the thermal cracked gas separation, the fraction change of these gas contents also need to be monitored. Table 38 indicates the volume/molar fraction of hydrogen, carbon monoxide and methane in the original MTCGM and each extractant's outlet gas during the desorption stage of the "*Extractive Distillation*" process. These results are

outside the experimental error estimates (± 0.005 vol.%).

Table 38. Other gases' fraction desorbed by extractant (i) to (iv) in the desorption stage of "*Extractive Distillation*" process for the MTCGM

Gas Content	MTCGM (vol.%)	n-hexane+DMC (vol.%) (i)	pure DMC (vol.%) (ii)	methanol+DMC (vol.%) (iii)	propylene carbonate+DMC (vol.%) (iv)
H_2 Fraction	**15.00%**	0.71%	0.76%	1.10%	0.74%
CO Fraction	**4.01%**	1.00%	0.89%	1.23%	0.67%
CH_4 Fraction	**24.76%**	23.56%	16.38%	15.16%	11.00%

Obviously, the molar fraction of hydrogen, carbon monoxide and methane in the outlet gas of all the extractants are reduced, means all the five extractants can remove these gas contents from the MTCGM successfully. The best performance is achieved when applied the mixture of propylene carbonate with DMC as the extractant in the "*Extractive Distillation*" process for the MTCGM.

5.2.5 Solvent for the "*Extractive Distillation*"

For the purpose of finding the most suitable solvent for "*Extractive Distillation*", the selectivity of the various candidate solvents need to be carefully considered. According to Prausnitz and Anderson, solvent selectivity within an "*Extractive Distillation*" process depends on two important aspects, the "*physical effect*" and the "*chemical effect*" between the solvent and the constituent solute.[34]

In their model framework, three points are included in the *physical effect* for consideration, and they are,

1) The different sizes between the solvent molecule and the solute, and between the various solutes to be separated;
2) The energy of vaporisation of the solvent;

3) The molar volume of the solvent.

The molecular kinetic diameters of the C2 and C3 alkenes and alkanes in our "*Extractive Distillation*" experiment are listed in Table 39. Through these kinetic diameters we find the molecular size of the alkenes is slightly larger than the size of the alkanes which have the same number of carbons. Based on Prausnitz and Anderson's theory, larger hydrocarbon will always have the larger activity coefficient.[34] That means in the "Extractive Distillation" process the solvent selectivity of larger alkenes is anticipated to be higher than the smaller alkanes. This principally confirms that the "*Extractive Distillation*" approach is able to separate alkenes and alkanes in the cracking gas.

Table 39. Molecular kinetic diameter of the C2 and C3 alkenes and alkanes[40]

C2 alkenes and alkanes	Molecular kinetic diameter (pm)	C3 alkenes and alkanes	Molecular kinetic diameter (pm)
Ethylene	390	Propylene	450
Ethane	380	Propane	430

One of the key factors to solvent selectivity lies in their term induction energy (ΔE^i), and since it is clear that if a polar host solvent can induce a larger energy of attraction in one hydrocarbon than in another, it will be selective.[34] Therefore, with regard to the second point, the polar energy of vaporisation of the solvent, the induction energy which represents the energy required to separate the dipole (solvent) and the dielectric (solute) must also be taken into account.[34]

In the absense of *chemical effects* it is possible, in principle, to compute the inductive energy between a polar molecule and a nonpolar but polarizable molecule by electrostatic theory.[34, 41] The inductive energy – ie that required to separate the

solvent from the solute – is given by[34]

$$\Delta E^i = \left(\frac{\epsilon - 1}{2\epsilon + 1}\right)\frac{\mu^2}{a^3} \qquad (14)$$

ϵ dielectric constant of the dielectric medium (solute);

μ dipole moment of solvent (D);

a the radius of solvent molecule (nm).

In this research, C2 and C3 alkenes and alkanes are the solutes which we require to be separated; and n-hexane, dimethyl carbonate (DMC), methanol and propylene carbonate are the solvent/extractant applied in the "*Extractive Distillation*" process. Table 40 and 41 list the corresponding data for computing the inductive energy between these solutes and solvents, and in Fig. 56 we plot the inductive energy of each solute with different solvents. The molecular radius of DMC ranges from 0.235 nm to 0.315 nm,[42] thus, the median value 0.275 nm is used here.

Table 40. Dielectric constant of C2 and C3 alkenes and alkanes[23]

Solute	**Dielectric constant ϵ**
Ethylene	1.00135
Ethane	1.00140
Propylene	1.00228
Propane	1.00203

Table 41. Dipole moment and molecular radius of different solvents[40, 42, 43]

Solvent	**Dipole moment μ (D)**	**Dipole moment μ (in C·m)**	**Molecular radius a (nm)**
n-hexane	0.08	$2.668*10^{-31}$	0.215
DMC	0.90	$3.002*10^{-30}$	0.275
Methanol	1.70	$5.671*10^{-30}$	0.182
Propylene carbonate	5.00	$1.668*10^{-29}$	0.305

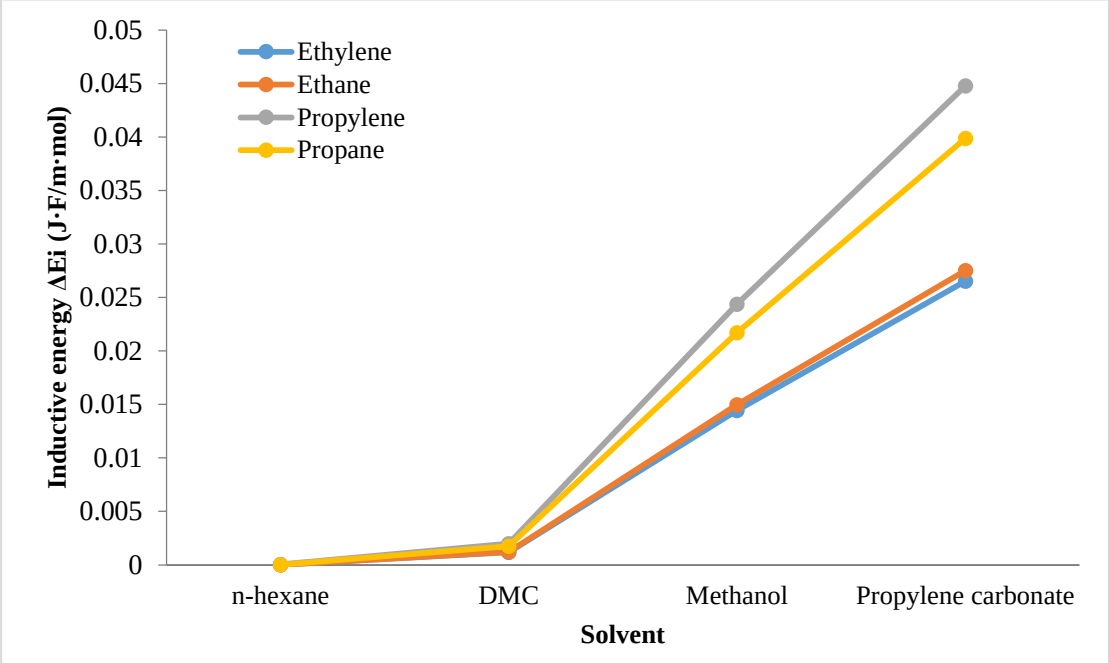

Fig. 56 Induction energy of each solute with different solvents calculated from Eq. (14)

For a more effective "*Extractive Distillation*" process, the the polar energy of vaporisation of the solvent should be large, that implies the induction energy, the energy required to separate the solvent and the solute should be large as well.[34] Compared to solvents n-hexane and DMC, methanol and propylene carbonate present much larger inductive energy with C2/C3 alkenes and alkanes (Fig. 56). Thus, methanol and propylene carbonate are more suitable for the "*Extractive Distillation*" process. From our previous experiment results methanol and propylene carbonate also present better separation performance than the others.

Moreover, since the dielectric constants of all hydrocarbons are very close to one another, being in the neighbourhood of 1, the inductive energy for a polar solvent-hydrocarbon solution therefore mainly depends on the dipole moment (μ) and size (a^3) of the solvent but very little on the nature of the hydrocarbon.[34] Hence, the solvent with larger dipole moment and smaller size will bring larger inductive energy

which leads to better selectivity.

It has been mentioned in Prausnitz and Anderson's research that the molar volume of solvent is also a critical point for the solvent selectivity.[34] They predicted that when one separates hydrocarbon of different molar volumes, the selectivity is sensitive to the polar solubility parameter.[34] This means that the effectiveness of a solvent depends on its polarity (dipole moment μ), which should be large, and on its molar volume, which should be small.[34] Table 42 lists the molar volume of various solvents utilised in our research, and among all the solvents methanol has the smallest molar volume $4.073*10^{-5}$ m^3/mol. Thus, from the viewpoint of molar volume methanol is a "*better*" solvent for use in the "*Extractive Distillation*" process than others.[34]

Table 42. Molar volume of various solvents[40]

Solvent	Molar volume (m^3/mol)
n-hexane	$13.045*10^{-5}$
DMC	$8.469*10^{-5}$
Methanol	$4.073*10^{-5}$
Propylene carbonate	$8.474*10^{-5}$

The "*chemical effect*" noted by Prausnitz and Anderson between the solvent and solute is another potentially important aspect that influences – or indeed can dominate – the solvent selectivity. The corresponding chemical viewpoint of solutions considers that any nonideality in solution arises because of association and solvation; in accordance with this concept the true species in solution can be loosely bonded aggregates consisting of two (or more) molecules of the same species (association) or of different species (solvation).[34]

We have demonstrated that unsaturated hydrocarbons may form complexes (hydrogen bonds) with various substances due to their π electron density which is strongly polarizable.[34] Thus, the solvent selectivity is, in many cases, related to the ability of a solvent to form complexes (hydrogen bonds) of different degrees of satbility with the hydrocarbons which are to be separated.[34]

In the "*Extractive Distillation*" process, since C2/C3 alkenes and alkanes of very similar size are to be separated by extractive distillation solvent (extractant), selectivity can be enhanced by choosing a solvent which will form a more stable complex with one hydrocarbon than with the other.[34] Comparing the alkanes in cracking gas with unsaturated alkenes, the alkenes form more stable hydrogen bond with hydrogen – bonded (bonding) polar solvent than alkanes.[34] Therefore, methanol and propylene carbonate, having larger dipole moments, can form more stable hydrogen bonds with the strongly polarizable alkenes, which means they are more suitable for separate alkenes and alkanes in the cracking gas than n-hexane and DMC through any such the "*Extractive Distillation*" process.

In general, then, the solvent selectivity depends primarily on the difference in size between the hydrocarbons to be separated (the larger the better), on the polar energy of vaporization of the solvent (which should be large), on the molar volume of the solvent (which should be small), and on the ability of a solvent to form complexes (hydrogen bonds) of different stability with various hydrocarbons in the solution (which should be large).[34] According to these points and combining with the experimental and computational chemistry results, it can be confirmed that methanol

is the best co-extractant in the "*Extractive Distillation*" process of the model catalytic cracking gas mixtures (MCCGM), and propylene carbonate is the best co-extractant in the "*Extractive Distillation*" process of the model thermal cracking gas mixtures (MTCGM).

5.3 Conclusions

In the previous chapter, the nature of the hydrogen bond interactions between various organic solutes (i.e. gaseous/liquid alkenes and thiophene) with the solvent methanol was studied. Due to the effect of hydrogen bond formation between the alkene/OSCs (thiophene) and methanol, it is believed that the alkenes and OSCs can be extracted/separated from various refinery products such as FCC gasoline and cracking gas mixtures through the "*Extractive Refining*" and "*Extractive Distillation*" approaches.

In this chapter the feasibility and effectiveness of the "*Extractive Refining*" approach for the FCC gasoline was investigated. Various methanol based extractant/extractant mixtures was applied in the "*Extractive Refining*" process for upgrading modelled FCC gasoline mixture and crude FCC gasoline (MFGM and CFG), and as the result of the hydrogen bond interaction between different extracts and extractants these extractants all showed excellent alkene reduction and desulfurization performance when dealing with MFGM and CFG.

On the other hand, through a series of tests of the feasibility and effectiveness of applying various organic solvents as the extractant in the "*Extractive Distillation*" process for separating the alkene contents and alkane contents in the modelled

catalytic and thermal cracked gases (MCCGM and MTCGM) was studied.

After analysing the results from the tests, it can be concluded that, during the "*Extractive Distillation*" process molecular dipole moment of the extractant shows a significant and clear correlation to the alkene/alkane separation performance. Compared with small dipole moment extractant such as n-hexane, the extractants with relative larger dipole moment do improve the separation performance. Moreover, through comparing the gas adsorption capacity results of the "*Extractive Distillation*" process for the MCCGM and MTCGM, it was found that, the process showed better performance when dealing with the MCCGM.

According to its relative better gaseous alkene/alkane separation performance and sustainable and economical characters, methanol is proposed as the key and ideal extractant for the "*Extractive Distillation*" process.

References

1 Z. Rusong, G. Junbin, Z. Juanjuan, *Petrochemical Technology* 2009, *3*, 009.

2 J. H. Gary, G. E. Handwerk, M. J. Kaiser, *Petroleum refining: technology and economics*. CRC press, Boca Raton, 2007.

3 N. Viswanadham, B. Negi, M. Garg, M. Sundaram, B. Sairam, A. Agarwal, *Fuel* 2007, *86*, 1290-1297.

4 Y. Fan, X. Bao, D. Lei, G. Shi, W. Wei, J. Xu, *Fuel* 2005, *84*, 435-442.

5 Y. Fan, X. Lin, G. Shi, H. Liu, X. Bao, *Microporous and Mesoporous Materials* 2007, *98*, 174-181.

6 P. Zhang, X. Guo, H. Guo, X. Wang, *Journal of Molecular Catalysis A: Chemical* 2007, *261*, 139-146.

7 Q. Huo, T. Dou, Z. Zhao, H. Pan, *Applied Catalysis A: General* 2010, *381*, 101-108.

8 L. Lin, G. Wang, H. Qu, J. Yang, Y. Wang, D. Shi, Y. Kong, *Journal of Membrane Science* 2006, *280*, 651-658.

9 C. Marcilly, *Studies in Surface Science and Catalysis* 2001, *135*, 37-60.

10 A. Ibrahim, S. B. Xian, Z. Wei, *Petroleum Science and Technology* 2003, *21*, 1555-1573.

11 E. Kowsari, in *Ionic Liquids - New Aspects for the Future*. InTech, Rijeka, 2013, Chap. 11.

12 M. Arias, D. Laurenti, C. Geantet, M. Vrinat, I. Hideyuki, Y. Yoshimura, *Catalysis Today* 2008, *130*, 190-194.

13 G. A. Huff Jr, O. S. Owen, B. D. Alexander, D. N. Rundell, W. J. Reagan, J. S. Yoo, US 5863419 A, 1999.

14 P. Xu, J. Feng, B. Yu, F. Li, C. Ma, in *Biotechnology in China I*, ed. by J.-J. Zhong, F.-W. Bai, W. Zhang, Springer, Berlin, 2009, Vol. 113, Chap. 16.

15 J. L. García-Gutiérrez, G. A. Fuentes, M. E. Hernández-Terán, F. Murrieta, J. Navarrete, F. Jiménez-Cruz, *Applied Catalysis A: General* 2006, *305*, 15-20.

16 L. Lin, Y. Zhang, Y. Kong, *Fuel* 2009, *88*, 1799-1809.

17 A. Samokhvalov, *Catalysis Reviews* 2012, *54*, 281-343.

18 W. E. Garwood, US 3894939 A, 1975.

19 C.-J. Yang, R. B. Jackson, *Energy Policy* 2012, *41*, 878-884.

20 V. Vishwanathan, K.-W. Jun, J.-W. Kim, H.-S. Roh, *Applied Catalysis A: General* 2004, *276*, 251-255.

21 R. C. Delgado, A. S. Araujo, V. J. Fernandes, *Fuel Processing Technology* 2007, *88*, 365-368.

22 J. F. Jansen, A. A. Dias, M. Dorschu, B. Coussens, *Macromolecules* 2002, *35*, 7529-7531.

23 W. M. Haynes, in *CRC handbook of chemistry and physics*. CRC press, Boca Raton, 2014, Sec. 9.

24 C. Bowman, D. Gordon, *The Journal of Chemical Physics* 1967, *46*, 1878-1883.

25 W. J. Hehre, J. A. Pople, *Journal of the American Chemical Society* 1975, *97*, 6941-6955.

26 CNCIC, in *Book Gas Market Research Report of China*. China National Chemical Information Center, 2012.
27 T. Brinck, J. S. Murray, P. Politzer, *Molecular Physics* 1992, *76*, 609-617.
28 K. L. Williamson, K. M. Masters, *Macroscale and Microscale Organic Experiments*. 6th Ed., Brooks Cole, Belmont, 2010.
29 A. F. M. Barton, *Chemical Reviews* 1975, *75*, 731-753.
30 A. F. Barton, *CRC handbook of solubility parameters and other cohesion parameters*. CRC press, Boca Raton, 1991.
31 K. Kowski, W. Lüttke, P. Rademacher, *Journal of Molecular Structure* 2001, *567–568*, 231-240.
32 K. Oku, H. Watanabe, M. Kubota, S. Fukuda, M. Kurimoto, Y. Tsujisaka, M. Komori, Y. Inoue, M. Sakurai, *Journal of the American Chemical Society* 2003, *125*, 12739-12748.
33 B. M. Kariuki, K. D. Harris, D. Philp, J. M. Robinson, *Journal of the American Chemical Society* 1997, *119*, 12679-12680.
34 J. Prausnitz, R. Anderson, *AIChE Journal* 1961, *7*, 96-101.
35 Z. Lei, C. Li, B. Chen, *Separation & Purification Reviews* 2003, *32*, 121-213.
36 W. Lewis, W. Whitman, *Industrial & Engineering Chemistry* 1924, *16*, 1215-1220.
37 R. Battino, H. L. Clever, *Chemical Reviews* 1966, *66*, 395-463.
38 G. E. Keller, A. E. Marcinkowsky, S. K. Verma, K. D. Williamson, *Olefin recovery and purification via silver complexation*. Marcel Dekker, New York, 1992.
39 D. J. Safarik, R. B. Eldridge, *Industrial & Engineering Chemistry Research* 1998, *37*, 2571-2581.
40 W. G. M. P.J. Linstrom, *NIST Chemistry WebBook*. National Institute of Standards and Technology, 2015.
41 C. J. F. Böttcher, *Theory of electric polarization*. Elsevier, Amsterdam, 1952.
42 X. Dong, Y. Lin, *Chemical Communications* 2013, *49*, 1196-1198.
43 D. T. L. Galhena, B. C. Bayer, S. Hofmann, G. A. J. Amaratunga, *ACS Nano* 2016, *10*, 747-754.

Chapter 6. Catalytic Conversion of Solvent Extraction Mixtures in a Micro-Reactor System

In our previous experiments, methanol based extractant mixtures showed both excellent alkene reduction and desulfurization performance when applied in the "*Extractive Refining*" approach for upgrading Model FCC Gasoline Mixture (MFGM) and crude FCC gasoline (CFG). The "*Extractive Refining*" process produces two phases of products that can be separated in vertical order. The first, the upper phase mixture (UPM), consists of upgraded high octane number clean FCC gasoline as the final product (Fig. 57). The second, lower phase mixture (LPM), contains methanol based extractant mixtures and extracts from the crude FCC gasoline, such as alkenes, alkanes, aromatics and OSCs (Fig. 57).

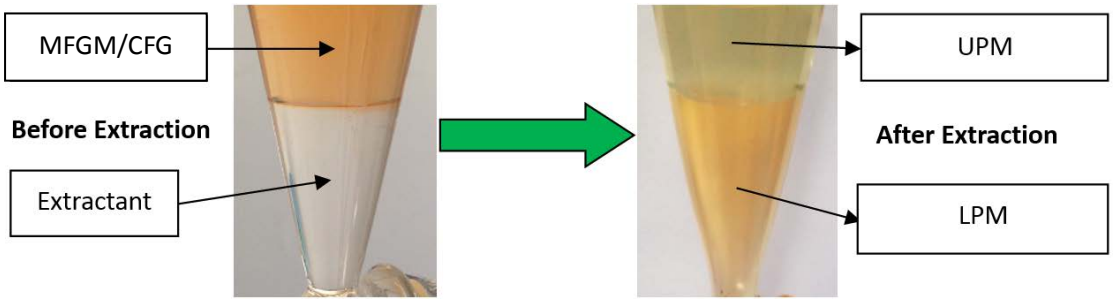

Fig. 57 The "*Extractive Refining*" approach

In order to sufficiently utilise all the products from the "*Extractive Refining*" approach, the LPMs utilised as the beginning in a subsequent extraction catalytic conversion process (Fig. 58). The nature and the performance of this catalytic conversion process is the subject of this chapter.

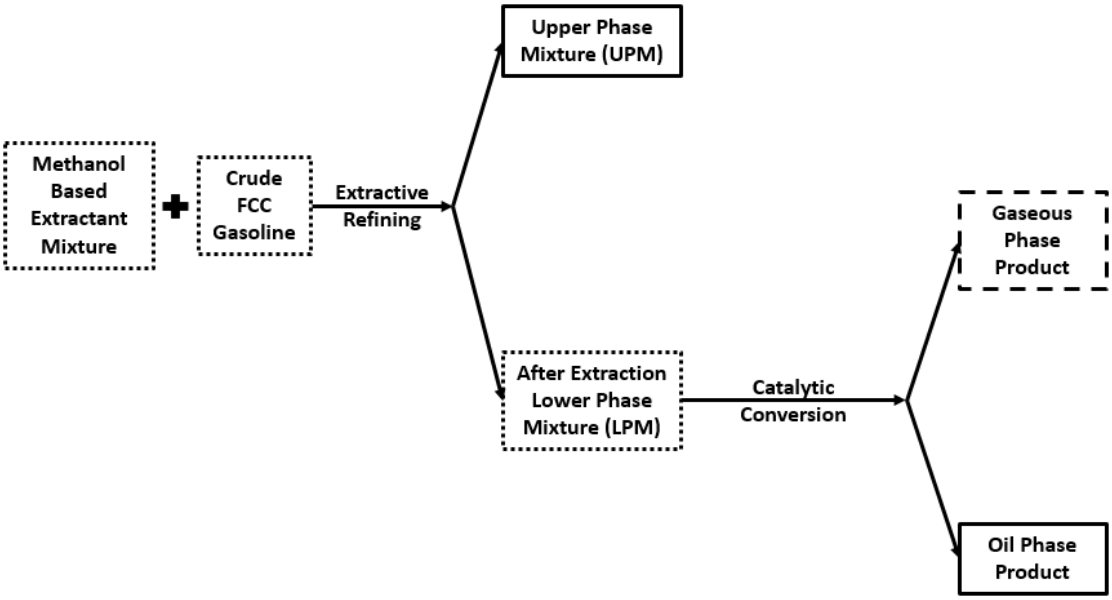

Fig. 58 Schematic step of the extraction refining and the catalytic conversion following extraction

The "Post extraction catalytic conversion" process is very similar to that of the established methanol to hydrocarbon (MTH) conversions, e.g., the methanol to gasoline (MTG) catalytic conversion process. Thus, in the first place, various organics (i.e. alkene, alkane, aromatics, OSCs and other alcohol content) existing in the LPM is individually co-fed, with methanol, as feedstock in the MTH process, with the aim of investigating other organics' co-feeding effects during the MTH process.

Secondly, the LPMs from the MFGM II "*Extractive Refining*" process, and from the CFG II "*Extractive Refining*" processes are used as the feedstocks in the post extraction catalytic conversion process, respectively (Fig. 58). For both, unmodified and modified HZSM-5 catalysts were applied in these post – extraction catalytic conversion processes. The conversion experiments are carried out in a fixed bed catalytic micro-reactor system. The conversion performances, the pre/post reaction catalysts and the final products of these catalytic conversion processes were

characterized.

Error estimates analyses for the experimental data are described in Appendix. Those for:

1) The analysis of the gaseous products' production rate in Appendix 3.8;
2) The analysis of the total yield of oil phase product from the catalytic conversion in Appendix 3.9;
3) The analysis of the liquid content's (BTX) distribution in Appendix 3.4;
4) The analysis of the OSCs fraction in Appendix 3.5;
5) The analysis of the sample's boiling point in Appendix 3.6;
6) The analysis of the spent catalyst's coke deposition in Appendix 3.6;

6.1 The Effects of Co-Feeding of Various Organics on Methanol Catalytic Conversion Process

Fig. 11, shows the dual-cycle concept for the methanol to hydrocarbon conversion over HZSM-5,[1-4] and this concept has been applied as the core to analysed the co-feeding effect of various organic on methanol catalytic conversion in conjunction with the experimental results.

In the experiments (presented in detail in Appendix 1), the conversion of methanol with various other organics existing in the LPMs were examined and analysed. During the experiments 1-hexene, n-octane, p-xylene, thiophene and ethylene glycol were chosen as the typical organic compounds to represent the alkene, alkane, aromatics, OSCs and other alcohol present in the LPMs, respectively. The analysis of the products from these co-feeding conversions was carried out using an on-line gas

chromatograph (GC), the total yield of the oil phase product and the specific yield of benzene, toluene and xylenes (BTX) in the oil phase product, which are the relative higher added value products are collected and analysed using an off-line gas chromatograph-mass spectrometer (GCMS), which are among all the organics produced from the conversions. The complete data and corresponding analyses of these co-feeding conversions are presented in Appendix 1.

The catalyst applied in these co-feeding conversions was unmodified HZSM-5 catalyst, and the silicon to aluminium Si/Al ratio of this catalyst is 60. These catalytic conversions were all tested at 400℃ and under atmosphere pressure (1atm). In the preparation step of each conversion 1.0 gram HZSM-5 catalyst was loaded into the tubular reactor, and during the conversion process, 2.0 grams of feedstock was pumped into the catalyst bed using the HPLC pump every hour, that means the weight hour space velocity (WHSV) of the process was 2 $hour^{-1}$.

6.1.1 Mechanism of the Co-Feeding Effect

The underpinning mechanism of the co-feeding effect of alkene, alkane, aromatics and co-extractant (alcohol/oxygenate) during the MTH catalytic conversion can be explained by the conversion mechanism of methanol. In the case of HZSM-5, a conversion mechanism involving methylation and subsequent cracking of higher alkenes is proposed in parallel with the aromatic-based hydrocarbon pool mechanism, *i.e.* the *dual-cycle* mechanism shown in Fig. 11.[1-5]

Through the *dual-cycle* mechanism it can be found that, when the alkene, alkane, aromatics and co-extractant (alcohol/oxygenate) is blended into methanol and came

into contact with catalyst in the reactor, all these co-feeding hydrocarbons act as the extra intermediates of the conversion process.

The added alkene and alkane promote the reactions in the ***Conversion cycle II*** (left) of the dual-cycle. The added alkenes can increase the yield and the selectivities to alkenes, which may be due to the competition for stronger acidic sites for the reactions of alkene with methanol.[6] On the other hand, methanol to hydrocarbons conversion is an exothermic reaction, co-feeding alkane into the MTH conversion might have compensated for the acid strengths and reduced temperature associated with the endothermic individual alkane cracking reaction, and this also leads to the enhancement of the yield and alkenes selectivities.[7]

The added aromatics promote the reactions in the ***Conversion cycle I*** (right), they are readily absorbed into the channels of HZSM-5 zeolite and promote the catalytic activity of the catalyst for conversion of methanol to hydrocarbons.[8] From the above experiments results, the promotion effect of the added aromatics (p-xylene) on the yield of MTH conversion was surely observed.

Moreover, the co-extractant (alcohol/oxygenate) promotes the reactions in both cycles. The co-extractant ethylene glycol utilised in this study provides higher carbon density ($2CH_2OH$) than methanol (CH_3OH). It produces more C3 and C4 alkanes when the conversion temperature is above 300 ℃, and it has a higher conversion rate than pure methanol feedstock.[9] Therefore, a higher oil phase yield was observed when ethylene glycol is co-fed with methanol during the MTH conversion than pure methanol as feedstock.

The preliminary purpose of examining the OSCs co-feeding effect on MTH conversion is to study its deactivation of catalyst during the conversion process, since there are always OSCs existing in the "*Extractive Refining*" process's post extraction LPMs, and these LPMs were utilised as the feedstock in the after "*Extractive Refining*" process LPM catalytic conversion process. Through the above co-feeding experiments, it has been found that relatively low concentration (1000-4000 ppm) OSCs (thiophene) does not increase the coke deposition rate and deactivate the HZSM-5 catalyst we used during the conversion process. During the conversion process with the hydrogen, which is one of the major gaseous products from the methanol conversion process, OSCs is converted into harmless and useful hydrocarbons, and sulphur is removed by the in-situ HDS process.[10] And surprisingly, the added OSCs (thiophene) even enhanced the yield of the co-feeding conversion's oil phase product. Thus, the post extraction LPM catalytic conversion process is believed able to remove sulphur from the feedstock by HDS during the catalytic reaction.

To sum up, the formation of the higher alkenes in the co-feeding systems is promotes by the added alkene and alkane. Thus, more liquid hydrocarbons are generated by the increasing amount of these higher alkenes. Moreover, the added aromatics promotes the catalytic activity of the catalyst for conversion of methanol to hydrocarbons.[8] Meanwhile, OSCs is removed by the HDS process during the conversion. As the final results, the total yield of the oil phase is improved by these added co-feeding raw materials, and the oil phase product should be clean which means low OSCs content.

6.2 Catalytic Conversion the Extracts of Model FCC Gasoline Mixture (MFGM)

From the above co-feeding experiments of various organics such as alkene, alkane, aromatics and co-extractant (alcohol/oxygenate) ethylene glycol with methanol, it is found that, importantly, compared with pure methanol feeding system, these co-feed organics all improve the MTH conversion performances, and the yield of the oil phase product from the MTH conversion was enhanced by adding these organics into the feedstock. The mechanisms of these alkene, alkane, aromatics and co-extractant (alcohol/oxygenate) co-feeding effects were also studied, respectively. Moreover, through the OSCs co-feeding experiments it is discovered that the added OSCs (thiophene) are removed by the in-situ HDS process of the catalytic MTH process.

Based on this analyses and practical experimental results it is confirmed that the MTG process can give a better yield of the oil phase product when applying the MFGM II's post extraction LPM from the "*Extractive Refining*" process as the feedstock than the pure methanol in the MTG conversion process. The schematic step of the catalytic conversion following the extraction process is presented in Fig. 59.

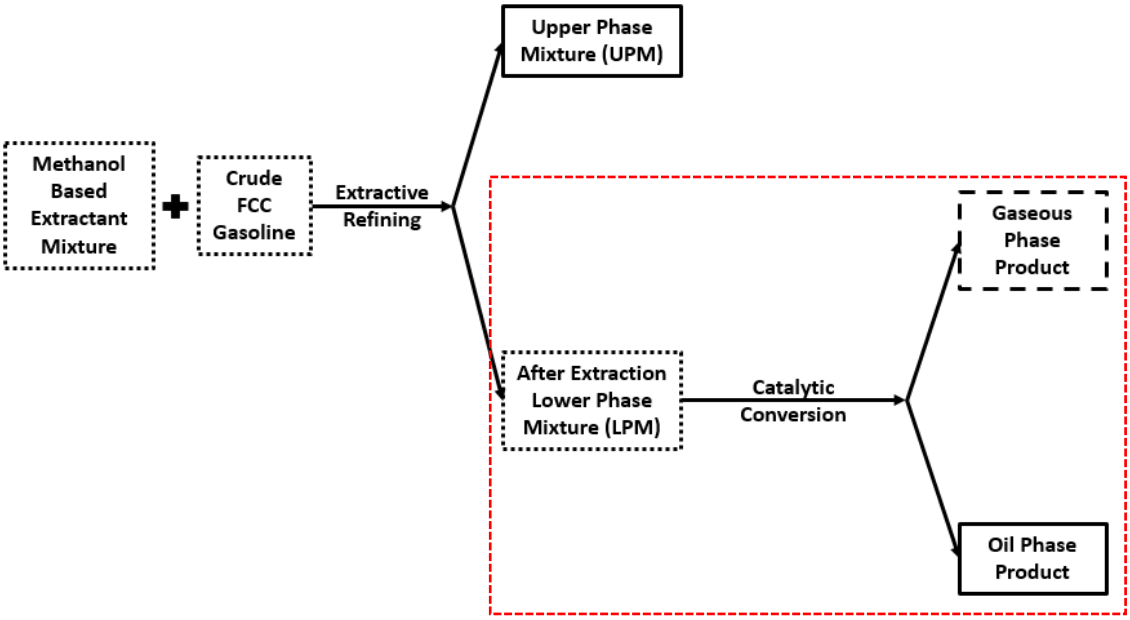

Fig. 59 Schematic step of the catalytic conversion following extraction (in red)

In these experiments, 25% in wt. ethylene glycol was mixed with 75% in wt. methanol at first to form the extractant mixture. Secondly, this extractant mixture was used to deal with the MFGM II during the "*Extractive Refining*" process. GCMS was employed to analyse the UPM and LPM from the MFGM II's "*Extractive Refining*" process.

The result indicated the OSCs (thiophene) was successfully removed from the MFGM II after the "*Extractive Refining*" process, and the mass fraction of alkene (1-hexene) and aromatics (p-xylene) were also reduced by the extraction process.

Therefore, from this novel "*Extractive Refining*" process two types of products are obtained. They are (1) the UPM which is the clean FCC gasoline (MFGM) of the post extraction mixture and (2) the LPM which is the feedstock for the post extraction catalytic conversion process at the Lower Phase of the post extraction mixture. The composition of each mixture in the after "*Extractive Refining*" process LPM of MFGM II is listed in Table 43.

Table 43. Composition of model FCC gasoline mixture (MFGM) II's post extraction lower phase mixture (LPM)

	methanol	**1-hexene**	**thiophene**	**Ethylene glycol**	**n-octane**	**p-xylene**
wt % (±0.05 %)	60.4	11.0	900±0.5 ppm	22.0	5.2	1.4

After carefully separating the UPM and LPM, the LPM from MFGM II's "*Extractive Refining*" process was pumped into the micro-reactor as the feedstock to proceed the MTG catalytic conversion process. The same procedure was adopted in all the co-feeding experiments, the catalyst used in these after "*Extractive Refining*" processes, LPM catalytic conversions are tested over the unmodified HZSM-5 with Si/Al ratio of 60. For the aim of finding the most suitable conversion conditions the process was examined at 400℃, 350℃, 300℃, respectively. Although at 400℃ and 350℃ the process presented very positive results, when the reaction temperature drops down to 300℃ the conversion rate of the feedstock decreases rapidly and very little oil phase product is collected. Thus, temperatures below 300℃ are regarded as non-effective reaction temperatures.

In the reaction preparation step, 1.0 gram of HZSM-5 catalyst with Si/Al ratio of 60 is loaded into the reactor tube. During reaction 2.0 grams of the LPM from the MFGM II's after "*Extractive Refining*" process is pumped into the microreactor every hour. Thus, the weight hour space velocity (WHSV) of the process is also equal to 2 $hour^{-1}$. The detailed experimental procedure of the catalytic conversion is shown in 3.4.2 of Chapter 3.

Gaseous products' production rates were obtained from the GC and the results

were presented in Fig. 60. These results are outside the experimental error estimates (± 0.005 ml/min). It was found that hydrogen production rate was decreased when MFGM II's after "*Extractive Refining*" process LPM were applied as the feedstock. Through the previous mechanism discussion this observation can be explained by the HDS process of the OSCs content (thiophene) which contains in the LPM.[11] The output of gaseous alkene reached the highest rate when the post extraction conversion process was carried out at 350℃. At this temperature the gaseous alkane's output rate was reduced too.

Since lower reaction temperature increases the alkylation of benzenes, and these alkylated benzenes deactivate the HZSM-5 catalyst by blocking the access to and from its active acid sites,[4, 12] the hydrogen transfer during the conversion is reduced with weaker/less active acid sites.[4, 13] Under this circumstance, less gaseous alkene is converted to gaseous alkane through hydrogen transfer. As a consequence, when the reaction temperature of post extraction LPM conversion is reduced from 400℃ to 350℃, the production of gaseous alkene is increased and the production of gaseous alkane is decreased.

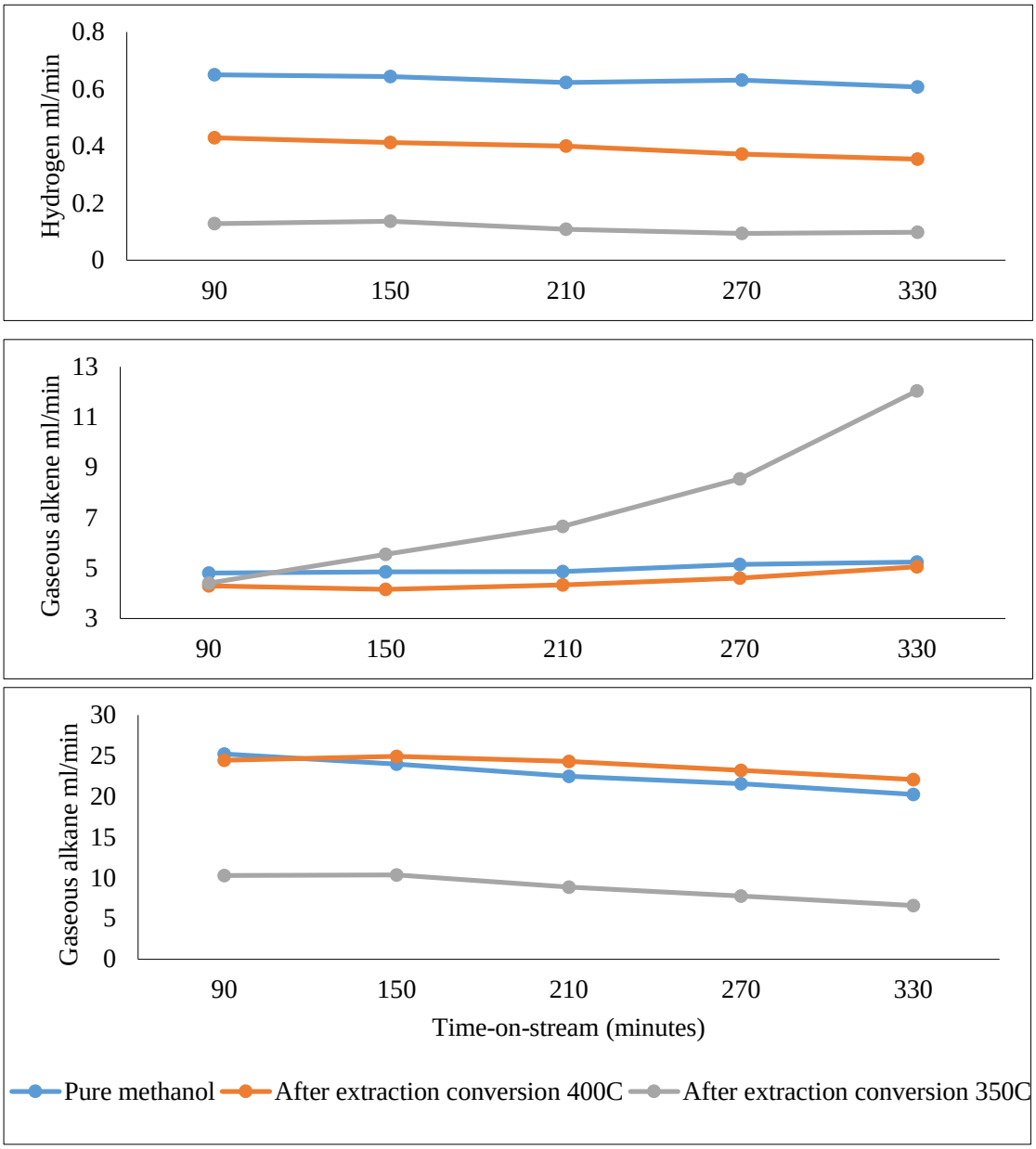

Fig. 60 Time-on-stream gaseous products' production rate of the model FCC gasoline mixture (MFGM) II's after "*Extractive Refining*" process lower phase mixture (LPM) conversions

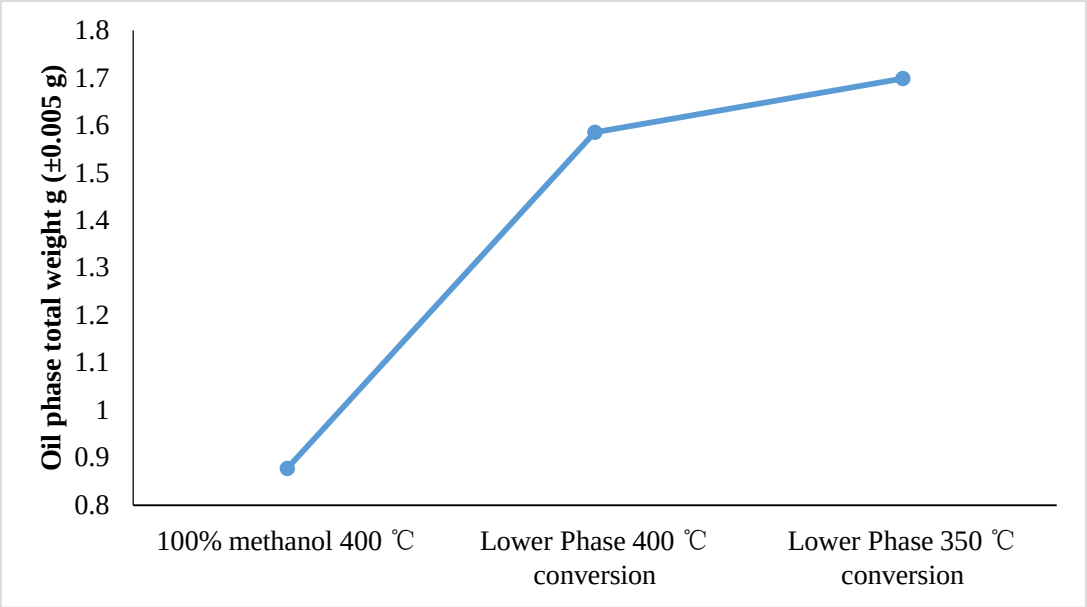

Fig. 61 Changes of oil phase product yield with the model FCC gasoline mixture (MFGM) II's after "*Extractive Refining*" process lower phase mixture (LPM) conversions

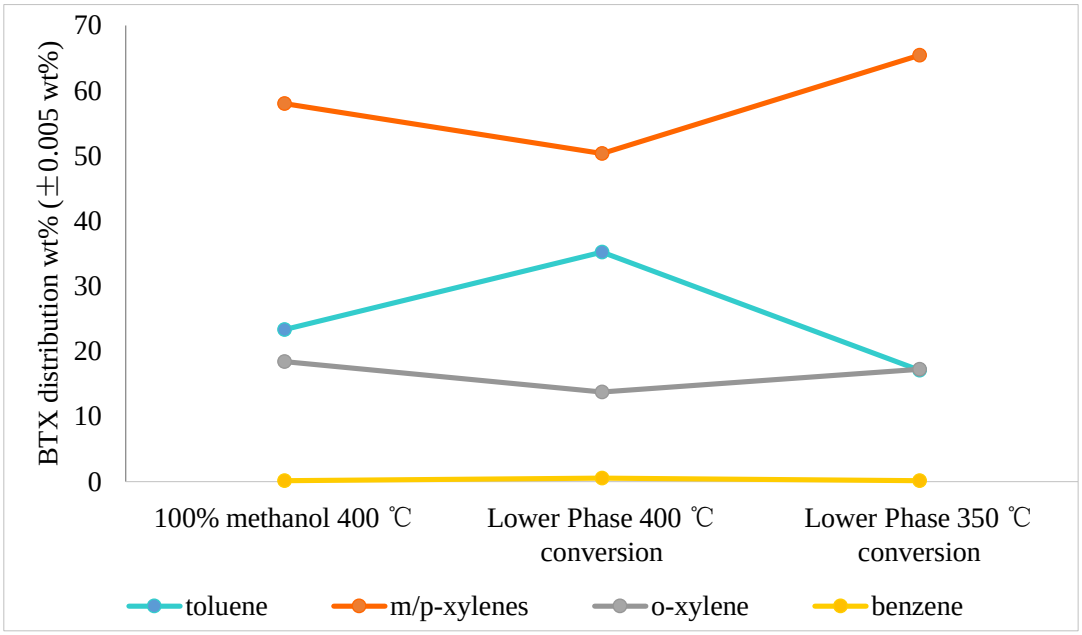

Fig. 62 Benzene, toluene, xylenes (BTX) distribution in the product of the model FCC gasoline mixture (MFGM) II's after "*Extractive Refining*" process lower phase mixture (LPM) conversions

The total yield of the oil phase product from the MFGM II's after "*Extractive Refining*" process LPM catalytic conversions at different reaction temperature are displayed in Fig. 61. From these total yield results of the oil phase product, a rapidy

increasing trend can be observed between pure methanol MTG process's and this LPM conversion's oil phase yield. That means, under the same reaction conditions, with the utilisation of MFGM II's after "*Extractive Refining*" process LPM, the total oil phase yield of the MTG catalytic conversion process was improved by nearly 81 wt%. Although, as described previously, the number/density of active acid sites is decreased by the lower reaction temperature, the overall catalyst performance is improved.[4, 12, 14] Therefore, the process achieved an even higher oil phase yield in the post extraction conversion process when the reaction temperature dropped to 350℃. Compared with pure methanol MTG process a 94% improvement of the total yield of oil phase at this temperature was obtained.

Moreover, from the GCMS analysis of the high added value aromatic compounds yield, it was found xylenes' distribution decreased and toluene and benzene's distribution increased by utilised the MFGM II's after "*Extractive Refining*" process LPM as feedstock rather than pure methanol during the MTG process at 400℃ (Fig. 62). The decreased fraction of methanol in the feedstock reduces the methylation of the formed benzene and toluene (Scheme 1).[5] Therefore, compared with pure methanol MTG conversion, the increase in consistent with toluene distribution and decrease in xylenes distribution were observed in the post extraction LPM conversion.

When the reaction temperature dropped to 350℃ the distribution of m/p-xylene increased to 65 wt% and toluene's distribution reduced to 17 wt%. O-xylene and benzene's distribution of this conversion was similar to pure methanol MTG conversion at 400℃. This is because a higher temperature above 350℃ leads to

dealkylation of alkylated benzene molecules such as C8/C8+ aromatics.[4, 12] This dealkylation process is restrained when the reaction temperature dropped from 400℃ to 350℃. As the methylation is quicker than the decomposition or further reaction of the benzenes species according to the hydrocarbon-pool mechanism with lower temperature,[4, 15-17] Fig. 62 shows that the xylenes distribution is increasing, toluene and benzene distribution is decreasing with the reduced temperature in the conversion of MFGM II's after "*Extractive Refining*" process LPM.

Therefore, through the above large improvement of the oil phase yield, it is confirmed that the MTG process can achieve better yield of the oil phase product when applying the MFGM II's post extraction LPM from the "*Extractive Refining*" process as the feedstock instead of the pure methanol.

6.3 Catalytic Conversion the Extracts of Crude FCC Gasoline (CFG)

The MFGM II's after "*Extractive Refining*" process LPM catalytic conversions showed very good performance, and compared with the conventional pure methanol MTG conversion the LPM conversion gives much higher yield of the oil phase product, implying the post extraction LPM conversion successfully enhances the effectiveness of the MTG process.

In order to examine the performance of the above post extraction LPM catalytic conversion process for the practical application, the LPM from the crude FCC gasoline (CFG) II's "*Extractive Refining*" processes were described in details in the above "*Methods*" and "*Performance Study of the Extractive Refining/Distillation Process*" parts is utilised as the feedstock for the catalytic conversion process.

During this series of conversion tests, the unmodified HZSM-5 Si/Al=60 and modified HZSM-5 Si/Al=60 (0.10C 60) zeolites are used as the catalyst. For the aim of obtaining the highest yield from the practical CFG II's after "*Extractive Refining*" process LPM catalytic conversion, the catalyst's performances under different reaction conditions such as different reaction temperatures and pressures were examined. 2.0 grams of catalyst is loaded into the reactor tube, and 4.0 grams of the above LPM was pumped into the microreactor as the feedstock every hour, thus, the WHSV of this process was 2 $hour^{-1}$. The detailed experimental procedure of the catalytic conversion is also shown in 3.4.2 of Chapter 3.

During the study, the unmodified HZSM-5 was firstly utilised as the catalyst in the CFG II's after "*Extractive Refining*" process LPM catalytic conversion process. The tests were carried out at 400℃ and under atmosphere pressure (1atm). Then, the modified ZSM-5 zeolite 0.10C60 was applied as the catalyst in the conversion process, the conditions of the conversion were kept the same, and after this conversion, the pressure during the following conversion process was set to 2bar higher than 1atm (1atm+2bar), the catalyst was still 0.10C60. In these catalytic tests, the conversion temperature was reduced to 350℃ and pressure was kept at 1atm+2bar, the catalyst was also 0.10C60.

6.3.1 Gaseous and Liquid Products from the Catalytic Conversion

The gaseous products' output rate from these conversion processes were obtained from the GC and the results were presented in Fig. 63. These results are outside the experimental error estimates (± 0.005 ml/min).

In all the figures of this section (6.3.1), "**Pure methanol 400C HZSM-5 60 1atm**" means pure methanol conversion with HZSM-5 catalyst with Si/Al ratio of 60 at 400℃ and under atmosphere pressure reaction conditions; "**CFG II 400C HZSM-5 60 1atm**" means crude FCC gasoline (CFG) II's after "*Extractive Refining*" process lower phase mixture (LPM) conversion with HZSM-5 catalyst with Si/Al ratio of 60 at 400℃ and under atmosphere pressure reaction conditions; "**CFG II 400C 0.10C 60 1atm**" means crude FCC gasoline (CFG) II's after "*Extractive Refining*" process lower phase mixture (LPM) conversion with the modified catalyst 0.10C60 at 400℃ and under atmosphere pressure reaction conditions; "**CFG II 400C 0.10C 60 1atm+2bar**" means crude FCC gasoline (CFG) II's after "*Extractive Refining*" process lower phase mixture (LPM) conversion with the modified catalyst 0.10C60 at 400℃ and under 2bar higher than atmosphere pressure reaction conditions; "**CFG II 350C 0.10C 60 1atm+2bar**" means crude FCC gasoline (CFG) II's after "*Extractive Refining*" process lower phase mixture (LPM) conversion with the modified catalyst 0.10C60 at 350℃ and under 2bar higher than atmosphere pressure reaction conditions.

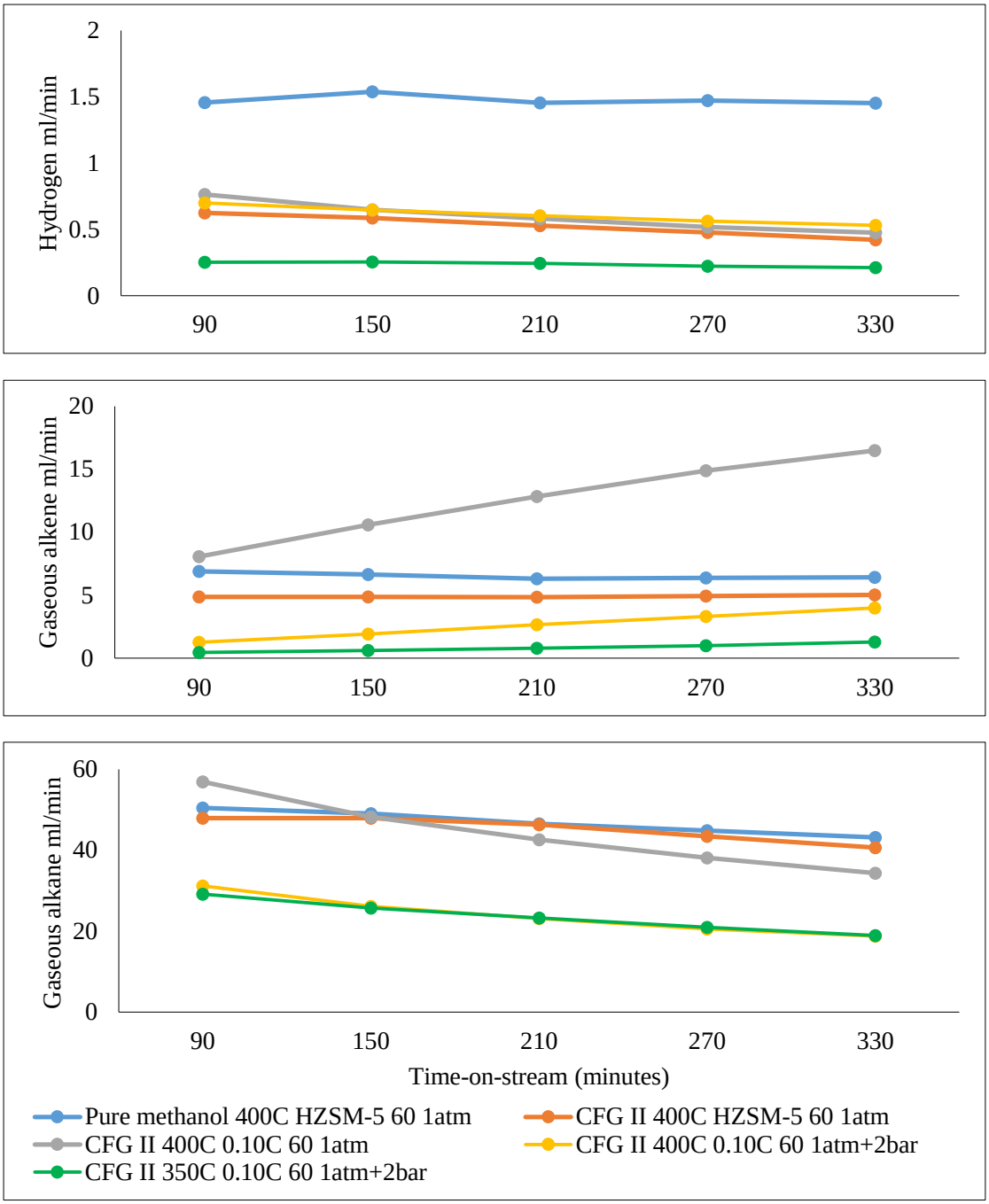

Fig. 63 Time-on-stream gaseous products' production rate of the crude FCC gasoline (CFG) II's after "*Extractive Refining*" process lower phase mixture (LPM) conversions

Similar to the MFGM II's after "*Extractive Refining*" process LPM catalytic conversion process, it can be found that hydrogen generation rate was also decreased when applying CFG II's after "*Extractive Refining*" process LPM as the feedstock (Fig. 63). This also can be explained by the HDS process of the OSCs content

(thiophene) which contains in the CFG II's LPM.[11] Whilst, the gaseous product generation rate results of these conversions indicate the hydrogen output rate was not affected by the increased pressure very much. However, the lower conversion temperature does have an influence on this rate. It can be observed that the decreased temperature reduced the hydrogen output rate significantly. This can be explained that the lower reaction temperature reduces the catalytic cracking of the methanol and hydrocarbons.[1-4, 18]

Since the modified catalyst 0.10C60 provides superior catalyst porosity, larger surface area, broader pore size, stronger acidity and more acid sites than the unmodified HZSM-5 catalyst,[19-21] the overall conversion is improved,[22] and more alkene is formed from methanol as the intermediate of the conversion.[4] Thus, the conversion over the modified catalyst 0.10C60 showed a higher generation rate of gaseous alkene than the unmodified HZSM-5 catalyst when the CFG II's after "*Extractive Refining*" process LPM conversion is carried out at the same temperature, e.g., 400℃ and atmosphere pressure conditions (Fig. 63). With the same HZSM-5 catalyst the CFG II's LPM conversions gaseous alkene output rate was slightly lower than pure methanol conversion at 400℃ and under atmosphere pressure. This is because the cycle II in Fig. 11 was suppressed when the feedstock was changed from methanol to post extraction LPM which contains aromatics.[1-5] Moreover, lower temperature (350℃) and higher pressure (1atm+2bar) enhance the aromatization of higher alkenes formed in the alkene-base cycle II, as shown in Fig. 11 of the methanol conversion.[1-5, 23, 24] As a consequence, the alkene output rate was reduced when higher

pressure was applied in the conversion process, and lower temperature (350℃) with higher pressure (1atm+2bar) presented the lowest gaseous alkene output rate.

On the other hand, compared with pure methanol as the feedstock, a slightly lower gaseous alkane output rate was achieved when the CFG II's after "*Extractive Refining*" process LPM was utilised as the feedstock at 400℃ and atmospheric pressure conditions (Fig. 63). This is also because the alkene-based cycle II in Fig. 11 was suppressed when the feedstock was changed from methanol to post extraction LPM which contains aromatics.[1-5] Meanwhile, under these conversion conditions, the unmodified HZSM-5 catalyst showed slightly higher output rate of gaseous alkane than the modified 0.10C60 catalyst, because the modified 0.10C60 catalyst is better at forming C5+ species than gaseous alkane.[25] Also, due to relative lower temperature (350℃) and higher pressure (1atm+2bar) enhancing the methanol conversion's aromatization process,[1-5, 23, 24] the pressure of the conversion process also indicated a negative correlation with the gaseous alkane output rate. At lower temperature (350℃) with higher pressure (1atm+2bar) lead to the lowest gaseous alkane output rates.

Regarding to the liquid product, the total yields of the oil phase product from the above conversions are presented in Fig. 64. From these results, it can be found that the yield of the oil phase was enhanced when the LPM from the CFG II's "*Extractive Refining*" process utilised as the feedstock in the catalytic conversion step. This result is due to the co-feeding effects of various organic contents with methanol which have been discussed in the previous part. As the result of these co-feeding effects, the extracts such as alkenes, alkanes, aromatics etc. existing in the CFG II's after

"*Extractive Refining*" process LPM enhanced the oil phase yield 45% in wt. when compare with pure methanol MTG process.

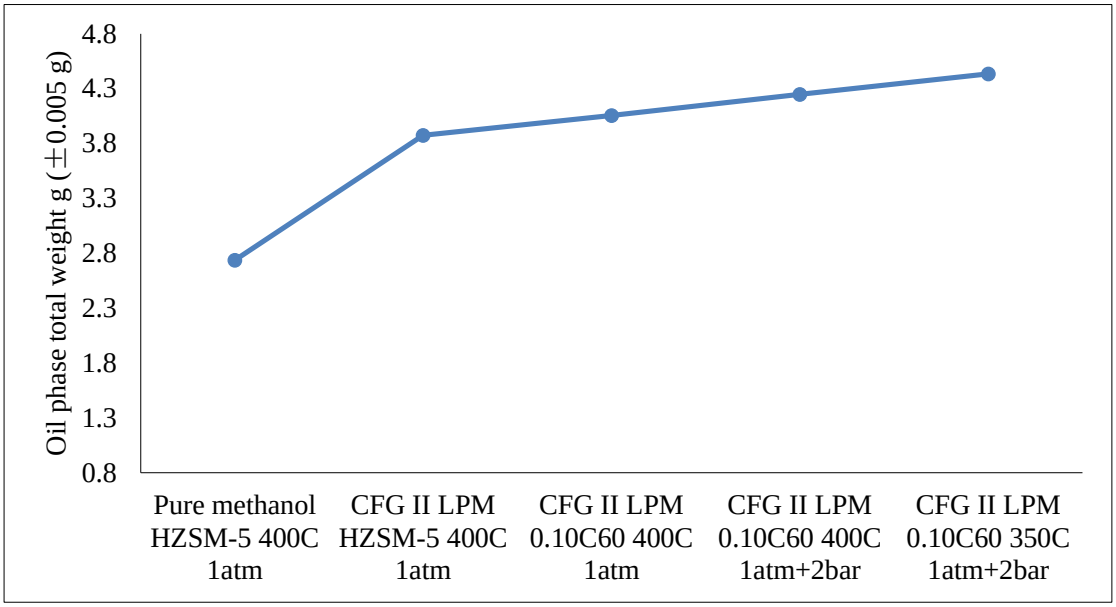

Fig. 64 Changes of oil phase product yield with the crude FCC gasoline (CFG) II's after "*Extractive Refining*" process lower phase mixture (LPM) conversions

In order to achieve the best oil phase yield, the modified catalyst 0.10C60 was used for the CFG II's after "*Extractive Refining*" process LPM conversion. The characterization and comparison of the modified catalyst and unmodified HZSM-5 is described in the following pre- and post-reaction catalyst properties part. Compared with the unmodified HZSM-5 catalytic MTG process, the oil phase yield of the conversion process achieved 5% in wt. improvement over the modified 0.10C60 catalyst.

Since higher pressure during the MTG conversion process can enhance the gasoline/oil phase yield,[26] and relatively low catalyst deactivation rate can be achieved with higher reaction pressure,[24] the 2bar above atmosphere pressure reaction condition was used in the CFG II's after "*Extractive Refining*" process LPM

conversion to maximize the oil phase yield and improve the catalyst performance. From the results it can be observed that compared with the conversion under atmosphere pressure, the oil phase yield has been enhanced by 5% in wt. with higher reaction pressure (1atm+2bar) (Fig. 64).

Moreover, under MTG reaction conditions, the catalyst undergoes two types of aging: a reversible loss results from coke formed on the catalyst as a reaction by-product and the reaction product stream also causes a gradual loss of activity.[27] High reaction temperature enhances this type of deactivation.[27] Therefore, a lower reaction temperature 350℃ was also examined in this series of tests. With the 0.10C60 catalyst and under 1atm+2bar pressure, another 5% enhancement for the oil phase yield was achieved at 350℃ reaction condition (Fig. 64).

The previous MFGM II's after "*Extractive Refining*" process LPM conversion results indicates that very little oil phase product was obtained at reaction temperature of 300℃, thus, it can be confirmed that for the practical CFG II's after "*Extractive Refining*" process LPM conversion, 350℃ and 1atm+2bar pressure is the suitable reaction conditions for MTG process.

The BTX distributions of the CFG II's after "*Extractive Refining*" process LPM conversions are presented in Fig. 65. It can be found that the majority content of the BTX yield from the process is m/p-xylene. The next majorities are toluene and o-xylene, and benzene always the least BTX content in the oil phase yield.

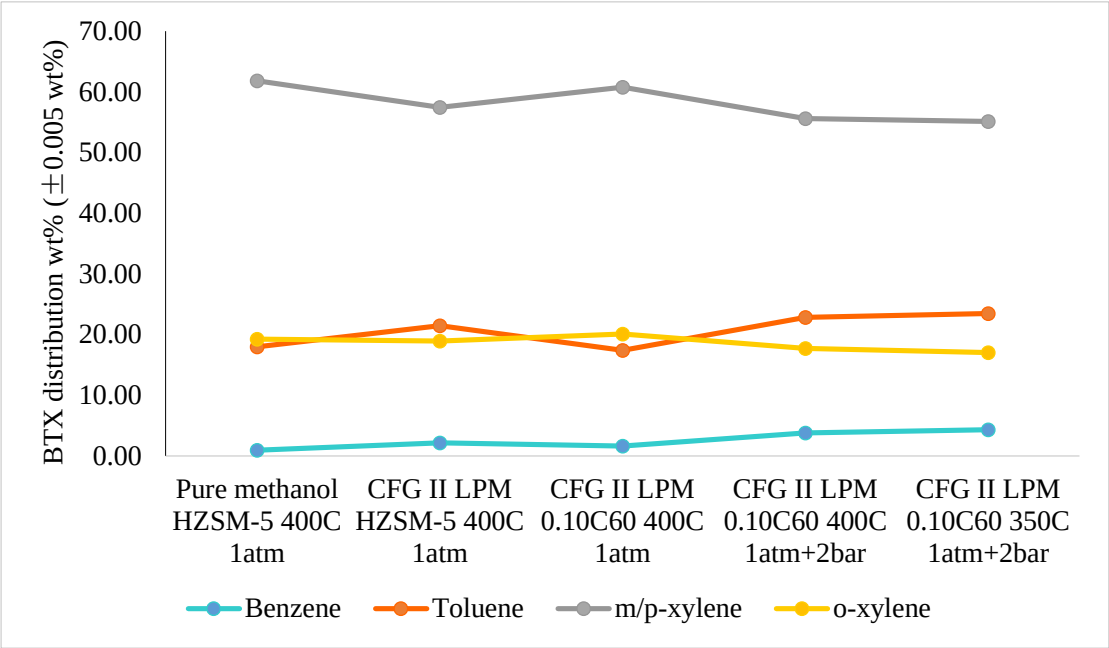

Fig. 65 Benzene, toluene, xylenes (BTX) distribution in the product of the crude FCC gasoline (CFG) II's after "*Extractive Refining*" process lower phase mixture (LPM) conversions

The decreased fraction of methanol in the feedstock reduces the methylation of the formed benzene and toluene (Appendix Scheme 1),[5] thus, when the catalytic conversion process utilised the LPM from the CFG II's "*Extractive Refining*" process as the feedstock instead of pure methanol, increase in toluene and benzene distribution and decrease in xylenes distribution were observed. The modified 0.10C60 catalyst increases the xylenes' distribution and reduces benzene and toluene's distribution since this catalyst favours the methylation of formed benzene and toluene.[21, 25, 28-30] Moreover, relative lower temperature (350℃) and higher pressure (1atm+2bar) enhances the methanol conversion's aromatization process,[1-5, 23, 24] therefore, reduction of xylenes' distribution and increase of toluene and benzene's distribution were observed when the conversion achieved relative higher pressure (1atm+2bar) and lower temperature (350℃) (Fig. 65).

In order to analyse the desulphurization performance of the LPM conversion, which applying the 0.10C60 catalyst with the optimum reaction conditions (350℃ and 1atm+2bar), the sulphur content in the feeds and the products are analysed using the ultraviolet (UV) fluorescent sulphur detector. The OSCs analysis results indicates that the OSCs level in the feedstock (CFG II's after "*Extractive Refining*" process LPM) is 260 ppm, and after catalytic conversion process this sulphur content has been reduced to 167 ppm in the oil phase product. Through these OSCs analysis results, the post extraction co-feeding conversion process is proved to be able to remove the OSCs in the feedstock.

As the best oil phase yield among all the CFG II's after "*Extractive Refining*" process LPM conversions, the oil phase product from the conversion by applying the 0.10C60 catalyst with these optimum reaction conditions was analysed using thermogravimetric analysis (TGA) to examine its boiling point. This analysis is to ensure the practicability of the oil phase product from this conversion, which means as a suitable gasoline fraction applied in the internal combustion engine the ebullition range of this oil phase product should be lower than 225℃.[31] The TGA analysis results of this oil phase product is presented in Fig. 66. This results are also outside the experimental error estimates (± 0.005% wt and ± 0.5℃).

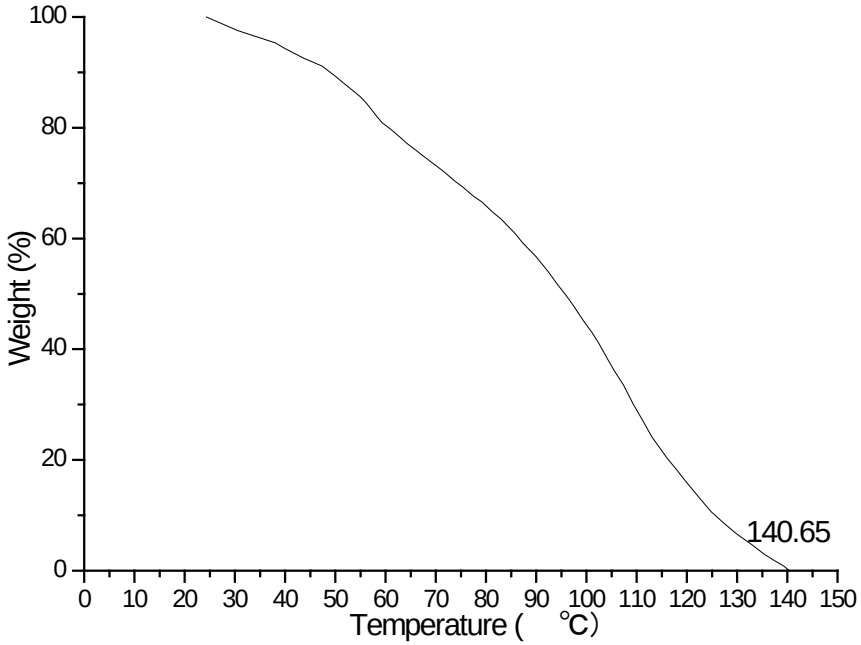

Fig. 66 Fraction (TGA) analysis result of the oil phase product from crude FCC gasoline (CFG) II's after "*Extractive Refining*" process lower phase mixture (LPM) conversion with 0.10C60+HDS catalyst and optimum reaction conditions (350℃ and 1atm+2bar)

From Fig. 66 it can be observed that all the contents in the oil phase product were evaporated before the temperature of the furnace reached 141℃ (Fig. 66). Therefore, through the boiling point analysis of the product from the CFG II's LPM conversion by applying the 0.10C60 catalyst with these optimum reaction conditions, it was confirmed that this oil phase product is in the gasoline range and can be directly used as the gasoline.

6.3.2 Characteristic Study of the Modified Catalyst

To characterize both the unmodified and modified catalyst, X-ray diffraction (XRD) was employed to analyse and compare the characteristic patterns between pristine unmodified HZSM-5 and modified 0.10C60 catalyst.

Fig. 67 shows the XRD pattern of 0.10C60 catalyst which was modified with Na_2CO_3 and additional CTAB in comparison to the unmodified HZSM-5. Visual inspection of the diffractograms from the XRD pattern of the catalyst samples show that both of the samples consist of a major MFI crystalline phase.[25] That means the crystallinity is well preserved for both Na_2CO_3+CTAB modified and unmodified samples, even though the [051], [033], and [313] peak of the alkaline treated zeolite is slightly reduced.[19, 32] The desilication treatment changes slightly the zeolite structure, a slight decrease in the intensities of the signals and therefore in crystallinity was detected. Moreover, no reflections were observed in the low angle 2θ-region (Fig. 67), indicating that the obtained mesopores by alkaline treated samples desilicated 0.10C60 is not well ordered.[19]

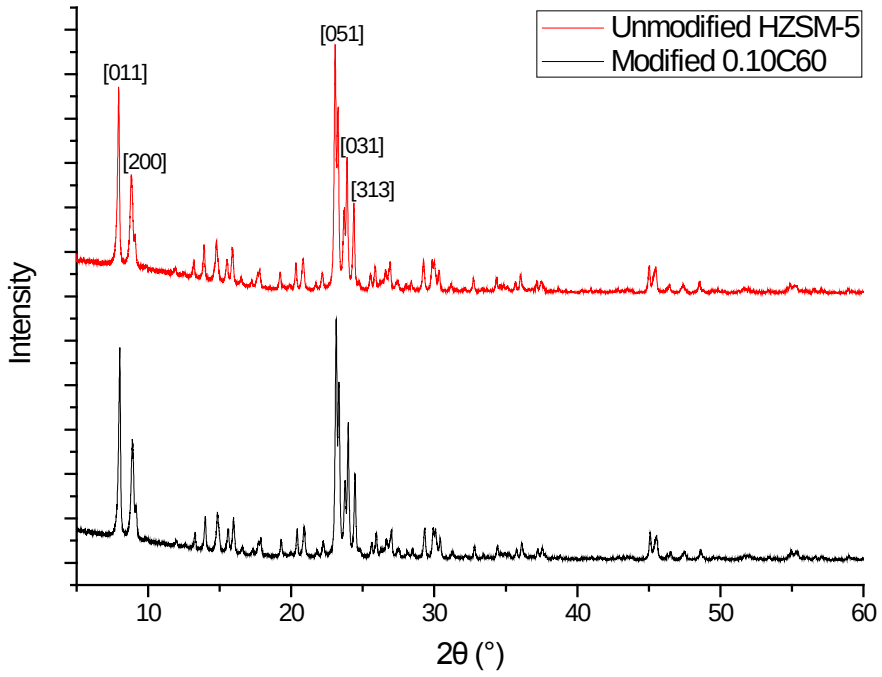

Fig. 67 XRD pattern of the unmodified HZSM-5 and modified 0.10C60 catalyst

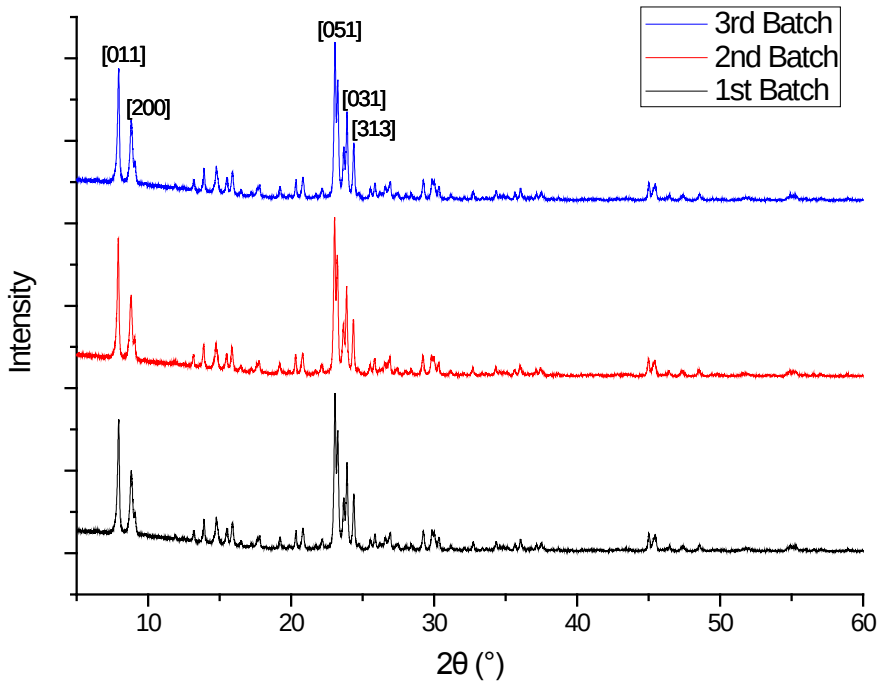

Fig. 68 XRD patterns of the three batches of the modified 0.10C60 catalyst

The reproducibility of our modified 0.10C60 catalyst has also been tested. Three batches of the 0.10C60 catalyst were made at different times. Through analysis of these catalysts' XRD patterns, it has been found that all the three batches of catalysts have exactly the same characterized structure, as their XRD patterns present almost no difference each other (Fig. 68). That means the modification process has excellent reproducibility.

6.3.3 Characteristic Study of the Post-reaction Catalyst

One of the main issues of the catalytic conversion process is related to the deactivation of the catalyst, due to coke deposition as a consequence of consecutive reactions between light alkenes over Brønsted or Lewis acid sites.[33, 34] This problem is caused by the limited diffusion of reactants/products within the zeolite materials.[27, 35] Thus, anti-coke performance of the catalyst during the conversion process is quite

important and critical.

Firstly, the formation of the coke deposited on the unmodified HZSM-5 and modified 0.10C60 catalysts during the above pure methanol MTG conversion and CFG II's after "*Extractive Refining*" process LPM conversions is analysed by Laser Raman spectroscopy, respectively. For all the post reaction (spent) unmodified HZSM-5 and modified 0.10C60 catalyst samples, two major Raman bands were observed in the spectra (Fig. 69): (i) 1425 cm^{-1}, which can be designated to the "breathing" vibrational mode of not-well-structured aromatics (*D*-band coke); (ii) 1600 cm^{-1}, *in*-plane stretching vibrational modes of well-structured aromatics (*G*-band coke).[36-38] With no doubt, coke has been formed on these catalysts during the catalytic conversion process.

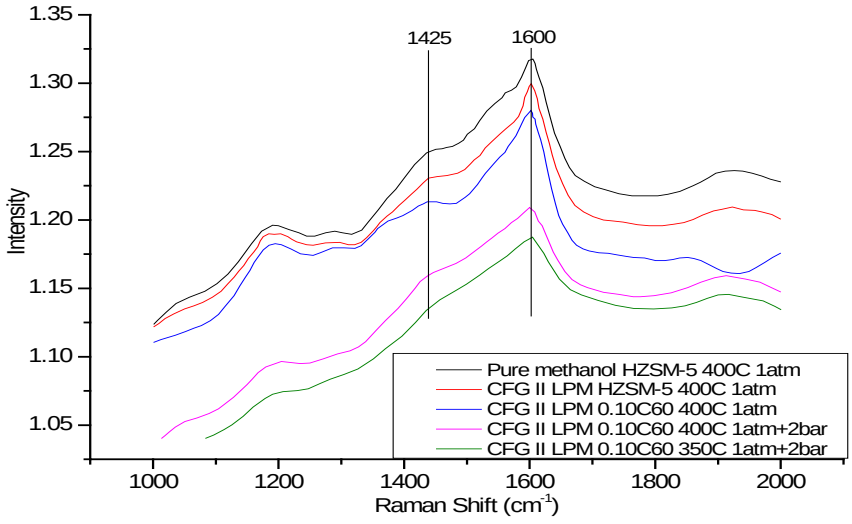

Fig. 69 Laser Raman spectra of post reaction unmodified HZSM-5 and modified 0.10C60+HDS mixed catalyst after pure methanol MTG conversion and crude FCC gasoline (CFG) II's after "*Extractive Refining*" process lower phase mixture (LPM) conversions with various reaction conditions

In order to compare the catalyst anti-coke (lifetime) performance during pure methanol MTG conversion and the CFG II's after "*Extractive Refining*" process LPM conversion, after these conversions under the same reaction conditions and the same unmodified HZSM-5 catalyst, the post reaction catalysts were examined by TGA to determine the coke content. The results obtained from the TGA analyser are shown in Fig. 70. These results are outside the experimental error estimates (± 0.005% wt).

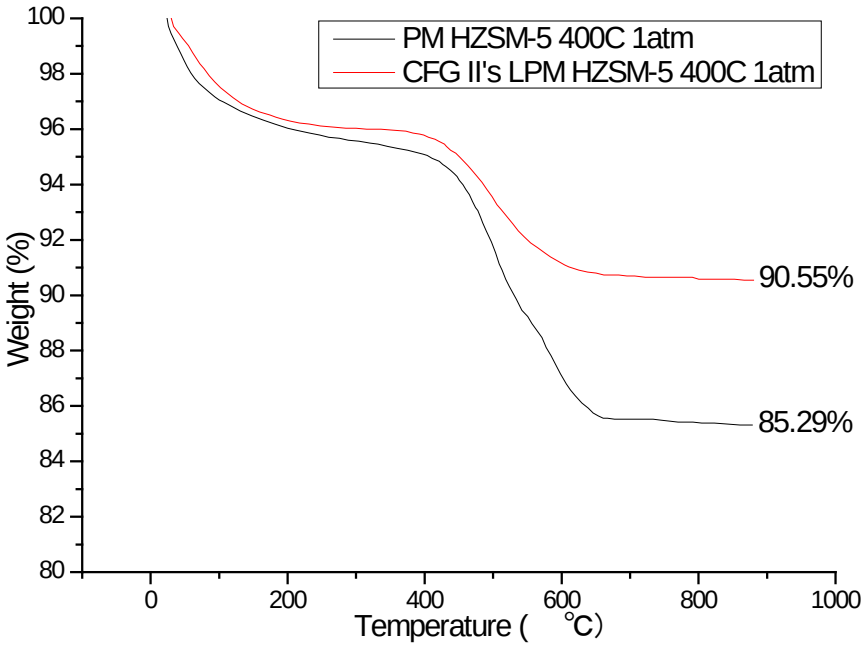

Fig. 70 Coke deposition (TGA) analysis results of unmodified HZSM-5 catalyst after pure methanol MTG conversion (black) and crude FCC gasoline (CFG) II's after "*Extractive Refining*" process lower phase mixture (LPM) conversion (red) with the same 400℃ and 1atm reaction conditions

After 6 hours reaction under the same conditions, the post reaction catalyst from CFG II's after "*Extractive Refining*" process LPM conversion presented much less coke deposition rate (9.45% in wt.) than pure methanol MTG conversion (14.71% in

wt.) (Fig. 70). That means, the catalyst lifetime during the conversion process can be improved by utilising CFG II's after "*Extractive Refining*" process LPM as the feedstock. The water from the methanol based extractant mixture which is contained in this feedstock can help to explain these results. Since in the MTG conversion the coke formation on the catalyst can be attenuated by the presence of water.[39] Water can moderate the formation of bulky hydrocarbon pool species that cannot diffuse through the small-pore material.[40] The occupation of the acid sites by water ultimately leads to reduced pore blocking, enhancing the diffusion of methanol and small alkenes deeper into the crystals to undergo reactive events.[40]

On the other hand, for comparing the catalysts anti-coke performance between unmodified HZSM-5 and modified 0.10C60 catalysts under the same reaction conditions (400℃ and 1atm) in CFG II's after "*Extractive Refining*" process LPM conversion, the post reaction samples of both catalysts were measured by TGA analyser. The TGA analysis results indicate that after the conversion, unmodified HZSM-5 catalyst contained 9.45% in wt. of coke (Fig. 71). The modified 0.10C60 catalyst's coke content is 8.98% in wt. which is lower than the unmodified HZSM-5 catalyst (Fig. 71). These results are outside the experimental error estimates (± 0.005% wt). Therefore, from this point of view it can be confirmed the modified 0.10C60 mixed catalyst has better anti-coke performance during the same conversion process than unmodified HZSM-5.

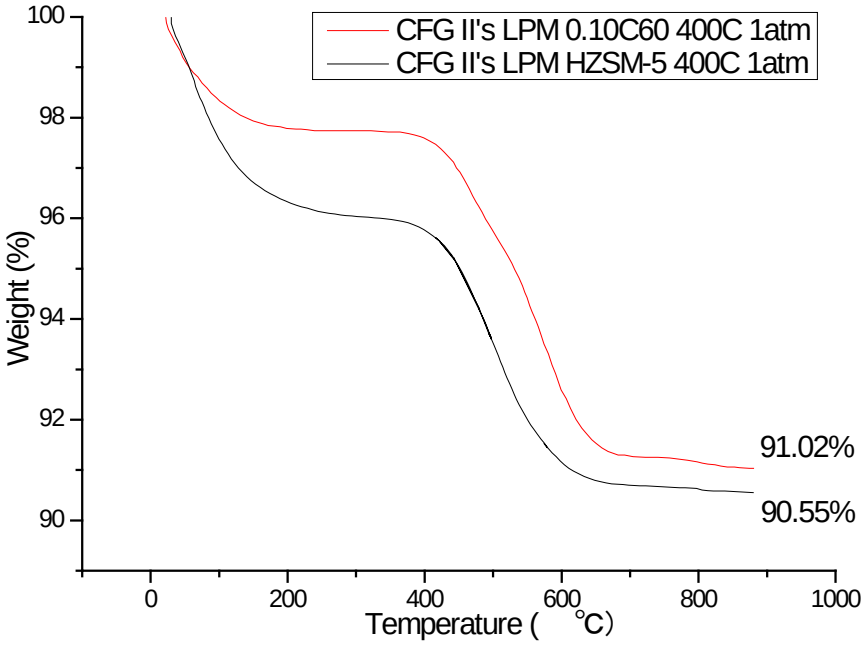

Fig. 71 Coke deposition (TGA) analysis results of unmodified HZSM-5 (black) and modified 0.10C60 (red) catalysts after crude FCC gasoline (CFG) II's after "*Extractive Refining*" process lower phase mixture (LPM) conversion with the same 400℃ and 1atm reaction conditions

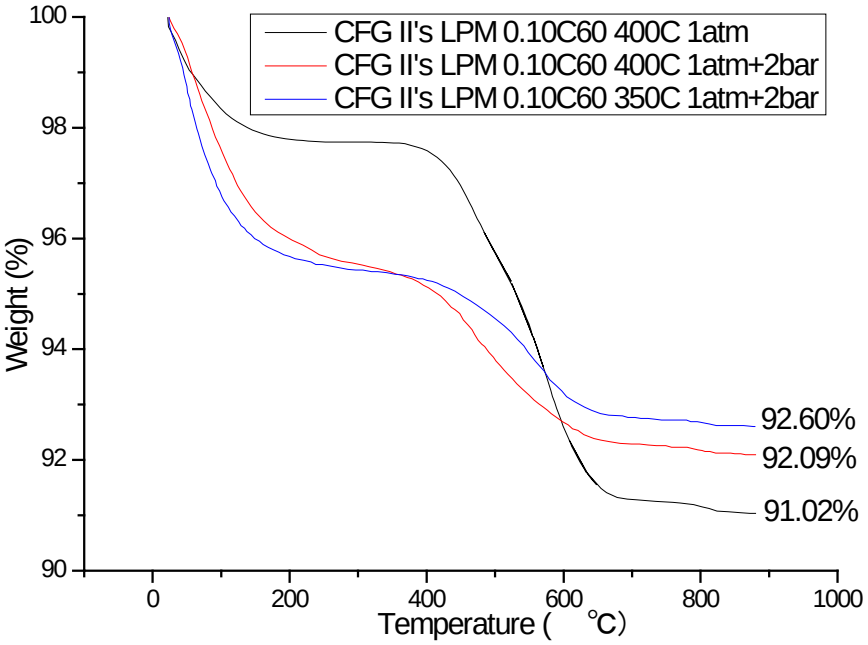

Fig. 72 Coke deposition (TGA) analysis results of modified 0.10C60 catalysts after crude FCC gasoline (CFG) II's after "*Extractive Refining*" process lower phase mixture (LPM) conversion with various reaction conditions

The coke depositions over the modified 0.10C60 catalyst after the CFG II's after "*Extractive Refining*" process LPM conversions with various reaction conditions such as higher reaction pressure (1atm+2bar) and lower reaction temperature (350℃) were also characterized by TGA analyser. These results are outside the experimental error estimates (± 0.005% wt) and presented in Fig. 72. Through these results, it can be observed that higher pressure (1atm+2bar) reaction gives rise to less coke deposition (7.91% in wt.) on the catalyst than atmosphere pressure (8.98% in wt.). Whilst, compared with 400℃, the modified 0.10C60 catalyst showed better coke-resistance performance (7.40% in wt.) at 350℃ during the CFG II's after "*Extractive Refining*" process LPM conversion under 1atm+2bar reaction pressure. As described in the

previous part, these results can be also explained as higher reaction pressure and lower reaction temperature reaction conditions achieve relatively low catalyst deactivation (coke deposition) rate during the MTG conversion process.[24, 27]

Therefore, from the above results of the CFG II's after "*Extractive Refining*" process LPM conversions, it can be concluded that that, compared with pure methanol MTG conversion, the CFG II's after "*Extractive Refining*" process LPM conversion gives higher oil phase product yield and less coke deposition. Meanwhile, this LPM conversion process can successfully remove the OSCs from feedstock during the catalytic reaction process. It also has been proved that under the optimum reaction conditions and over modified 0.10C60 catalyst this conversion process can achieve even better overall performance such as higher oil phase yield, higher coking tolerance and better desulphurisation performance. Furthermore, the most important oil phase product from this conversion was confirmed to be in the gasoline range by boiling point analysis. To sum up, the practical feasibility of the after "*Extractive Refining*" process LPM conversion is confirmed.

6.4 Conclusions

For the aim of effectively utilising all the products from the "*Extractive Refining*" approach, the LPMs from previous "*Extractive Refining*" processes with various extractant mixtures were utilised as the feedstocks in the post extraction catalytic conversion process during this part of the research.

In this chapter, the co-feeding conversion effect of methanol with various other organics such as 1-hexene, n-octane, p-xylene, thiophene and ethylene glycol which

were chosen as the typical organic compounds to represent the alkene, alkane, aromatics, OSCs and other alcohol contents existing in the LPMs were first examined and analysed, respectively. It can be observed from the results of these conversions that the formation of the higher alkenes is promoted by the co-fed alkene and alkane. Meanwhile, the co-fed aromatics promotes the catalytic activity of the catalyst for conversion of methanol to hydrocarbons.[8] OSCs, such as thiophene is also removed by the HDS process during the conversion. As the final results, the total yield of the oil phase product and high added value BTX contents are improved by these added co-feeding raw materials, and the oil phase product is light colorcleaner which means low OSCs.

Before applying the LPMs from the crude FCC gasoline's "*Extractive Refining*" processes in the catalytic conversion process, the LPM from the modelled FCC gasoline mixture "*Extractive Refining*" process was used as the feedstock in the catalytic conversion to examine the feasibility of the after "*Extractive Refining*" conversion process. Through the impressive improvement of the oil phase and high added value BTX contents yield, it is confirmed that the MTG process can achieve better yield of the oil phase product when apply the MFGM II's post extraction LPM from the "*Extractive Refining*" process as the feedstock instead of the pure methanol. This also confirms the feasibility of the after "*Extractive Refining*" conversion process.

Following the MFGM II's after "*Extractive Refining*" process conversion, the LPM from the crude FCC gasoline CFG II's "*Extractive Refining*" process was

utilised as the feedstock in the catalytic conversions. From the results of the CFG II's after "*Extractive Refining*" process LPM conversions, it can be confirmed that, compared with pure methanol MTG conversion, this LPM's conversion presents better oil phase and BTX yield and less coke deposition. This LPM conversion process can also successfully remove the OSCs from feedstock. Moreover, with optimum reaction conditions (350℃ and 1atm+2bar) and modified 0.10C60 catalyst this conversion process can achieve even better overall performance. Through the boiling point analysis the oil phase product from this conversion was confirmed in the gasoline range. Therefore, the theoretical practicability of the after "*Extractive Refining*" process LPM conversion in the refinery industry is confirmed.

References

1 S. Svelle, F. Joensen, J. Nerlov, U. Olsbye, K.-P. Lillerud, S. Kolboe, M. Bjørgen, *Journal of the American Chemical Society* 2006, *128*, 14770-14771.
2 M. Bjørgen, S. Svelle, F. Joensen, J. Nerlov, S. Kolboe, F. Bonino, L. Palumbo, S. Bordiga, U. Olsbye, *Journal of Catalysis* 2007, *249*, 195-207.
3 M. Bjørgen, K.-P. Lillerud, U. Olsbye, S. Svelle, *Studies in Surface Science and Catalysis* 2007, *167*, 463-468.
4 U. Olsbye, S. Svelle, M. Bjørgen, P. Beato, T. V. Janssens, F. Joensen, S. Bordiga, K. P. Lillerud, *Angewandte Chemie International Edition* 2012, *51*, 5810-5831.
5 X. Sun, S. Mueller, H. Shi, G. L. Haller, M. Sanchez-Sanchez, A. C. van Veen, J. A. Lercher, *Journal of Catalysis* 2014, *314*, 21-31.
6 X. Wu, R. Anthony, *Applied Catalysis A: General* 2001, *218*, 241-250.
7 G. Roohollahi, M. Kazemeini, A. Mohammadrezaee, R. Golhosseini, *Journal of Industrial and Engineering Chemistry* 2013, *19*, 915-919.
8 T. Mole, J. A. Whiteside, D. Seddon, *Journal of Catalysis* 1983, *82*, 261-266.
9 E. G. Derouane, J. B. Nagy, P. Dejaifve, J. H. van Hooff, B. P. Spekman, J. C. Védrine, C. Naccache, *Journal of Catalysis* 1978, *53*, 40-55.
10 S. Bhatia, J. Beltramini, D. Do, *Catalysis Reviews—Science and Engineering* 1989, *31*, 431-480.
11 E. Kowsari, in *Ionic Liquids - New Aspects for the Future*. InTech, Rijeka, 2013, Chap. 11.
12 H. Schulz, *Catalysis Today* 2010, *154*, 183-194.
13 L.-T. Yuen, S. Zones, T. Harris, E. Gallegos, A. Auroux, *Microporous Materials* 1994, *2*, 105-117.
14 S. Campbell, D. Bibby, J. Coddington, R. Howe, *Journal of Catalysis* 1996, *161*, 350-358.
15 M. Bjørgen, U. Olsbye, D. Petersen, S. Kolboe, *Journal of Catalysis* 2004, *221*, 1-10.
16 M. Bjørgen, S. Akyalcin, U. Olsbye, S. Benard, S. Kolboe, S. Svelle, *Journal of Catalysis* 2010, *275*, 170-180.
17 W. Song, J. B. Nicholas, A. Sassi, J. F. Haw, *Catalysis Letters* 2002, *81*, 49-53.
18 P. M. Mortensen, J.-D. Grunwaldt, P. A. Jensen, K. Knudsen, A. D. Jensen, *Applied Catalysis A: General* 2011, *407*, 1-19.
19 F. Schmidt, M. R. Lohe, B. Büchner, F. Giordanino, F. Bonino, S. Kaskel, *Microporous and Mesoporous Materials* 2013, *165*, 148-157.
20 R. Wei, C. Li, C. Yang, H. Shan, *Journal of Natural Gas Chemistry* 2011, *20*, 261-265.
21 P. L. Benito, A. G. Gayubo, A. T. Aguayo, M. Olazar, J. Bilbao, *Journal of Chemical Technology and Biotechnology* 1996, *66*, 183-191.
22 M. Ogura, S.-y. Shinomiya, J. Tateno, Y. Nara, M. Nomura, E. Kikuchi, M. Matsukata, *Applied Catalysis A: General* 2001, *219*, 33-43.
23 C. Chang, W. Lang, R. Smith, *Journal of Catalysis* 1979, *56*, 169-173.
24 S. Sie, *Applied Catalysis A: General* 2001, *212*, 129-151.

25 S. Fathi, M. Sohrabi, C. Falamaki, *Fuel* 2014, *116*, 529-537.
26 A. C. Gujar, V. K. Guda, M. Nolan, Q. Yan, H. Toghiani, M. G. White, *Applied Catalysis A: General* 2009, *363*, 115-121.
27 F. J. Keil, *Microporous and Mesoporous Materials* 1999, *29*, 49-66.
28 A. A. Rownaghi, F. Rezaei, J. Hedlund, *Catalysis Communications* 2011, *14*, 37-41.
29 A. A. Rownaghi, J. Hedlund, *Industrial & Engineering Chemistry Research* 2011, *50*, 11872-11878.
30 M. Bjørgen, F. Joensen, M. S. Holm, U. Olsbye, K.-P. Lillerud, S. Svelle, *Applied Catalysis A: General* 2008, *345*, 43-50.
31 R. C. Delgado, A. S. Araujo, V. J. Fernandes, *Fuel Processing Technology* 2007, *88*, 365-368.
32 A. S. Al-Dughaither, H. de Lasa, *Industrial & Engineering Chemistry Research* 2014, *53*, 15303-15316.
33 M. Milina, S. Mitchell, P. Crivelli, D. Cooke, J. Pérez-Ramírez, *Nature Communications* 2014, *5*, 3922.
34 A. A. Rownaghi, F. Rezaei, J. Hedlund, *Microporous and Mesoporous Materials* 2012, *151*, 26-33.
35 M. Stöcker, *Microporous and Mesoporous Materials* 1999, *29*, 3-48.
36 B. Guichard, M. Roy-Auberger, E. Devers, B. Rebours, A. Quoineaud, M. Digne, *Applied Catalysis A: General* 2009, *367*, 1-8.
37 B. Valle, P. Castaño, M. Olazar, J. Bilbao, A. G. Gayubo, *Journal of Catalysis* 2012, *285*, 304-314.
38 B. M. Vogelaar, A. D. van Langeveld, S. Eijsbouts, J. A. Moulijn, *Fuel* 2007, *86*, 1122-1129.
39 G. Qi, Z. Xie, W. Yang, S. Zhong, H. Liu, C. Zhang, Q. Chen, *Fuel Processing Technology* 2007, *88*, 437-441.
40 K. De Wispelaere, C. S. Wondergem, B. Ensing, K. Hemelsoet, E. J. Meijer, B. M. Weckhuysen, V. Van Speybroeck, J. Ruiz-Martínez, *ACS Catalysis* 2016, 1991-2002.

Chapter 7. Summary

7.1 Green and Sustainable Refinery Processes

7.1.1 FCC Gasoline Upgrading and Gas Mixtures Separation

Global demand for transportation fuels continues to grow, and this demand will continue to be met largely by gasoline and diesel fuels. As a major product which is produced from the "*Fluid Catalytic Cracking*" (FCC) process, FCC gasoline is a significant transportation fuel used in Internal Combustion Engines (ICE). In gasoline the contents of alkenes and organosulfur compounds (OSCs) are required to meet increasingly stringent environmental regulations.[1] The current upgrading technologies such as hydroisomerization, aromatization and hydrodesulphurisation (HDS) processes etc. can convert or remove the alkene contents and OSCs from FCC gasoline effectively.[2] However, these processes require severe conditions such as high temperature and pressure, complex procedures and specific chemicals or materials, particularly the need for large amounts of hydrogen-typically produced from the CO_2 intensive steam reforming of methane[3]

On the other hand, mixtures of light gaseous alkene and alkane produced in the petroleum refining process are often used as important refinery fuel and feedstock,[4] and recovery of alkenes in these streams would be a substantial conservation of resources.[5] Conventional alkene/alkane separations mixture gas separation processes in the chemical and petrochemical industry rely heavily upon energy intensive technologies, such as cryogenic distillation.[6-8] With all these challenging problems, developing green and sustainable technologies for the above refinery processes is

becoming increasingly important.

In my research, I have explored new routes, based on new, innovative chemistry, to improve the considerable energy consumption and overcome the environmental disadvantages in current FCC gasoline upgrading and gaseous alkene and alkane separating, and to develop a lower cost, less energy-intensive approach to the problem.

Therefore, to overcome the shortcomings in current FCC gasoline upgrading processes, and achieve high alkene and sulphur removal efficiency, a novel and sustainable "*Extractive Refining*" technology has been developed in this study. Under simple and very safe operation conditions (room temperature and atmosphere pressure), and without the need for hydrogen, the new "*Extractive Refining*" technology can purify FCC gasoline with much lower energy consumption, much less operation and capital cost than the conventional HDS and other upgrading processes.

Moreover, to overcome the shortcomings in current gaseous alkene/alkane separation processes, a new "*Extractive Distillation*" approach in advanced here in this research. Under the mild and much safe operation conditions, the new "*Extractive Distillation*" approach also can efficiently separate gaseous alkene/alkane in the gas mixtures with much lower energy consumption and capital cost than the conventional cryogenic distillation and other separation processes.

7.2 Methanol as a Platform for Future Petroleum Extraction and Conversion Technologies

As a future sustainable technology, the feedstock utilised during the process also

needs to be green and sustainable. Methanol can fit all these requirements, since it is easy to produce from fossil-fuel-based syn-gas, shale gas and bio-mass, it can also be prepared by direct oxidative conversion of natural gas (methane) or reductive conversion of atmospheric carbon dioxide with hydrogen.[9] Meanwhile, with the enormous production capability, excellent utilizabillity and transformability, methanol opens up the possibility of an alternative energy source to diminishing oil and gas resources and would lead to a feasible “methanol economy”.[9, 10] Therefore, the major solvent methanol was utilised as the basic extractant in the above extractive approaches. For convenience, the overall process is again shown here Fig. 73.

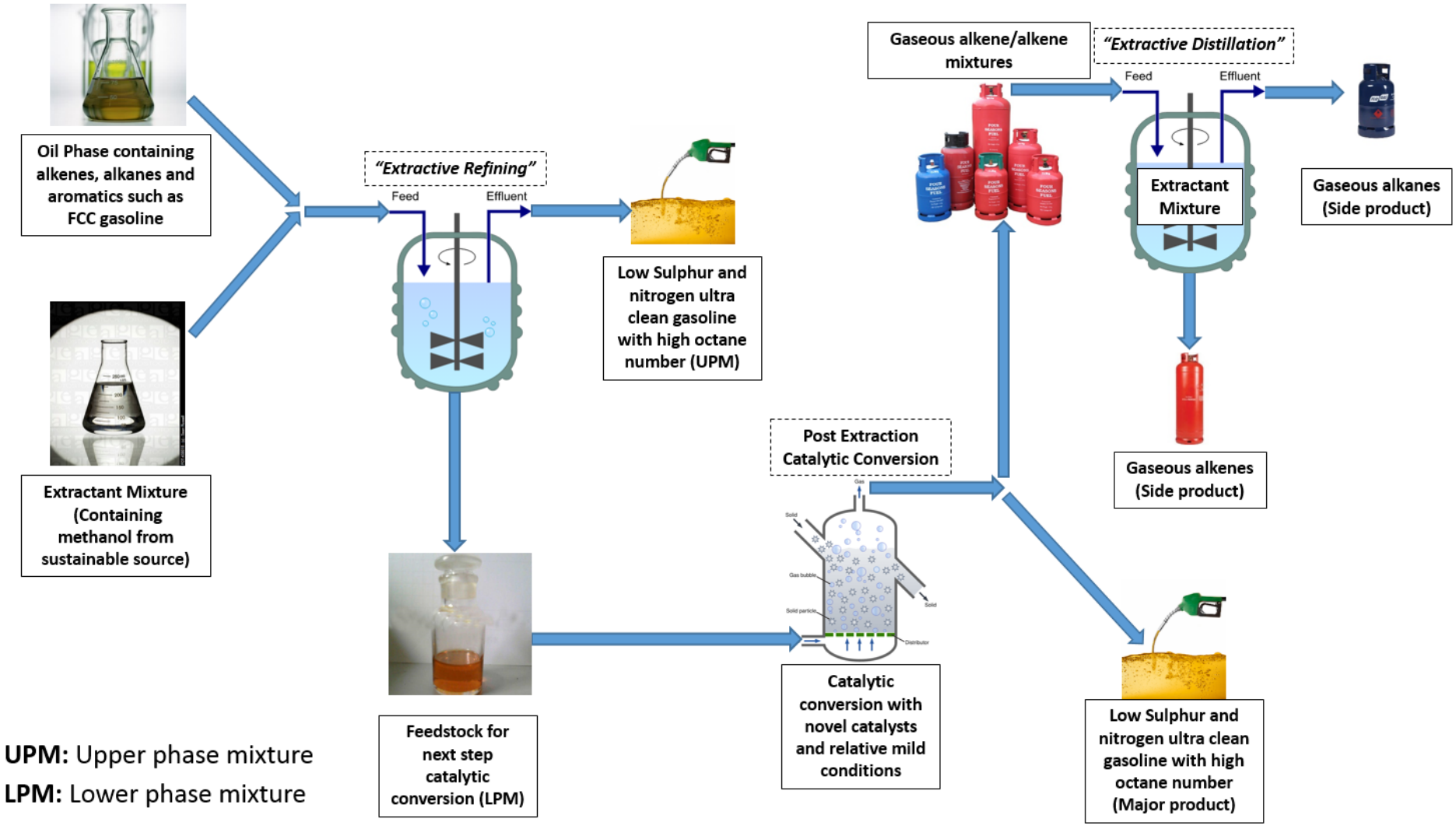

Fig. 73 Potential New Sustainable Technologies for Refinery Product Upgrading/Separating and Methanol Utilization

7.2.1 Methanol based "Extractive Refinery" and "Extractive Distillation"

Before applied these extractive approaches into the practical process, the mechanism of the underlying solvent (methanol) extraction or solubilisation processes was studied firstly, and the feasibility of the "*Extractive Refining*" and "*Extractive Distillation*" processes has been studied from the theoretical aspect.

In the mechanism study, through the results from the analyses of computational quantum chemical calculations, FTIR and Proton Nuclear Magnetic Resonance (^{1}H-NMR) spectroscopies, the weak hydrogen bonds are confirmed form between methanol and alkenes through the interaction of the π-electron cloud of alkenes and methanol's hydroxyl group (O—H···π),[11, 12] together with the interaction of a proton of these alkenes and the oxygen atom of methanol's hydroxyl group (C—H···O).[13] The results also suggest that the hydrogen bond formed between thiophene the most typical OSCs in FCC gasoline and methanol is bridged by the thiophene's sulphur atom and methanol's hydroxyl group (O—H···S).[14] Moreover, it was also found that alkenes' dipole moment presents positive correlation with the strength of these hydrogen bond, and this affects the solubility of gaseous alkenes in methanol. And Low temperature can weaken the hydrogen bond between different solutes and solvent methanol.

For the aim of proving the "*Extractive Refining*" and "*Extractive Distillation*" approaches' feasibility practically, both approaches were applied to dealing with the modelled or real commercial raw materials and their performances were analysed in the following study, respectively.

Various methanol based extractant/extractant mixtures was applied in the "*Extractive Refining*" process for upgrading modelled FCC gasoline mixture and commercial FCC gasoline (MFGM and CFG), and as the result of the hydrogen bond interaction between different extracts and extractants these extractants all showed excellent alkene reduction and desulfurization performance when dealing with MFGM and CFG.

On the other hand, through series of tests the feasibility and effectiveness of applying various organic solvents as the extractant in the "*Extractive Distillation*" process for separating the alkene contents and alkane contents in the modelled catalytic and thermal cracked gases mixtures (MCCGM and MTCGM) were studied. The "*Extractive Distillation*" approach proved successful to separate the alkene and alkane contents in the gaseous mixtures. Whilst, due to its strong effect on the hydrogen bond formed between alkene and extractant, the molecular dipole moment of the extractant shows a positive correlation to the alkene/alkane separation performance during the "*Extractive Distillation*" process.

7.2.2 Post Extraction Catalytic Conversion

Furthermore, in order to sufficiently utilise all the products from the "*Extractive Refining*" approach, the lower phase mixtures (LPMs) from previous "*Extractive Refining*" processes were utilised as the feedstocks in the post extraction catalytic conversion process.

The co-feeding conversion effect of methanol with various other organics contents existing in the LPMs were first examined and analysed during the methanol to

gasoline (MTG) conversion. The total yield of the oil phase product and high added value BTX contents are improved by these added co-feeding raw materials as the result of their co-feeding effect. Meanwhile, since the OSCs is removed by the HDS process during the conversion, low OSCs level oil phase products can be obtained through this conversion process. Therefore, it was proposed utilise these LPMs as the feedstock can improve the yield and performance of the MTG process.

Through the impressive improvement on yield of the oil phase and high added value BTX products, it was confirmed that the MTG process can achieve a better yield and performance when applying the model FCC gasoline's post extraction LPM as the feedstock instead of the pure methanol. This also verified the feasibility of the post "*Extractive Refining*" process LPM conversion in the practical application.

Then, the LPM from the commercial FCC gasoline's "*Extractive Refining*" process was utilised as the feedstock in the catalytic conversions. Compared with pure methanol MTG conversion, it is found that this LPM's conversion presents better gasoline range oil phase and BTX yield and longer catalyst lifetime. Whilst, this LPM conversion process successfully removes the OSCs from feedstock without external hydrogen supplement. Moreover, with optimum reaction conditions (350℃ and 1atm+2bar) and modified 0.10C60 catalyst this conversion process can achieve even better overall performance.

Therefore, as an important platform, the "alternative energy source" methanol can be not only utilised as the basic extractant to reduce the alkene and OSCs contents or separate the gaseous alkene contents during the green and sustainable "*Extractive*

Refining" and "*Extractive Distillation*" approaches, respectively, but also through the post extraction catalytic conversion process, the feedstock methanol is also able to be efficiently converted into high added value product such as gasoline, BTX etc..

7.3 The Future Refinery

To sum up, this research developed in this thesis presents a series of alternative green and sustainable methanol based approaches to replace the conventional energy intensive, complex and costly process in the petroleum refinery industry in the future. During this research, the underpinning, fundamental science and application performance of these newly developed approaches were investigated. The results determine the underlying concepts and the all-important influences of the hydrogen bond interaction and the molecular dipole moment, respectively. Whilst, the feasibilities and advantages of these approaches have been verified.

Looking ahead, although facing a lot of difficulties during the technological and economic transformations,[15] low carbon process is constantly the ultimate objective and development trend of the world industries.[15] Thus, for the future development tendency of the refinery, more and more energy intensive and inefficient conventional processes need to be replaced by greener and more sustainable processes such as the approaches developed in this research (Fig. 87). Meanwhile, as the Nobel Laureate George A. Olah and many other scientists pointed out, traditional feedstock in the petroleum industry i.e. fossil fuel can be utilised more effectively by introducing the sustainable and renewable energy resources such as methanol into the refinery process, and the utilisation of these renewable resources also protect the diminishing oil and

gas resources.[9, 16, 17] The newly developed green and sustainable approaches in this research fulfil all these objectives and should be highly desirable in future refineries.

References

1 E. Kowsari, in *Ionic Liquids - New Aspects for the Future*. InTech, Rijeka, 2013, Chap. 11.
2 Y. Fan, X. Bao, D. Lei, G. Shi, W. Wei, J. Xu, *Fuel* 2005, *84*, 435-442.
3 A. Ibrahim, S. B. Xian, Z. Wei, *Petroleum Science and Technology* 2003, *21*, 1555-1573.
4 R. B. Eldridge, *Industrial & Engineering Chemistry Research* 1993, *32*, 2208-2212.
5 D. J. Safarik, R. B. Eldridge, *Industrial & Engineering Chemistry Research* 1998, *37*, 2571-2581.
6 R. Yang, E. Kikkinides, *AIChE Journal* 1995, *41*, 509-517.
7 A. Ortiz, L. María Galán, D. Gorri, A. B. de Haan, I. Ortiz, *Industrial & Engineering Chemistry Research* 2010, *49*, 7227-7233.
8 G. E. Keller, A. E. Marcinkowsky, S. K. Verma, K. D. Williamson, *Olefin recovery and purification via silver complexation*. Marcel Dekker, New York, 1992.
9 G. A. Olah, *Angewandte Chemie International Edition* 2005, *44*, 2636-2639.
10 C.-J. Yang, R. B. Jackson, *Energy Policy* 2012, *41*, 878-884.
11 K. Kowski, W. Lüttke, P. Rademacher, *Journal of Molecular Structure* 2001, *567–568*, 231-240.
12 K. Oku, H. Watanabe, M. Kubota, S. Fukuda, M. Kurimoto, Y. Tsujisaka, M. Komori, Y. Inoue, M. Sakurai, *Journal of the American Chemical Society* 2003, *125*, 12739-12748.
13 B. M. Kariuki, K. D. Harris, D. Philp, J. M. Robinson, *Journal of the American Chemical Society* 1997, *119*, 12679-12680.
14 D. K. Singh, S. K. Srivastava, A. K. Ojha, B. P. Asthana, *Journal of Molecular Structure* 2008, *892*, 384-391.
15 P. J. Pearson, T. J. Foxon, *Energy Policy* 2012, *50*, 117-127.
16 A. Demirbas, *Energy Sources* 2004, *26*, 715-730.
17 S. Xiu, A. Shahbazi, *Renewable and Sustainable Energy Reviews* 2012, *16*, 4406-4414.

Appendixes

Appendix 1: Chemicals

Table Appendix 1 Chemicals

Chemical	Supplier	Purity (minimum)	Impurities
ethylene (gas)	BOC	99.92%	ethane and other hydrocarbons
propylene (gas)	BOC	99.50%	propane and other hydrocarbons
1-butene (gas)	BOC	99.00%	butane and other hydrocarbons
isobutylene (gas)	BOC	99.00%	butane and other hydrocarbons
cis-2-butene (gas)	BOC	99.00%	butane and other hydrocarbons
trans-2-butene (gas)	BOC	99.00%	butane and other hydrocarbons
1-pentene (liquid)	Sigma Aldrich Company	99.50%	other hydrocarbons
1-hexene (liquid)	Sigma Aldrich Company	99.80%	other hydrocarbons
thiophene (liquid)	Sigma Aldrich Company	99.50%	less than 0.200% benzene
methanol (liquid)	Sigma Aldrich Company	99.90%	other organics
methanol-d_4 (liquid)	Sigma Aldrich Company	99.80 atom % D	less than 0.025% water
benzene-d_6 (liquid)	Sigma Aldrich Company	99.60 atom % D	other hydrocarbons
tetramethylsilane (TMS) (liquid)	Sigma Aldrich Company	99.50%	other organics
n-octane (liquid)	Sigma Aldrich Company	99.00%	less than 0.002% water
ethylbenzene (liquid)	Sigma Aldrich Company	99.90%	less than 0.002% water
ethylene glycol (liquid)	Sigma Aldrich Company	99.00%	less than 0.050% water
dimethyl carbonate (DMC) (liquid)	Sigma Aldrich Company	99.00%	less than 0.005% water
p-xylene (liquid)	Sigma Aldrich Company	99.00%	less than 0.030% water
n-hexane (liquid)	Sigma Aldrich	97.00%	less than 0.0005%

	Company		non-volatile matter, 0.001% free acid (as CH_3COOH) and 0.01% water
propylene carbonate (PC) (liquid)	Sigma Aldrich Company	99.70%	less than 0.002% water
Potassium bromide (KBr) (solid)	Sigma Aldrich Company	99.00%	trace metals basis
sodium carbonate (Na_2CO_3) (solid)	Sigma Aldrich Company	99.95%	less than 0.005% silica and 0.01% insolubles
cetyl trimethyl ammonium bromide (CTAB) (solid)	Sigma Aldrich Company	99.00%	less than 0.001% phosphorus (P) and 0.1% insoluble matter
Ammonium nitrate (NH_4NO_3) (solid)	Sigma Aldrich Company	99.50%	less than 0.0005% phosphorus (P) and 0.005% insoluble matter
HZSM-5 Si/Al=60 (solid)	ZEOLYST international Company	99.90%	other zeolites

Appendix 2: Supplied Samples

2.1 Crude FCC gasoline from SINOPEC Company, China (CFG I):

Table Appendix 2.1 Group composition of CFG I from SINOPEC Company, China

Alkane	Wt %	Alkene	Wt %	Aromatics	Wt %	OSCs	ppm
n-paraffins	7.25		49.27		5.05		750
i-paraffins	18.12						
Naphthenes	20.31						
Total	45.68		49.27		5.05		750

2.2 Crude FCC gasoline from Petroineos Manufacturing Scotland LTD, UK (CFG II):

Table Appendix 2.2 Group composition of CFG II from Petroineos Manufacturing Scotland LTD, UK

Alkane	Wt %	Alkene	Wt %	Aromatics	Wt %	OSCs	ppm
n-paraffins	4.23		30.39		31.80		960
i-paraffins	20.31						
Naphthenes	13.27						
Total	37.81		30.39		31.80		960

2.3 Model catalytic cracking gas mixture from CK Special Gases Ltd, UK (MCCGM):

Table Appendix 2.3 Composition of model catalytic cracking gas mixture (MCCGM) from CK Special Gases Ltd, UK

Content	ethylene	ethane	propylene	propane
Fraction (mol%)	14.97%	24.97%	19.87%	40.19%

2.4 Model thermal cracking gas mixture from CK Special Gases Ltd, UK (MTCGM):

Table Appendix 2.4 Composition of model thermal cracking gas mixture (MTCGM) from CK Special Gases Ltd, UK

Content	hydrogen	carbon monoxide	methane	ethylene	ethane	propylene	propane
Fraction (mol%)	15.00%	4.01%	24.76%	45.21%	4.99%	5.02%	1.01%

Appendix 3: Error Estimates Analysis

3.1 Gaseous alkenes solubility

Gaseous alkene solubility in methanol experiments were repeated three times for each gaseous alkene, and the result adopted in Chapter 4 is the mean value of three times tests' results. Through these results it was observed that the maximum difference appear in the solubility tests is 2 ml compare with the result adopted in Chapter 4, hence, the ±2 ml error estimate of the gaseous alkenes solubility in methanol is adopted.

3.2 Proton Nuclear Magnetic Resonance (^{1}HNMR) spectrum

The ^{1}HNMR spectrum of each sample was carefully measured across ten recordings and the obtained chemical shift results reveal excellent reproducibility. According to the reference,[1] the adopted error estimates of the chemical shifts obtained from the ^{1}HNMR spectrum test in Chapter 4 is ±0.004 ppm.

3.3 Mass (weight) loss

Mass (weight) loss is the reduced weight when comparing the original weight of the added gasoline as a feed to the weight of the after "*Extractive Refining*" process upper phase mixture (UPM) as a product. In order to obtain its error estimates, the mean value of three "*Extractive Refining*" tests' mass loss under same conditions was adopted as the mass loss result in Chapter 5. The maximum difference observed in these tests is 0.05 g, thus, the error estimates for the mass loss analysis is adopted as ±0.05 g.

3.4 Liquid content's composition/distribution from Gas Chromatography Mass Spectrometry (GCMS)

The GCMS test of each liquid sample was repeated three times to obtain the composition/distribution (mass fraction % in wt.) of various contents in it. In Chapter 5 and 6 the adopted composition/product distribution result of each sample is the mean value of three tests' results. These results reveal excellent reproducibility, and the error estimates for the group composition is ±0.005% in wt. which is the maximum difference appears in these results.

3.5 Organic Sulphur Contents (OSCs) fraction from Ultraviolet (UV) fluorescent sulphur detector

To obtain the OSCs fraction of the samples, each sample was test by the UV fluorescent sulphur detector three times. Every OSCs fraction in Chapter 5 and 6 is the mean value of three tests' results. These results reveal excellent reproducibility, and the error estimates of the OSCs fraction is ±0.005% in wt. which is the maximum difference appears in these results.

3.6 Sample's boiling point/coke deposition from Thermogravimetric Analysis (TGA)

Liquid sample's boiling point and spent catalyst's coke deposition are tested by the TGA detector. Each sample was tested three times, and the result showed in Chapter 5 and 6 is the mean value of three tests' results. These results reveal excellent reproducibility. According to TGA detector's instrument error and the maximum difference observed in these tests, the error estimates adopted for the sample's boiling

point and coke deposition is ± 0.5℃ and ± 0.005% in wt., respectively.

3.7 Total adsorbed gas volume through the "*Extractive Distillation*" approach

The total adsorbed gas volume through the "*Extractive Distillation*" approach was tested three times with each extractant/extractant mixture. The final results indicate in Chapter 5 is the mean value of three tests' results. The error estimates of the total adsorbed gas volume is ± 5 ml, which is the maximum difference appears in these results.

3.8 Gaseous content's composition/product's production rate from Gas Chromatography (GC)

The GC test of each gaseous sample was repeated three times to obtain the various contents' composition (volume/molar fraction % in vol.) in the sample, or to obtain the production rate (ml/min) of various products. In Chapter 5 and 6 the result of the composition for gaseous samples or the gaseous product's production rate is the mean value of three tests' results. These results reveal excellent reproducibility, and the error estimates for the gaseous content's composition is ±0.005% in vol. and for gaseous product's production rate is ±0.005 ml/min, both are the maximum differences appear in the tests' results.

3.9 Total yield of oil phase product from the catalytic conversion

Two liquid phases are produced from the catalytic conversion process, the lower phase is the water phase product and the upper phase is the oil phase product. Each catalytic conversion test was repeated three times under the same reaction conditions for obtaining the mean value of oil phase product yield. This mean value is adopted as

the total yield of oil phase product from each catalytic conversion in Chapter 6. The error estimates of the total yield of oil phase product is ± 0.005 g, which is the maximum difference observed in these tests.

Appendix 4: Data and Corresponding Analyses of Various Organics of Co-Feeding Experiment

4.1 Alkene as the Co-Feed

The co-feeding effect of alkene on the MTH catalytic conversion process was examined. In this series of tests, 1-hexene was chosen as the co-feeding raw material and mix with methanol at different mass fraction from 5% to 20%. The time-on-stream gaseous products' production rates are displayed in Appendix Fig. 1. These results are obtained from the on-line GC analysis, and they are outside of the experimental error estimates (± 0.005 ml/min).

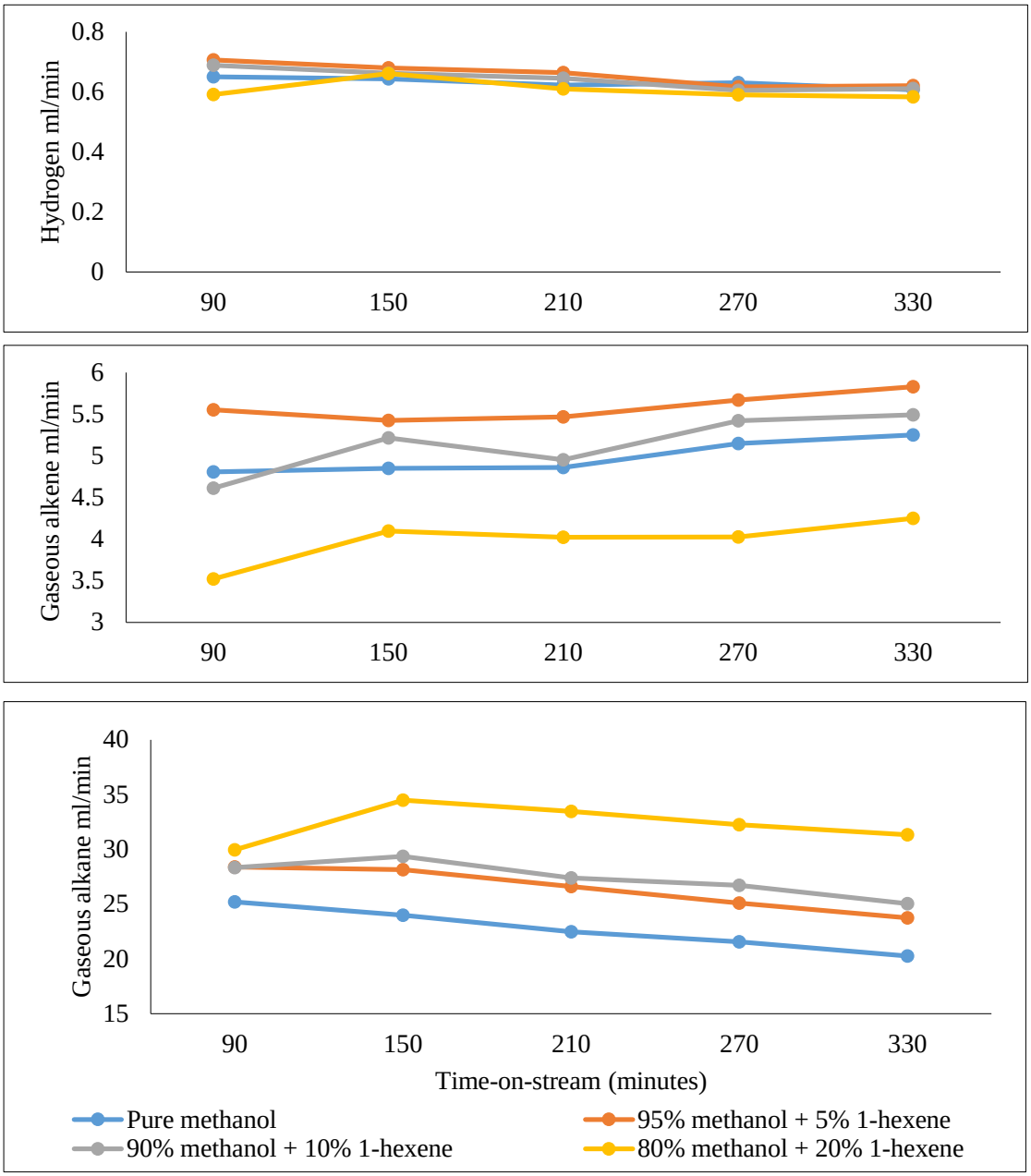

Appendix Fig. 1 Time-on-stream gaseous products' production rate of the alkene co-feeding conversions

Compared with the pure methanol MTH conversion process, the hydrogen output rate does not show an obvious change when the process is modified to methanol and 1-hexene as the feedstock. From the on-line GC results during the conversion process, it can be observed that, the output rate of gaseous alkene (C1-C4 alkene) was enhanced when the 1-hexene's mass fraction is more than 10%, the production of

alkene is reduced. However, the gaseous alkane's (C1-C4 alkane) output shows a positive correlation with increasing 1-hexene fraction. The gaseous product analysis results indicate that, during the MTH process the co-feeding alkene (1-hexene) can enhance the production of gaseous products (hydrogen, gaseous alkenes and gaseous alkanes).

These results can be explained by the catalytic mechanism of the MTH conversion (Appendix Fig. 2). The co-fed 1-hexene is very reactive in this conversion.[2] As a consequence only some 1-hexene desorbed as product, some molecules were cracked to propene, and some further methylated to heptene, which either desorbs as a minor product or undergoes cracking (major) to form propene and butenes.[2] Therefore, the increase of gaseous alkene production has been observed during the above 1-hexene co-feeding conversions. Moreover, addition of alkenes favours hydrogen transfer in the MTH conversion (Appendix Fig. 2),[2] thus, when 1-hexene was co-fed with methanol in the conversion process, more gaseous alkane was produced from cracked alkene by hydrogen transfer. With higher 1-hexene fraction (20%) in the feedstock, more cracked alkene has been converted into alkane through the hydrogen transfer. Hence, a drop and a rise in the gaseous alkene and gaseous alkane production was observed, respectively (Appendix Fig. 1).

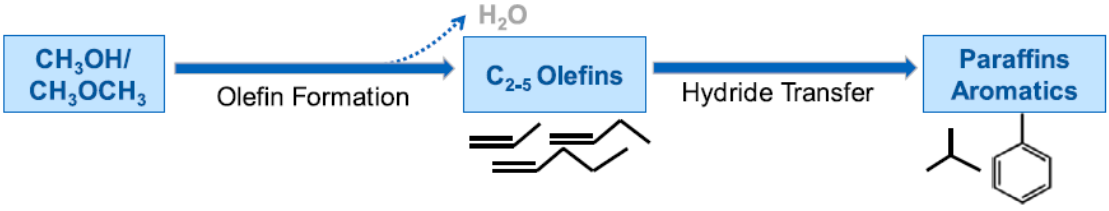

Appendix Fig. 2 A simplified reaction pathway of methanol conversion over HZSM-5 catalysts[2]

Moreover, the total yield of oil phase product (two liquid phases are produced

from the catalytic conversion process, the lower phase is the water phase product and the upper phase is the oil phase product) from the alkene co-feeding conversions with different methanol and 1-hexene mixing ratio are presented in Appendix Fig. 3. A fairly clear and positive correlation between the 1-hexene's mass fraction in the methanol-alkene mixture (feedstock) and the total yield of the oil phase product can be observed from Appendix Fig. 3. That means the oil phase yield can be enhanced by the adding 1-hexene. With the raw material of 80% methanol and 20% 1-hexene, the oil phase yield has been improved by nearly 30% (29.8%) compared with pure methanol MTH conversion. According to these results, it can be concluded that the total oil phase yield of the MTH process can be enhanced by the addition of an alkene (1-hexene).

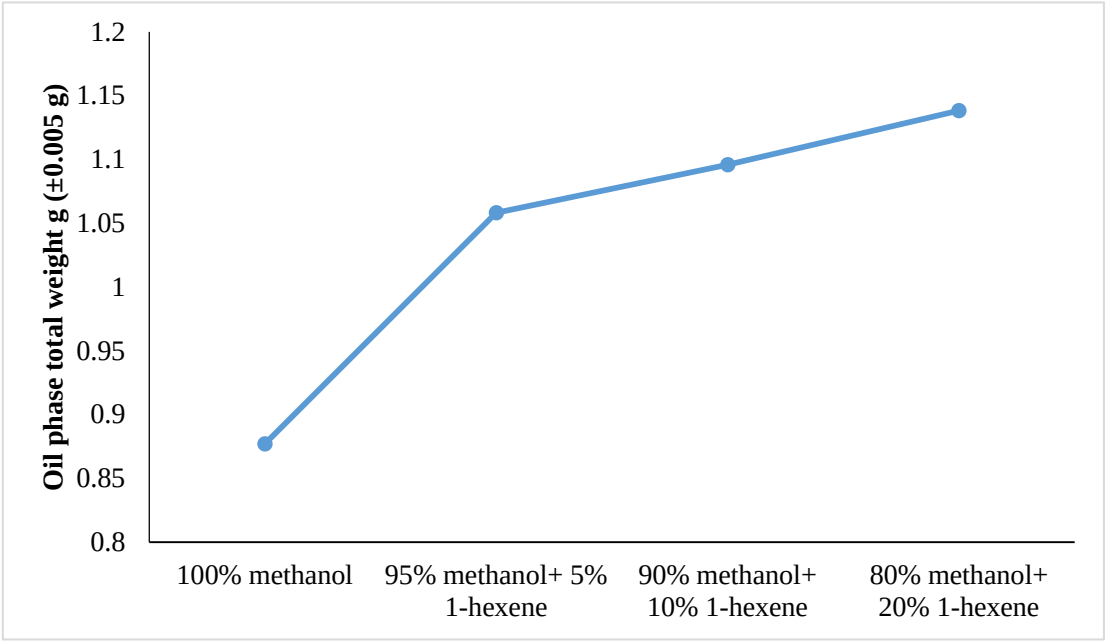

Appendix Fig. 3 Changes of oil phase product yield with the alkene co-feeding conversions

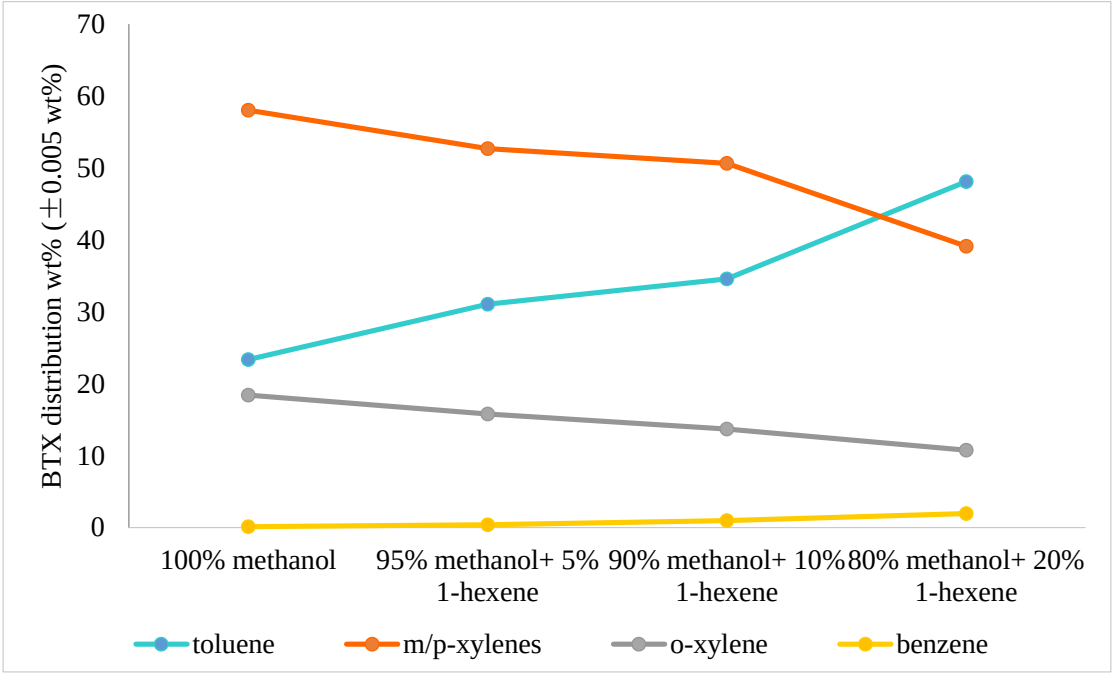

Appendix Fig. 4 Benzene, toluene, xylenes (BTX) distribution in the product of the alkene

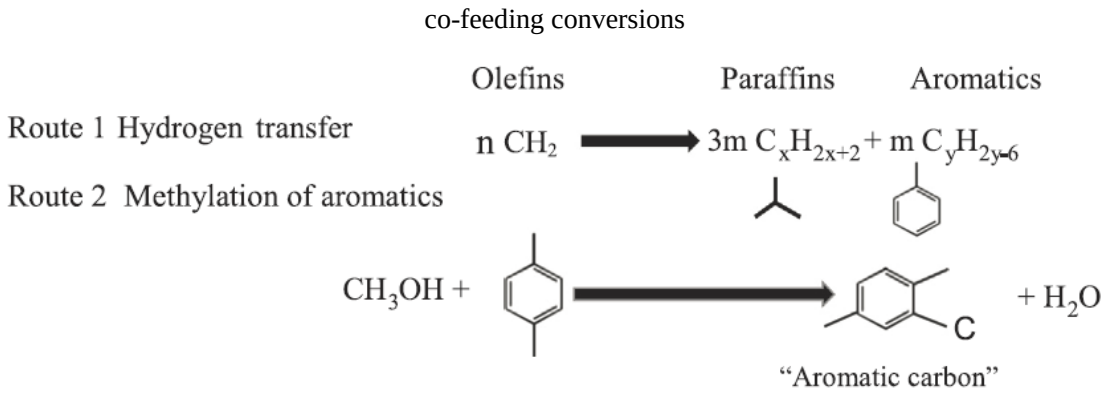

Scheme 1 Two representative routes for aromatics increment[2]

On the other hand, GCMS analysis results of the BTX in the oil phase products (Appendix Fig. 4), indicates the distribution of toluene and benzene in the oil-phase product increases with increasing percentage of added 1-hexene in the feedstock; this arises because the addition of alkene also favours the formation of aromatics.[2] The decreased fraction of methanol in the feedstock reduces the methylation of the benzene and toluene (Scheme 1),[2] as a result, xylenes' distribution shows a decreasing trend with larger 1-hexene mixing ratio.

4.2 Alkane as the Co-Feed

In order to examine the alkane co-feeding effect on MTH conversion, n-octane was mixed with methanol at 5%, 10% and 15% mass fraction, and these mixtures were utilised as the feedstocks in the MTH catalytic conversion processes, respectively.

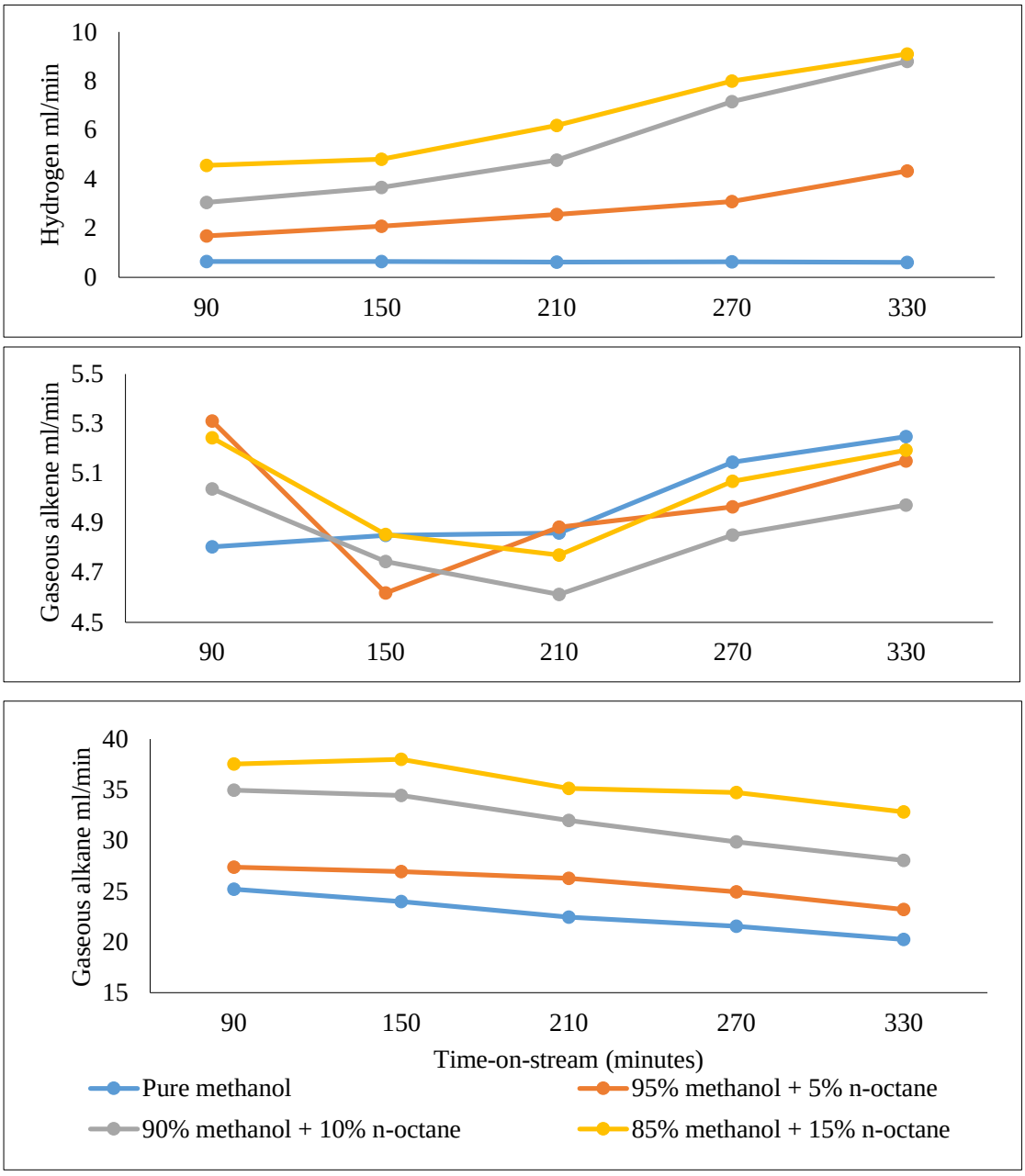

Appendix Fig. 5 Time-on-stream gaseous products' production rate of the alkane co-feeding conversions

From the gaseous product's analysis results it is found the generation rate of hydrogen has increased with the larger fraction of n-octane in the raw material (Appendix Fig. 5). These results are outside of the experimental error estimates (± 0.005 ml/min). This can be explained that the dehydrogenation performance of the process is promoted by the added n-octane, which is more easily dehydrogenated than methanol.

Moreover, the results indicate that the gaseous alkane generation rate is promoted by the added n-octane, and gaseous alkene generation rate is enhanced at first and then restrained slightly. In general, during the MTH process the production rate of gaseous product is unquestionably improved by the addition of alkane (in this case, n-octane). Similar to the alkene co-feeding conversions, co-feeding alkane into the MTH conversion favours the endothermic individual alkane cracking reaction, and this leads to the enhancement of the gaseous alkane production (Appendix Fig. 5).[3]

Through the catalytic conversion process, different yields of the oil phase product were obtained from the mixtures with various methanol and n-octane mass fractions. The total oil phase yield results are presented in Appendix Fig. 6. The total yield of the oil phase product indicates an obvious positive correlation with the increasing fraction of n-octane in the feedstock. It achieved 20% improvement of the total oil phase yield when applied the 85% methanol and 15% n-octane as the feedstock instead of the pure methanol. Through analysing the above results, it is confirmed that, the oil phase yield of the MTH process can be enhanced by the added alkane (n-octane).

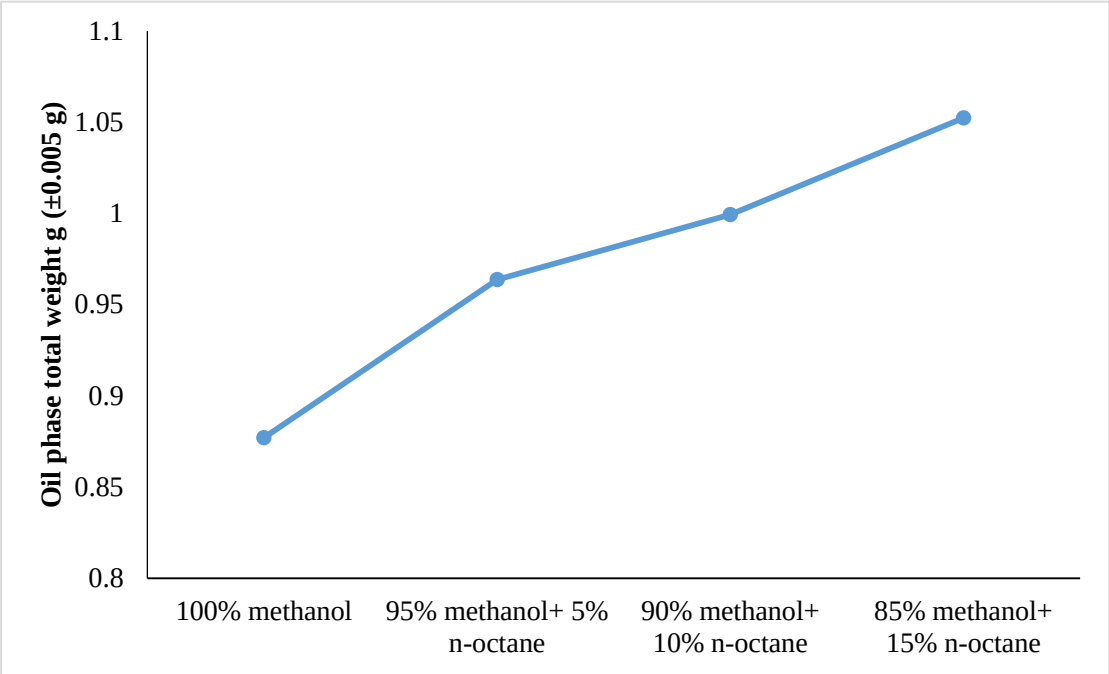

Appendix Fig. 6 Changes of oil phase product yield with the alkane co-feeding conversions

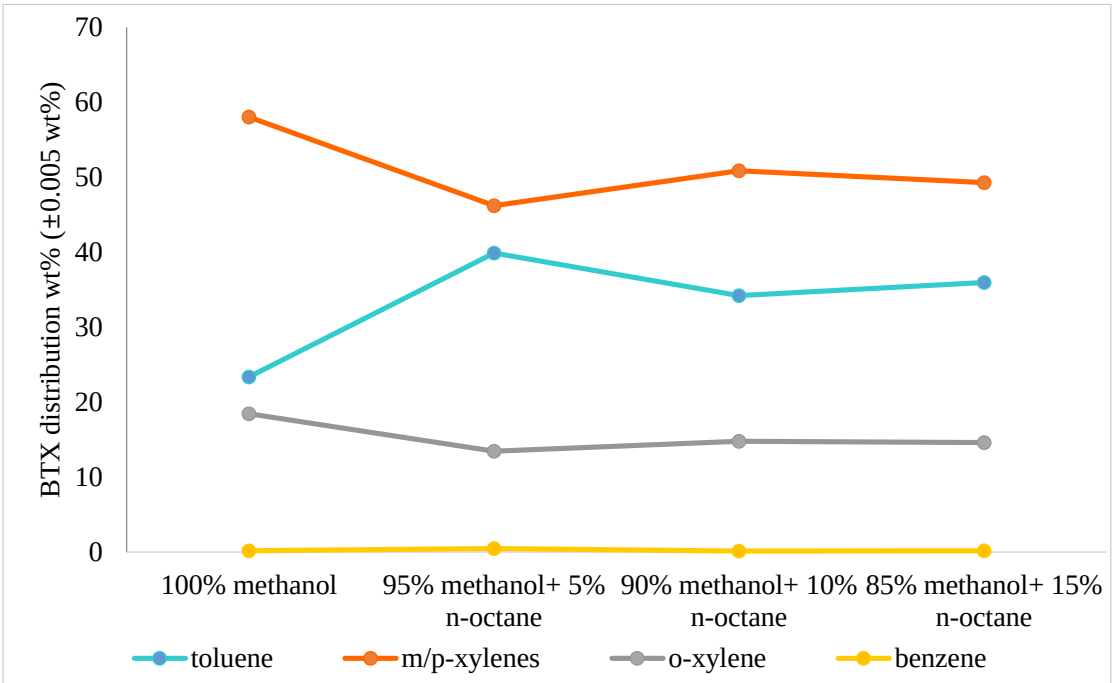

Appendix Fig. 7 BTX distribution in the product of the alkane co-feeding conversions

The BTX distribution results of the alkane co-feeding conversions are shown in Appendix Fig. 7. Since added alkane enhances the alkene selectivity of the conversion (Fig. 56),[3] the addition of 1-octane also favours the hydrogen transfer and formation

of aromatics shown in Scheme 1.[2] As the results, toluene distribution is improved when the process co-fed n-octane arises in the feedstock. With lower fraction of methanol in the feedstock, the methylation of the aromatics has been restrained.[2] Therefore, the distribution of xylenes shows a decline with the amount of n-octane in the feedstock. Compare of with pure methanol's conversion, the distribution of benzene does not present a significant change.

4.3 Aromatics as the Co-Feed

In the aromatics co-feeding conversions in this study, p-xylene is chosen as the co-feeding raw material. It is mixed with methanol at 5%, 10% and 20% mass fraction in the feedstock.

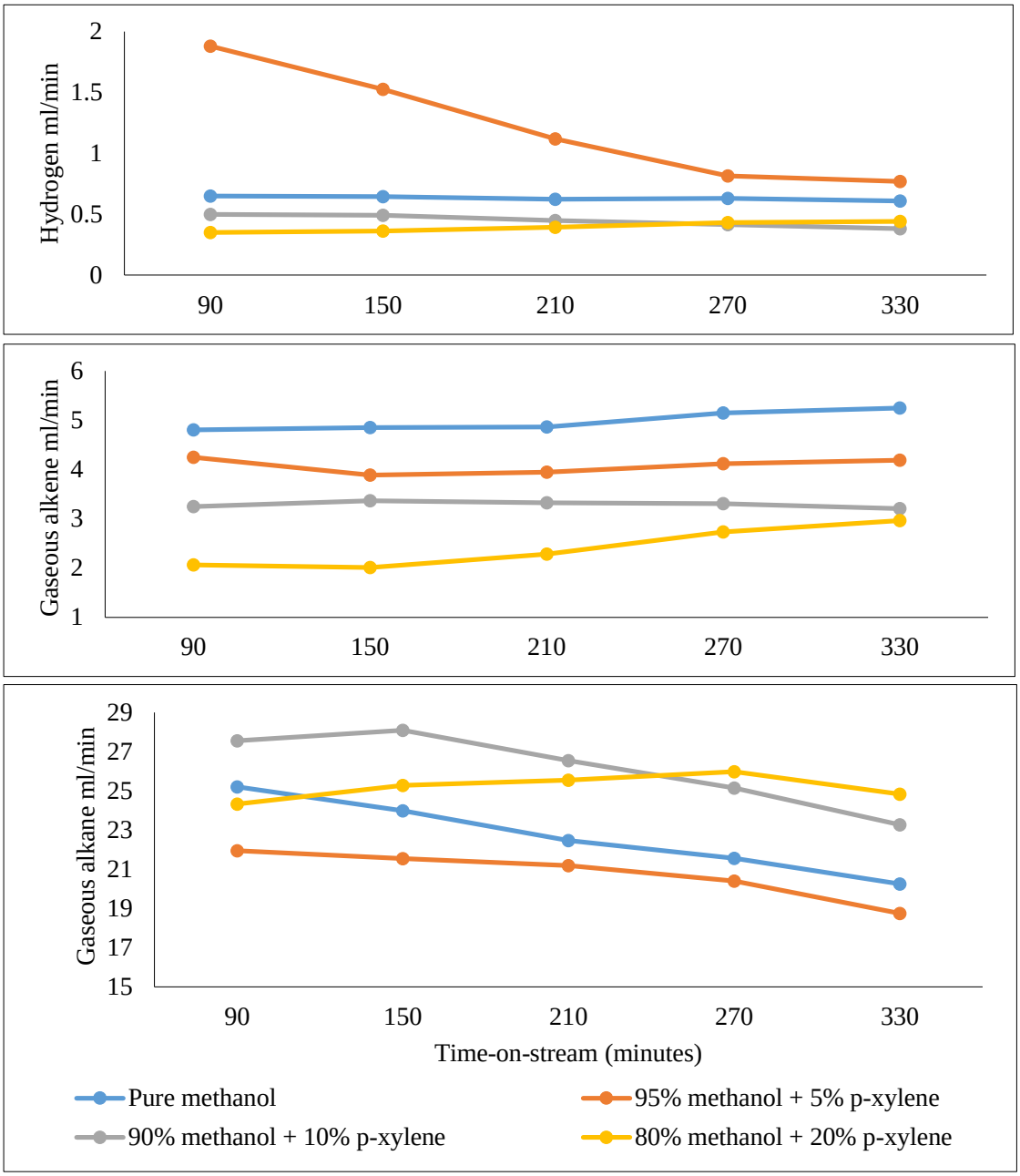

Appendix Fig. 8 Time-on-stream gaseous products' production rate of the aromatics co-feeding conversions

In the aromatics co-feeding conversions, the gaseous products production rate did not show an obvious enhancement upon the addition of the co-fed p-xylene. Except for the case of 95% methanol + 5% p-xylene, methanol and p-xylene with other mixing ratio present reduced hydrogen output rate (Appendix Fig. 8). These results are also outside of the experimental error estimates (± 0.005 ml/min).

From the on-line GC analysis results, it is found that the production rate of the gaseous alkenes exhibited a negative correlation with the mass fraction of the added p-xylene. This is because the cycle II shown in Fig. 56 was suppressed when p-xylene was co-fed.[2, 4-7] In regard to the gaseous alkane production rate, 95% methanol + 5% p-xylene showed lower rate than the pure methanol because low concentration of co-fed p-xylene suppresses the alkene-based cycle II in Fig. 56.[2, 4-7] Methanol with 10% and 20% of p-xylene gives higher gaseous alkane production rate than pure methanol (Appendix Fig. 8). This result is due to the high concentration of co-fed p-xylene enhance the dealkylation of aromatics, and the formed alkene from the dealkylation promotes the hydrogen transfer conversion. The hydrogen transfer conversion forms alkane from alkene. Therefore, when high concentration (10% and 20%) p-xylene was co-fed with methanol in the MTH conversion, higher gaseous alkane production rate than pure methanol conversion was obtained.

Different yields of the oil phase product are also observed from the co-feeding processes of various methanol and p-xylene mixtures, and these results are given in Appendix Fig. 9. Again, the total yield of the oil phase product presented a very clear positive correlation with the increasing mass fraction of p-xylene in the feedstock. With 20% p-xylene and 80% methanol in the feedstock the conversion process achieved nearly 160% improvement in the total oil phase yield than the pure methanol through the co-feeding MTH conversion process. These results suggest, importantly, that the co-fed aromatics is beneficial to enhance the oil phase yield of the MTH process.

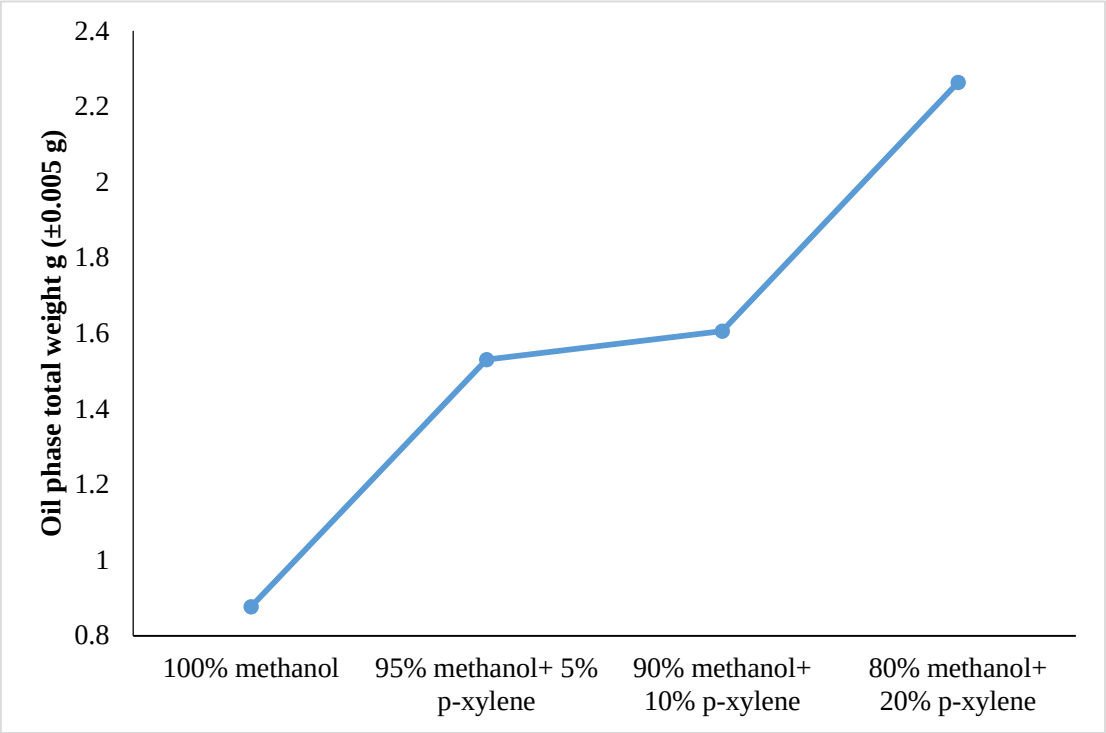

Appendix Fig. 9 Changes of oil phase product yield with the aromatics co-feeding conversions

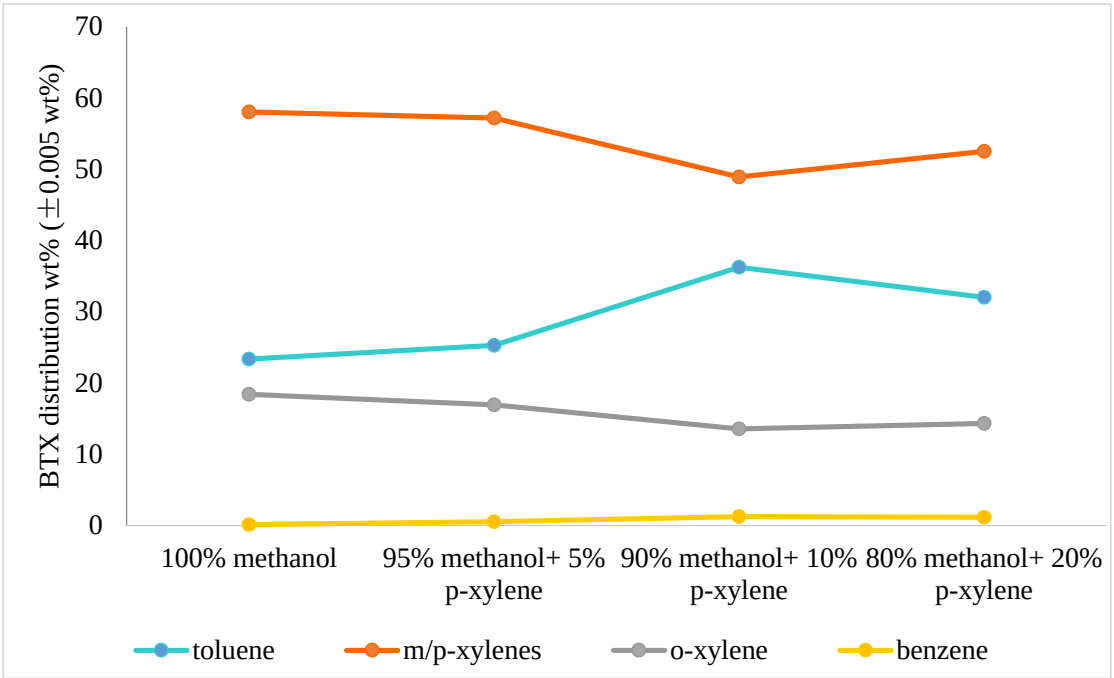

Appendix Fig. 10 Benzene, toluene, xylenes (BTX) distribution in the product of the aromatics co-feeding conversions

Considering the distribution of the specific high added value compounds, namely toluene and benzene', their distribution from the conversion process shows an

increase when p-xylene is blended into methanol as the co-feeding raw material. This can be observed from Appendix Fig. 10. Similar to the situation of the alkene and alkane co-feeding conversions, the co-feed p-xylene in the feedstock also results in a decreased yield of xylene. Sun et al. note that co-feeding low concentration of p-xylene with methanol during the MTH conversion promotes the aromatics-based cycle I in Fig. 56,[2, 4-7] and this enhances the methylation of aromatics to form trimethylbenzenes and tetramethylbenzenes as a consequence.[2] The added p-xylene also promotes the dealkylation of aromatics.[2] Whilst, less fraction of methanol restrains the methylation of benzene and toluene which are formed from the methanol conversion (Scheme 1).[2] Hence, increased distributions of toluene and benzene, but decreased distributions of xylenes were observed in these p-xylene co-feeding MTH conversions' oil phase products.

4.4 Other Solvent Co-extractants as the Co-Feed

Ethylene glycol is another alcohol and oxygenate, and it was used as other solvent co-extractant in our previous MFGM "*Extractive Refining*" (Chapter 5). Thus, it was examined as one of the co-feeds in those post extraction LPMs. In this study, in order to examine the co-feeding effect of co-extractant (alcohol/oxygenate) in the MTH conversion process, ethylene glycol was blended with methanol at 5%, 10% and 20% mass fraction to form the feedstocks of the co-feeding conversions.

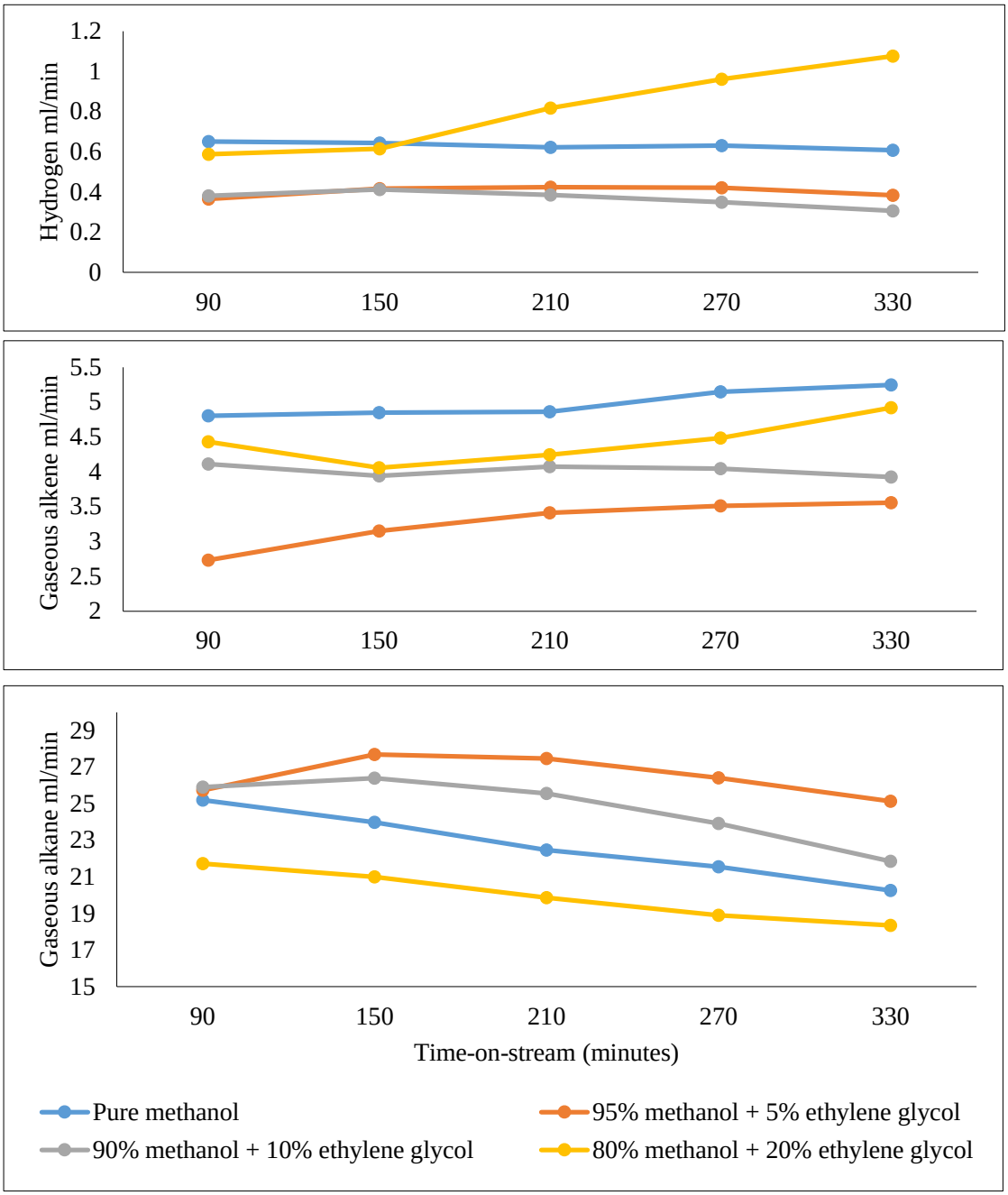

Appendix Fig. 11 Time-on-stream gaseous products' production rate of the co-extractant co-feeding conversions

Through the on-line GC analysis, it has been found that the hydrogen output rate only increased by using 80% methanol + 20% ethylene glycol as the feed stream, otherwise, the co-feeding conversion process only achieved lower hydrogen output rate than pure methanol conversion (Appendix Fig. 11).

Although the output of gaseous alkene's was restrained by the added ethylene glycol, higher ethylene glycol ratio still enhances the process to achieve higher alkene output. Moreover, 95% methanol + 5% ethylene glycol obtains highest alkane output rate, and with higher ethylene glycol mass ratio in the feedstock the gaseous alkane output rate became lower. With 20% ethylene glycol and 80% methanol the gaseous alkane output rate even became lower than the pure methanol conversion (Appendix Fig. 11).

The reason for the above results is the co-extractant ethylene glycol utilised in these conversions provides higher carbon density ($2CH_2OH$) than methanol (CH_3OH). Thus, it has a higher conversion rate than methanol solely and produces more C3 and C4 alkane when the conversion temperature is above 300 ℃.[8] Therefore, co-feeding low concentrations (5%) of ethylene glycol with methanol during the MTH conversion increases the production of gaseous alkane and reduces the production of gaseous alkene (Appendix Fig. 11).

With higher ethylene glycol concentration (10% and 20%) in the feedstock more C3 and C4 alkanes are produced from the reaction. Then, these C3 and C4 alkanes lead improvement in gaseous alkene production while reduction in light alkane yield (Appendix Fig. 11).[3] All these gaseous product results are outside of the experimental error estimates (± 0.005 ml/min).

The total yields of the oil phase product from various mixing ratio ethylene glycol+methanol mixtures after the catalytic conversion process are displayed in Appendix Fig. 12.

The results indicate the oil phase yield of these conversions present a positive correlation with the mass fraction of the co-extractant ethylene glycol in the mixture feedstock. With 20% ethylene glycol and 80% methanol in the feedstock, the co-feeding conversion process yields nearly 50% more oil phase product than the pure methanol MTH process. Therefore, the enhancement of the oil phase yield from the co-extractant (alcohol/oxygenate) ethylene glycol was confirmed by these co-feeding conversion test results.

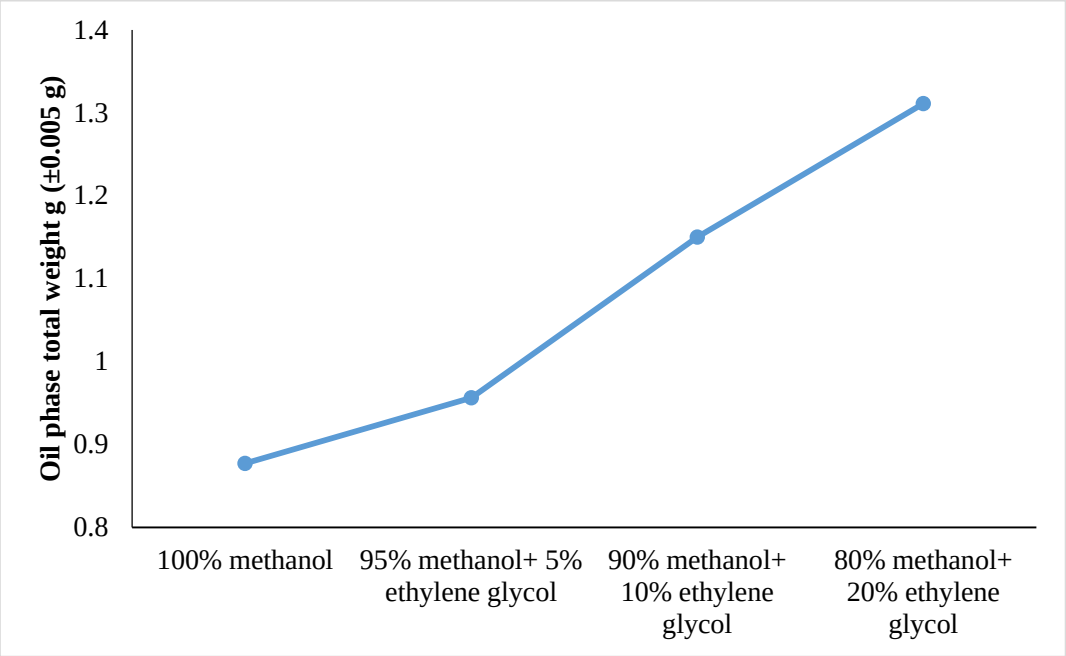

Appendix Fig. 12 Changes of oil phase product yield with the co-extractant co-feeding conversions

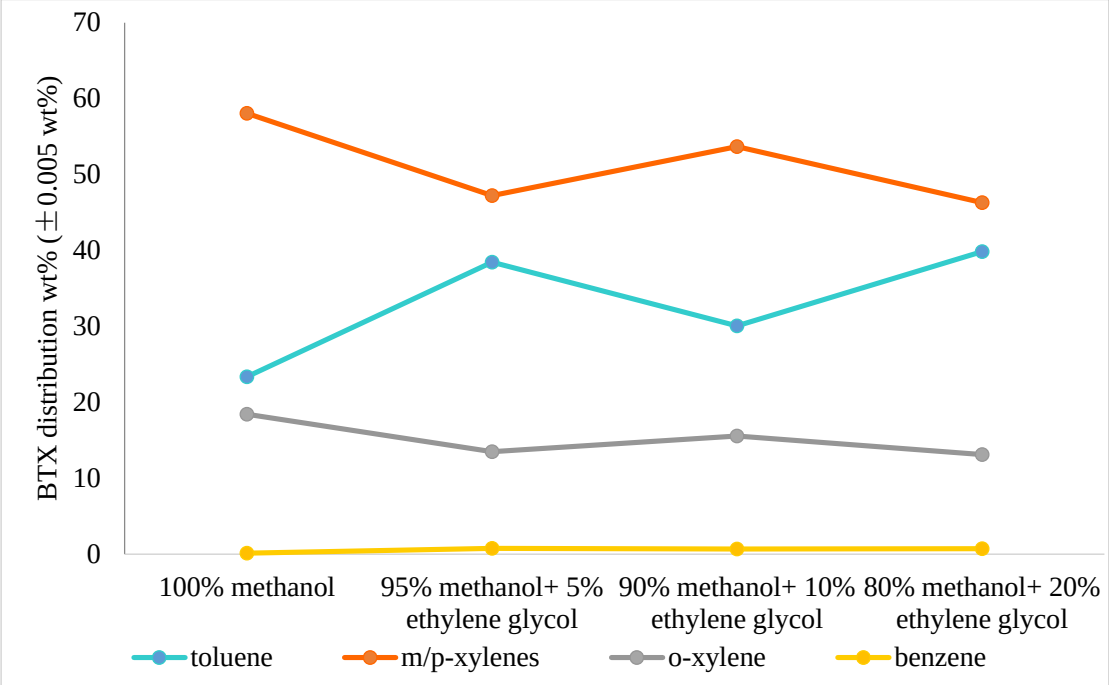

Appendix Fig. 13 Benzene, toluene, xylenes (BTX) distribution in the product of the co-extractant co-feeding conversions

Due to the decreased fraction of methanol in the feedstock, the methylation of the formed benzene and toluene (Scheme 1) is restrained.[2] Thus, xylenes distribution presented a decline with the co-feed ethylene glycol (Appendix Fig. 13). Whilst, the ethylene glycol co-feeding conversions also present a larger toluene and benzene distribution percentage than pure methanol conversion. These results are similar to the alkene, alkane and aromatics co-feeding conversions.

4.5 Organic Sulphur Compounds as the Co-Feed

Organic sulphur compounds (OSCs) are another group of extracts that exist in the "*Extractive Refining*" post extraction LPMs. Thus, it is necessary to examine the influence of the OSCs during the post extraction catalytic conversion process or MTH process. In order to investigate the OSCs co-feeding effect in the MTH conversion process, thiophene which has the most contribution to FCC gasoline's sulphur-content

is utilised as the target OSCs in the process.[9-11] Thiophene was blended into the methanol feed stream at the concentrations of 1000, 2000 and 4000 ppm.

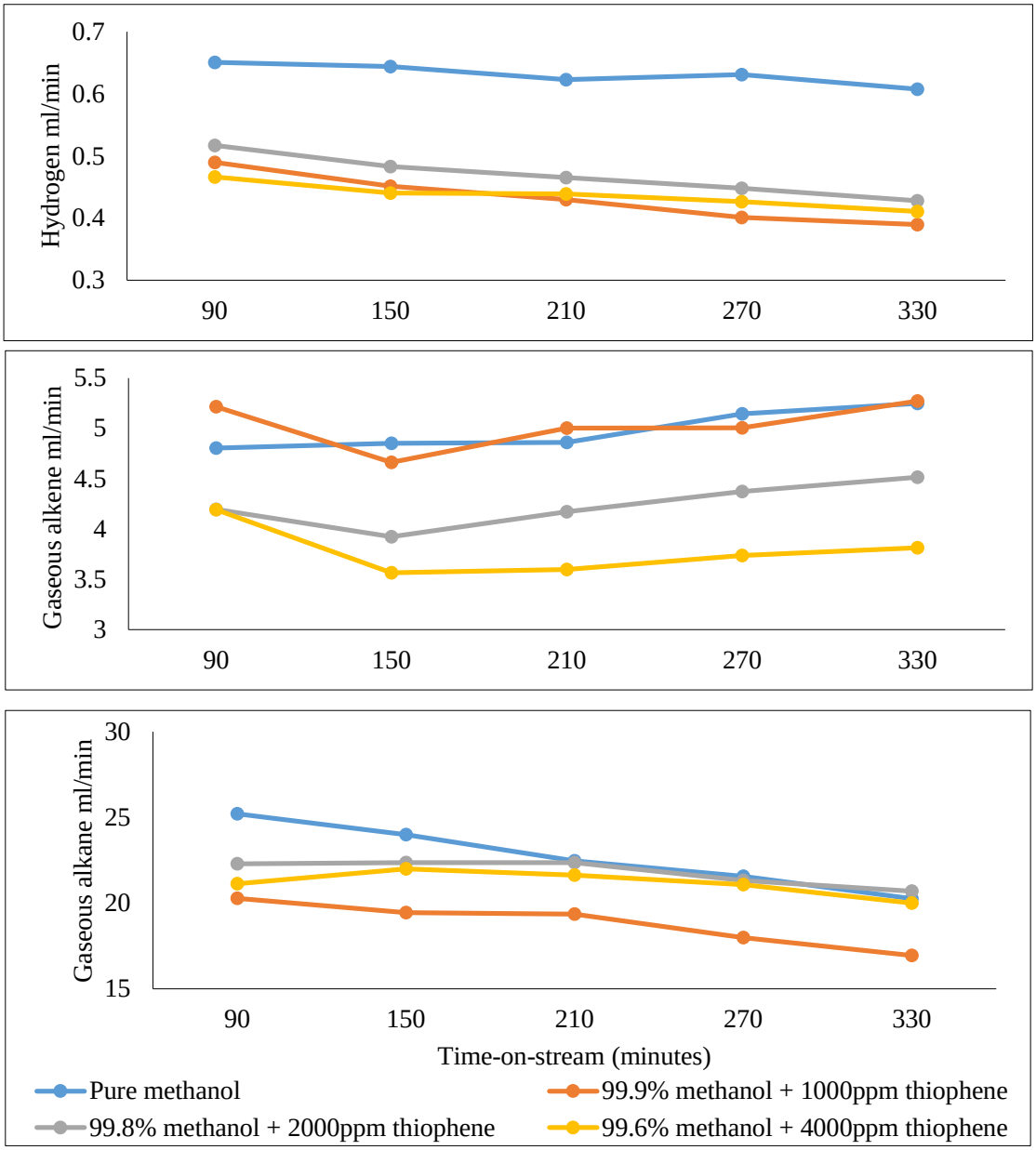

Appendix Fig. 14 Time-on-stream gaseous products' production rate of the OSCs co-feeding conversions

The on-line GC analysis results are shown in Appendix Fig. 14, these results are outside of the experimental error estimates (± 0.005 ml/min). We find the hydrogen generation rate decreases with higher concentration of thiophene added in the

feedstock (Appendix Fig. 14). This observation can be explained by the HDS process, which can be defined as a by-process of the OSCs co-feeding MTH conversion process.

Hydrogen is one of the major gaseous products from the methanol conversion process. OSCs (thiophene) in the feed stock reacts with hydrogen. Therefore, this by-reaction consumes the hydrogen produced by the methanol conversion process. As a result, the hydrogen output rate is reduced when OSCs (thiophene) has been added into the feed stock. Based on these results, it can be confirmed that the post extraction conversion process is able to remove the OSCs in the feedstock through the HDS by-process over HZSM-5 catalyst.

Moreover, the alkene's output rate was restrained by the addition of thiophene, and a negative correlation between the concentration of the thiophene and gaseous alkene's output was observed (Appendix Fig. 14). The alkane's output rate of the conversion processes with the feedstock which contain thiophene are also lower than the pure methanol conversion.

According to the literature, OSCs such as mercaptans, thiophenes, etc., present in the feedstock may deactivate the zeolite catalyst due to poisoning.[12] From the above on-line GC results, relatively constant gaseous products output rate was observed. Interestingly, it can be confirmed that, when the OSCs (thiophene) is added into the feedstock during the co-feeding MTH conversions the catalyst's deactivation (coke deposition) rate does not become faster than the pure methanol conversion process.

The total yield of the oil phase product from OSCs co-feeding conversion

processes are presented in Appendix Fig. 15. The results indicate that, the addition of the thiophene in the feedstock did not reduce the oil phase yield. On the contrary, the oil phase yield showed positive correlation with the concentration of thiophene in the feedstock mixture. These results also confirm the above conclusion that co-feed OSCs does not deactivate the H-ZSM-5 catalyst during the MTH conversion process. It was observed that with 4000 ppm thiophene, the OSCs co-feeding process achieved 9% increase in the total yield of the oil phase.

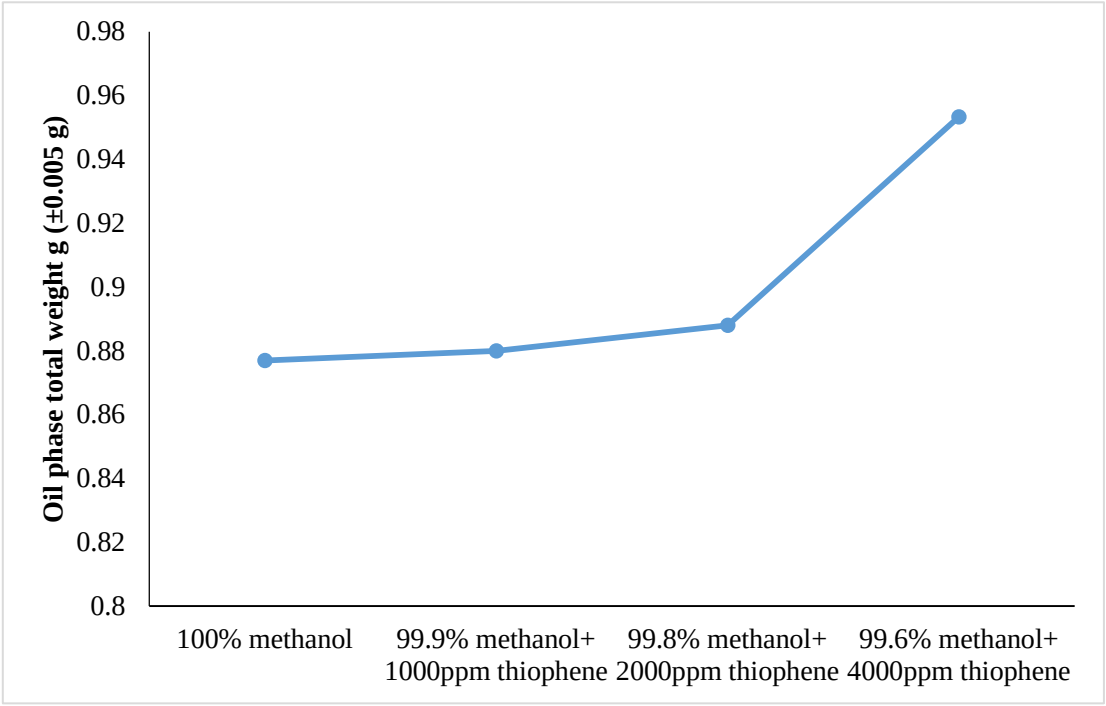

Appendix Fig. 15 Changes of oil phase product yield with the OSCs co-feeding conversions

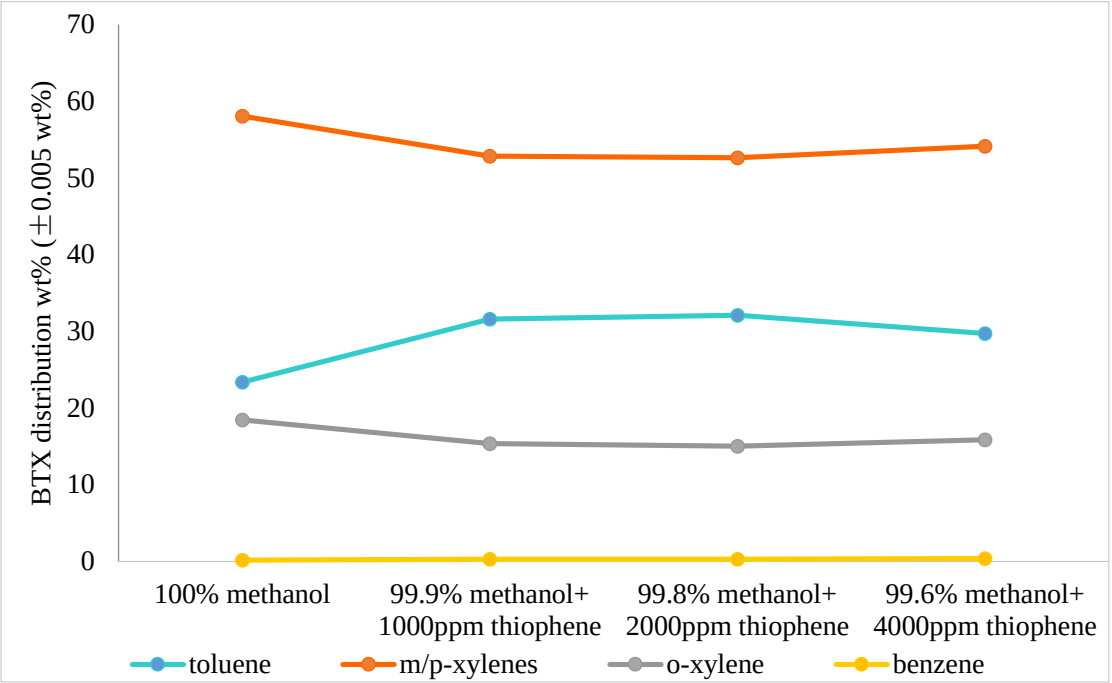

Appendix Fig. 16 Benzene, toluene, xylenes (BTX) distribution in the product of the OSCs co-feeding conversions

Similar to all the other co-feeding conversions, toluene's distribution in the BTX yield slightly increases when co-feeding thiophene in the feedstock (Appendix Fig. 16). The distribution of benzene does not show an obvious change with added OSCs (Appendix Fig. 16). In these thiophene co-feeding conversions, slightly reduction in xylenes' distribution was observed when comparing with the xylenes distribution of pure methanol MTH conversion. The minor decreased fraction of methanol in the feedstock slightly reduces the methylation of the formed benzene and toluene (Scheme 1).[2] Thus, during these OSCs (thiophene) co-feeding conversions, increase in toluene distribution and decrease in xylenes distribution were observed, respectively.

Through analysing the gaseous and liquid products, we can conclude that low concentration of OSCs (thiophene) influences neither the total oil phase yield nor the

deactivation rate of the HZSM-5 catalyst during the MTH process.

References

1 R. E. Hoffman, *Magnetic Resonance in Chemistry* 2006, *44*, 606-616.
2 X. Sun, S. Mueller, H. Shi, G. L. Haller, M. Sanchez-Sanchez, A. C. van Veen, J. A. Lercher, *Journal of Catalysis* 2014, *314*, 21-31.
3 G. Roohollahi, M. Kazemeini, A. Mohammadrezaee, R. Golhosseini, *Journal of Industrial and Engineering Chemistry* 2013, *19*, 915-919.
4 S. Svelle, F. Joensen, J. Nerlov, U. Olsbye, K.-P. Lillerud, S. Kolboe, M. Bjørgen, *journal of the American Chemical Society* 2006, *128*, 14770-14771.
5 M. Bjørgen, S. Svelle, F. Joensen, J. Nerlov, S. Kolboe, F. Bonino, L. Palumbo, S. Bordiga, U. Olsbye, *Journal of Catalysis* 2007, *249*, 195-207.
6 M. Bjørgen, K.-P. Lillerud, U. Olsbye, S. Svelle, *Studies in Surface Science and Catalysis* 2007, *167*, 463-468.
7 U. Olsbye, S. Svelle, M. Bjørgen, P. Beato, T. V. Janssens, F. Joensen, S. Bordiga, K. P. Lillerud, *Angewandte Chemie International Edition* 2012, *51*, 5810-5831.
8 E. G. Derouane, J. B. Nagy, P. Dejaifve, J. H. van Hooff, B. P. Spekman, J. C. Védrine, C. Naccache, *Journal of Catalysis* 1978, *53*, 40-55.
9 T. G. Albro, P. A. Dreifuss, R. F. Wormsbecher, *Journal of High Resolution Chromatography* 1993, *16*, 13-17.
10 W.-C. Cheng, G. Kim, A. Peters, X. Zhao, K. Rajagopalan, M. Ziebarth, C. Pereira, *Catalysis Reviews* 1998, *40*, 39-79.
11 M. Absi-Halabi, J. Beshara, H. Qabazard, A. Stanislaus, in *Catalysts in Petroleum Refining and Petrochemical Industries 1995*. Elsevier, Amsterdam, 1996, Chap. 3.
12 S. Bhatia, J. Beltramini, D. Do, *Catalysis Reviews—Science and Engineering* 1989, *31*, 431-480.